ELECTROMAGNETIC FIELDS INDUCED IN AND SCATTERED BY BIOLOGICAL SYSTEMS EXPOSED TO NONIONIZING ELECTROMAGNETIC RADIATION

> Dissertation for the Degree of Ph. D. MICHIGAN STATE UNIVERSITY DONALD EDWARD LIVESAY 1975





This is to certify that the

thesis entitled

"Electromagnetic Fields Induced in and Scattered by Biological Systems Exposed to Nonionizing Electromagnetic Radiation"

presented by

Donald Edward Livesay

has been accepted towards fulfillment of the requirements for

Ph. D. degree in EE

Major professor

Date May 13, 1975

O-7639



093/38

ABSTRACT

ELECTROMAGNETIC FIELDS INDUCED IN AND SCATTERED BY BIOLOGICAL SYSTEMS EXPOSED TO NONIONIZING ELECTROMAGNETIC RADIATION

 $\mathbf{B}\mathbf{v}$

Donald Edward Livesay

This thesis presents a technique for calculating the electric field induced in a finite biological body having arbitrary shape and composition, when the body is irradiated by an electromagnetic wave. A knowledge of the induced field is important to researchers investigating the biological effects of nonionizing radiation.

As an introduction to the study of induced electromagnetic fields in biological media, a plane slab model of a human trunk is analyzed. The electromagnetic field induced in the model by a uniform plane wave is obtained by two methods: (1) by a direct application of boundary conditions, and (2) by transmission line techniques. A group of numerical examples illustrates the behavior of the human trunk model at various frequencies from 100 Hz to 10 GHz.

The problem of calculating the electric field induced in a finite body is considered next. An integral equation for the induced electric field is derived using the free-space dyadic Green's function. The method of moments is then used to transform the integral equation to a matrix equation for numerical solution. Techniques for calculating the external scattered field, and for using symmetry to reduce the matrix size, are

included. A variety of numerical examples, along with some experimental data, are presented to illustrate the versatility and the accuracy of the moment solution. In addition, the computer program used to calculate the numerical examples is described, and instructions for its use are given.

ELECTROMAGNETIC FIELDS INDUCED IN AND SCATTERED BY BIOLOGICAL SYSTEMS EXPOSED TO NONIONIZING ELECTROMAGNETIC RADIATION

By

Donald Edward Livesay

A DISSERTATION

Submitted to
Michigan State University
in partial fulfillment of the requirements
for the degree of

DOCTOR OF PHILOSOPHY

Department of Electrical Engineering and Systems Science

This thesis is fondly dedicated to Dr. Ralph Kron.
Without his encouragement, kindness, and understanding,
it might never have been written.

ACKNOWLEDGMENTS

The author wishes to express his appreciation to his major professor, Dr. K. M. Chen, for his guidance and encouragement throughout the course of this work.

He also wishes to thank the other members of his guidance committee, Dr. D. P. Nyquist, Dr. M. M. Gordon, Dr. B. Ho, and Dr. J. Asmussen, for their time and assistance.

A special note of thanks is extended to the National Science Foundation for the Graduate Traineeship which helped the author complete this study. The research reported in this thesis was supported in part by the National Science Foundation under Grant ENG 74-12603.

TABLE OF CONTENTS

		Page
LIST	OF TABLES	vi
LIST	OF FIGURES	vii
I.	INTRODUCTION	1
П.	INTERACTION OF AN ELECTROMAGNETIC PLANE WAVE WITH A PLANE SLAB MODEL	
	OF A PHYSIOLOGICAL SYSTEM	3
	2.1 Qualitative Description of the Plane Slab Model	3
	2.2 Maxwell's Equations and Plane Wave Solutions	
	for a General N-Slab System	5
	2.3 Boundary Conditions	7
	2.4 Matrix Representation of Boundary Conditions	8
	2.5 Solution by Transmission Line Analogy 2.6 Numerical Results for a Plane Slab Model of	10
	the Human Trunk	15
III.	INTERACTION OF AN ELECTROMAGNETIC WAVE WITH AN ARBITRARY PHYSIOLOGICAL	
	SYSTEM	31
	3.1 Description of Problem and Method of Solution	31
	3.2 Integral Equation for Internal Electric Field	33
		37
	3.4 Calculation of Matrix Elements	42
	Cross-Sectional Symmetry	51
	3.6 Calculation of External Scattered Field	60
	3.7 Numerical and Experimental Results	61
	A. Testing and Convergence	62
	B. Internal Electric Field	65
	C. External Scattered Field	96
	D. Symmetric and Antisymmetric Modes	98
IV.	A DESCRIPTION OF THE COMPUTER PROGRAM USED TO DETERMINE THE INDUCED ELECTRIC FIELD IN AN ARBITRARY, FINITE PHYSIOLOGICAL	
	SYSTEM	111
	4.1 Description of the Program	111
	4.2 Structure of the Data File	113

																							Page
	4.3	Desc	rip	tion	1 0	f ti	he	In	pu	t \	Va:	ria	abl	es		•						•	117
	4.4	Using	g ti	ne F	Pro	gr	am	1	•	•	•		•	•	•	•	•	•	•	•	•	•	123
	4.5	Listi	ng	of I	Pro	gı	an	n a	and	i S	ut	orc	out	in	es	•	•	•	•	•	•	•	130
v.	SUM	MARY	•	• •	•	•	•	•	•	•	•		•	•	•		•	•	•	•		•	139
APPI	ENDIX	Α.	•	• •	•	•	•	•		•,	•	•	•	•	•	•	•	•			•		141
BIBL	IOGRA	APHY			•	•		•	•	•	•	•	•	•		•		•	•	•	•		144

LIST OF TABLES

	Page
Frequency Dependence of Conductivity and Relative Permittivity for Muscle, Skin, Fat, and Bone	17
Induced electric field at the center of the muscle cubes shown in Figure 3.10 for various numbers of subvolumes. $ \vec{E}^i = 1 \text{ V/m}$	67
The structure of the data file for PRØGRAM BLØCK. If any of the variables marked with an asterisk does not match its prescribed codes, the program will be aborted	114
	Relative Permittivity for Muscle, Skin, Fat, and Bone Induced electric field at the center of the muscle cubes shown in Figure 3.10 for various numbers of subvolumes. $ \vec{E}^i = 1 \text{ V/m}$ The structure of the data file for PRØGRAM BLØCK. If any of the variables marked with

LIST OF FIGURES

Figure		Page
2.1	An arbitrary N-slab system	4
2.2	Boundary condition solution of N-slab system	9
2.3	Transmission line solution of N-slab system	12
2.4	7-slab model used for calculations	16
2.5	Electric field and power density in 7-slab model at 100 Hz, for $0 \le z \le 8.5$ cm. Incident field is a plane wave, with $ \vec{E}^i = 1 \text{ V/m} \cdot \cdot \cdot \cdot \cdot \cdot \cdot \cdot \cdot$.	19
2.6	Electric field and power density in 7-slab model at 1 kHz, for $0 \le z \le 8.5$ cm. Incident field is a plane wave, with $ \vec{E}^i = 1$ V/m	20
2.7	Electric field and power density in 7-slab model at 1 MHz, for $0 \le z \le 8.5$ cm. Incident field is a plane wave, with $ \vec{E}^i = 1$ V/m	21
2.8	Electric field and power density in 7-slab model at 10 MHz, for $0 \le z \le 8.5$ cm. Incident field is a plane wave, with $ \vec{E}^i = 1$ V/m	22
2.9	Electric field and power density in 7-slab model at 100 MHz, for $0 \le z \le 8.5$ cm. Incident field is a plane wave, with $ \vec{E}^i = 1$ V/m	23
2.10	Electric field and power density in 7-slab model at 300 MHz, for $0 \le z \le 8.5$ cm. Incident field is a plane wave, with $ \vec{E}^1 = 1$ V/m	24
2, 11	Electric field and power density in 7-slab model at 600 MHz, for $0 \le z \le 8.5$ cm. Incident field is a plane wave, with $ \vec{E}^i = 1$ V/m	25
2.12	Electric field and power density in 7-slab model at 900 MHz, for $0 \le z \le 8.5$ cm. Incident field is a plane wave, with $ \vec{E}^i = 1$ V/m	26
2.13	Electric field and power density in 7-slab model at 1.5 GHz, for $0 \le z \le 8.5$ cm. Incident field is a plane wave, with $ \vec{E}^1 = 1$ V/m	27

Figure		Page
2.14	Electric field and power density in 7-slab model at 2.45 GHz, for $0 \le z \le 8.5$ cm. Inset shows power density in skin layer. Incident field is a plane wave, with $ \vec{E}^i = 1$ V/m	28
2.15	Electric field and power density in 7-slab model at 5 GHz, for $0 \le z \le 8.5$ cm. Inset shows power density in skin layer. Incident field is a plane wave, with $ \vec{E}^1 = 1$ V/m	29
2.16	Electric field and power density in 7-slab model at 10 GHz, for $0 \le z \le 8.5$ cm. Inset shows power density in skin layer. Incident field is a plane wave, with $ \vec{E}^i = 1 \text{ V/m} \dots \dots$	30
3.1	An arbitrarily shaped biological body in free space, illuminated by an electromagnetic field. In general, the body is inhomogeneous and nonmagnetic	32
3, 2	A physiological system partitioned into N subvolumes, showing a typical arrangement of the cells	39
3.3	(a) Scattered field \vec{E}^s in subvolume V_m produced by a unit current in subvolume V_n when cylindrical body is perpendicular to \vec{E}^i . (b) Scattered field \vec{E}^s in subvolume V_m produced by a unit current in subvolume V_n when cylindrical body is parallel to \vec{E}^i . \vec{E}^s in (b) is about twice as large as \vec{E}^s in (a)	44
3.4	(a) Equivalent sphere S_n , centered about \overrightarrow{r}_n , used to calculate the diagonal elements of each submatrix. (b) Spherical coordinate system defined in S_n	48
3, 5	A cubical body partitioned into symmetrical quadrants. The quadrants are designated by Roman numerals	52
3.6	A cubical body partitioned into symmetrical octants, designated by Roman numerals. The origin of the coordinate system is located at the center of the cube	56
3.7	Cubical body excited by (a) the symmetric mode \vec{E}_s^i , and (b) the anti-symmetric mode \vec{E}_a^i . The octants of the cube are numbered as in Figure 3.6	58

Figure		Page
3.8	A cylinder of muscle partitioned into (a) 6, (b) 48, and (c) 162 subvolumes. The cylinder is illuminated by a 2.45 GHz plane wave, with the incident electric field \vec{E}^i parallel to the axis of the cylinder. $ \vec{E}^i = 1 \text{ V/m} \dots \dots$	63
3.9	Electric field intensity along the axis of the cylinder shown in Figure 3.8, for models (a), (b), and (c). $ \vec{E}^i = 1 \text{ V/m}$. One wavelength in the cylinder is 1.76 cm	64
3.10	Two cubes of muscle illuminated by a 2.45 GHz plane wave, treated as single cells in (a) and (c), and divided into 27 cubical subvolumes in (b) and (d). The edges of the cubes measure one wavelength and 1/4 wavelength, respectively	66
3, 11	Electric field induced at the center of a dielectric cube, for various values of frequency and dielectric constant. Incident electric field is a plane wave	68
3, 12	Plane conducting layer exposed to a 300 MHz plane wave, with \vec{E}^i perpendicular to the plane of the layer	70
3.13	Electric field induced in the layer of Figure 3.12, with $\epsilon = 70 \epsilon_0$ and $\sigma = 1 \text{ mho/m}$. Only half of the layer is shown above. Ey and Ez are negligible	71
3, 14	A 300 MHz plane wave impinges upon a plane conducting layer, with \vec{E}^i parallel to the plane of the layer	72
3.15	The x-component of the electric field induced in the layer of Figure 3.14, with $\epsilon = 70 \epsilon_0$ and $\sigma = 1$ mho/m. Only half of the layer is shown above	73
3.16	The z-component of the electric field induced in the layer of Figure 3.14, with $\epsilon = 70 \epsilon_0$ and $\sigma = 1$ mho/m. Only half of the layer is shown above	74
3.17	A block of tissue composed of a fat layer and a muscle layer, illuminated by a plane wave at 100 MHz	75

3.18 The electric field induced in the block of tissue pictured in Figure 3.17. Only 1/4 of each layer		
is shown above. For a corresponding plane slab model, $E_x = 0.197$ V/m at the center of the fat layer, and $E_x = 0.210$ V/m at the center of the muscle layer.	•	76
3.19 A saltwater cylinder of half-length h illuminated by a 9.45 GHz plane wave. The cross-section of the cylinder measures 1.8 mm x 1.8 mm	•	78
 Electric field E along the axis of the saltwater cylinder shown in Figure 3.19, for h/λ = 0.113, 0.227, 0.510, and 0.737. Concentration of the salt solution is 1 Normal, and the frequency is 9.45 GHz	•	79
Power density P along the axis of the saltwater cylinder shown in Figure 3.19, and total absorbed power P_t , for $h/\lambda_0 = 0.113$, 0.227, 0.510, and 0.737. Concentration of the salt solution is 1 Normal, and the frequency is 9.45 GHz	•	80
3.22 Electric field E along the axis of the saltwater cylinder shown in Figure 3.19, for $h/\lambda_0 = 0.113$, 0.227, 0.510, and 0.737. Concentration of the salt solution is 2 Normal, and the frequency is 9.45 GHz	•	81
3.23 Power density P along the axis of the saltwater cylinder shown in Figure 3.19, and total absorbed power P_t , for $h/\lambda_0 = 0.113$, 0.227, 0.510, and 0.737. Concentration of the salt solution is 2 Normal, and the frequency is 9.45 GHz	•	82
3.24 Electric field E along the axis of the saltwater cylinder shown in Figure 3.19, for $h/\lambda_0 = 0.113$, 0.227, 0.510, and 0.737. Concentration of the salt solution is 5 Normal, and the frequency is 9.45 GHz	•	83
Power density P along the axis of the saltwater cylinder shown in Figure 3.19, and total absorbed power P_t , for $h/\lambda_0 = 0.113$, 0.227, 0.510, and 0.737. Concentration of the salt solution is 5 Normal, and the frequency is 9.45 GHz	•	84
3.26 (a) A homogeneous muscle cylinder, and (b) an inhomogeneous muscle cylinder irradiated by a 2.45 GHz plane wave	•	85

Figure		Page
3.27	(a) Induced electric field E, and (b) power density P along the axes of the muscle cylinders shown in Figure 3.26. The frequency is 2.45 GHz, and $ \vec{E}^{i} = 1 \text{ V/m}$. Each cylinder was partitioned lengthwise into 100 subvolumes of equal size	. 86
3.28	(a) A homogeneous fat cylinder, and (b) an inhomogeneous fat cylinder irradiated by a 2.45 GHz plane wave	. 88
3.29	(a) Induced electric field E, and (b) power density P along the axes of the fat cylinders shown in Figure 3.28. The frequency is 2.45 GHz, and $ \vec{E}^i = 1$ V/m. Each cylinder was partitioned lengthwise into 100 subvolumes of equal size	. 89
3.30	An inhomogeneous fat layer illuminated by a uniform plane wave at 600 MHz	. 90
3.31	The x-component of the electric field induced in the layer illustrated in Figure 3.30. The incident field is polarized along the x-axis	. 91
3,32	The y-component of the electric field induced in the layer illustrated in Figure 3.30. The incident field is polarized along the x-axis	. 92
3, 33	A homogeneous layer of muscle, illuminated only in the shaded area by a 600 MHz plane wave	. 93
3.34	The x-component of the electric field induced in the layer pictured in Figure 3.33. The incident field is polarized along the x-axis, and irradiates only the shaded portion of the layer	. 94
3.35	The y-component of the electric field induced in the layer pictured in Figure 3.33. The incident field is polarized along the x-axis, and irradiates only the shaded portion of the layer	. 95
3.36	Backscattering from three different homogeneous cylinders exposed to a 10 GHz plane wave. The magnitude of τ was 100 in each case, but the respective values of the phase angle of τ were 0° , 45° , and 90° . The observation point was 30 cm from each cylinder	. 97

Figure		Page
3.37	Comparison of theory and experiment for back- scattering from a saltwater cylinder of 1 Normal concentration at 9.45 GHz. The observation point was 15 cm from the cylinder	99
3,38	Comparison of theory and experiment for back- scattering from a saltwater cylinder of 5 Normal concentration at 9.45 GHz. The observation point was 15 cm from the cylinder	100
3,39	Comparison of theory and experiment for back- scattering from a brass cylinder at 9.45 GHz. The observation point was 15 cm from the cylinder	101
3.40	Comparison of theory and experiment for relative backscattering from a brass cylinder and a saltwater cylinder of 1 Normal concentration. The frequency was 9.45 GHz, and the observation point was 15 cm from each cylinder	102
3.41	The symmetric mode of the electric field in a muscle layer exposed to a 1 GHz plane wave. The symmetric mode is induced by the symmetric component ($\cos k_0 z \hat{k}$) of \vec{E}^i . Only 1/4 of the layer is shown above	104
3.42	The antisymmetric mode of the electric field in a muscle layer exposed to a 1 GHz plane wave. The antisymmetric mode is induced by the antisymmetric component (- j $\sin k_0 z \hat{x}$) of \vec{E}^i . Only 1/4 of the layer is shown above	105
3,43	The total electric field induced in a muscle layer by a 1 GHz plane wave. Only 1/4 of the layer is shown above	106
3.44	A square loop of muscle irradiated by a 100 MHz plane wave. \vec{E}^i lies in the plane of the loop, while \vec{H}^i is normal to the plane of the	107
3.45	The symmetric mode of the electric field in the loop of muscle shown in Figure 3.44. The symmetric mode is induced by the symmetric component (cos k _o z k) of the incident field. Only 1/4 of the loop is shown above	107
3.46	The antisymmetric mode of the electric field in the loop of muscle shown in Figure 3.44. The antisymmetric mode is induced by the antisymmetric component (-j sink _o z x) of the incident field. Only 1/4 of the loop is shown	
	here	110

Figure		Page
4.1	An electromagnetic plane wave, incident normally upon a rectangular block of tissue	112
4.2	A block of tissue partitioned into rows, columns, and layers of subvolumes along the x-, y-, and z-axes, respectively	115
4.3	A block of tissue divided into 4 symmetrical quadrants. If the incident field is likewise symmetrical, calculating the induced field in only one quadrant will determine the induced field in the entire block	119
4. 4	A spherical polar coordinate system used in calculations of the external scattered field. This system is used unless the program user changes it	122
4.5	An alternate spherical polar coordinate system for scattering calculations. This system uses the y-axis as the polar axis	124
4.6	A block of tissue composed of a homogeneous fat layer and a homogeneous layer of muscle, illuminated by a 915 MHz plane wave	125
4. 7	An inhomogeneous layer of fat, illuminated only in one corner by a 915 MHz plane wave	127

CHAPTER I

INTRODUCTION

In recent years there has been a growing concern over the possible health hazards of nonionizing electromagnetic radiation. A variety of responses to such radiation have been observed in humans and animals. Some of these reactions are caused by an increase in body temperature, while others are triggered directly by the induced electromagnetic field. Before valid safety standards for exposure to nonionizing radiation can be established, the conditions which elicit a particular response must be known. Thus, it is necessary to determine the electric field intensity which produces a nonthermal reaction, and to establish the temperature at which a heat-induced effect occurs. The temperature, however, can be derived from the intensity of the internal electric field. Consequently, valuable insight into both thermal and nonthermal effects can be gained if the induced electric field can be calculated.

The mathematical complexity of the problem is enormous. It is therefore necessary, in a practical theoretical study, to approximate the biological system of interest by a relatively simple model which can be readily analyzed. Some commonly used models are the plane slab [7], [16], the conducting sphere [6], [17], and the dielectric cylinder [4]. However, these models are often grossly oversimplified, and the conclusions drawn from their behavior have only limited validity.

This thesis presents a technique for calculating the electric field induced inside a finite biological body having arbitrary shape and

composition, when the body is irradiated by an electromagnetic wave.

The free-space dyadic Green's function [1] is used to derive an integral equation for the induced electric field; the method of moments is then used to solve the equation numerically. The calculation of the scattered field is also discussed.

A plane slab model of a human trunk is studied in Chapter II. Two methods of calculating the induced field due to a uniform plane wave are presented: (1) solving the system of linear equations generated by the boundary conditions on the electric and magnetic fields, and (2) using transmission line techniques. A number of numerical examples illustrate the behavior of the human trunk model at various frequencies from 100 Hz to 10 GHz.

Chapter III is devoted to calculating the induced field in a finite biological body having arbitrary shape and composition. An integral equation for the induced electric field is derived using the free-space dyadic Green's function. The method of moments is then used to convert the integral equation to a matrix equation for numerical solution. Details for using symmetry to reduce the matrix size, and for calculating the scattered field, are given. The chapter concludes with a variety of examples illustrating the versatility of this numerical technique. Some calculations of the scattered field from saltwater cylinders are compared with experimental data, with good agreement.

Chapter IV contains a description and listing of the computer program used to obtain the numerical results presented in Chapter III.

Instructions for its use, along with some illustrative examples, are also included.

CHAPTER II

INTERACTION OF AN ELECTROMAGNETIC PLANE WAVE WITH A PLANE SLAB MODEL OF A PHYSIOLOGICAL SYSTEM

Since humans and animals have such complicated shapes and structures, an attempt to directly analyze their electromagnetic absorption and scattering properties would be a formidable task. It is therefore necessary to approximate these complex physiological systems by simpler models for which the scattering problem can be readily solved. In this chapter we will discuss the often-used plane slab model, which, in some cases, can provide useful data about heating patterns in the original system.

2.1. Qualitative Description of the Plane Slab Model

A general N-slab system, shown in Figure 2.1, consists of N contiguous plane layers of tissue, each having uniform thickness and infinite cross-section. The tissue composing each layer is linear, homogeneous, and isotropic, although its electrical properties do vary with frequency. We assume that the entire array contains no sources, and that the incoming electromagnetic field is a uniform plane wave, incident normally upon the first slab. The coordinates are defined so that one axis is perpendicular to all of the boundaries in the model. Both of the vacuum regions enclosing the system extend to infinity along this axis, so that no reflected wave exists in the vacuum on the right. Before considering a specific example, we shall discuss two methods of

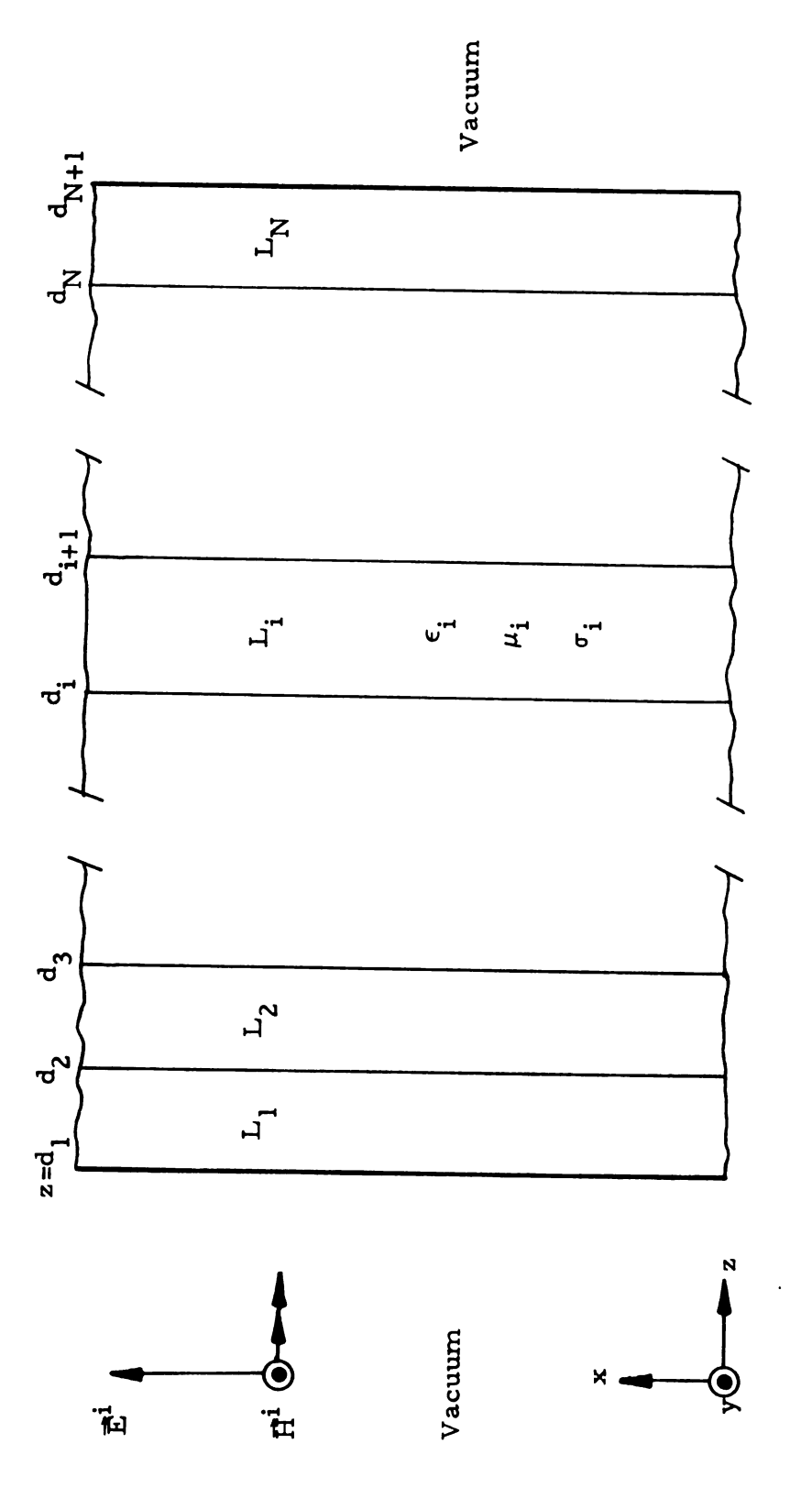


Figure 2.1. An arbitrary N-slab system.

determining the electromagnetic field inside an arbitrary N-slab configuration.

2.2. Maxwell's Equations and Plane Wave Solutions for a General N-Slab System

For a mathematical description of the model, we refer again to Figure 2.1. We have chosen the coordinates so that the z-axis is perpendicular to all of the boundaries in the system. The incident wave impinges on the array from the left, traveling in the +z direction, with the electric field vector linearly polarized along the x-axis. At any point \vec{r} , $\vec{E}(\vec{r})$ denotes the electric field while $\vec{H}(\vec{r})$ represents the magnetic field. The space occupied by the $n^{\frac{th}{L}}$ layer will be indicated by L_n . In the discussion which follows, we can economize on our descriptions by regarding the vacuum regions as additional "layers" of the system; we will refer to the region $z < d_1$ as L_0 , while we denote the region $z > d_{N+1}$ by L_{N+1} . With this notation in mind, let us select a layer at random, say L_1 , and investigate the behavior of the electromagnetic field within it.

As indicated in Figure 2.1, the $i\frac{th}{-}$ layer has permittivity ϵ_i Farad/meter, permeability μ_i Henry/meter, and conductivity σ_i mho/meter. Its input plane is located at $z = d_i$, where " d_0 " is at - ∞ . It will be convenient to represent the electric and magnetic fields inside L_i by $\vec{E}_i(\vec{r})$ and $\vec{H}_i(\vec{r})$, respectively. Thus, for $\vec{r} \in L_i$,

$$\vec{\mathbf{E}}(\vec{\mathbf{r}}) = \vec{\mathbf{E}}_{\mathbf{i}}(\vec{\mathbf{r}}) \tag{2.2.1a}$$

$$\vec{\mathbf{H}}(\vec{\mathbf{r}}) = \vec{\mathbf{H}}_{\mathbf{i}}(\vec{\mathbf{r}})$$

$$\mathbf{i} = 0, 1, \dots, N+1.$$
(2.2.1b)

We assume a harmonic time variation of $e^{j\omega t}$, which we shall henceforth suppress. Since each layer is linear, homogeneous, isotropic, and source-free, Maxwell's equations for L_i are

$$\nabla \times \vec{E}_{i}(\vec{r}) = -j\omega \mu_{i} \vec{H}_{i}(\vec{r}) \qquad (2.2.2a)$$

$$\nabla \times \vec{\mathbf{H}}_{i}(\vec{\mathbf{r}}) = (\sigma_{i} + j\omega \epsilon_{i}) \vec{\mathbf{E}}_{i}(\vec{\mathbf{r}})$$
 (2.2.2b)

$$\nabla \cdot \vec{E}_i(\vec{r}) = 0 \tag{2.2.2c}$$

$$\nabla \cdot \vec{\mathbf{H}}_{\mathbf{i}}(\vec{\mathbf{r}}) = 0 \tag{2.2.2d}$$

$$i = 0, 1, ..., N+1.$$

Maxwell's equations may be combined in the usual manner to obtain the vector Helmholtz equation for $\vec{E}_i(\vec{r})$:

$$\nabla^2 \vec{E}_i(\vec{r}) + k_i^2 \vec{E}_i(\vec{r}) = 0$$
 (2.2.3a)

where
$$k_i^2 = \omega^2 \mu_i \epsilon_i - j\omega \mu_i \sigma_i$$
 (2.2.3b)
 $i = 0, 1, ..., N+1.$

Since the incoming uniform plane wave is incident normally on the first slab, we expect to obtain uniform plane waves in each layer of the Therefore, we anticipate a solution to Equation (2.2.3a) of the form

$$\vec{E}_{i}(\vec{r}) = \vec{E}_{i}(z) = x(A_{i}e^{-jk_{i}z} + B_{i}e^{jk_{i}z})$$

$$i = 0, 1, \dots, N+1$$

$$(2.2.4)$$

where A_i and B_i are complex constants, as yet undetermined. A_i specifies the amplitude and phase of a wave traveling in the +z direction, while B; gives the amplitude and phase of a wave moving in the -z direction. A_{Ω} represents the incident wave, and is known in advance. Also, since our model precludes any reflections in L_{N+1} , we must take $B_{N+1} = 0$.

From Equation (2.2.2a), $\vec{H}_i(\vec{r})$ is given by

$$\vec{H}_{i}(\vec{r}) = \frac{j}{\omega \mu_{i}} [\nabla \times \vec{E}_{i}(\vec{r})] . \qquad (2.2.5a)$$

Substituting Equation (2.2.4) in Equation (2.2.5a) yields

$$\vec{H}_{i}(\vec{r}) = \vec{H}_{i}(z) = \sqrt[A]{\frac{(A_{i}e^{-jk_{i}z} - B_{i}e^{jk_{i}z})}{\zeta_{i}}}$$

$$i = 0, 1, ..., N+1$$
(2.2.5b)

where ζ_i denotes the characteristic wave impedance of L_i , and is given by

$$\zeta_{i} = \frac{\omega \mu_{i}}{k_{i}} = \sqrt{\frac{\mu_{i}}{\epsilon_{i} - j(\sigma_{i}/\omega)}}$$
 $i = 0, 1, ..., N+1.$ (2.2.5c)

Let
$$k_i = \beta_i - ja_i$$
.

Then, using Equation (2.2.3b), we obtain

$$\beta_{i} = \operatorname{Re}(k_{i}) = \omega \left[\frac{\mu_{i} \epsilon_{i}}{2} \left(\sqrt{1 + \left(\frac{\sigma_{i}}{\omega \epsilon_{i}} \right)^{2} + 1} \right) \right]^{1/2}. \tag{2.2.7a}$$

 β_i is the wave number in the $i^{\frac{th}{2}}$ layer; it is also defined by

$$\beta_{i} = \frac{2\pi}{\lambda_{i}} \tag{2.2.7b}$$

where λ_i is the wavelength in L_i . α_i represents the attenuation constant in L_i , and it is given by

$$a_i = -\operatorname{Im}(k_i) = \omega \left[\frac{\mu_i \epsilon_i}{2} \left(\sqrt{1 + \left(\frac{\sigma_i}{\omega \epsilon_i} \right)^2} - 1 \right) \right]^{1/2}$$
 (2.2.8)

2.3. Boundary Conditions

To completely specify the electromagnetic field in the $i \stackrel{th}{=} slab$, we must determine the constants A_i and B_i in Equations (2.2.4) and (2.2.5b). We can do so by imposing boundary conditions on $\vec{E}(\vec{r})$ and $\vec{H}(\vec{r})$. Electromagnetic theory tells us that the component of $\vec{E}(\vec{r})$ and the component of $\vec{H}(\vec{r})$ which is tangent to an interface between disparate media must be continuous there. A reference to Figure 2.1 and to Equations (2.2.4) and (2.2.5b) shows that both $\vec{E}(\vec{r})$ and $\vec{H}(\vec{r})$ are tangent to all boundaries in our model. Therefore, the boundary conditions imply

that $\vec{E}(\vec{r})$ and $\vec{H}(\vec{r})$ must be continuous throughout the system. We may use Equation (2.2.4) to express the continuity of the electric field at $z = d_n$ by

$$(A_{n-1}e^{-jk_{n-1}d_n} + B_{n-1}e^{jk_{n-1}d_n}) = (A_ne^{-jk_nd_n} + B_ne^{jk_nd_n})$$
 (2.3.1)

From Equation (2.2.5b), we obtain the expression for the continuity of the magnetic field:

$$\frac{(A_{n-1}e^{-jk_{n-1}d_n} - B_{n-1}e^{jk_{n-1}d_n})}{\zeta_{n-1}} = \frac{(A_ne^{-jk_nd_n} - B_ne^{jk_nd_n})}{\zeta_n}$$
 (2.3.2)

These relationships are illustrated in Figure 2.2. For convenience, we shall take $d_1 = 0$ with no loss of generality.

2.4. Matrix Representation of Boundary Conditions

As the index n of the previous section assumes all possible values, Equations (2.3.1) and (2.3.2) generate a set of 2N + 2 simultaneous linear equations relating the unknown A's and B's. This algebraic system has a solution if the A's and B's also number 2N + 2.

The N tissue layers contribute 2N unknowns, since there are two for each slab. In addition, we must evaluate B_0 and A_{N+1} . A_0 and B_{N+1} , of course, have already been specified. The system of equations therefore contains 2N+2 unknowns, enabling us to solve it.

We define the following column vectors:

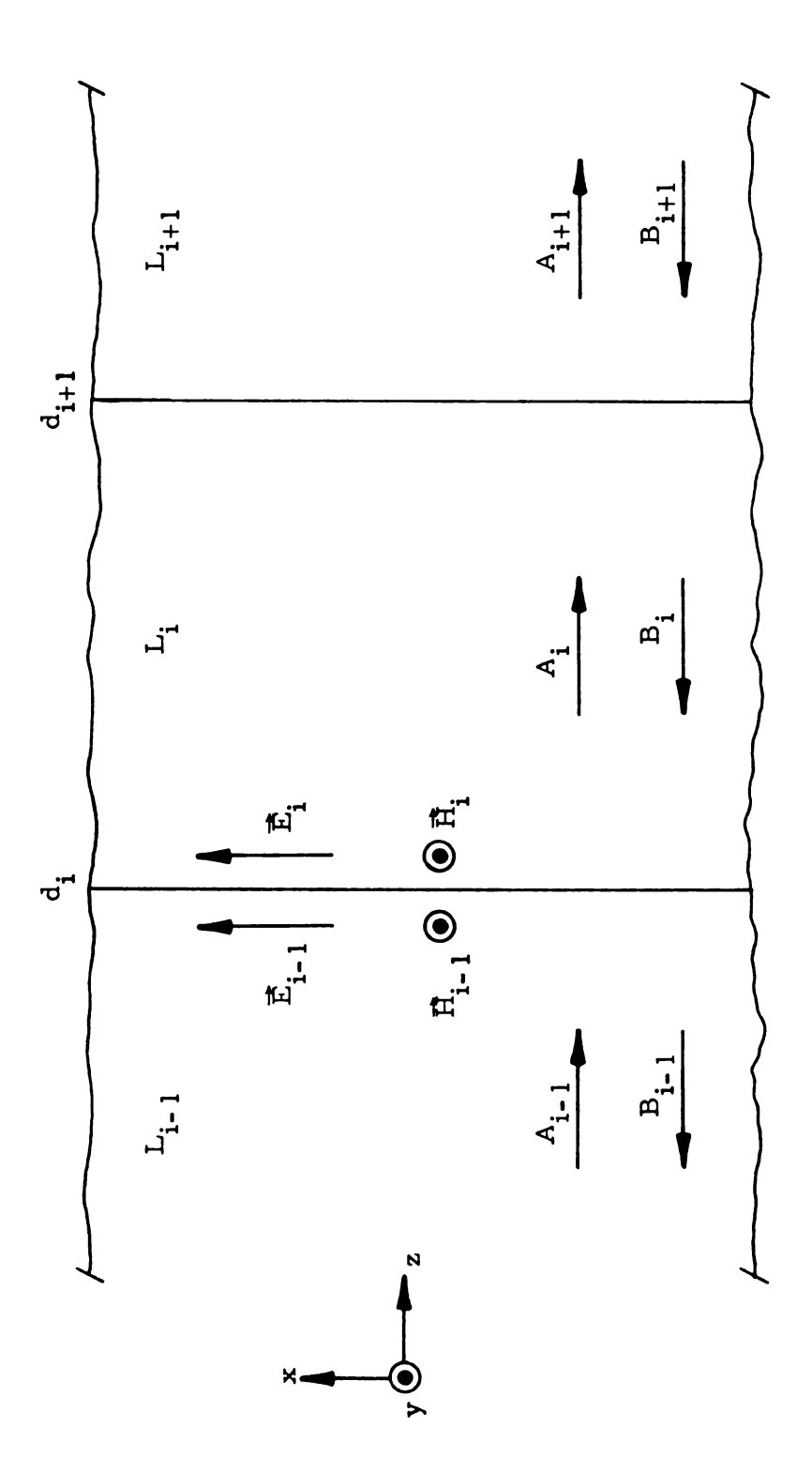


Figure 2.2. Boundary condition solution of N-slab system.

$$\psi = \begin{bmatrix}
B_{0} \\
A_{1} \\
B_{1} \\
A_{2} \\
\vdots \\
B_{N-1} \\
A_{N} \\
B_{N} \\
A_{N+1}
\end{bmatrix} (2.4.1a) \qquad \psi_{0} = A_{0} \begin{bmatrix}
1 \\
1 \\
0 \\
0 \\
0 \\
\vdots \\
0 \\
0 \\
0
\end{bmatrix} (2.4.1b)$$

The system of 2N + 2 linear equations may then be cast into the form

$$[C]\psi = \psi_{O} \tag{2.4.2}$$

where [C] is the $(2N + 2) \times (2N + 2)$ matrix shown on page 11.

The vector ψ may be written as

$$\psi = [C]^{-1} \psi_{0}. \tag{2.4.3}$$

After the A's and B's have been evaluated, the electromagnetic field in L_i can be found by using Equations (2.2.4) and (2.2.5b)

2.5. Solution by Transmission Line Analogy

Equation (2.4.2) will be solved by a computer in most cases. Since the boundary conditions relate the coefficients in adjacent layers only, most of the elements of [C] are zero. Thus, particularly if N is large, considerable computer storage will be wasted, making the matrix method uneconomical to use. We can calculate the coefficients in Equations (2.2.4) and (2.2.5b) a different way, by exploiting the similarities between our slab model and a uniform transmission line [12].

The pertinent quantities are shown in Figure 2.3. As before, the input plane of L_i is located at $z = d_i$. The input impedance to L_i is denoted by Z_{in}^i . Clearly, Z_{in}^i is the "load" impedance for L_{i-1} . At

	<i>-</i>						
0	ο.			0	0	-jk _o d _{N+1}	-jkodn+1
0	0			j ^k N ^d n	j ^k n ^d n e ⁵ n	j ^k N ^d N+1	$\int_{0}^{jk} N^{d}N+1$
		0	0		$-\frac{\mathrm{jk_N}\mathrm{d_N}}{\xi_N}$	-j ^k n ^d n+1	-jk _N d _{N+1}
		jk ₂ d ₂ - e	jk2d2 e		$\frac{\mathrm{jk_{N-1}d_{N}}}{\xi_{N-1}}$	0	0
0	0	-jk2 ^d 2	$-jk_2d_2$ $\frac{-jk_2d_2}{\xi_2}$		-j ^k N-1 ^d N		
1	-50/51	jk ₁ d ₂	jk ₁ d ₂	0	0		
1	ξ ₀ /ξ ₁	-jk ₁ d ₂	-jk ₁ d ₂			0	0
	-	0	0		• •	. 0	· · · · · · · · · · · · · · · · · · ·

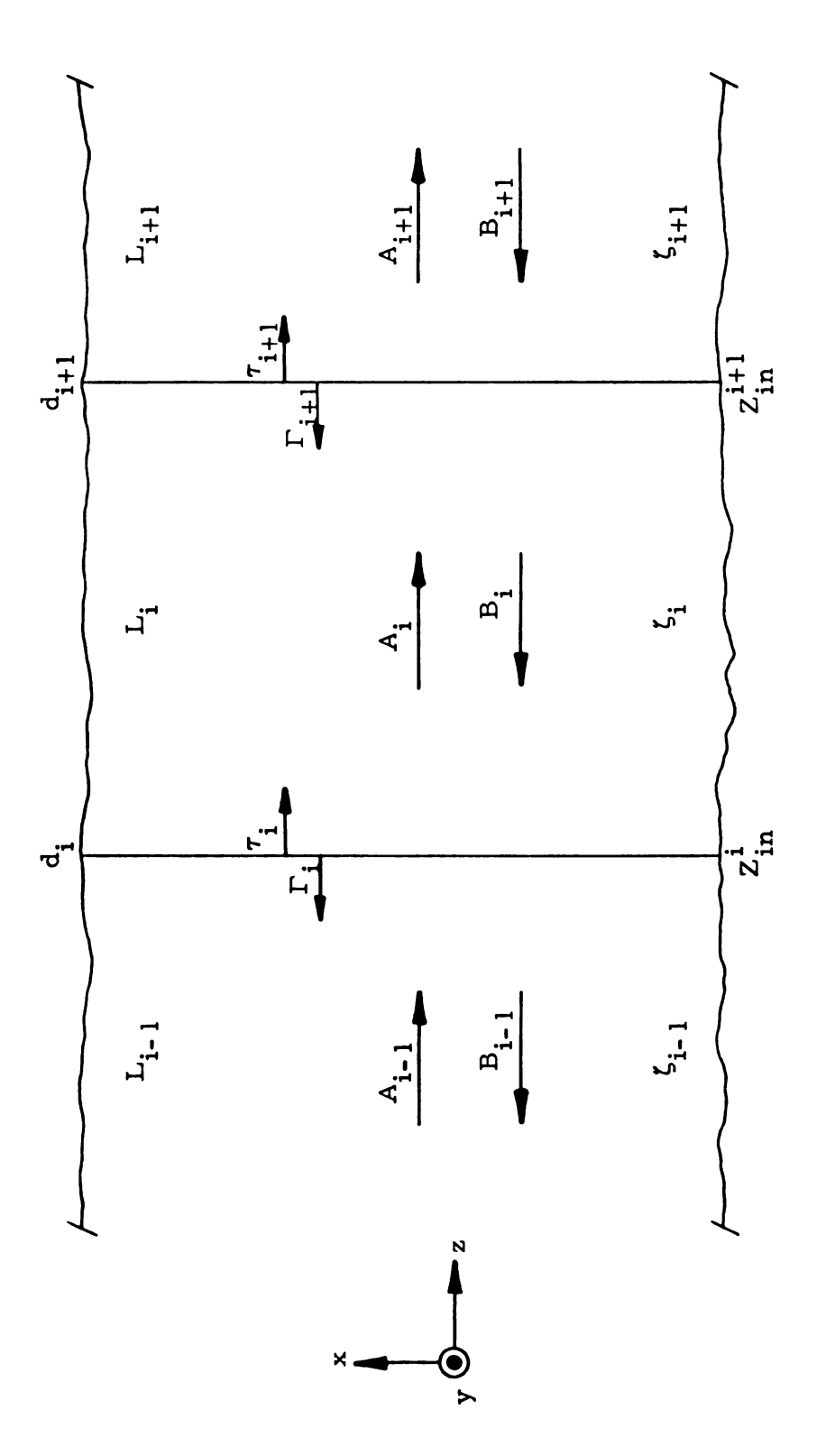


Figure 2.3. Transmission line solution of N-slab system.

the boundary $z = d_i$, we define a reflection coefficient Γ_i and a transmission coefficient τ_i :

$$\Gamma_{\mathbf{i}} = \frac{B_{\mathbf{i}-1}}{A_{\mathbf{i}-1}} \tag{2.5.1a}$$

$$\tau_{i} = \frac{A_{i}}{A_{i-1}}$$
 $i = 1, ..., N+1$. (2.5.1b)

We will derive expressions for Γ_i and τ_i by using the boundary conditions on $\vec{E}(\vec{r})$ and $\vec{H}(\vec{r})$ at $z = d_i$, and by using the definition of impedance.

The impedance $Z_{i}(z)$ in L_{i} is given by

$$Z_{i}(z) \equiv \frac{E_{ix}(z)}{H_{iy}(z)} = \zeta_{i} \frac{\left[A_{i}e^{-jk_{i}z} + B_{i}e^{jk_{i}z}\right]}{\left[A_{i}e^{-jk_{i}z} - B_{i}e^{-jk_{i}z}\right]}$$
(2.5.2)

where ζ_i is the characteristic impedance of L_i , given by Equation (2.2.5c).

Thus, Zin may be written as

$$Z_{in}^{i} \equiv Z_{i}(z=d_{i}) = \zeta_{i} \frac{[A_{i}e^{-jk_{i}d_{i}} + B_{i}e^{jk_{i}d_{i}}]}{[A_{i}e^{-jk_{i}d_{i}} - B_{i}e^{jk_{i}d_{i}}]}$$
 (2.5.3a)

01

$$Z_{in}^{i} = \zeta_{i} \frac{\left[1 + \Gamma_{i+1} e^{j2k_{i}d_{i}}\right]}{\left[1 - \Gamma_{i+1} e^{j2k_{i}d_{i}}\right]}$$
(2.5.3b)

The boundary conditions at $z = d_i$ are

$$A_{i-1} e^{-jk_{i-1}d_i} + B_{i-1} e^{jk_{i-1}d_i} = A_i e^{-jk_i d_i} + B_i e^{jk_i d_i}$$
(2.5.4a)

$$\frac{A_{i-1}e^{-jk_{i-1}d_{i}} - B_{i-1}e^{jk_{i-1}d_{i}}}{\zeta_{i-1}} = \frac{A_{i}e^{-jk_{i}d_{i}} - B_{i}e^{jk_{i}d_{i}}}{\zeta_{i}}$$
(2.5.4b)

By using the relationship expressed in Equation (2.5.3a), we rewrite Equation (2.5.4b) as

$$\frac{A_{i-1} e^{-jk_{i-1}d_i} - B_{i-1} e^{jk_{i-1}d_i}}{\zeta_{i-1}} = \frac{A_i e^{-jk_i d_i} + B_i e^{jk_i d_i}}{Z_{in}^i}$$
(2.5.5)

Substituting Equation (2.5.4a) into Equation (2.5.5) and dividing by A_{i-1} yields

$$\frac{e^{-jk_{i-1}d_{i}} - \Gamma_{i}e^{jk_{i-1}d_{i}}}{\zeta_{i-1}} = \frac{e^{-jk_{i-1}d_{i}} + \Gamma_{i}e^{jk_{i-1}d_{i}}}{Z_{in}^{i}}$$
(2.5.6)

We can readily solve Equation (2.5.6) for Γ_i :

$$\Gamma_{i} = \frac{(Z_{in}^{i} - \zeta_{i-1})}{(Z_{in}^{i} + \zeta_{i-1})} e^{-j2k_{i-1}d_{i}}$$

$$i = 1, ..., N+1.$$
(2.5.7)

We may rewrite Equation (2.5.4a) as

$$A_{i-1}[e^{-jk_{i-1}d_i} + \Gamma_i e^{jk_{i-1}d_i}] = A_i[e^{-jk_id_i} + \Gamma_{i+1} e^{jk_id_i}]$$
 (2.5.8)

Hence, τ_i is given by

$$\tau_{i} = \frac{\left[e^{-jk_{i-1}d_{i}} + \Gamma_{i}e^{jk_{i-1}d_{i}}\right]}{\left[e^{-jk_{i}d_{i}} + \Gamma_{i+1}e^{jk_{i}d_{i}}\right]}$$
(2.5.9a)

By substituting Equation (2.5.7) into Equation (2.5.9a), we obtain

$$\tau_{i} = \frac{2 Z_{in}^{i}}{Z_{in}^{i} + \zeta_{i-1}} \frac{e^{j(k_{i}^{-}k_{i-1})d_{i}}}{[1 + \Gamma_{i+1}e^{j2k_{i}d_{i}}]}$$
(2.5.9b)

By examining Equations (2.5.3b), (2.5.7), and (2.5.9b), we see that we can determine Z_{in}^{i} , Γ_{i} , and τ_{i} if we know Γ_{i+1} . Our procedure is motivated by this observation.

Since $B_{N+1} = 0$, it follows that $\Gamma_{N+2} = 0$. Thus, from Equation (2.5.3b), Z_{in}^{N+1} is simply ζ_0 , the characteristic impedance of free space. Using Equations (2.2.5c), (2.5.7), and (2.5.9b), we calculate Γ_{N+1} and τ_{N+1} . We then repeat the procedure, evaluating Z_N , Γ_N , τ_N , Z_{N-1} , and so on, until Γ and τ have been determined at each boundary. Next, we calculate the coefficients, using Equations (2.5.1a) and (2.5.1b):

$$B_0 = \Gamma_1 A_0$$
 (2.5.10a)

$$A_1 = \tau_1 A_0$$
 (2.5.10b)

$$B_1 = \Gamma_2 A_1 = \Gamma_2 \tau_1 A_0 \qquad (2.5.10c)$$

$$A_2 = \tau_2 A_1 = \tau_2 \tau_1 A_0$$
, (2.5.10d)

and so forth. In general, A; and B; are given by

$$A_i = \tau_i \tau_{i-1} \tau_{i-2} \dots \tau_2 \tau_1 A_0$$
 (2.5.11a)

$$B_{i} = \Gamma_{i+1} \tau_{i} \tau_{i-1} \dots \tau_{2} \tau_{1} A_{0}$$
 (2.5.11b)

Finally, we use Equations (2.2.4) and (2.2.5b) to determine the electromagnetic field in L_i .

2.6. Numerical Results for a Plane Slab Model of the Human Trunk

The model depicted in Figure 2.4 was chosen to represent a human trunk. The system is 19.9 cm thick, and comprises 7 layers: two layers of skin, each 0.2 cm thick; two layers of fat, each 3.0 cm thick; two layers of muscle, each 5.0 cm thick; and a layer of bone, 3.5 cm thick.

Table 2.1 lists the electrical properties of each type of tissue at various frequencies from 100 Hz to 10 GHz. Since physiological tissues are essentially nonmagnetic, it has been assumed that $\mu_{\hat{1}} = \mu_{\hat{0}}$ in each slab.

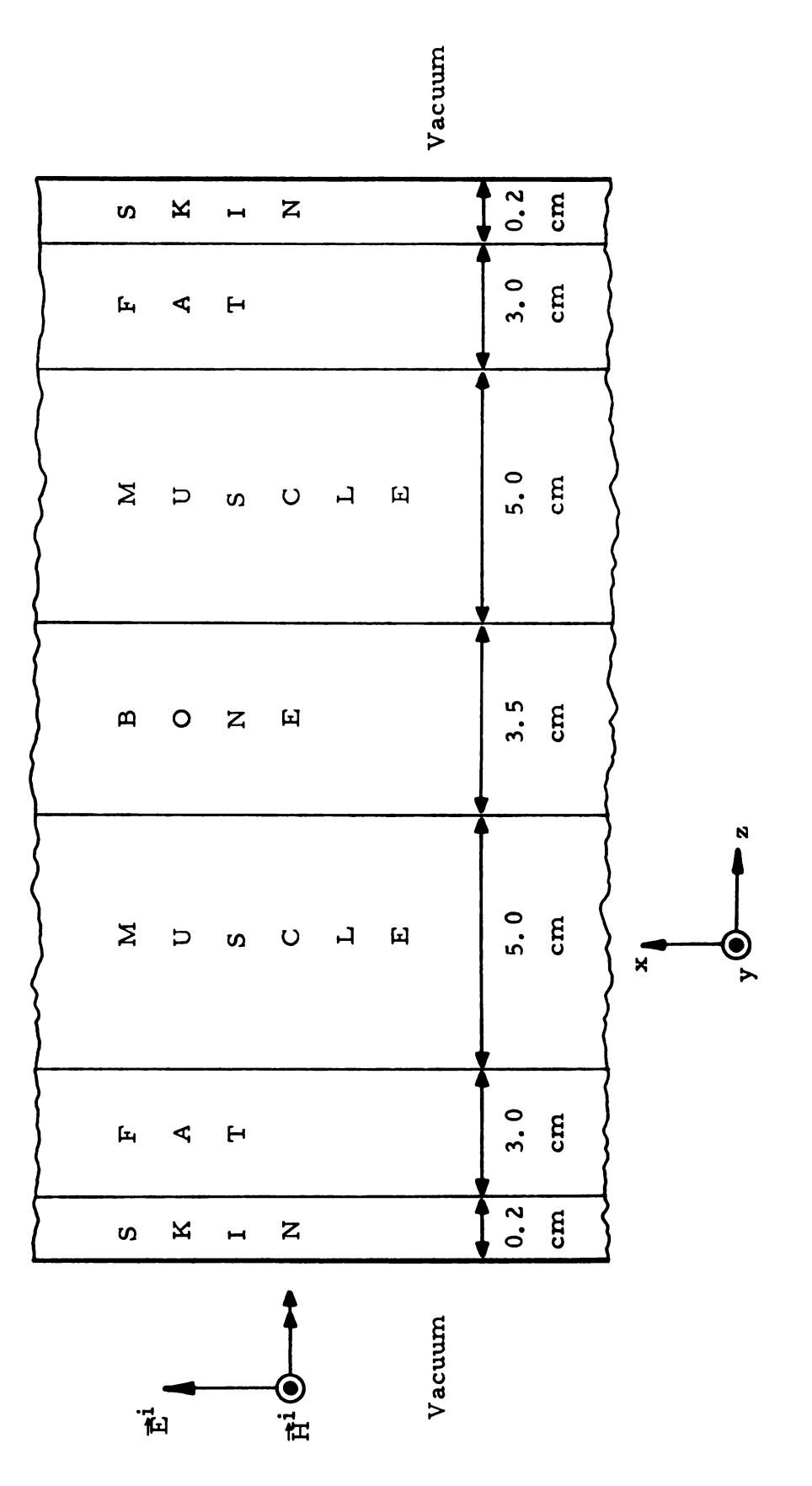


Figure 2. 4. 7-slab model used for calculations.

Frequency	Muscle,	Skin	Fat,	Bone
(Hz)	$\epsilon/\epsilon_{ m o}$	σ(mho/m)	$\epsilon/\epsilon_{_{ m O}}$	σ(mho/m)
10 ²	1,438,039	0.2	71,902	0.04
10 ³	539,265	0.2	21,571	0.04
10 ⁶	2,000.0	0.4	200.0	0.043
107	160.0	0.625	40.0	0.045
108	71.7	0.889	7.45	0.048
3×10^8	54.0	1.37	5.7	0. 069
6 x 10 ⁸	52.47	1.49	5.6	0. 086
9 x 10 ⁸	51.09	1.59	5.6	0. 101
1.5 x 10 ⁹	49.0	1.77	5.6	0. 121
2.45 x 10 ⁹	47.0	2.21	5.5	0. 155
5 x 10 ⁹	44.0	3.92	5.5	0.236
10 ¹⁰	39.9	10.3	4.5	0.437

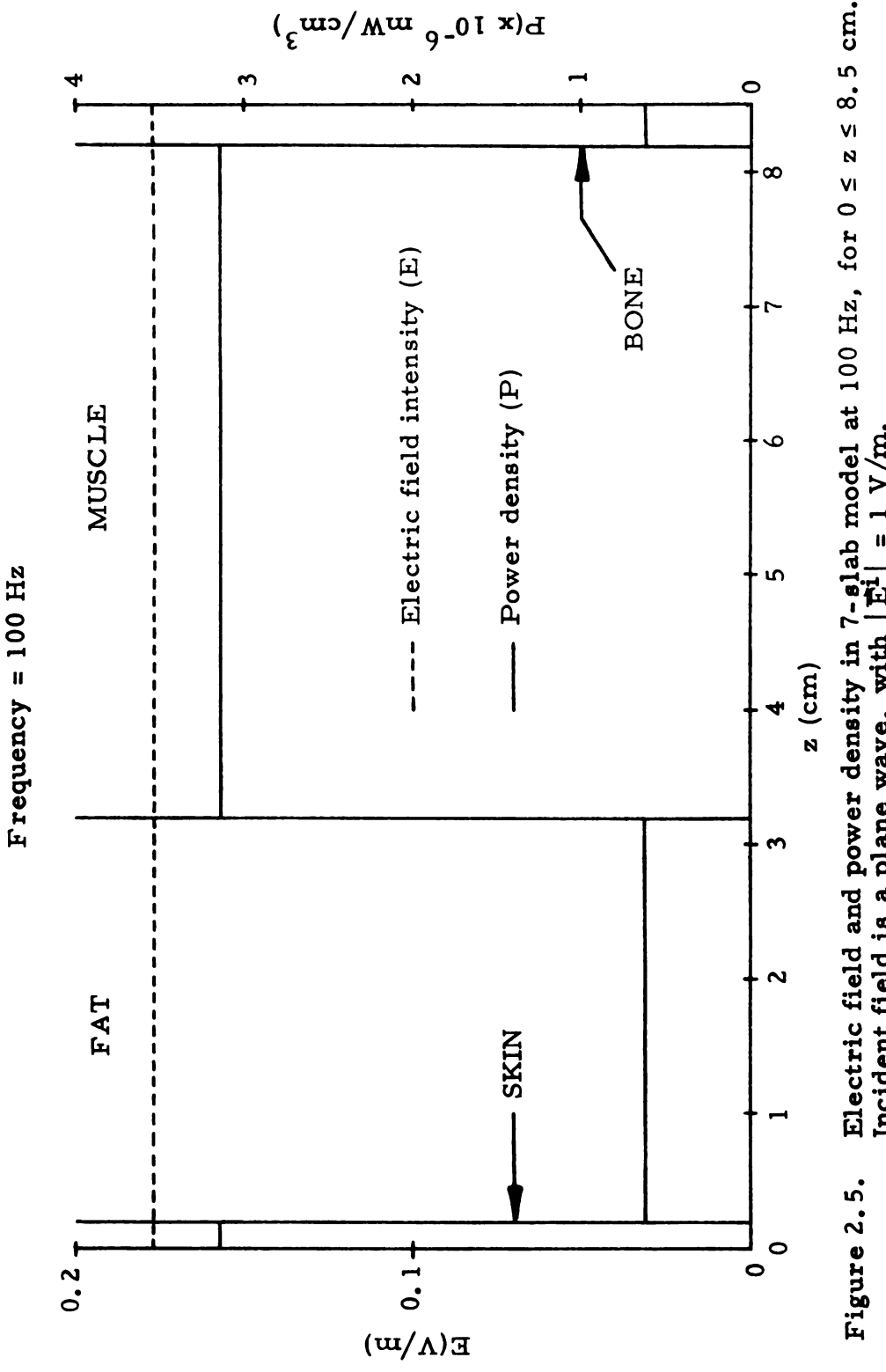
Table 2.1. Frequency Dependence of Conductivity and Relative Permittivity for Muscle, Skin, Fat, and Bone.

The electric field intensity E and the power density P have been calculated in each layer of the system at each of the frequencies given in Table 2.1, and the results are shown in Figures 2.5 through 2.16. Ao has been taken to be 1. The distributions of E and P at each frequency are plotted only for $0 \le z \le 8.5$ cm, as explained below.

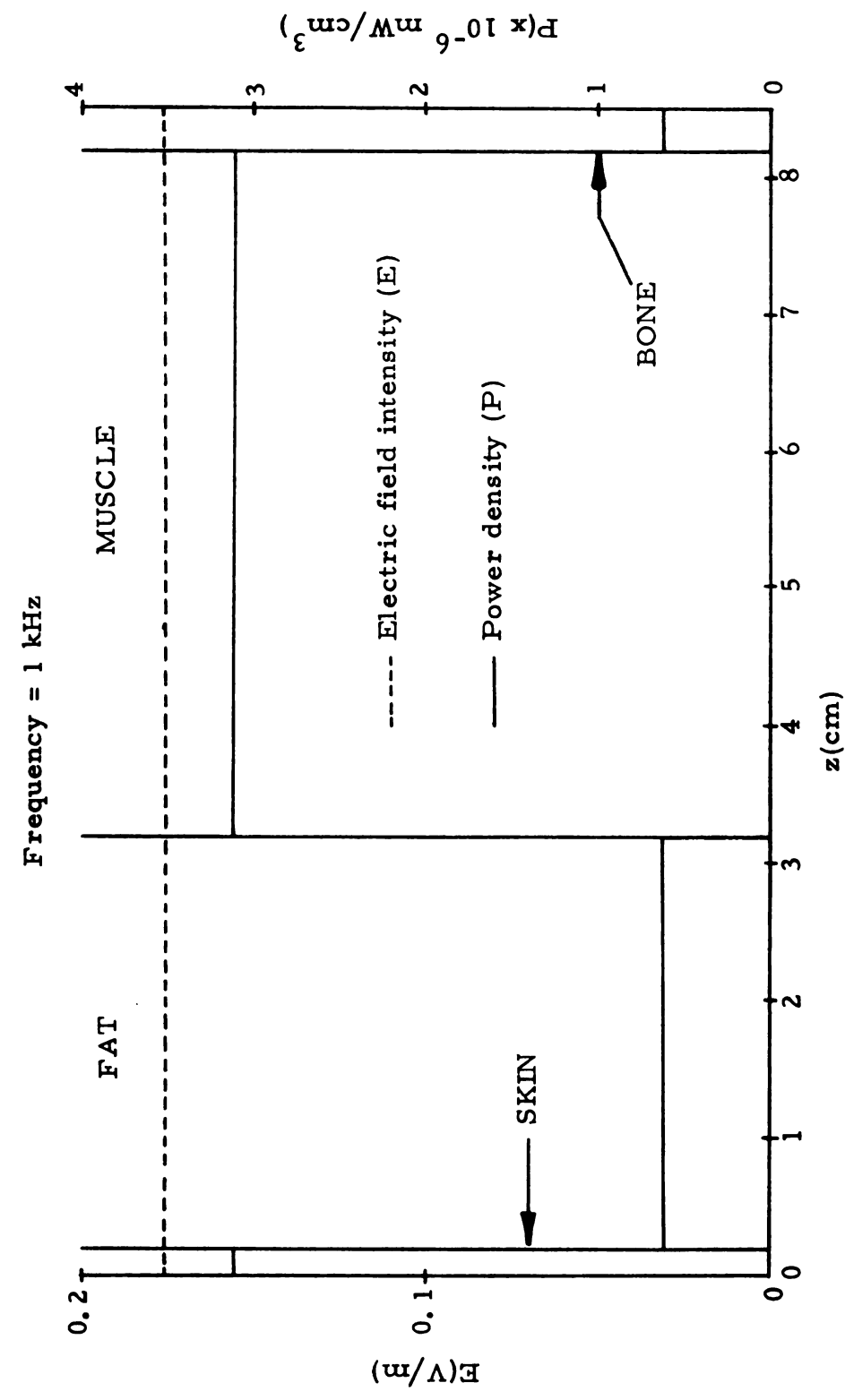
At low frequencies, up to about 10 MHz, the electric field is nearly constant throughout the entire model. Therefore, the power density in the second half of the system is merely a mirror image of that in the first half. At higher frequencies (100 MHz and above), the power density is nearly zero beyond the first muscle layer; hence, the latter portions of the system are of little interest.

As noted before, the electric field is nearly constant throughout the system for frequencies up to 10 MHz. The heating of each layer is therefore uniform, with the skin and muscle layers heated the most.

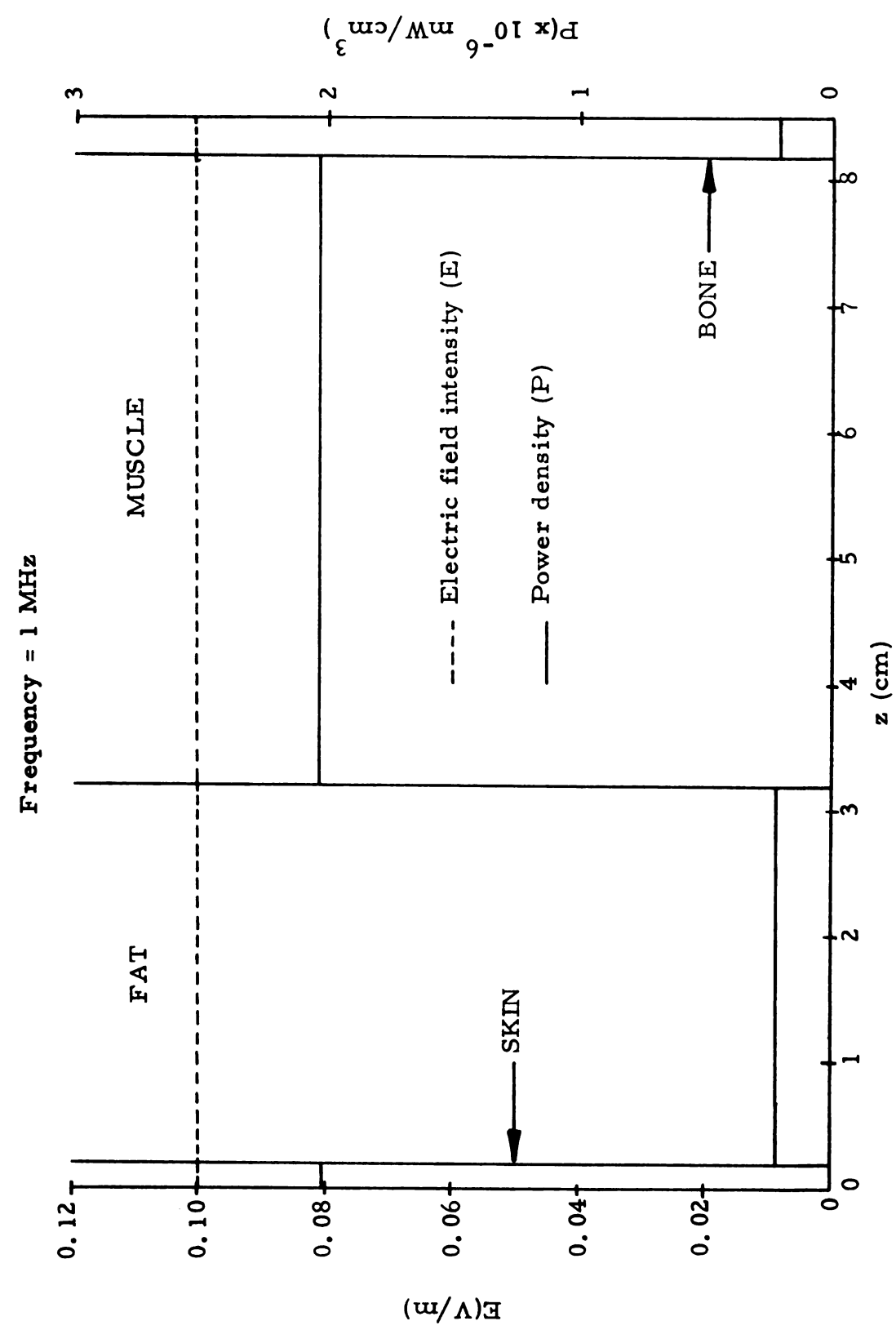
We also note that E and P are generally larger at frequencies above 100 MHz than they are at lower frequencies. The maximum value of E occurs in the skin layer at 600 MHz. At 600 MHz and above, the ratio of the power density in the skin to that in the muscle becomes large. Thus, most of the power in the incident wave is dissipated in the skin layer; relatively little penetrates to deeper layers of tissue. Based on this model, the use of high frequencies for diathermy is questionable, since little heating would occur deep in the body. Indeed, a patient would suffer severe burns on the skin before he would experience any significant heating of internal structures. Of course, this model does not take into account the cooling effects of perspiration and circulation of the blood. In addition, the accuracy with which the system of Figure 2.4 represents an actual human trunk is questionable.



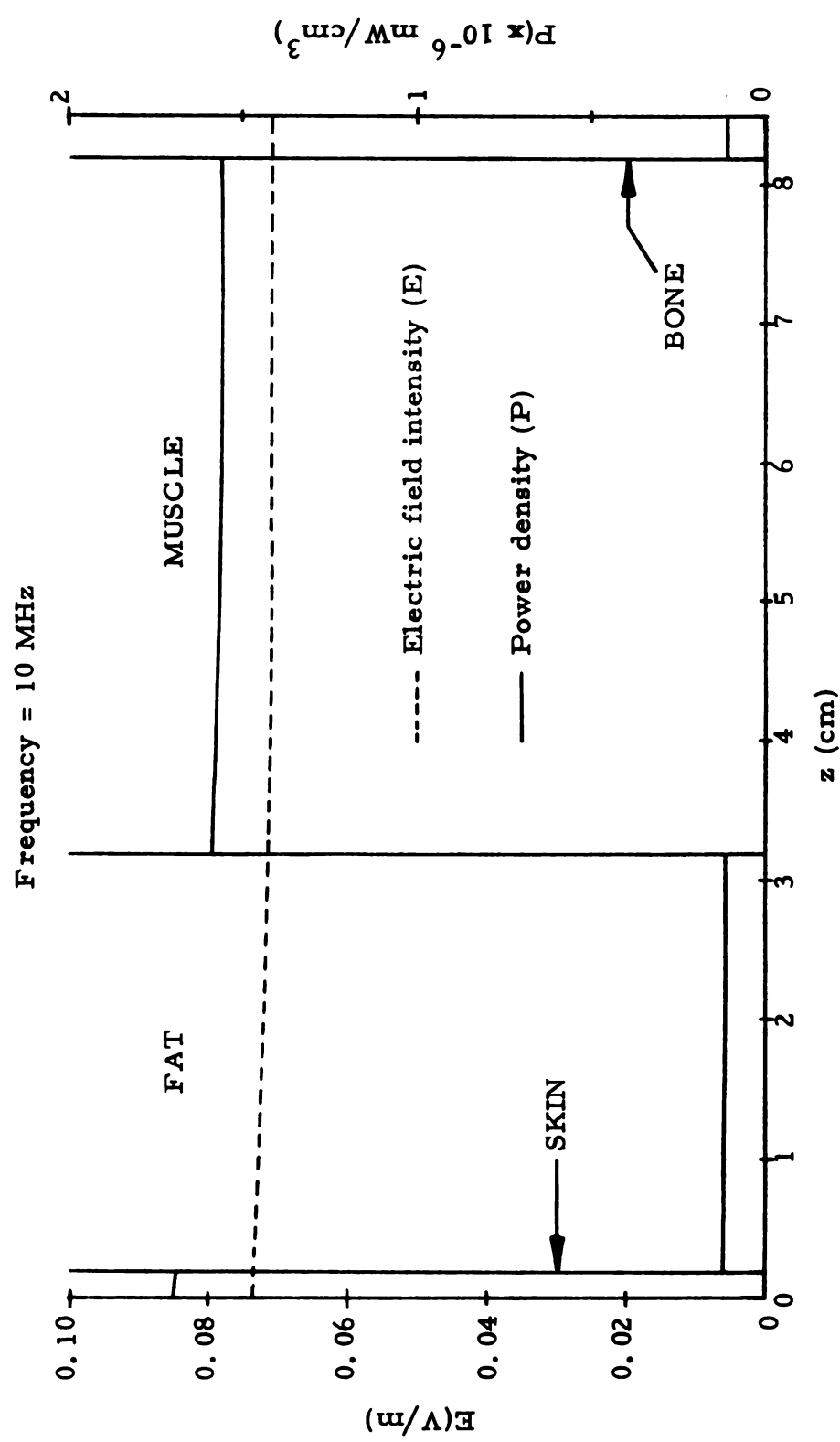
Electric field and power density in 7-slab model at $100~{\rm Hz}$, for $0 \le z \le 8.5~{\rm cm}$. Incident field is a plane wave, with $|\vec{E}^i|=1~{\rm V/m}$.



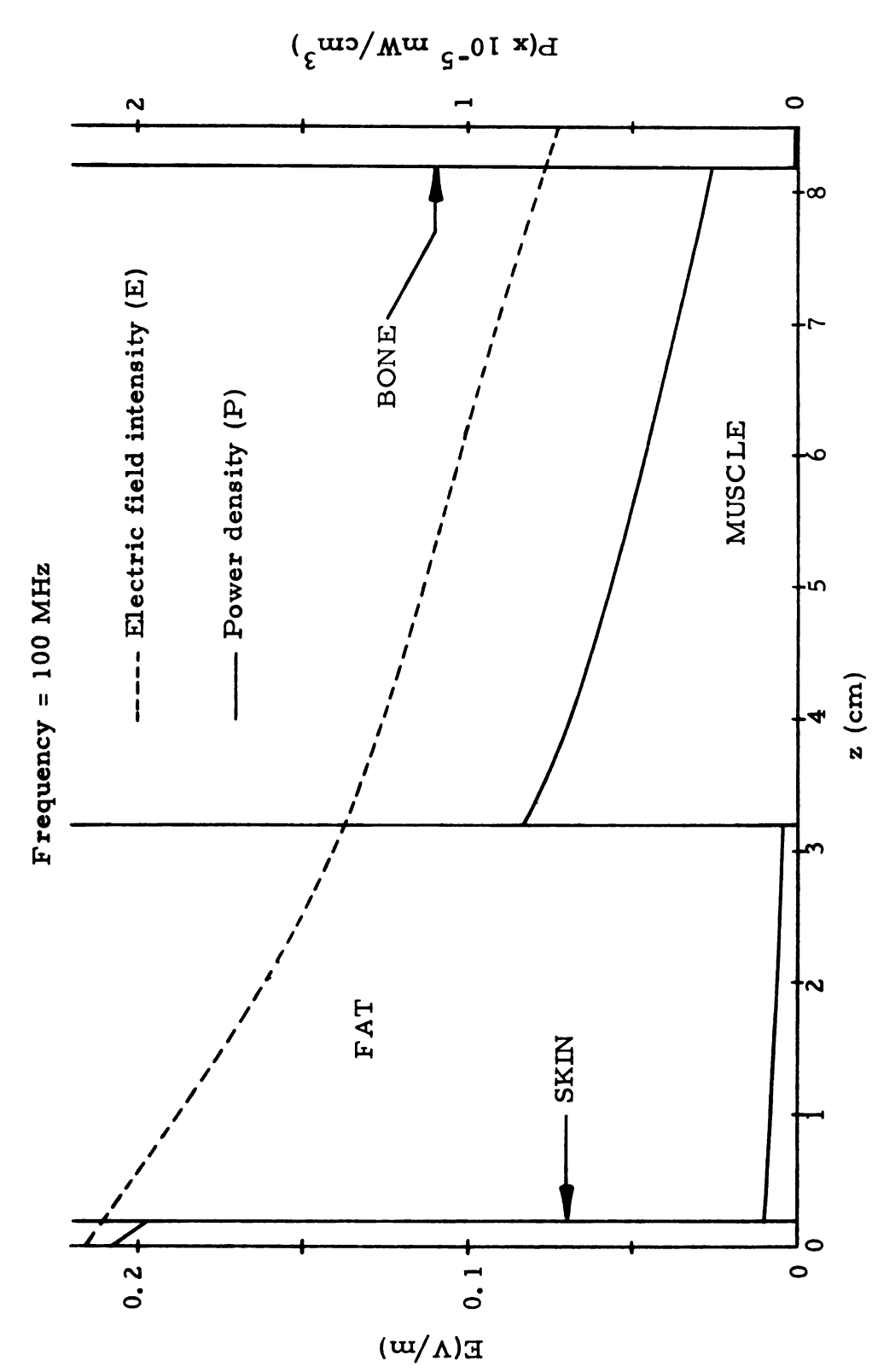
Electric field and power density in 7-slab model at 1 kHz, for $0 \le z \le 8.5$ cm. Incident field is a plane wave, with $|\vec{E}^i|=1$ V/m. Figure 2.6.



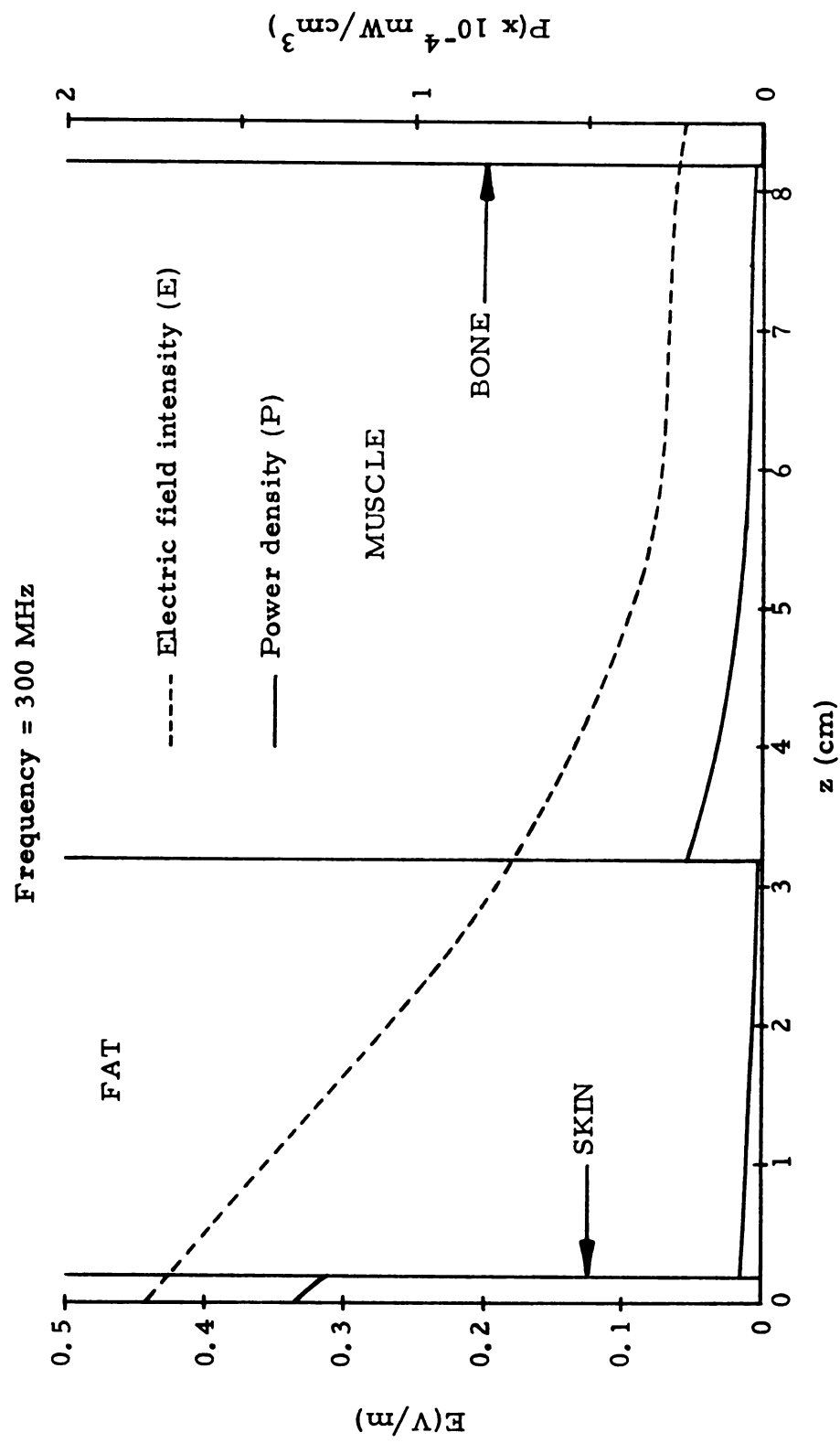
Electric field and power density in 7-slab model at 1 MHz, for $0 \le z \le 8.5$ cm. Incident field is a plane wave, with $|\vec{E}^i| = 1 \text{ V/m}$. Figure 2.7.



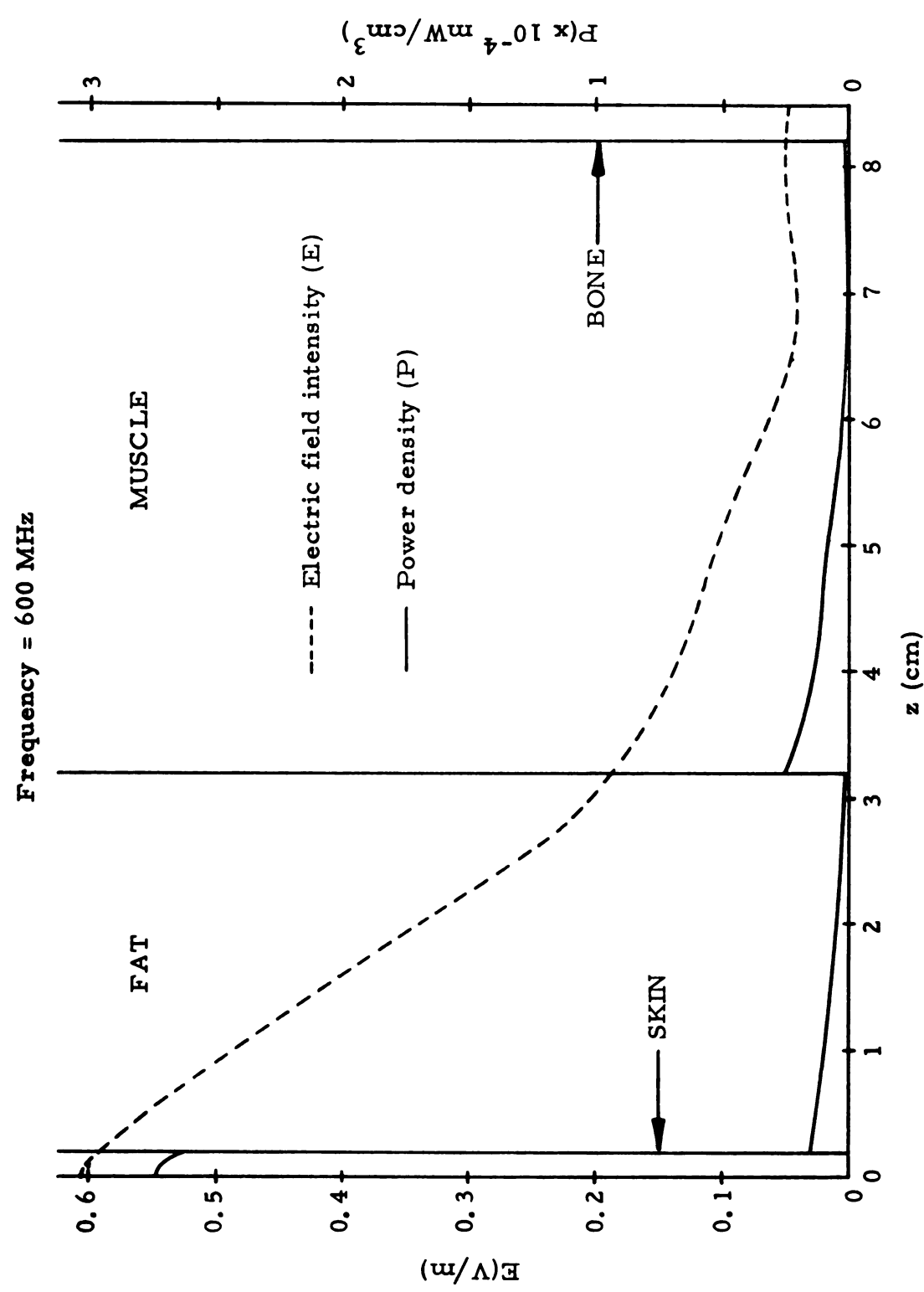
Electric field and power density in 7-slab model at 10 MHz, for $0 \le z \le 8.5$ cm. Incident field is a plane wave, with $|\vec{E}^i| = 1 \text{ V/m}$. Figure 2.8.



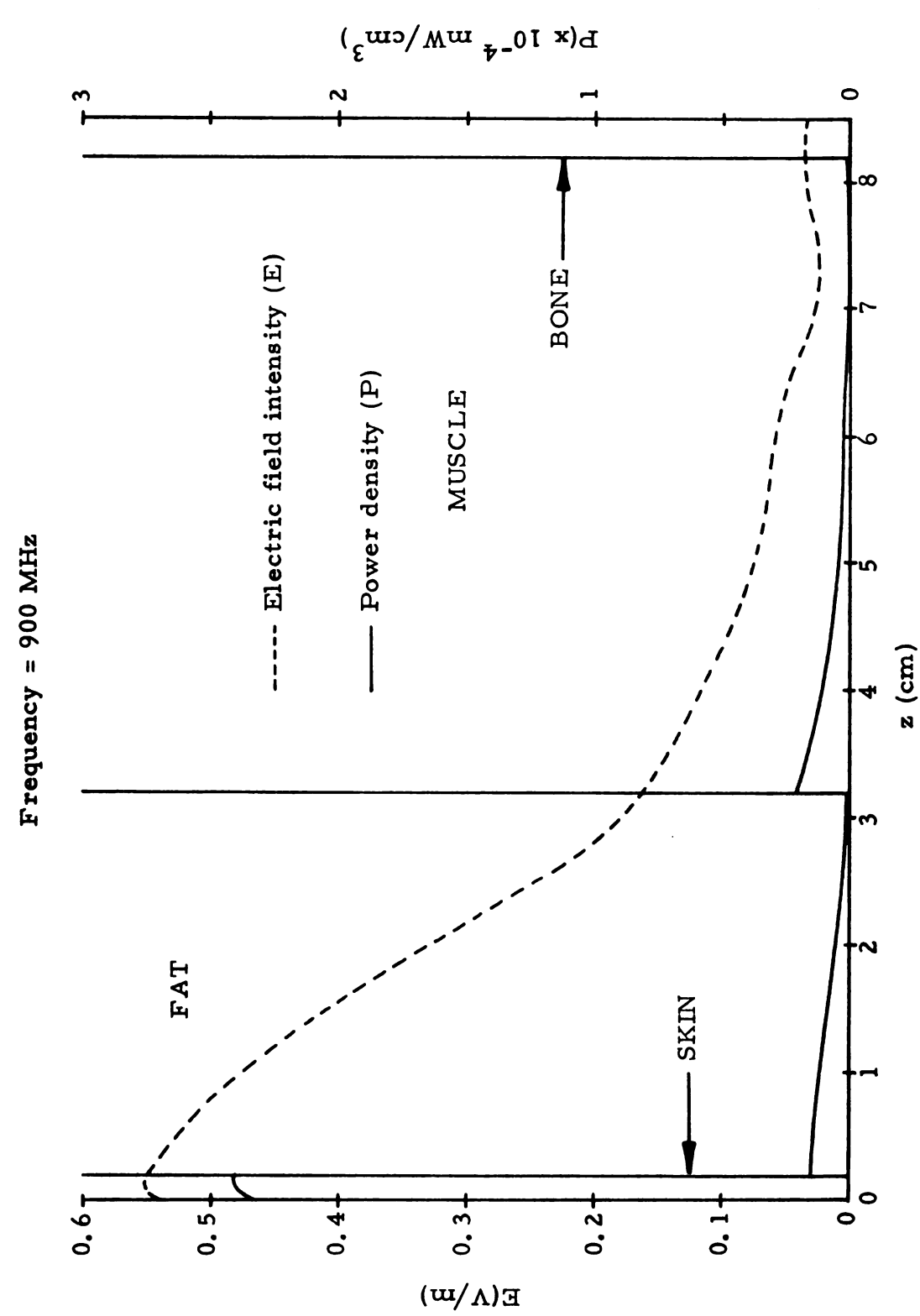
Electric field and power density in 7-slab model at 100 MHz, for $0 \le z \le 8.5$ cm. Incident field is a plane wave, with $|\vec{E}^i| = 1 \text{ V/m}$. Figure 2.9.



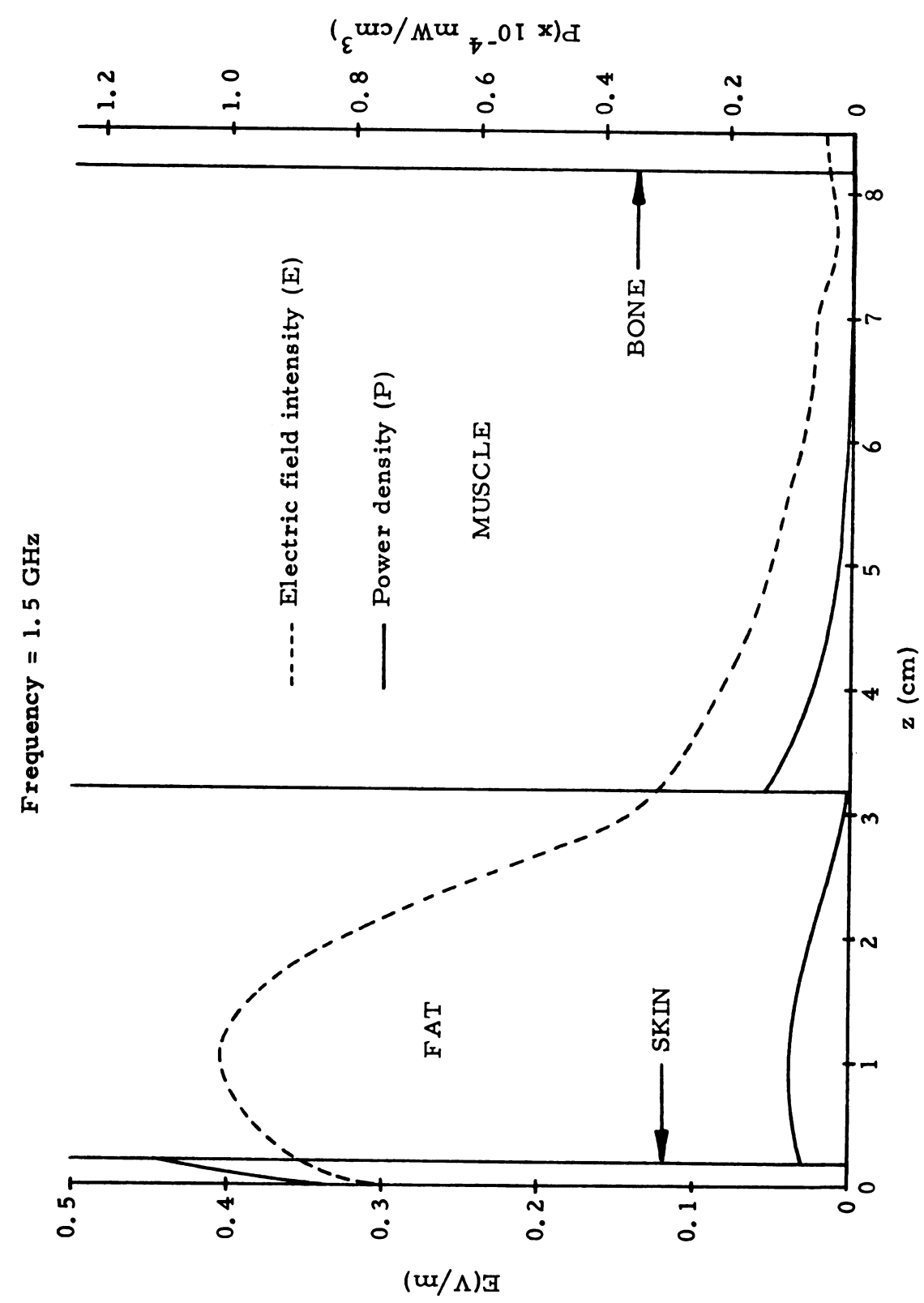
Electric field and power density in 7-slab model at 300 MHz, for $0 \le z \le 8.5$ cm. Incident field is a plane wave, with $|\vec{E}^i| = 1 \text{ V/m}$. Figure 2. 10.



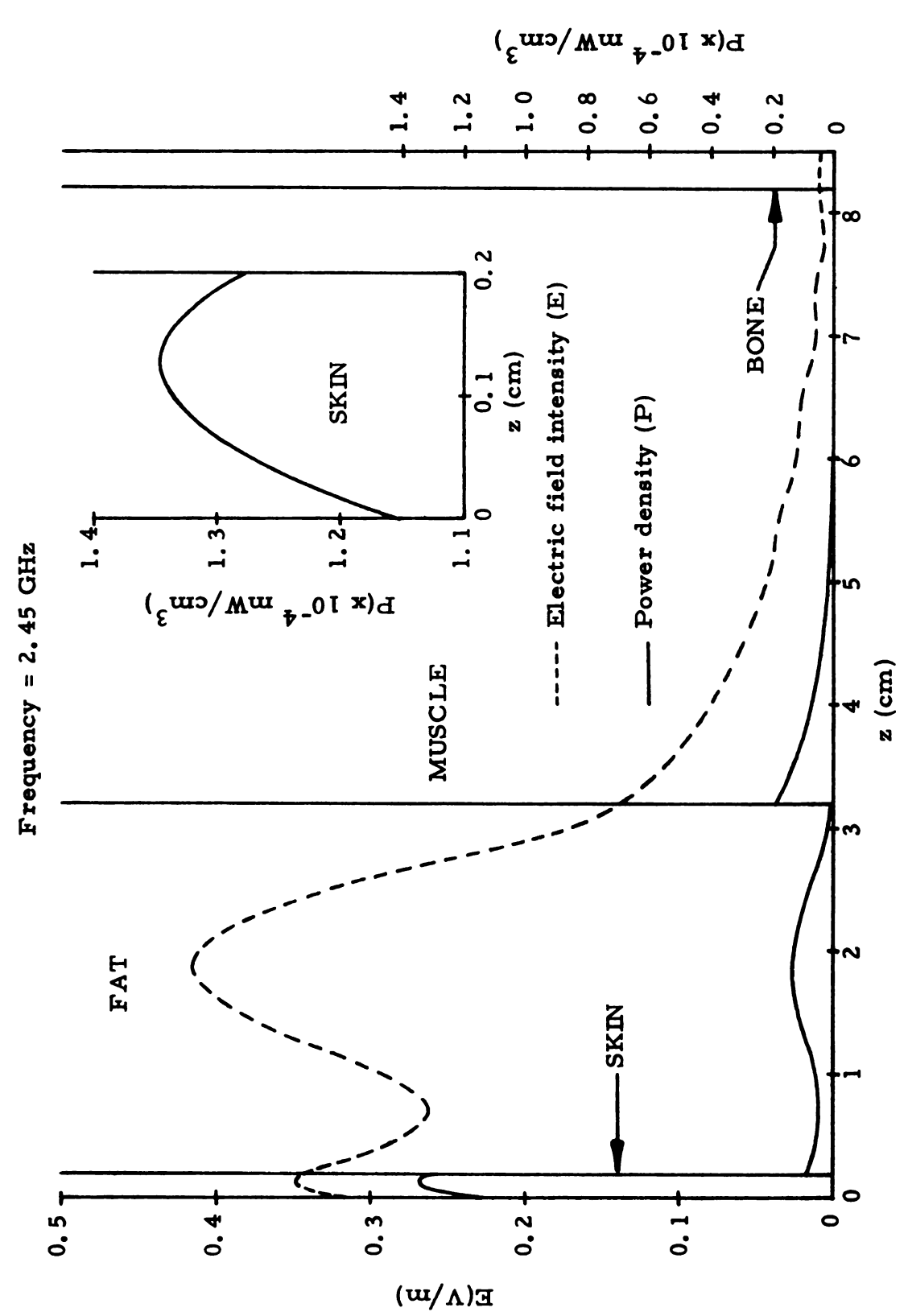
Electric field and power density in 7-slab model at 600 MHz, for $0 \le z \le 8.5$ cm. Incident field is a plane wave, with $|\mathbf{E}^i| = 1 \text{ V/m}$. Figure 2. 11.



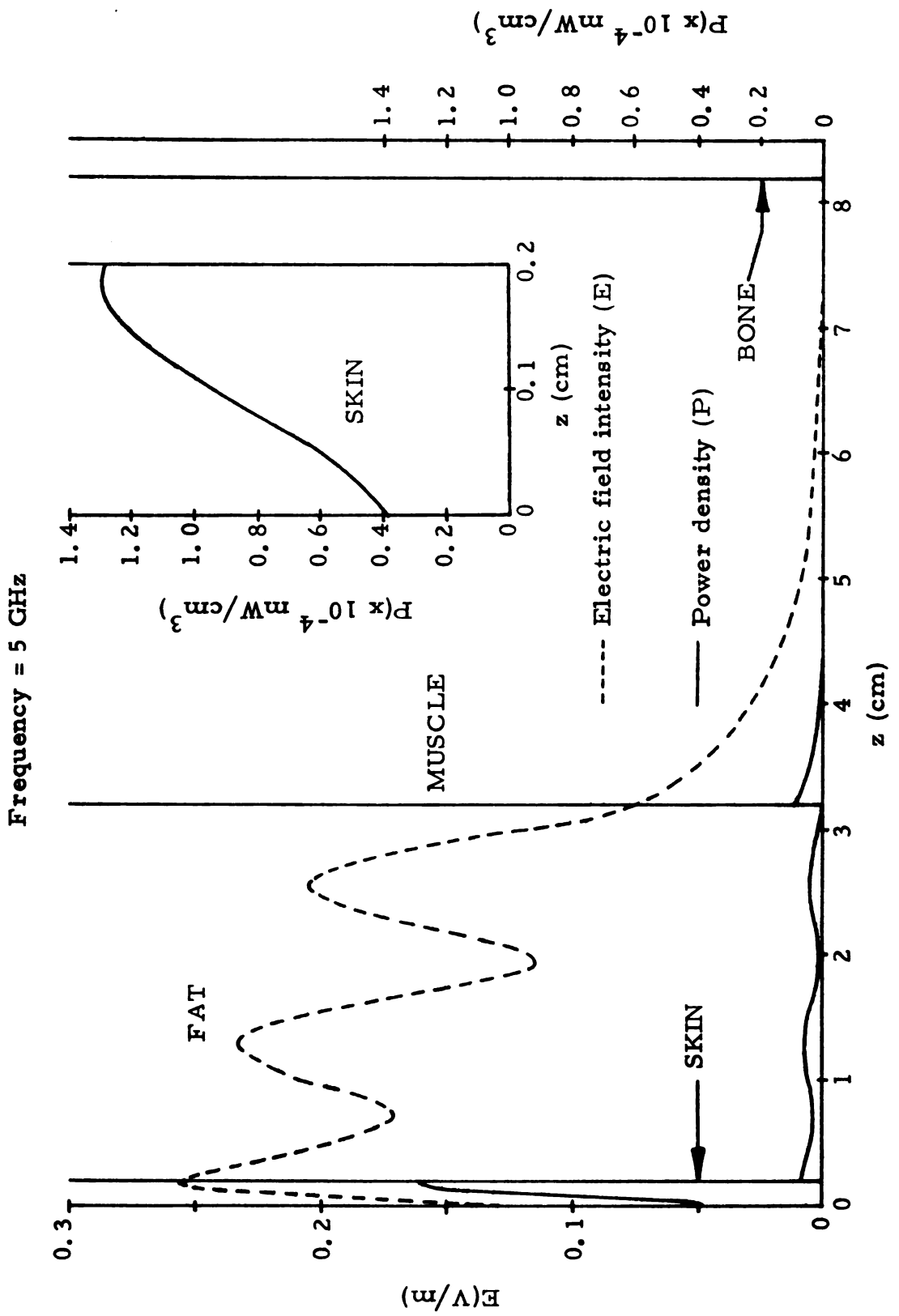
Electric field and power density in 7-slab model at 900 MHz, for $0 \le z \le 8.5$ cm. Incident field is a plane wave, with $|\vec{E}^i| = 1 \text{ V/m}$. Figure 2. 12.



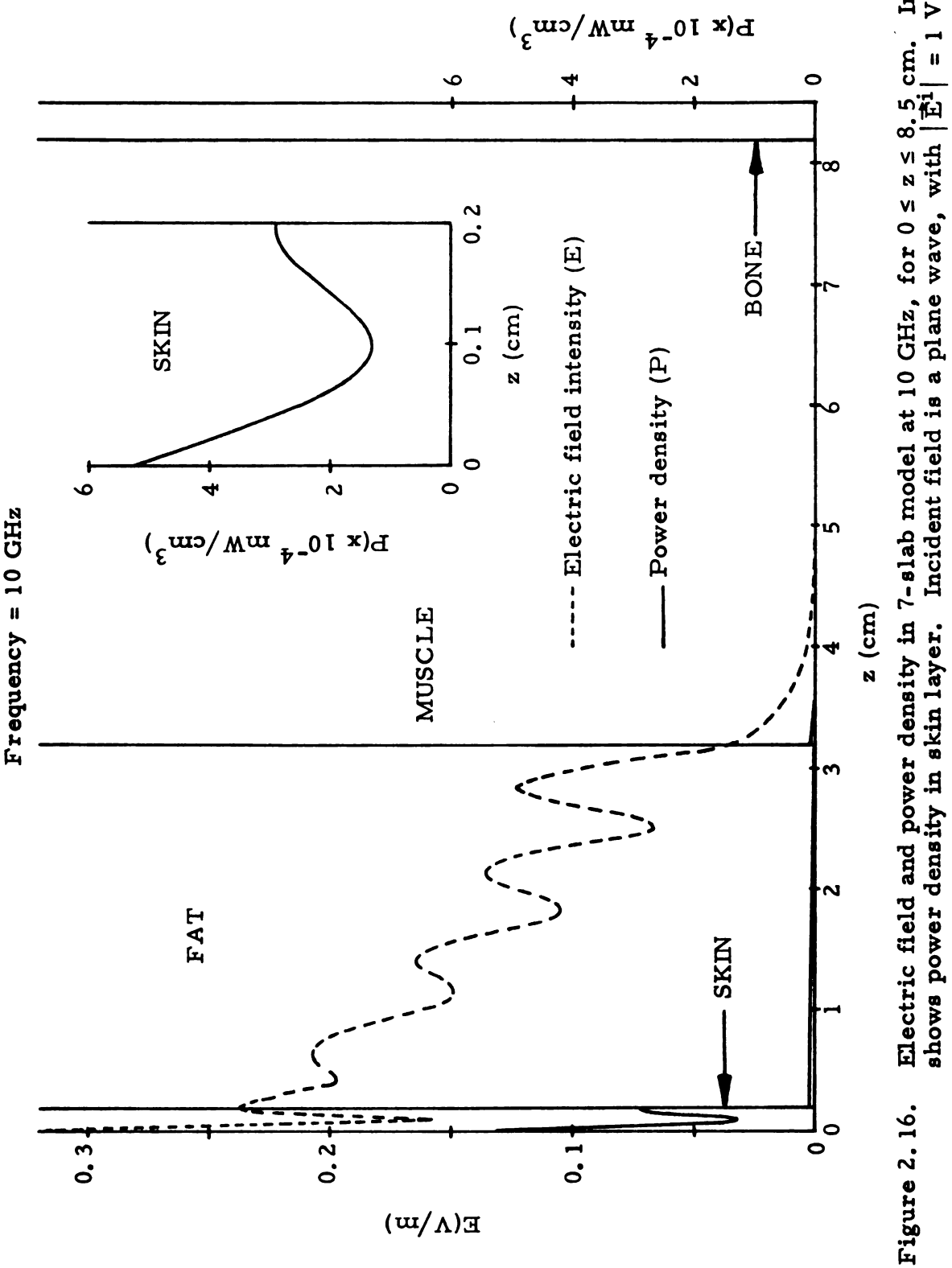
Electric field and power density in 7-slab model at 1.5 GHz, for $0 \le z \le 8.5$ cm. Incident field is a plane wave, with $|\vec{E}^i| = 1 \text{ V/m}$. Figure 2, 13.



= 1 V/m. Electric field and power density in 7-slab model at 2.45 GHz, for $0 \le z \le 8.5$ cm. shows power density in skin layer. Incident field is a plane wave, with $|\vec{E}^i| = 1$ V Figure 2, 14.



Electric field and power density in 7-slab model at 5 GHz, for $0 \le z \le 8.5$ cm. Inset shows power density in skin layer. Incident field is a plane wave, with $|\vec{E}^1| = 1 \text{ V/m}$. Figure 2. 15.



cm. Inset = 1 V/m.

CHAPTER III

INTERACTION OF AN ELECTROMAGNETIC WAVE WITH AN ARBITRARY PHYSIOLOGICAL SYSTEM

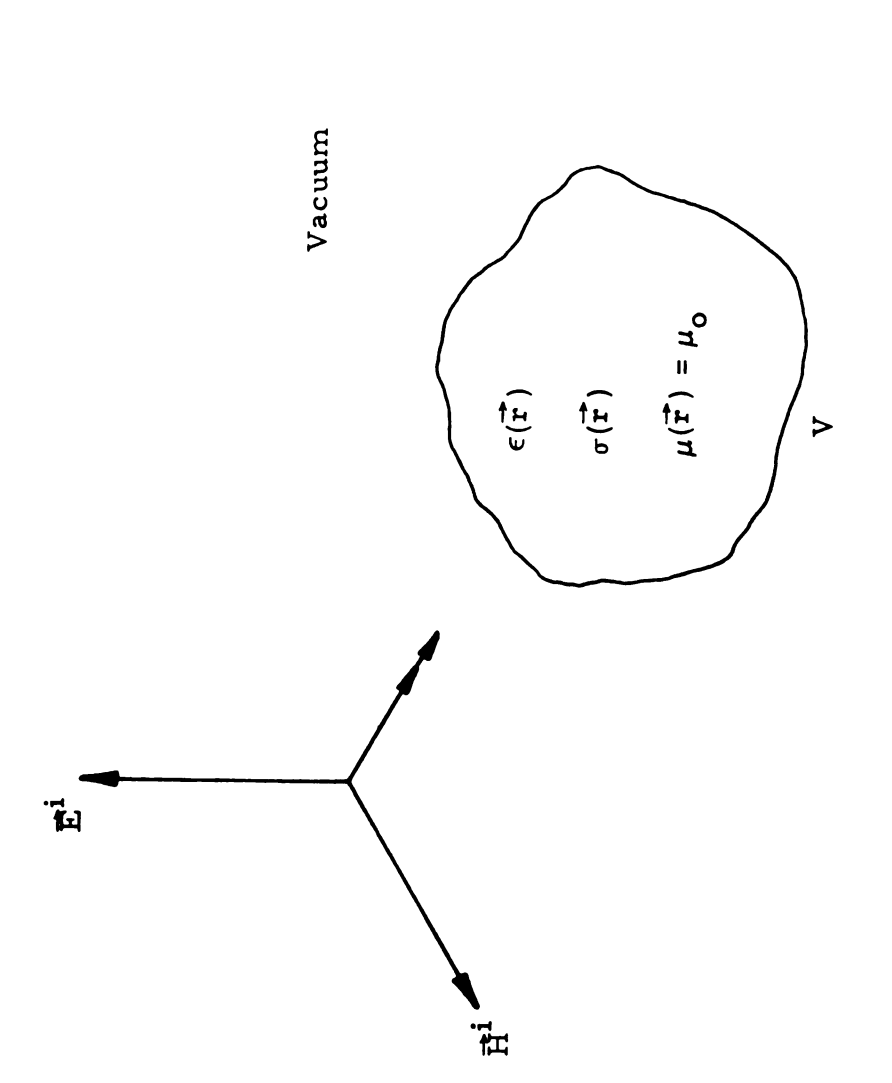
Although the plane slab model is a useful analytical tool, it has several obvious limitations. There are many important biological structures which cannot be represented by a plane slab model. Therefore, we need to develop a method of analyzing finite physiological systems with arbitrary shapes.

3.1. Description of Problem and Method of Solution

In this chapter we will develop a numerical method for studying the electromagnetic absorption and scattering characteristics of a finite, source-free physiological system. The system, also referred to as a biological body, has an arbitrary shape and composition, and is located in a source-free region of free space. The body is illuminated by an electromagnetic field having an assumed harmonic time variation of $e^{j\omega t}$, as shown in Figure 3.1.

Although the system is, in general, inhomogeneous, we assume it to be linear and isotropic. The permeability, permittivity, and conductivity of the biological body are $\mu(\vec{r})$, $\epsilon(\vec{r})$, and $\sigma(\vec{r})$, respectively. All losses in the system may be accounted for by the conductivity; thus, $\epsilon(\vec{r})$ is real. Since biological tissues are essentially nonmagnetic, we can assume that $\mu(\vec{r}) = \mu_0$ with negligible error.

By manipulating Maxwell's equations for the incident electromagnetic field and for the total electromagnetic field, we obtain a tensor



An arbitrarily shaped biological body in free space, illuminated by an electromagnetic field. In general, the body is inhomogeneous and nonmagnetic. Figure 3.1.

integral equation for the unknown electric field inside the system. Then, using a pulse-function expansion of the unknown field in conjunction with point-matching, we employ the method of moments [2] to solve the integral equation numerically. Once the internal electric field has been determined, we may, if desired, calculate the field scattered externally by the body.

3. 2. Integral Equation for Internal Electric Field

The constituent vectors $\vec{E}^i(\vec{r})$ and $\vec{H}^i(\vec{r})$ of the incident electromagnetic field satisfy Maxwell's equations for a source-free region of free space:

$$\nabla \times \vec{E}^{i}(\vec{r}) = -j\omega_{\mu_{0}} \vec{H}^{i}(\vec{r}) \qquad (3.2.1a)$$

$$\nabla \times \vec{\mathbf{H}}^{i}(\vec{\mathbf{r}}) = j\omega \in \vec{\mathbf{E}}^{i}(\vec{\mathbf{r}})$$
 (3.2.1b)

$$\nabla \cdot \vec{\mathbf{E}}^{\mathbf{i}}(\vec{\mathbf{r}}) = 0 \tag{3.2.1c}$$

$$\nabla \cdot \vec{\mathbf{H}}^{\mathbf{i}}(\vec{\mathbf{r}}) = 0 \tag{3.2.1d}$$

 μ_0 and ϵ_0 are the permeability and permittivity, respectively, of free space. $\vec{E}^i(\vec{r})$ and $\vec{H}^i(\vec{r})$, of course, are known functions of \vec{r} .

When the incident electromagnetic field impinges on the physiological system shown in Figure 3.1, it creates a distribution of induced charges and currents throughout the system. These charges and currents are the sources for a secondary or scattered field, denoted by $\vec{E}^{S}(\vec{r})$ and $\vec{H}^{S}(\vec{r})$. Thus, $\vec{E}(\vec{r})$ and $\vec{H}(\vec{r})$, representing the total electromagnetic field at each point, may be written as the sum of the two partial fields:

$$\vec{E}(\vec{r}) = \vec{E}^{i}(\vec{r}) + \vec{E}^{s}(\vec{r})$$
 (3.2.2a)

$$\vec{H}(\vec{r}) = \vec{H}^{i}(\vec{r}) + \vec{H}^{s}(\vec{r})$$
 (3.2.2b)

Since $\vec{E}^i(\vec{r})$ is known, the problem will be solved if we can obtain an expression for $\vec{E}^s(\vec{r})$ inside the body.

First, we must relate $\vec{E}^{s}(\vec{r})$ to its sources through Maxwell's equations. We begin with Maxwell's equations for the total electromagnetic field inside the physiological system:

$$\nabla \times \vec{E}(\vec{r}) = -j\omega_{\mu_0} \vec{H}(\vec{r}) \qquad (3.2.3a)$$

$$\nabla \times \vec{\mathbf{H}}(\vec{\mathbf{r}}) = \sigma(\vec{\mathbf{r}}) \vec{\mathbf{E}}(\vec{\mathbf{r}}) + \mathbf{j}\omega \in (\vec{\mathbf{r}}) \vec{\mathbf{E}}(\vec{\mathbf{r}})$$
(3.2.3b)

$$\nabla \cdot [\sigma(\vec{r}) \vec{E}(\vec{r}) + j\omega \epsilon(\vec{r}) \vec{E}(\vec{r})] = 0$$
 (3.2.3c)

$$\nabla \cdot \vec{\mathbf{H}}(\vec{\mathbf{r}}) = 0 \tag{3.2.3d}$$

Since Maxwell's equations are linear, we substitute Equations (3.2.2a) and (3.2.2b) into Equations (3.2.3a) and (3.2.3b), and obtain

$$\nabla \times \vec{E}^{i}(\vec{r}) + \nabla \times \vec{E}^{s}(\vec{r}) = -j\omega_{\mu_{O}}\vec{H}^{i}(\vec{r}) - j\omega_{\mu_{O}}\vec{H}^{s}(\vec{r})$$
(3.2.4a)

$$\nabla \times \vec{\mathbf{H}}^{\mathbf{i}}(\vec{\mathbf{r}}) + \nabla \times \vec{\mathbf{H}}^{\mathbf{s}}(\vec{\mathbf{r}}) = \sigma(\vec{\mathbf{r}}) \vec{\mathbf{E}}(\vec{\mathbf{r}}) + j\omega[\vec{\mathbf{e}}(\vec{\mathbf{r}}) - \epsilon_{0}] \vec{\mathbf{E}}(\vec{\mathbf{r}}) + j\omega\epsilon_{0}[\vec{\mathbf{E}}^{\mathbf{i}}(\vec{\mathbf{r}}) + \vec{\mathbf{E}}^{\mathbf{s}}(\vec{\mathbf{r}})]$$
(3.2.4b)

Subtracting Equations (3.2.1a) and (3.2.1b) from Equations (3.2.4a) and (3.2.4b), respectively, we have

$$\nabla \times \vec{E}^{S}(\vec{r}) = -j\omega_{\mu_{O}} \vec{H}^{S}(\vec{r})$$
 (3.2.5a)

$$\nabla \times \vec{\mathbf{H}}^{\mathbf{S}}(\vec{\mathbf{r}}) = \{ \sigma(\vec{\mathbf{r}}) + j\omega[\epsilon(\vec{\mathbf{r}}) - \epsilon_{0}] \} \vec{\mathbf{E}}(\vec{\mathbf{r}}) + j\omega\epsilon_{0} \vec{\mathbf{E}}^{\mathbf{S}}(\vec{\mathbf{r}})$$
(3.2.5b)

Defining an equivalent volume current density $\vec{J}_{eq}(\vec{r})$ by

$$\vec{J}_{eq}(\vec{r}) = \tau(\vec{r}) \vec{E}(\vec{r}), \qquad (3.2.6a)$$

where
$$\tau(\vec{r}) = \sigma(\vec{r}) + j\omega[\vec{r}] - \epsilon_0$$
, (3.2.6b)

we may rewrite Equation (3.2.5b) as

$$\nabla \times \vec{\mathbf{H}}^{\mathbf{s}}(\vec{\mathbf{r}}) = \vec{\mathbf{J}}_{eq}(\vec{\mathbf{r}}) + j\omega \epsilon_{o} \vec{\mathbf{E}}^{\mathbf{s}}(\vec{\mathbf{r}})$$
 (3.2.7)

The equivalent current density is non-zero only inside the physiological system, and has two components: $\sigma(\vec{r}) \vec{E}(\vec{r})$ represents the conduction current flowing in the body, while $j\omega[\epsilon(\vec{r}) - \epsilon_0] \vec{E}(\vec{r})$ gives the polarization current.

The equation of continuity for $\vec{J}_{eq}(\vec{r})$ defines an equivalent volume charge density $\rho_{eq}(\vec{r})$:

$$\nabla \cdot \vec{J}_{eq}(\vec{r}) + j\omega \rho_{eq}(\vec{r}) = 0$$
 (3.2.8a)

from which

$$\rho_{eq}(\vec{r}) = \frac{j}{\omega} \nabla \cdot \vec{J}_{eq}(\vec{r})$$
 (3.2.8b)

Taking the divergence of Equation (3.2.7) and using Equation (3.2.8b) gives

$$\nabla \cdot \vec{E}^{s}(\vec{r}) = \frac{\rho_{eq}(\vec{r})}{\epsilon_{o}}$$
 (3.2.9)

Finally, taking the divergence of Equation (3.2.5a), we have

$$\nabla \cdot \vec{\mathbf{H}}^{\mathbf{S}}(\vec{\mathbf{r}}) = 0 \tag{3.2.10}$$

Equations (3.2.5a), (3.2.7), (3.2.9), and (3.2.10) constitute Maxwell's equations for $\vec{\mathbb{E}}^s(\vec{r})$ and $\vec{\mathbb{H}}^s(\vec{r})$:

$$\nabla \times \vec{E}^{S}(\vec{r}) = -j\omega_{\mu_{O}} \vec{H}^{S}(\vec{r})$$
 (3.2.11a)

$$\nabla \times \vec{H}^{S}(\vec{r}) = \vec{J}_{eq}(\vec{r}) + j\omega \in \vec{E}^{S}(\vec{r})$$
 (3.2.11b)

$$\nabla \cdot \vec{E}^{S}(\vec{r}) = \frac{1}{\epsilon_{O}} \rho_{eq}(\vec{r})$$
 (3.2.11c)

$$\nabla \cdot \vec{\mathbf{H}}^{\mathbf{S}}(\vec{\mathbf{r}}) = 0 \tag{3.2.11d}$$

Since $\rho_{eq}(\vec{r})$ is related to $\vec{J}_{eq}(\vec{r})$ by Equation (3.2.8b), we can express $\vec{E}^{s}(\vec{r})$ as a function of $\vec{J}_{eq}(\vec{r})$ only. Furthermore, we may think of $\vec{J}_{eq}(\vec{r})$ as a current existing in free space, since only μ_{o} and ϵ_{o} appear in Equations (3.2.11a) through (3.2.11d). Note, however, that $\vec{J}_{eq}(\vec{r})$ depends upon the total electric field $\vec{E}(\vec{r})$, which is still unknown. It is this fact which leads us to an integral equation for $\vec{E}(\vec{r})$.

The scattered electric field $\vec{E}^{s}(\vec{r})$ can be written in terms of $\vec{J}_{eq}(\vec{r})$ by using the free-space tensor Green's function $\vec{G}(\vec{r},\vec{r})$ [1], given by

$$\vec{G}(\vec{r}, \vec{r'}) = -j\omega_{\mu_0} \left[\vec{T} + \frac{\nabla\nabla}{k_0^2}\right] \psi(\vec{r}, \vec{r'}), \qquad (3.2.12a)$$

where

$$\psi(\vec{\mathbf{r}}, \vec{\mathbf{r}}') = \frac{e^{-j\mathbf{k}_{0}|\vec{\mathbf{r}} - \vec{\mathbf{r}}'|}}{4\pi|\vec{\mathbf{r}} - \vec{\mathbf{r}}'|}, \qquad (3.2.12b)$$

$$\vec{I} = \hat{x}\hat{x} + \hat{y}\hat{y} + \hat{z}\hat{z} , \qquad (3.2.12c)$$

and $k_0 = \omega \sqrt{\mu_0 \epsilon_0}$.

or

Let V denote the volume occupied by the physiological system. If \vec{r} is outside of V, the relation between $\vec{E}^{s}(\vec{r})$ and $\vec{J}_{eq}(\vec{r}')$ is simply

$$\vec{\mathbf{E}}^{\mathbf{S}}(\vec{\mathbf{r}}) = \int_{\mathbf{V}} \vec{\mathbf{J}}_{\mathbf{eq}}(\vec{\mathbf{r}}') \cdot \vec{\mathbf{G}}(\vec{\mathbf{r}}, \vec{\mathbf{r}}') dV' \qquad (3.2.13)$$

If \vec{r} is inside V, however, difficulties arise because $\vec{G}(\vec{r}, \vec{r}^1)$ is singular at $\vec{r}^1 = \vec{r}$. We can remedy the difficulties by using a modified tensor Green's function $\tilde{G}(\vec{r}, \vec{r}^1)$, first introduced by Van Bladel [18]. $\tilde{G}(\vec{r}, \vec{r}^1)$ is given by

$$\vec{G}(\vec{r}, \vec{r}^{\dagger}) = P.V.\vec{G}(\vec{r}, \vec{r}^{\dagger}) - \frac{\hat{T}\delta(\vec{r} - \vec{r}^{\dagger})}{3j\omega\epsilon_{0}}$$
(3.2.14)

where $\vec{G}(\vec{r}, \vec{r}')$ is defined by Equation (3.2.12a), and the P. V. symbol denotes the Principal Value, to be defined presently.

Thus, when \overrightarrow{r} is inside the physiological system, Equation (3.2.13) is replaced by

$$\vec{\mathbf{E}}^{\mathbf{s}}(\vec{\mathbf{r}}) = \int_{\mathbf{V}} \vec{\mathbf{q}}(\vec{\mathbf{r}}') \cdot \left[\mathbf{P. V. } \vec{\mathbf{G}}(\vec{\mathbf{r}}, \vec{\mathbf{r}}') - \frac{\vec{\mathbf{T}}\delta(\vec{\mathbf{r}} - \vec{\mathbf{r}}')}{3j\omega\epsilon_{\mathbf{o}}} \right] dV' \qquad (3.2.15a)$$

 $\vec{\mathbf{E}}^{\mathbf{g}}(\vec{\mathbf{r}}) = \mathbf{P.} \mathbf{V.} \int_{\mathbf{V}} \vec{\mathbf{J}}_{eq}(\vec{\mathbf{r}}') \cdot \vec{\mathbf{G}}(\vec{\mathbf{r}}, \vec{\mathbf{r}}') \, d\mathbf{V}' - \frac{\vec{\mathbf{J}}_{eq}(\vec{\mathbf{r}})}{3j\omega\epsilon_{o}}$ (3.2.15b)

The P. V. symbol, then, refers to the principal value of the integral in Equation (3.2.15b), obtained by excluding from V a small sphere of radius η centered at \vec{r} , then taking the limit as $\eta \to 0$.

By substituting Equation (3.2.15b) into Equation (3.2.2a) and rearranging terms, recalling that $\vec{J}_{eq}(\vec{r}) = \tau(\vec{r})\vec{E}(\vec{r})$, we obtain the desired

integral equation for $\vec{E}(\vec{r})$:

$$\left[1 + \frac{\tau(\vec{\mathbf{r}})}{3j\omega}\right] \vec{\mathbf{E}}(\vec{\mathbf{r}}) - \mathbf{P.} \mathbf{V.} \int_{\mathbf{V}} \tau(\vec{\mathbf{r}}') \vec{\mathbf{E}}(\vec{\mathbf{r}}') \cdot \vec{\mathbf{G}}(\vec{\mathbf{r}}, \vec{\mathbf{r}}') dV' = \vec{\mathbf{E}}^{i}(\vec{\mathbf{r}}) \quad (3.2.16)$$

Equation (3.2.16) may be classified as a Fredholm integral equation of the second kind. $\vec{E}^i(\vec{r})$ and $\tau(\vec{r})$ are, of course, known quantities. $\vec{E}(\vec{r})$ is the unknown total electric field inside the body. A solution to Equation (3.2.16), based on the method of moments, will be discussed in the next section.

3.3. Moment Solution of Integral Equation

The inner product of $\vec{E}(\vec{r})$ and $\vec{G}(\vec{r}, \vec{r})$ in Equation (3.2.16) may be represented as a matrix product:

$$\vec{E}(\vec{r}') \cdot \vec{G}(\vec{r}, \vec{r}') = \begin{bmatrix} G_{xx}(\vec{r}, \vec{r}') & G_{xy}(\vec{r}, \vec{r}') & G_{xz}(\vec{r}, \vec{r}') \\ G_{yx}(\vec{r}, \vec{r}') & G_{yy}(\vec{r}, \vec{r}') & G_{yz}(\vec{r}, \vec{r}') \\ G_{zx}(\vec{r}, \vec{r}') & G_{zy}(\vec{r}, \vec{r}') & G_{zz}(\vec{r}, \vec{r}') \end{bmatrix} \begin{bmatrix} E_{x}(\vec{r}') \\ E_{y}(\vec{r}') \\ E_{z}(\vec{r}') \end{bmatrix}$$

$$(3.3.1)$$

To make the analysis as general as possible, it will be convenient to introduce the following notation:

$$x_1 = x$$
 $x_2 = y$ $x_3 = z$ (3.3.2)

Physically, $G_{x_p}^{(\vec{r},\vec{r}')}$ is the x_p component of the electric field at the observation point \vec{r} maintained by a unit x_q component of current at the point \vec{r}' .

If the expression for $\vec{G}(\vec{r}, \vec{r'})$ given in Equation (3.2.12a) is used to evaluate the inner product of $\vec{E}(\vec{r'})$ and $\vec{G}(\vec{r}, \vec{r'})$, and if the resulting expression is compared to Equation (3.3.1), we find that

$$G_{\mathbf{x}_{\mathbf{p}}\mathbf{x}_{\mathbf{q}}}(\vec{\mathbf{r}}, \vec{\mathbf{r}}^{1}) = -j\omega\mu_{\mathbf{o}} \left[\delta_{\mathbf{p}\mathbf{q}} + \frac{1}{k_{\mathbf{o}}^{2}} \frac{\partial^{2}}{\partial \mathbf{x}_{\mathbf{q}} \partial \mathbf{x}_{\mathbf{p}}}\right] \psi(\vec{\mathbf{r}}, \vec{\mathbf{r}}^{1})$$

$$p, q = 1, 2, 3.$$
(3.3.3)

where δ_{pq} is Kronecker's delta. A straightforward evaluation of Equation (3.3.3) (see Appendix A) gives, after some rearranging,

$$G_{\mathbf{x}_{\mathbf{p}}\mathbf{x}_{\mathbf{q}}}(\vec{\mathbf{r}}, \vec{\mathbf{r}}') = \frac{-j\omega\mu_{\mathbf{o}}k_{\mathbf{o}}e^{-j\alpha}}{4\pi\alpha^{3}}[(\alpha^{2} - 1 - j\alpha)\delta_{\mathbf{p}\mathbf{q}} + \cos\theta_{\mathbf{x}_{\mathbf{p}}}\cos\theta_{\mathbf{x}_{\mathbf{q}}}(3 - \alpha^{2} + 3j\alpha)]$$
(3.3.4)

where

$$\alpha = k_0 R$$

$$R = |\vec{r} - \vec{r}|$$

$$\cos \theta_{\mathbf{x}_p} = \frac{\mathbf{x}_p - \mathbf{x}_p'}{R}$$

$$\cos \theta_{\mathbf{x}_q} = \frac{\mathbf{x}_q - \mathbf{x}_q'}{R}$$

$$\vec{r} = (\mathbf{x}_1, \mathbf{x}_2, \mathbf{x}_3)$$

$$\vec{r}' = (\mathbf{x}_1', \mathbf{x}_2', \mathbf{x}_3')$$

Equation (3.2.16) comprises three coupled scalar integral equations.

Using Equation (3.3.1), we write each scalar component of Equation

(3.2.16) as

$$\left[1 + \frac{\tau(\vec{r})}{3j\omega\epsilon_{o}}\right] E_{\mathbf{x}p}(\vec{r}) - P. V. \int_{V} \tau(\vec{r}') \left[\sum_{q=1}^{3} G_{\mathbf{x}p} \mathbf{x}_{q}(\vec{r}, \vec{r}') E_{\mathbf{x}q}(\vec{r}')\right] dV' = E_{\mathbf{x}p}^{i}(\vec{r})$$

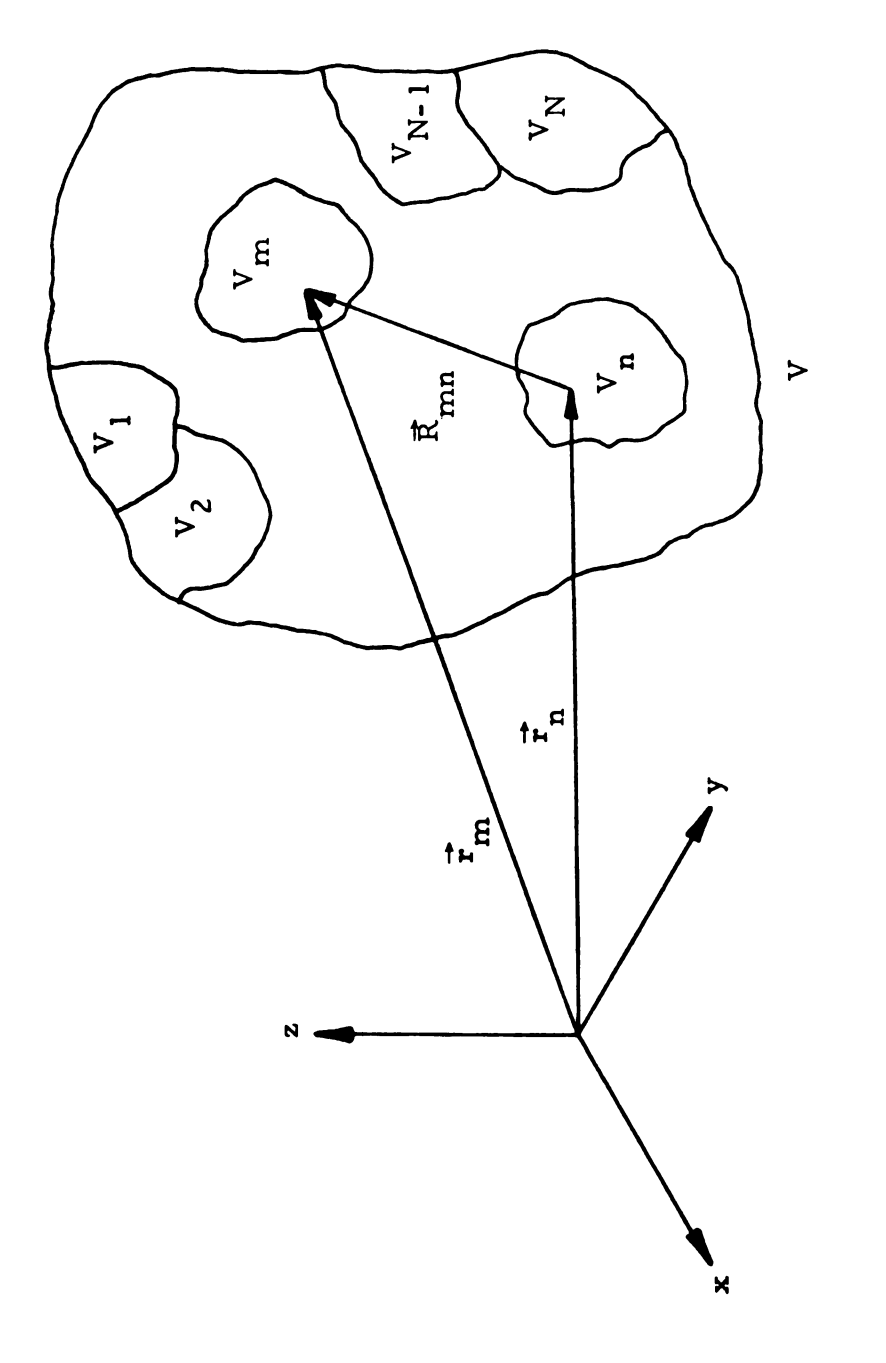
$$p = 1, 2, 3. \qquad (3.3.5)$$

We can use the method of moments to transform Equation (3, 3, 5) into a matrix equation for each value of p. The resulting coupled matrix equations may then be combined into a single matrix equation for $\vec{E}(\vec{r})$.

First, we partition the body into N cells, or subvolumes, and assume that $\tau(\vec{r})$ and $\vec{E}(\vec{r})$ are constant throughout each cell. We denote the mth subvolume by V_m , and we let \vec{r}_m denote the position of a representative interior point of V_m , as shown in Figure 3.2. Thus, the integral in Equation (3.3.5) may be written as

P. V.
$$\int_{\mathbf{V}} \tau(\vec{\mathbf{r}}') \begin{bmatrix} \frac{3}{\Sigma} G_{\mathbf{x}_{\mathbf{p}} \mathbf{x}_{\mathbf{q}}} (\vec{\mathbf{r}}, \vec{\mathbf{r}}') E_{\mathbf{x}_{\mathbf{q}}} (\vec{\mathbf{r}}') \end{bmatrix} dV'$$

$$= \frac{3}{\Sigma} P. V. \int_{\mathbf{V}} \tau(\vec{\mathbf{r}}') G_{\mathbf{x}_{\mathbf{p}} \mathbf{x}_{\mathbf{q}}} (\vec{\mathbf{r}}, \vec{\mathbf{r}}') E_{\mathbf{x}_{\mathbf{q}}} (\vec{\mathbf{r}}') dV'$$
(3.3.6a)



A physiological system partitioned into N subvolumes, showing a typical arrangement of the cells. Figure 3.2.

$$= \sum_{q=1}^{3} \sum_{n=1}^{N} P. V. \int_{V_n} \tau(\vec{r}) G_{\mathbf{x}p} \mathbf{x}_q(\vec{r}, \vec{r}) E_{\mathbf{x}_q}(\vec{r}) dV'$$
 (3.3.6b)

$$= \sum_{q=1}^{3} \sum_{n=1}^{N} \tau(\vec{r}_n) E_{\mathbf{x}_q}(\vec{r}_n) P. V. \int_{V_n} G_{\mathbf{x}_p} \mathbf{x}_q(\vec{r}, \vec{r}') dV'$$
(3.3.6c)

Hence, Equation (3.3.5) becomes

$$\left[1 + \frac{\tau(\vec{r})}{3j\omega\epsilon_{o}}\right] E_{\mathbf{x}p}(\vec{r}) - \sum_{q=1}^{3} \sum_{n=1}^{N} \tau(\vec{r}_{n}) E_{\mathbf{x}q}(\vec{r}_{n}) P. V. \int_{V_{n}} G_{\mathbf{x}p} \mathbf{x}_{q}(\vec{r}, \vec{r}') dV' = E_{\mathbf{x}p}^{i}(\vec{r})$$
(3.3.7)

Next, we require that Equation (3.3.7) be satisfied at each \vec{r}_{m} .

That is.

$$\begin{bmatrix}
1 + \frac{\tau(\vec{r}_{m})}{3j\omega\epsilon_{o}}
\end{bmatrix} E_{\mathbf{x}p}(\vec{r}_{m}) - \sum_{q=1}^{3} \sum_{n=1}^{N} \tau(\vec{r}_{n}) E_{\mathbf{x}q}(\vec{r}_{n}) P. V. \int_{V_{n}} G_{\mathbf{x}p} \mathbf{x}_{q}(\vec{r}_{m}, \vec{r}') dV'$$

$$= E_{\mathbf{x}p}^{i}(\vec{r}_{m})$$

$$= 1, 2, ..., N.$$

$$p = 1, 2, 3.$$

Equation (3.3.8) can be rewritten in the following form:

$$\sum_{\mathbf{q}=1}^{3} \sum_{\mathbf{n}=1}^{N} \left[\tau(\vec{\mathbf{r}}_{\mathbf{n}}) P. V. \int_{\mathbf{V}_{\mathbf{n}}} G_{\mathbf{x}_{\mathbf{p}} \mathbf{x}_{\mathbf{q}}} (\vec{\mathbf{r}}_{\mathbf{m}}, \vec{\mathbf{r}}') dV' - \delta_{\mathbf{p}\mathbf{q}} \delta_{\mathbf{m}\mathbf{n}} \left(1 + \frac{\tau(\vec{\mathbf{r}}_{\mathbf{m}})}{3j\omega \epsilon_{\mathbf{o}}} \right) \right] E_{\mathbf{x}_{\mathbf{q}}} (\vec{\mathbf{r}}_{\mathbf{n}})$$

$$= - E_{\mathbf{x}_{\mathbf{p}}}^{i} (\vec{\mathbf{r}}_{\mathbf{m}})$$

$$= - E_{\mathbf{x}_{\mathbf{p}}}^{i} (\vec{\mathbf{r}}_{\mathbf{m}})$$

$$= 1, 2, ..., N.$$

$$p = 1, 2, 3.$$
(3.3.9)

Let $[G_{x_p}^{x_q}]$ be the $N \times N$ matrix whose elements $G_{x_p}^{mn}$ are given by

$$G_{\mathbf{x}_{\mathbf{p}}\mathbf{x}_{\mathbf{q}}}^{\mathbf{mn}} = \tau(\vec{\mathbf{r}}_{\mathbf{n}}) P. V. \int_{V_{\mathbf{n}}} G_{\mathbf{x}_{\mathbf{p}}\mathbf{x}_{\mathbf{q}}}(\vec{\mathbf{r}}_{\mathbf{m}}, \vec{\mathbf{r}}^{\dagger}) dV^{\dagger} - \delta_{\mathbf{p}\mathbf{q}} \delta_{\mathbf{mn}} \left[1 + \frac{\tau(\vec{\mathbf{r}}_{\mathbf{m}})}{3j\omega \epsilon_{\mathbf{o}}} \right]$$

$$m, n = 1, 2, \dots, N.$$

$$p, q = 1, 2, 3.$$
(3.3.10)

Then, Equation (3.3.9) is simply

$$\sum_{q=1}^{3} \sum_{n=1}^{N} G_{\mathbf{x}_{p} \mathbf{x}_{q}}^{mn} E_{\mathbf{x}_{q}}(\vec{\mathbf{r}}_{n}) = -E_{\mathbf{x}_{p}}^{i}(\vec{\mathbf{r}}_{m})$$

$$m = 1, 2, ..., N$$

$$p = 1, 2, 3.$$
(3.3.11)

We also define the N-dimensional column vectors $\begin{bmatrix} E_{x} \\ p \end{bmatrix}$ and $\begin{bmatrix} E_{x}^{i} \\ p \end{bmatrix}$, given by

$$\begin{bmatrix} \mathbf{E}_{\mathbf{x}_{\mathbf{p}}} \end{bmatrix} = \begin{bmatrix} \mathbf{E}_{\mathbf{x}_{\mathbf{p}}}^{(\mathbf{\vec{r}}_{\mathbf{l}})} \\ \vdots \\ \mathbf{E}_{\mathbf{x}_{\mathbf{p}}}^{(\mathbf{\vec{r}}_{\mathbf{N}})} \end{bmatrix}, \quad (3.3.12a) \quad \begin{bmatrix} \mathbf{E}_{\mathbf{x}_{\mathbf{p}}}^{\mathbf{i}} \end{bmatrix} = \begin{bmatrix} \mathbf{E}_{\mathbf{x}_{\mathbf{p}}}^{\mathbf{i}} (\mathbf{\vec{r}}_{\mathbf{l}}) \\ \vdots \\ \mathbf{E}_{\mathbf{x}_{\mathbf{p}}}^{\mathbf{i}} (\mathbf{\vec{r}}_{\mathbf{N}}) \end{bmatrix}. \quad (3.3.12b)$$

$$p = 1, 2, 3.$$

The summation over n in Equation (3.3.11) represents the inner product of the mth row of $\begin{bmatrix} G_{x_p} \\ q \end{bmatrix}$ with $\begin{bmatrix} E_{x_q} \\ q \end{bmatrix}$. As m ranges over all values from 1 to N, Equation (3.3.11) becomes

$$\sum_{q=1}^{3} [G_{x_p}^{x_q}][E_{x_q}] = -[E_{x_p}^i]. p = 1, 2, 3. (3.3.13)$$

After performing the summation over q for each value of p, we obtain the following set of linear equations:

$$[G_{xx}][E_x] + [G_{xy}][E_y] + [G_{xz}][E_z] = -[E_x^i]$$
 (3.3.14a)

$$[G_{yx}][E_x] + [G_{yy}][E_y] + [G_{yz}][E_z] = -[E_y^i]$$
 (3.3.14b)

$$[G_{zx}][E_x] + [G_{zy}][E_y] + [G_{zz}][E_z] = -[E_z^1]$$
 (3.3.14c)

Equivalently, we have

$$\begin{bmatrix} \begin{bmatrix} G_{xx} \end{bmatrix} & \begin{bmatrix} G_{xy} \end{bmatrix} & \begin{bmatrix} G_{xz} \end{bmatrix} \\ \begin{bmatrix} G_{yx} \end{bmatrix} & \begin{bmatrix} G_{yz} \end{bmatrix} & \begin{bmatrix} E_{x} \end{bmatrix} \\ \begin{bmatrix} G_{yx} \end{bmatrix} & \begin{bmatrix} G_{yz} \end{bmatrix} & \begin{bmatrix} E_{y} \end{bmatrix} \\ \begin{bmatrix} G_{zx} \end{bmatrix} & \begin{bmatrix} G_{zy} \end{bmatrix} & \begin{bmatrix} G_{zz} \end{bmatrix} & \begin{bmatrix} E_{z} \end{bmatrix} \end{bmatrix}$$

$$(3.3.15)$$

Equation (3.3.15) may be written in compact form as

$$[G][E] = -[E^{i}]$$
 (3.3.16)

Equation (3.3.16) is the matrix representation of Equation (3.2.16).

[G] is a 3N x 3N matrix, while [E] and [Eⁱ] each have 3N components.

We can find the total electric field in each of the N subvolumes by solving Equation (3.3.16) for [E].

3.4. Calculation of Matrix Elements

In this section we develop explicit expressions for the elements of each N x N submatrix $[G_{x_p x_q}]$, p,q = 1,2,3. The m,nth element of $[G_{x_p x_q}]$ is defined by Equation (3.3.10):

$$G_{\mathbf{x}_{p}\mathbf{x}_{q}}^{\mathbf{mn}} = \tau(\vec{\mathbf{r}}_{n}) P. V. \int_{V_{n}} G_{\mathbf{x}_{p}\mathbf{x}_{q}}(\vec{\mathbf{r}}_{m}, \vec{\mathbf{r}}^{\dagger}) dV' - \delta_{pq} \delta_{mn} \left[1 + \frac{\tau(\vec{\mathbf{r}}_{m})}{3j\omega\epsilon_{o}}\right]$$
(3.4.1)

We will first evaluate the off-diagonal elements; i.e., $m \neq n$. Since $\vec{r}_m \neq V_n$, the integrand in Equation (3.4.1) is continuous throughout V_n , so we need not take the principal value. Thus, the off-diagonal elements of $[G_{x_p}]$ are given by

$$G_{\mathbf{x}_{\mathbf{p}}\mathbf{x}_{\mathbf{q}}}^{\mathbf{m}\mathbf{n}} = \tau(\vec{\mathbf{r}}_{\mathbf{n}}) \int_{\mathbf{V}_{\mathbf{n}}} G_{\mathbf{x}_{\mathbf{p}}\mathbf{x}_{\mathbf{q}}} (\vec{\mathbf{r}}_{\mathbf{m}}, \vec{\mathbf{r}}') \, dV'$$

$$m \neq n$$

$$\mathbf{p}, \mathbf{q} = 1, 2, 3.$$
(3.4.2)

The integral in Equation (3.4.2) can be evaluated numerically by any convenient method.

If the dimensions of V_n are small compared to the free-space wavelength λ_0 , we can approximate $G_{\mathbf{x}_{\mathbf{p}}\mathbf{x}_{\mathbf{q}}}^{\mathbf{mn}}$ by assuming that the integrand in Equation (3.4.2) is constant over the region of integration. With this assumption, Equation (3.4.2) becomes

$$G_{\mathbf{x}_{\mathbf{p}}\mathbf{x}_{\mathbf{q}}}^{\mathbf{m}\mathbf{n}} = \tau(\vec{\mathbf{r}}_{\mathbf{n}}) G_{\mathbf{x}_{\mathbf{p}}\mathbf{x}_{\mathbf{q}}}(\vec{\mathbf{r}}_{\mathbf{m}}, \vec{\mathbf{r}}_{\mathbf{n}}) \Delta V_{\mathbf{n}}$$

$$m \neq \mathbf{n}$$
(3.4.3a)

where

$$\Delta V_{n} = \int_{V_{n}} dV' \qquad . \tag{3.4.3b}$$

Writing \vec{r}_m and \vec{r}_n as

$$\vec{r}_{m} = (x_{1}^{m}, x_{2}^{m}, x_{3}^{m})$$
 (3.4.4a)

$$\vec{r}_n = (x_1^n, x_2^n, x_3^n)$$
, (3.4.4b)

and using Equation (3.3.4) to evaluate $G_{x_p x_q}(\vec{r}_m, \vec{r}_n)$, we obtain an approximate expression for the off-diagonal matrix elements. The result is

$$G_{\mathbf{x}_{p}\mathbf{x}_{q}}^{mn} = \frac{-j\omega_{\mu_{o}} k_{o} \tau(\vec{r}_{n}) \Delta V_{n} e^{-j\alpha_{mn}}}{4\pi \alpha_{mn}^{3}} [(\alpha_{mn}^{2} - 1 - j\alpha_{mn}) \delta_{pq} + \cos\theta_{\mathbf{x}_{q}}^{mn} \cos\theta_{\mathbf{x}_{q}}^{mn} (3 - \alpha_{mn}^{2} + 3j\alpha_{mn})]$$
(3.4.5a)

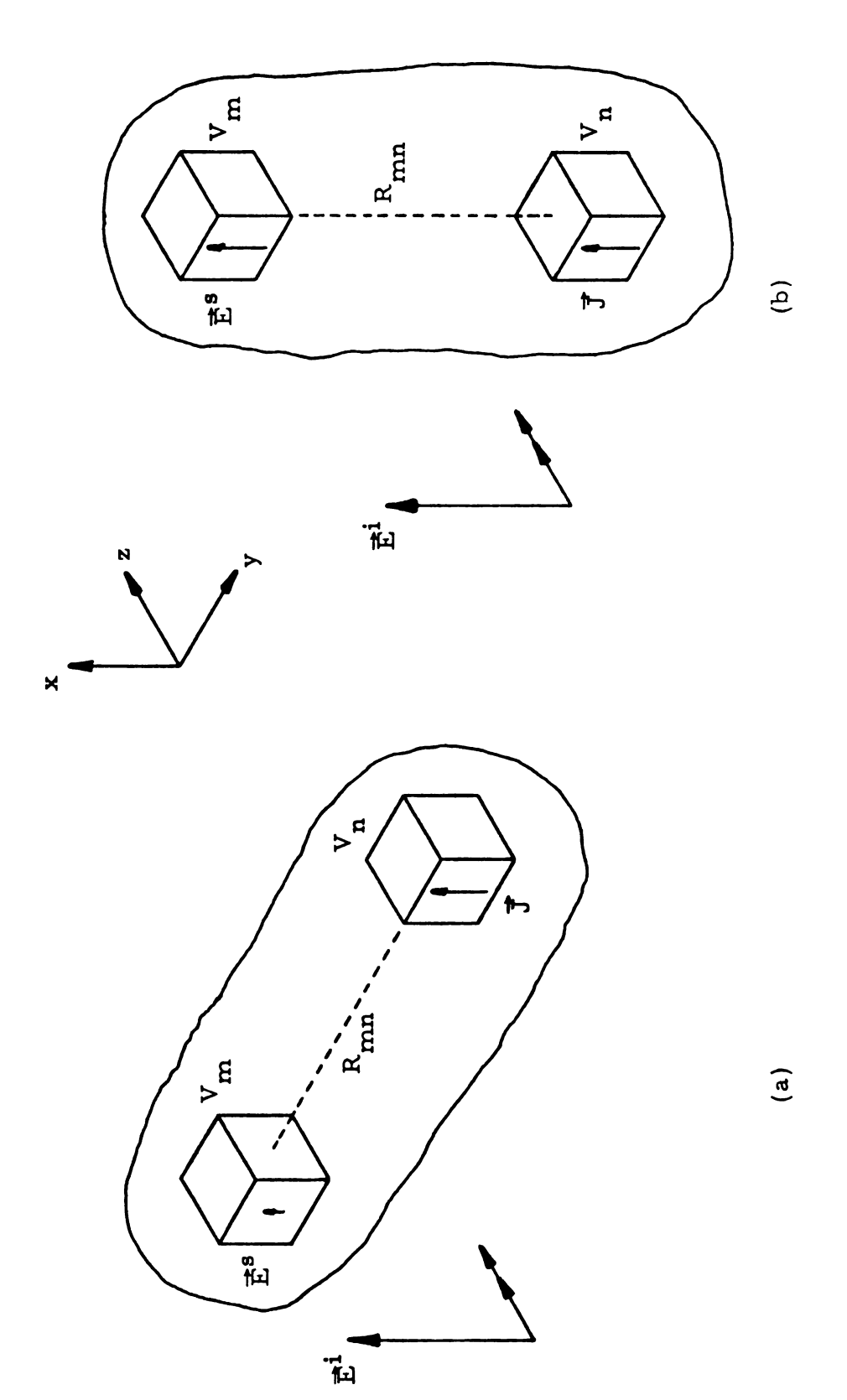
where

$$a_{mn} = k_0 R_{mn}$$
 , $R_{mn} = |\vec{r}_m - \vec{r}_n|$ (3.4.5b)

$$\cos \theta_{\mathbf{x}_{\mathbf{p}}}^{\mathbf{mn}} = \frac{\mathbf{x}_{\mathbf{p}}^{\mathbf{m}} - \mathbf{x}_{\mathbf{p}}^{\mathbf{n}}}{R_{\mathbf{mn}}}, \quad \cos \theta_{\mathbf{x}_{\mathbf{q}}}^{\mathbf{mn}} = \frac{\mathbf{x}_{\mathbf{q}}^{\mathbf{m}} - \mathbf{x}_{\mathbf{q}}^{\mathbf{n}}}{R_{\mathbf{mn}}}$$
 (3.4.5c)

If the biological body is cylindrical, experience has shown that using Equation (3.4.5a) often produces inaccurate data. When the cylinder axis is perpendicular to $\vec{E}^i(\vec{r})$, numerical integration of Equation (3.4.2) leads to nearly the same solution as using Equation (3.4.5a). The two methods generate different solutions, however, when the axis of the cylinder is parallel to $\vec{E}^i(\vec{r})$. We will soon see why.

Figure 3.3 shows a cylindrical body illuminated by a uniform plane wave at normal incidence, with $\vec{E}^{i}(\vec{r})$ linearly polarized along the x-axis.



(a) Scattered field \vec{E}^s in subvolume V_m produced by a unit current in subvolume V_n when cylindrical body is perpendicular to \vec{E}^i . (b) Scattered field \vec{E}^s in subvolume V_m produced by a unit current in subvolume V_m when cylindrical body is parallel to \vec{E}^i . \vec{E}^s in (b) is about twice as large as \vec{E}^s in (a). Figure 3.3.

The only significant component of both $\vec{E}(\vec{r})$ and $\vec{E}^{S}(\vec{r})$ is the x-component. Therefore, it will be instructive to compare the values of $G_{xx}(\vec{r}_{m}, \vec{r}_{n})$ for the two cases illustrated in Figure 3.3.

In Figure 3.3a, the axis of the cylinder is perpendicular to $\vec{E}^i(\vec{r})$, so that \vec{r}_m and \vec{r}_n have very nearly the same x-coordinate. Thus, according to Equation (3.4.5c),

$$\left(\cos\theta_{\mathbf{x}}^{\mathbf{mn}}\right)^{2} \simeq 0. \tag{3.4.6a}$$

 $G_{xx}(\vec{r}_m, \vec{r}_n)$, the Green's function for perpendicular polarization, is therefore given approximately by

$$G_{xx}(\vec{r}_{m}, \vec{r}_{n})_{\perp} \simeq \frac{-j\omega_{\mu_{o}}k_{o}e^{-j\alpha_{mn}}}{4\pi \alpha_{mn}^{3}} (\alpha_{mn}^{2} - 1 - j\alpha_{mn})$$
 (3.4.6b)

If $a_{mn}^2 \ll 1$, we can neglect the a_{mn}^2 term in Equation (3.4.6b), obtaining

$$G_{xx}(\vec{r}_m, \vec{r}_n) \perp \simeq \frac{j\omega\mu_0 k_0 e^{-j\alpha_{mn}}}{4\pi \alpha_{mn}^3} (1 + j\alpha_{mn})$$
 (3.4.6c)

The axis of the body is parallel to $\vec{E}^i(\vec{r})$ in Figure 3.3b, so that \vec{r}_m and \vec{r}_n have approximately the same y- and z-coordinates. Hence,

$$\left(\cos\theta_{\mathbf{x}}^{\mathbf{mn}}\right)^{2} \simeq 1 \tag{3.4.7a}$$

 $G_{xx}(\vec{r}_m, \vec{r}_n)_{||}$, the Green's function for parallel polarization, is approximately

$$G_{xx}(\vec{r}_{m}, \vec{r}_{n})_{||} \simeq \frac{-j\omega\mu_{o}k_{o}e^{-ja_{mn}}}{4\pi a_{mn}^{3}}[(a_{mn}^{2} - 1 - ja_{mn}) + (3 - a_{mn}^{2} + 3ja_{mn})]$$
(3.4.7b)

$$= -2 \frac{j\omega_{\mu_0} k_0 e^{-ja_{mn}}}{4\pi a_{mn}^3} (1 + ja_{mn})$$
 (3.4.7c)

Therefore,

$$|G_{\mathbf{x}\mathbf{x}}(\vec{\mathbf{r}}_{\mathbf{m}}, \vec{\mathbf{r}}_{\mathbf{n}})| \simeq 2|G_{\mathbf{x}\mathbf{x}}(\vec{\mathbf{r}}_{\mathbf{m}}, \vec{\mathbf{r}}_{\mathbf{n}})|$$

$$if \quad a_{\mathbf{m}\mathbf{n}}^{2} << 1.$$
(3.4.7d)

Since $G_{x_p x_q}(\vec{r}, \vec{r}^i)$ varies as $(a)^{-3}$ for small a, the largest matrix elements are those for which $a_{mn}^2 << 1$. These elements are approximately twice as large for parallel polarization as they are when $\vec{E}^i(\vec{r})$ is perpendicular to the cylinder axis. Thus, for parallel polarization, the matrix elements should be evaluated more accurately to obtain reliable data.

The diagonal elements of $[G_{\mathbf{x}_{\mathbf{p}}\mathbf{x}_{\mathbf{q}}}]$ may be written as $G_{\mathbf{x}_{\mathbf{p}}\mathbf{x}_{\mathbf{q}}}^{\mathbf{n}\mathbf{n}} = \tau(\vec{\mathbf{r}}_{\mathbf{n}})I_{\mathbf{x}_{\mathbf{p}}\mathbf{x}_{\mathbf{q}}}^{\mathbf{n}} - \delta_{\mathbf{p}\mathbf{q}}\left[1 + \frac{\tau(\vec{\mathbf{r}}_{\mathbf{n}})}{3j\omega\epsilon_{\mathbf{0}}}\right]$ (3.4.8a)

where

$$I_{x_{p}x_{q}}^{n} = P. V. \int_{V_{n}} G_{x_{p}x_{q}}(\vec{r}_{n}, \vec{r}') dV'$$
 (3.4.8b)

It is easily verified that $G_{\mathbf{x}_{\mathbf{p}}\mathbf{x}_{\mathbf{q}}}(\vec{\mathbf{r}},\vec{\mathbf{r}'})$, defined in Equation (3.3.3), is also given by

$$G_{\mathbf{x}_{\mathbf{p}}\mathbf{x}_{\mathbf{q}}}(\vec{\mathbf{r}},\vec{\mathbf{r}}^{1}) = -j\omega\mu_{\mathbf{o}}\left[\delta_{\mathbf{p}\mathbf{q}} + \frac{1}{\mathbf{k}_{\mathbf{o}}^{2}} \frac{\partial^{2}}{\partial\mathbf{x}_{\mathbf{p}}^{1}\partial\mathbf{x}_{\mathbf{q}}^{1}}\right]\psi(\vec{\mathbf{r}},\vec{\mathbf{r}}^{1})$$
(3.4.9)

All derivatives in Equation (3.4.9) are taken with respect to the variables of integration, so we may set $\vec{r} = \vec{r}_n$ at the outset. Then, since $G_{x_p x_q}(\vec{r}_n, \vec{r}_1)$ is a function of $(x^n - x^1)$, $(y^n - y^1)$, and $(z^n - z^1)$ only, we can define a coordinate system centered at \vec{r}_n , and set $\vec{r}_n = \vec{0}$. Thus,

$$\psi(\vec{0}, \vec{r}') = \psi(\vec{r}') = \psi(r') = \frac{e}{4\pi r'}$$
(3.4.10)

where

$$\mathbf{r}^{\dagger} = |\vec{\mathbf{r}}^{\dagger}|$$
.

Consequently,

$$G_{\mathbf{x}_{\mathbf{p}}\mathbf{x}_{\mathbf{q}}}(\vec{\mathbf{0}}, \vec{\mathbf{r}}^{1}) = G_{\mathbf{x}_{\mathbf{p}}\mathbf{x}_{\mathbf{q}}}(\vec{\mathbf{r}}^{1}) = -j\omega\mu_{\mathbf{0}}\left[\delta_{\mathbf{p}\mathbf{q}} + \frac{1}{k_{\mathbf{0}}^{2}} \frac{\partial^{2}}{\partial \mathbf{x}_{\mathbf{p}}^{1} \partial \mathbf{x}_{\mathbf{q}}^{1}}\right]\psi(\mathbf{r}^{1})$$
(3.4.11)

To evaluate $I_{\mathbf{x}_{p}\mathbf{x}_{q}}^{n}$, we will approximate V_{n} by a sphere S_{n} of equal volume centered about the origin of the new coordinate system, as shown in Figure 3.4a. The radius a_{n} of the sphere is given by

$$a_n = \left(\frac{3\Delta V_n}{4\pi}\right)^{1/3}$$
 (3.4.12)

Thus,

$$I_{x_{p}x_{q}}^{n} \simeq P. V. \int_{S_{n}} G_{x_{p}x_{q}}(\vec{r}') dV'$$
 (3.4.13)

The variables of integration are merely dummy variables, so we will omit the primes from here on.

It is easily shown that

$$\frac{\partial^2 \psi(\mathbf{r})}{\partial \mathbf{x}_{\mathbf{p}} \partial \mathbf{x}_{\mathbf{q}}} = \frac{d^2 \psi(\mathbf{r})}{d\mathbf{r}^2} \frac{\mathbf{x}_{\mathbf{p}}}{\mathbf{r}} \frac{\mathbf{x}_{\mathbf{q}}}{\mathbf{r}} + \frac{1}{\mathbf{r}} \frac{d \psi(\mathbf{r})}{d\mathbf{r}} \left[\delta_{\mathbf{p}\mathbf{q}} - \frac{\mathbf{x}_{\mathbf{p}}}{\mathbf{r}} \frac{\mathbf{x}_{\mathbf{q}}}{\mathbf{r}} \right]$$
(3.4.14)

In the spherical coordinate system illustrated in Figure 3.4b, we have

$$\frac{x}{r} = \sin\theta \cos\phi \tag{3.4.15a}$$

$$\frac{y}{r} = \sin\theta \sin\phi \tag{3.4.15b}$$

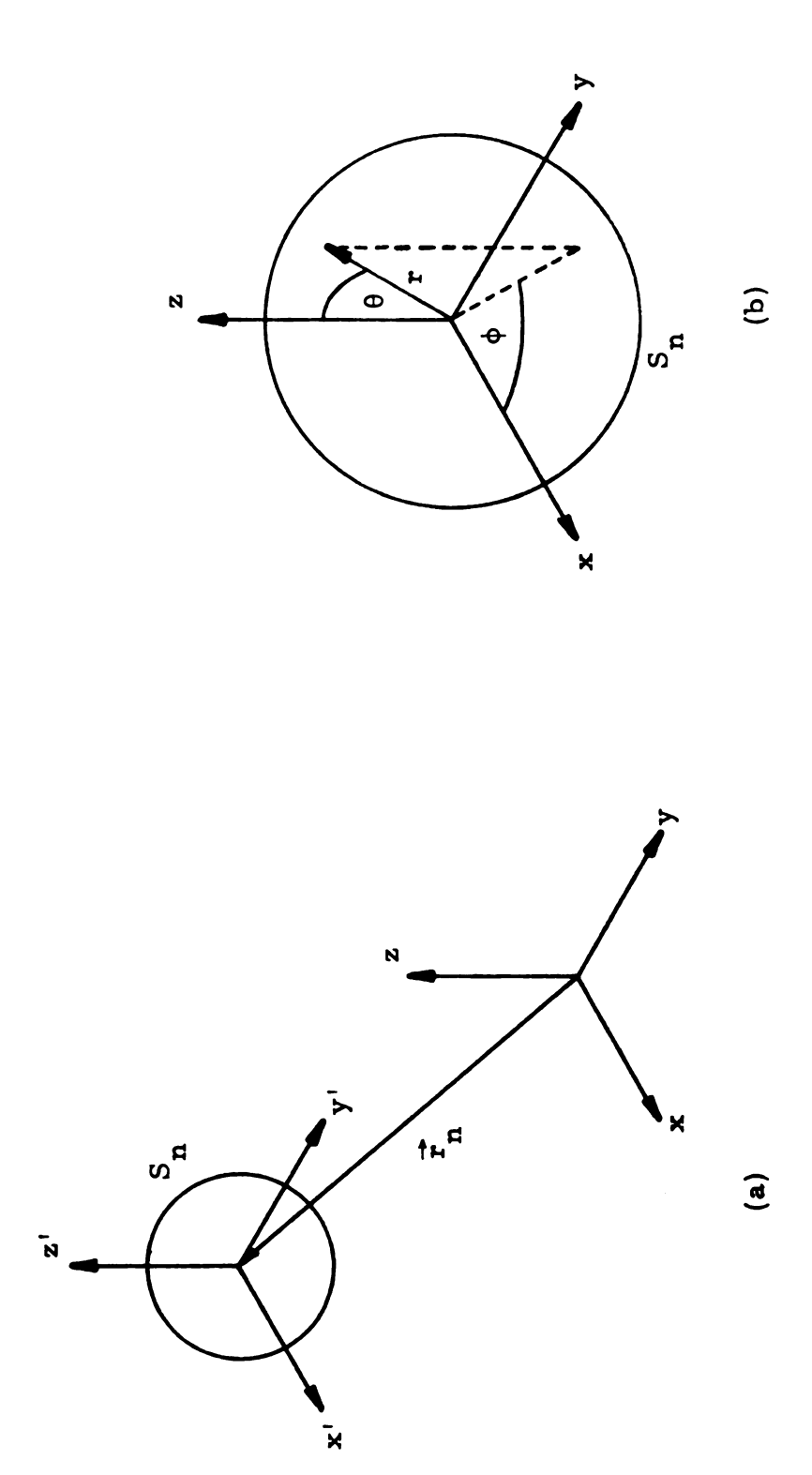
$$\frac{z}{r} = \cos \theta \tag{3.4.15c}$$

$$dV = r^2 \sin\theta \, dr \, d\theta \, d\phi \qquad (3.4.15d)$$

Therefore, since the ratio of x,y, or z to r is a function of θ and ϕ only, we write

$$f_{x_p x_q}(\theta, \phi) = \frac{x_p}{r} \frac{x_q}{r}$$
 p, q = 1,2,3. (3.4.16)

Then, using Equations (3.4.16) and (3.4.14), Equation (3.4.11) becomes



(a) Equivalent sphere S_n , centered about \vec{r}_n , used to calculate the diagonal elements of each submatrix. (b) Spherical coordinate system defined in S_n . Figure 3. 4.

$$G_{\mathbf{x}_{\mathbf{p}}\mathbf{x}_{\mathbf{q}}}(\vec{\mathbf{r}}) = -j\omega\mu_{\mathbf{o}} \left\{ \psi(\mathbf{r}) \delta_{\mathbf{p}\mathbf{q}} + \frac{1}{k_{\mathbf{o}}^{2}} \left[\frac{d^{2}\psi(\mathbf{r})}{d\mathbf{r}^{2}} f_{\mathbf{x}_{\mathbf{p}}\mathbf{x}_{\mathbf{q}}}(\theta, \phi) + \frac{1}{\mathbf{r}} \frac{d\psi(\mathbf{r})}{d\mathbf{r}} \left(\delta_{\mathbf{p}\mathbf{q}} - f_{\mathbf{x}_{\mathbf{p}}\mathbf{x}_{\mathbf{q}}}(\theta, \phi) \right) \right] \right\}$$
(3.4.17)

We now substitute Equation (3.4.17) into Equation (3.4.13) to obtain

$$\begin{split} I_{\mathbf{x}_{\mathbf{p}}\mathbf{x}_{\mathbf{q}}}^{\mathbf{n}} &= -j\omega_{\mu_{\mathbf{o}}} \lim_{\eta \to 0} \left\{ \delta_{\mathbf{p}\mathbf{q}} \int_{\eta}^{\mathbf{a}\mathbf{n}} \psi(\mathbf{r}) \, \mathbf{r}^{2} \, \mathrm{d}\mathbf{r} \int_{\mathbf{o}}^{2\pi} \mathrm{d}\phi \int_{\mathbf{o}}^{\pi} \sin\theta \, \mathrm{d}\theta \right. \\ &+ \frac{1}{k^{2}_{\mathbf{o}}} \int_{\eta}^{\mathbf{a}\mathbf{n}} \frac{\mathrm{d}^{2}\psi(\mathbf{r})}{\mathrm{d}\mathbf{r}^{2}} \, \mathbf{r}^{2} \, \mathrm{d}\mathbf{r} \int_{\mathbf{o}}^{2\pi} \mathrm{d}\phi \int_{\mathbf{o}}^{\pi} f_{\mathbf{x}_{\mathbf{p}}\mathbf{x}_{\mathbf{q}}}(\theta, \phi) \sin\theta \, \mathrm{d}\theta \\ &+ \frac{1}{k^{2}_{\mathbf{o}}} \int_{\eta}^{\mathbf{a}\mathbf{n}} \frac{\mathrm{d}\psi(\mathbf{r})}{\mathrm{d}\mathbf{r}} \, \mathbf{r} \, \mathrm{d}\mathbf{r} \int_{\mathbf{o}}^{2\pi} \mathrm{d}\phi \int_{\mathbf{o}}^{\pi} [\delta_{\mathbf{p}\mathbf{q}} - f_{\mathbf{x}_{\mathbf{p}}\mathbf{x}_{\mathbf{q}}}(\theta, \phi)] \sin\theta \, \mathrm{d}\theta \\ &+ \frac{1}{k^{2}_{\mathbf{o}}} \int_{\eta}^{\mathbf{a}\mathbf{n}} \frac{\mathrm{d}\psi(\mathbf{r})}{\mathrm{d}\mathbf{r}} \, \mathbf{r} \, \mathrm{d}\mathbf{r} \int_{\mathbf{o}}^{2\pi} \mathrm{d}\phi \int_{\mathbf{o}}^{\pi} [\delta_{\mathbf{p}\mathbf{q}} - f_{\mathbf{x}_{\mathbf{p}}\mathbf{x}_{\mathbf{q}}}(\theta, \phi)] \sin\theta \, \mathrm{d}\theta \\ &+ \frac{1}{k^{2}_{\mathbf{o}}} \int_{\eta}^{\mathbf{a}\mathbf{n}} \frac{\mathrm{d}\psi(\mathbf{r})}{\mathrm{d}\mathbf{r}} \, \mathbf{r} \, \mathrm{d}\mathbf{r} \int_{\mathbf{o}}^{2\pi} \mathrm{d}\phi \int_{\mathbf{o}}^{\pi} [\delta_{\mathbf{p}\mathbf{q}} - f_{\mathbf{x}_{\mathbf{p}}\mathbf{x}_{\mathbf{q}}}(\theta, \phi)] \sin\theta \, \mathrm{d}\theta \\ &+ \frac{1}{k^{2}_{\mathbf{o}}} \int_{\eta}^{\mathbf{a}\mathbf{n}} \frac{\mathrm{d}\psi(\mathbf{r})}{\mathrm{d}\mathbf{r}} \, \mathbf{r} \, \mathrm{d}\mathbf{r} \int_{\mathbf{o}}^{2\pi} \mathrm{d}\phi \int_{\mathbf{o}}^{\pi} [\delta_{\mathbf{p}\mathbf{q}} - f_{\mathbf{x}_{\mathbf{p}}\mathbf{x}_{\mathbf{q}}}(\theta, \phi)] \sin\theta \, \mathrm{d}\theta \\ &+ \frac{1}{k^{2}_{\mathbf{o}}} \int_{\eta}^{\mathbf{a}\mathbf{n}} \frac{\mathrm{d}\psi(\mathbf{r})}{\mathrm{d}\mathbf{r}} \, \mathbf{r} \, \mathrm{d}\mathbf{r} \int_{\mathbf{o}}^{2\pi} \mathrm{d}\phi \int_{\mathbf{o}}^{\pi} [\delta_{\mathbf{p}\mathbf{q}} - f_{\mathbf{x}_{\mathbf{p}}\mathbf{x}_{\mathbf{q}}}(\theta, \phi)] \sin\theta \, \mathrm{d}\theta \\ &+ \frac{1}{k^{2}_{\mathbf{o}}} \int_{\eta}^{\mathbf{a}\mathbf{n}} \frac{\mathrm{d}\psi(\mathbf{r})}{\mathrm{d}\mathbf{r}} \, \mathbf{r} \, \mathrm{d}\mathbf{r} \int_{\mathbf{o}}^{2\pi} \mathrm{d}\phi \int_{\mathbf{o}}^{\pi} [\delta_{\mathbf{p}\mathbf{q}} - f_{\mathbf{p}\mathbf{q}}\mathbf{r}] \, \mathbf{r} \, \mathrm{d}\phi \, \mathbf{r} \, \mathrm{$$

Integrating the second term of Equation (3.4.18) by parts and combining the result with the third term gives

$$I_{\mathbf{x}_{\mathbf{p}}\mathbf{x}_{\mathbf{q}}}^{\mathbf{n}} = -j\omega_{\mu_{o}} \lim_{\eta \to 0} \left\{ \delta_{\mathbf{p}\mathbf{q}} \int_{\eta}^{a_{\mathbf{q}}} \psi(\mathbf{r}) \, \mathbf{r}^{2} \, d\mathbf{r} \int_{o}^{2\pi} d\phi \int_{o}^{\pi} \sin\theta \, d\theta \right.$$

$$\left. + \frac{1}{k_{o}^{2}} \left[\mathbf{r}^{2} \frac{d\psi(\mathbf{r})}{d\mathbf{r}} \Big|_{\eta}^{a_{\mathbf{q}}} \right] \int_{o}^{2\pi} d\phi \int_{o}^{\pi} \mathbf{x}_{\mathbf{p}}\mathbf{x}_{\mathbf{q}}^{(\theta,\phi)} \sin\theta \, d\theta \right.$$

$$\left. + \frac{1}{k_{o}^{2}} \int_{\eta}^{a_{\mathbf{q}}} \frac{d\psi(\mathbf{r})}{d\mathbf{r}} \, \mathbf{r} \, d\mathbf{r} \int_{o}^{2\pi} d\phi \int_{o}^{\pi} [\delta_{\mathbf{p}\mathbf{q}} - 3f_{\mathbf{x}_{\mathbf{p}}\mathbf{x}_{\mathbf{q}}^{(\theta,\phi)}}] \sin\theta \, d\theta \right\}$$

$$(3.4.19)$$

In the third term of Equation (3.4.19), $\int_{\eta}^{a} \frac{d\psi(r)}{dr} r dr$ becomes infinite as $\eta \to 0$. However, using Equation (3.4.16) and Equations (3.4.15a) through (3.4.15c), it is readily verified that

$$\int_{0}^{2\pi} d\phi \int_{0}^{\pi} \left[\delta_{pq} - 3f_{x_{p}x_{q}}(\theta, \phi) \right] \sin\theta d\theta = 0$$

$$p, q = 1, 2, 3.$$
(3.4.20)

The third term of Equation (3.4.19) is therefore zero for all finite values of η , and contributes nothing as $\eta \rightarrow 0$. Thus, Equation (3.4.19)

becomes

$$I_{\mathbf{x}_{\mathbf{p}}\mathbf{x}_{\mathbf{q}}}^{\mathbf{n}} = -j\omega_{\mu_{0}} \lim_{\eta \to 0} \left\{ 4\pi \delta_{\mathbf{p}\mathbf{q}} \int_{\eta}^{\mathbf{a}_{\mathbf{n}}} \psi(\mathbf{r}) \mathbf{r}^{2} d\mathbf{r} + \frac{1}{k_{0}^{2}} \left[\mathbf{r}^{2} \frac{d\psi(\mathbf{r})}{d\mathbf{r}} \Big|_{\eta}^{\mathbf{a}_{\mathbf{n}}} \right] \int_{0}^{2\pi} d\phi \int_{0}^{\pi} \mathbf{x}_{\mathbf{p}}^{\mathbf{x}_{\mathbf{q}}}(\theta, \phi) \sin\theta d\theta \right\}$$
(3.4.21)

It can be readily demonstrated that

$$\int_{0}^{2\pi} d\phi \int_{0}^{\pi} f_{\mathbf{x}_{\mathbf{p}} \mathbf{x}_{\mathbf{q}}}(\theta, \phi) \sin \theta d\theta = \frac{4\pi}{3} \delta_{\mathbf{pq}}$$
 (3.4.22)

We then have

$$I_{\mathbf{x}_{\mathbf{p}}\mathbf{x}_{\mathbf{q}}}^{\mathbf{n}} = -j\omega_{\mu_{0}} 4\pi \delta_{\mathbf{p}\mathbf{q}} \lim_{\eta \to 0} \left\{ \int_{\eta}^{a_{\mathbf{n}}} \psi(\mathbf{r}) \mathbf{r}^{2} d\mathbf{r} + \frac{1}{3k_{0}^{2}} \left[\mathbf{r}^{2} \frac{d\psi(\mathbf{r})}{d\mathbf{r}} \Big|_{\eta}^{a_{\mathbf{n}}} \right] \right\}$$

$$-jk_{0}\mathbf{r}$$

$$(3.4.23)$$

Recalling that $\psi(r) = \frac{e^{-jk} r}{4\pi r}$, we obtain

$$I_{\mathbf{x}_{\mathbf{p}}\mathbf{x}_{\mathbf{q}}}^{\mathbf{n}} = -j\omega_{\mu_{\mathbf{0}}} \delta_{\mathbf{p}\mathbf{q}} \lim_{\eta \to 0} \left\{ \int_{\eta}^{a_{\mathbf{n}}} e^{-jk_{\mathbf{0}}\mathbf{r}} r \, d\mathbf{r} + \frac{1}{3k_{\mathbf{0}}^{2}} \left[r^{2} \frac{d}{d\mathbf{r}} \left(\frac{e^{-jk_{\mathbf{0}}\mathbf{r}}}{\mathbf{r}} \right) \right]_{\eta}^{a_{\mathbf{n}}} \right\}$$
(3.4.24)

A straightforward evaluation of Equation (3.4.24) gives

$$I_{\mathbf{x}_{\mathbf{p}}\mathbf{q}}^{\mathbf{n}} = \frac{-2 j \omega \mu_{0} \delta_{\mathbf{p}\mathbf{q}}}{3 k_{0}^{2}} \left[e^{-jk_{0}a_{\mathbf{n}}} (1 + j k_{0} a_{\mathbf{n}}) - 1 \right]$$
(3.4.25)

The desired expression for the diagonal matrix elements is found by substituting Equation (3.4.25) into Equation (3.4.8a):

$$G_{x_{\mathbf{p}}x_{\mathbf{q}}}^{\mathbf{nn}} = -\delta_{\mathbf{pq}} \left\{ \frac{2j\omega_{\mu_{o}}\tau(\vec{\mathbf{r}}_{\mathbf{n}})}{3k_{o}^{2}} \left[e^{-jk_{o}a_{\mathbf{n}}} (1+jk_{o}a_{\mathbf{n}}) - 1 \right] + \left[1 + \frac{\tau(\vec{\mathbf{r}}_{\mathbf{n}})}{3j\omega\epsilon_{o}} \right] \right\}$$
(3. 4. 26a)

$$G_{\mathbf{x}_{\mathbf{p}}\mathbf{x}_{\mathbf{q}}}^{\mathbf{n}\mathbf{n}} = \frac{j\omega_{\mu_{\mathbf{o}}}\delta_{\mathbf{p}\mathbf{q}}}{3k_{\mathbf{o}}^{2}} \left\{ 3\left[\tau(\mathbf{r}_{\mathbf{n}}) + j\omega\epsilon_{\mathbf{o}}\right] - 2\tau(\mathbf{r}_{\mathbf{n}}) e^{-jk_{\mathbf{o}}\mathbf{a}_{\mathbf{n}}} (1 + jk_{\mathbf{o}}\mathbf{a}_{\mathbf{n}}) \right\}$$
(3.4.26b)

If the actual shape of V_n differs appreciably from that of a sphere, Equation (3.4.25) can be applied to a small sphere surrounding \vec{r}_n ; the integration over the remainder of V_n can be done numerically.

3.5. Reduction of Matrix Size for Special Cases of Cross-Sectional Symmetry

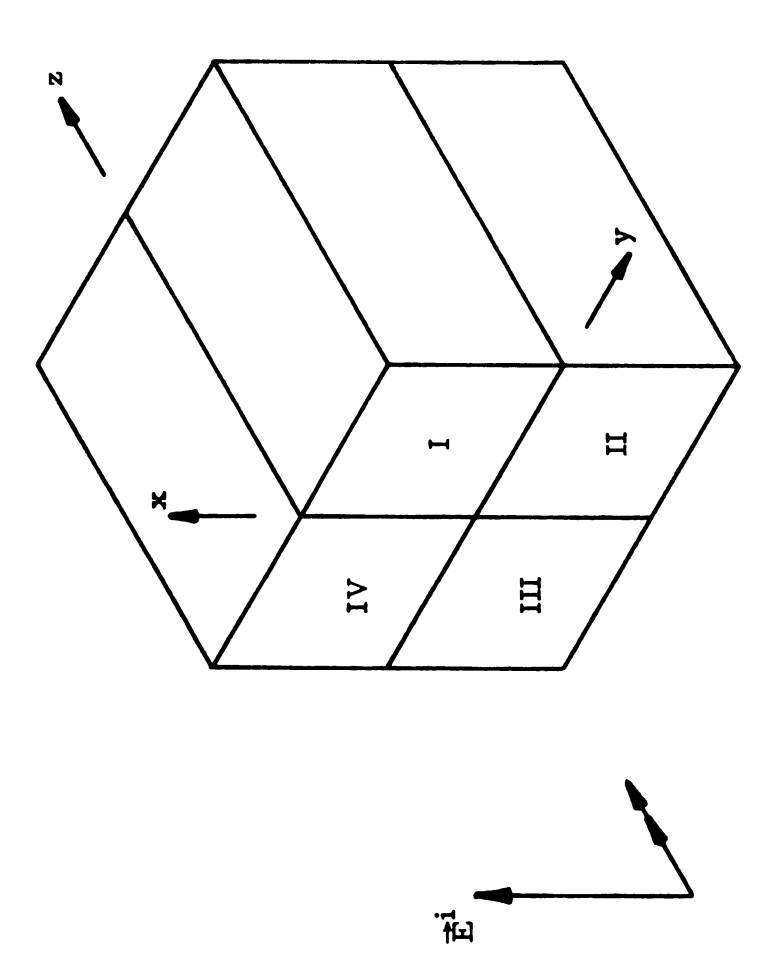
It is possible in some cases to reduce the number of unknowns in Equation (3.3.16), thereby effecting a substantial saving in computer storage space. To illustrate the method, we will consider the cubical body shown in Figure 3.5.

We will assume that the incident electric field is a plane wave, given by

$$\vec{\mathbf{E}}^{i}(\vec{\mathbf{r}}) = \mathbf{\hat{x}} \mathbf{E}_{o} e^{-j\mathbf{k}_{o} \mathbf{z}} , \qquad (3.5.1)$$

and that $\vec{E}^{i}(\vec{r})$ is incident normally upon the face of the cube.

The body's cross section is symmetrical about the z-axis, and about the planes x = 0 and y = 0. We will assume that the electrical properties of the cube are likewise symmetrical. The planes of symmetry divide the cube into four quadrants, which are indicated by Roman numerals in Figure 3.5. We could proceed with the calculation of $\vec{E}(\vec{r})$ inside the body in a purely straightforward manner; that is, we could partition the cube into, say, 4N subvolumes (N in each quadrant), and compute $\vec{E}(\vec{r})$ in each cell. However, under the assumed conditions, we need only determine $\vec{E}(\vec{r})$ in one quadrant; the electric field in the other quadrants can be obtained by utilizing the symmetry of the body. Thus, as we shall show, we can determine $\vec{E}(\vec{r})$ at 4N points in the cube by solving a matrix equation involving the unknown electric field at only N points.



The quadrants A cubical body partitioned into symmetrical quadrants. are designated by Roman numerals. Figure 3.5.

Following a procedure similar to that used in Section 3.3, we partition the first quadrant into N cells, or subvolumes, and assume that $\tau(\vec{r})$ and $\vec{E}(\vec{r})$ are constant throughout each cell. We denote the mth subvolume by V_{m_1} , and its location by \vec{r}_{m_1} , where the subscript "1" refers to the first quadrant. By reflecting V_{m_1} and \vec{r}_{m_1} about the plane x = 0, the z-axis, and the plane y = 0, we obtain their respective images in the other quadrants: V_{m_2} and \vec{r}_{m_2} in the second quadrant, V_{m_3} and \vec{r}_{m_3} in the third, and V_{m_4} and \vec{r}_{m_4} in the fourth. By assumption,

$$\tau(\vec{r}_{m_1}) = \tau(\vec{r}_{m_2}) = \tau(\vec{r}_{m_3}) = \tau(\vec{r}_{m_4})$$
 (3.5.2)

We require that Equation (3.2.16) be satisfied at each \vec{r}_{m_1} . Proceeding as in Section 3.3, we have

$$\sum_{q=1}^{3} \sum_{n=1}^{N} \left[G_{x_{p} x_{q}}^{mn_{1}} E_{x_{q}}(\vec{r}_{n_{1}}) + G_{x_{p} x_{q}}^{mn_{2}} E_{x_{q}}(\vec{r}_{n_{2}}) + G_{x_{p} x_{q}}^{mn_{3}} E_{x_{q}}(\vec{r}_{n_{3}}) + G_{x_{p} x_{q}}^{mn_{4}} E_{x_{q}}(\vec{r}_{n_{4}}) \right] = -E_{x_{p}}^{i}(\vec{r}_{m_{1}}) \qquad (3.5.3a)$$

$$m = 1, 2, ..., N,$$

$$p = 1, 2, 3,$$

where

$$G_{\mathbf{x}_{\mathbf{p}}\mathbf{x}_{\mathbf{q}}}^{\mathbf{mn}_{\mathbf{1}}} = \tau(\vec{\mathbf{r}}_{\mathbf{n}_{\mathbf{1}}}) P. V. \int_{V_{\mathbf{n}_{\mathbf{1}}}} G_{\mathbf{x}_{\mathbf{p}}\mathbf{x}_{\mathbf{q}}} (\vec{\mathbf{r}}_{\mathbf{m}_{\mathbf{1}}}, \vec{\mathbf{r}}') dV' - \delta_{\mathbf{p}\mathbf{q}} \delta_{\mathbf{mn}} \left[1 + \frac{\tau(\vec{\mathbf{r}}_{\mathbf{m}_{\mathbf{1}}})}{3j\omega\epsilon_{\mathbf{0}}} \right]$$
(3.5.3b)

and

$$G_{\mathbf{x}_{\mathbf{p}}\mathbf{q}}^{\mathbf{m}_{\mathbf{j}}} = \tau(\vec{\mathbf{r}}_{\mathbf{n}_{1}}) \int_{V_{\mathbf{n}_{\mathbf{j}}}} G_{\mathbf{x}_{\mathbf{p}}\mathbf{q}}(\vec{\mathbf{r}}_{\mathbf{m}_{1}}, \vec{\mathbf{r}}') dV', \qquad (3.5.3c)$$

The principal value has been omitted in Equation (3.5.3c) because the integrands are continuous throughout the regions of integration.

Under the assumed conditions of symmetry and normal incidence, with $\vec{E}^{i}(\vec{r})$ linearly polarized along the x-axis, we can determine by inspection (and verify by computation) the following relations:

$$E_{\mathbf{x}}(\vec{r}_{n_1}) = E_{\mathbf{x}}(\vec{r}_{n_2}) = E_{\mathbf{x}}(\vec{r}_{n_3}) = E_{\mathbf{x}}(\vec{r}_{n_4})$$
 (3.5.4a)

$$E_{y}(\vec{r}_{n_{1}}) = -E_{y}(\vec{r}_{n_{2}}) = E_{y}(\vec{r}_{n_{3}}) = -E_{y}(\vec{r}_{n_{4}})$$
 (3.5.4b)

$$E_{z}(\vec{r}_{n_{1}}) = -E_{z}(\vec{r}_{n_{2}}) = -E_{z}(\vec{r}_{n_{3}}) = E_{z}(\vec{r}_{n_{4}})$$
 (3.5.4c)

Thus, Equation (3.5.3a) may be rewritten as

$$\sum_{n=1}^{N} \left[G_{x_{p}x}^{mn_{1}} + G_{x_{p}x}^{mn_{2}} + G_{x_{p}x}^{mn_{3}} + G_{x_{p}x}^{mn_{4}} \right] E_{x}(\vec{r}_{n_{1}})
+ \sum_{n=1}^{N} \left[G_{x_{p}y}^{mn_{1}} - G_{x_{p}y}^{mn_{2}} + G_{x_{p}y}^{mn_{3}} - G_{x_{p}y}^{mn_{4}} \right] E_{y}(\vec{r}_{n_{1}})
+ \sum_{n=1}^{N} \left[G_{x_{p}z}^{mn_{1}} - G_{x_{p}z}^{mn_{2}} - G_{x_{p}z}^{mn_{3}} + G_{x_{p}z}^{mn_{4}} \right] E_{z}(\vec{r}_{n_{1}}) = - E_{x_{p}}^{i}(\vec{r}_{m_{1}})$$
(3.5.5)

$$m = 1, 2, ..., N$$
, $p = 1, 2, 3$.

Let $[\mathcal{A}_{x_D x}]$, $[\mathcal{A}_{x_D y}]$, and $[\mathcal{A}_{x_D z}]$ be NxN matrices whose respective

$$A_{x_p}^{mn} = G_{x_p}^{mn_1} + G_{x_p}^{mn_2} + G_{x_p}^{mn_3} + G_{x_p}^{mn_4}$$
 (3.5.6a)

$$x_{py}^{mn} = G_{x_{py}}^{mn_1} - G_{x_{py}}^{mn_2} + G_{x_{py}}^{mn_3} - G_{x_{py}}^{mn_4}$$
 (3.5.6b)

$$\mathcal{A}_{\mathbf{x}_{p}\mathbf{x}}^{mn} = G_{\mathbf{x}_{p}\mathbf{x}}^{mn_{1}} + G_{\mathbf{x}_{p}\mathbf{x}}^{mn_{2}} + G_{\mathbf{x}_{p}\mathbf{x}}^{mn_{3}} + G_{\mathbf{x}_{p}\mathbf{x}}^{mn_{4}}$$

$$\mathcal{A}_{\mathbf{x}_{p}\mathbf{y}}^{mn} = G_{\mathbf{x}_{p}\mathbf{y}}^{mn_{1}} - G_{\mathbf{x}_{p}\mathbf{y}}^{mn_{2}} + G_{\mathbf{x}_{p}\mathbf{y}}^{mn_{3}} - G_{\mathbf{x}_{p}\mathbf{y}}^{mn_{4}}$$

$$\mathcal{A}_{\mathbf{x}_{p}\mathbf{z}}^{mn} = G_{\mathbf{x}_{p}\mathbf{z}}^{mn_{1}} - G_{\mathbf{x}_{p}\mathbf{z}}^{mn_{2}} - G_{\mathbf{x}_{p}\mathbf{z}}^{mn_{3}} + G_{\mathbf{x}_{p}\mathbf{z}}^{mn_{4}}$$

$$\mathcal{A}_{\mathbf{x}_{p}\mathbf{z}}^{mn} = G_{\mathbf{x}_{p}\mathbf{z}}^{mn_{1}} - G_{\mathbf{x}_{p}\mathbf{z}}^{mn_{2}} - G_{\mathbf{x}_{p}\mathbf{z}}^{mn_{3}} + G_{\mathbf{x}_{p}\mathbf{z}}^{mn_{4}}$$
(3.5.6c)

$$p = 1, 2, 3.$$

Equation (3.5.5) then becomes

$$\sum_{q=1}^{3} \sum_{n=1}^{N} \sum_{x_{p} \neq q}^{mn} E_{x_{q}}(\vec{r}_{n_{1}}) = -E_{x_{p}}^{i}(\vec{r}_{m_{1}})$$

$$m = 1, 2, ..., N,$$

$$p = 1, 2, 3.$$
(3.5.7)

As explained in Section 3.3, Equation (3.5.7) is equivalent to the following as m and p range over all possible values:

$$\begin{bmatrix}
[\mathcal{A}_{xx}] & [\mathcal{A}_{xy}] & [\mathcal{A}_{xz}] \\
[\mathcal{A}_{yx}] & [\mathcal{A}_{yy}] & [\mathcal{A}_{yz}] \\
[\mathcal{A}_{zx}] & [\mathcal{A}_{zy}] & [\mathcal{A}_{zz}]
\end{bmatrix}
\begin{bmatrix}
[E_{x}]_{1} \\
[E_{y}]_{1} \\
[E_{z}]_{1}
\end{bmatrix} = -\begin{bmatrix}
[E_{x}^{i}]_{1} \\
[E_{y}^{i}]_{1} \\
[E_{z}^{i}]_{1}
\end{bmatrix}$$
(3.5.8)

where $\begin{bmatrix} E_x \\ p \end{bmatrix}$ and $\begin{bmatrix} E_x^i \\ p \end{bmatrix}$, p = 1, 2, 3, are defined by Equations (3.3.12a) and (3.3.12b), respectively. The subscript "1" again refers to values in the first quadrant.

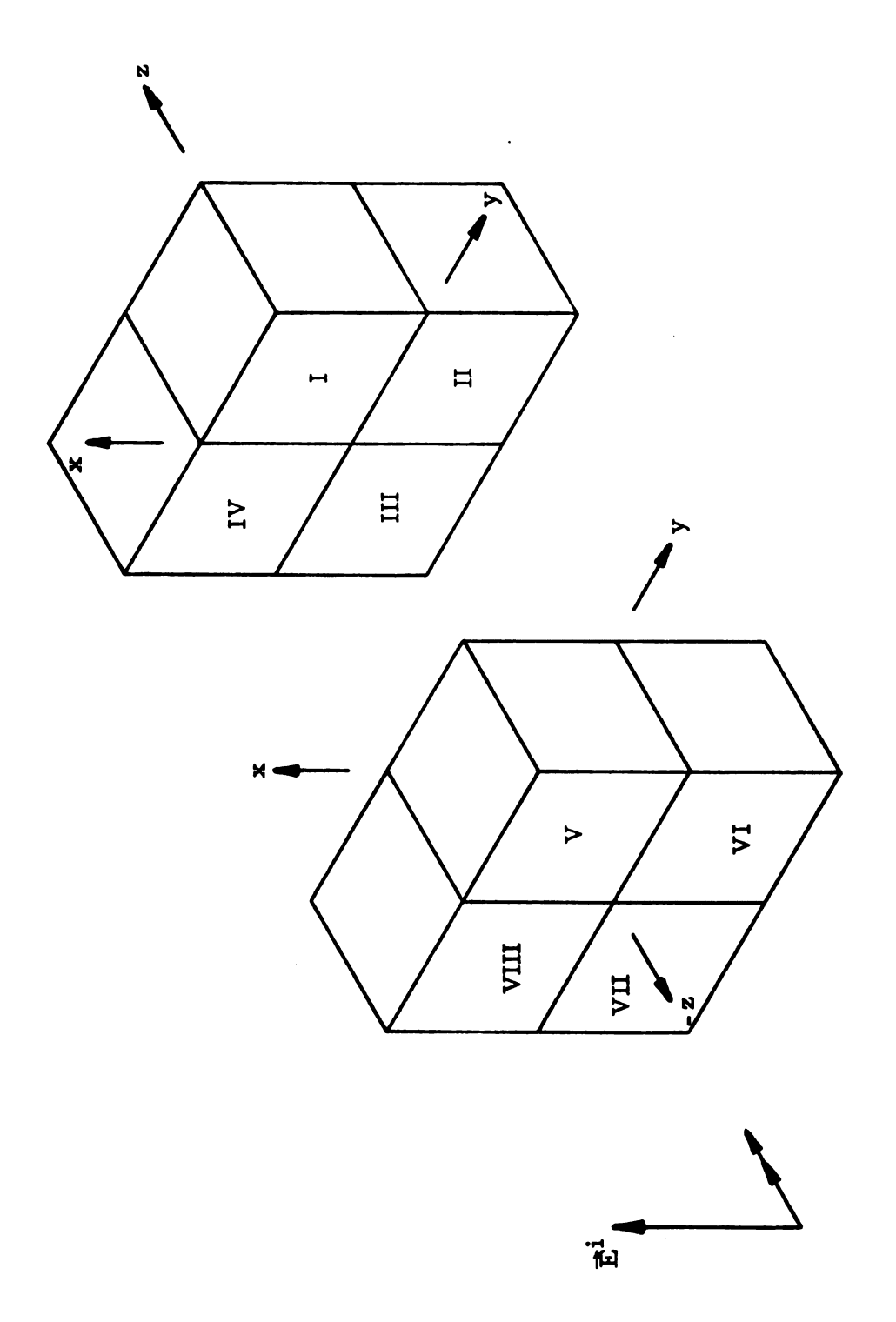
We may write Equation (3.5.8) in more compact form:

$$[\mathcal{A}][\mathbf{E}]_{1} = -[\mathbf{E}^{\mathbf{i}}]_{1} \tag{3.5.9}$$

where [\$\mathbb{4}\$] is a 3N x 3N matrix, and both [E]₁ and [E¹]₁ have 3N components. After we solve Equation (3.5.9) for [E]₁, we obtain [E]₂, [E]₃, and [E]₄ via Equations (3.5.4a) through (3.5.4c). Had we solved Equation (3.3.16) for [E] in the entire body, we would have had 12N unknowns. Thus, we have reduced the number of unknowns (and the matrix size) by a factor of 4. However, the amount of computation needed to evaluate each matrix element has increased by the same factor.

We can sometimes reduce the number of unknowns by an additional factor of 2, at the expense of computation time, by decomposing the incident plane wave into symmetric and anti-symmetric modes. We will again use the cubical body to briefly outline the method.

The origin of the coordinate system will be located at the center of the cube, with the axes oriented as shown in Figure 3.6. The planes x = 0, y = 0, and z = 0 divide the cube into eight octants. We partition the first octant into N subvolumes, as before, and denote the mth



A cubical body partitioned into symmetrical octants, designated by Roman numerals. The origin of the coordinate system is located at the center of the numerals. cube. Figure 3.6.

subvolume and its location by V_{m_1} and \vec{r}_{m_1} , respectively. Again, V_{m_1} and \vec{r}_{m_1} have images in each of the other octants. We assume that

$$\tau(\vec{r}_{m_1}) = \tau(\vec{r}_{m_2}) = \tau(\vec{r}_{m_3}) = \tau(\vec{r}_{m_4})$$

$$= \tau(\vec{r}_{m_5}) = \tau(\vec{r}_{m_6}) = \tau(\vec{r}_{m_7}) = \tau(\vec{r}_{m_8}), \qquad (3.5.10)$$

where the numerical subscript once again refers to the octant in which the point is located.

The incident electric field, given by Equation (3.5.1), can be written as

$$\vec{\mathbf{E}}^{i}(\vec{\mathbf{r}}) = \vec{\mathbf{E}}_{s}^{i}(\vec{\mathbf{r}}) + \vec{\mathbf{E}}_{a}^{i}(\vec{\mathbf{r}}), \qquad (3.5.11a)$$

where

$$\vec{E}_{s}^{i}(\vec{r}) = \hat{x} E_{o} \cos k_{o} z \qquad (3.5.11b)$$

$$\vec{E}_a^i(\vec{r}) = - \hat{x} j E_0 \sin k_0 z. \qquad (3.5.11c)$$

 $\vec{E}_{s}^{i}(\vec{r})$ represents a symmetric mode of exciting the cube, while $\vec{E}_{a}^{i}(\vec{r})$ is an anti-symmetric mode. $\vec{E}_{s}^{i}(\vec{r})$ and $\vec{E}_{a}^{i}(\vec{r})$ are illustrated in Figures 3.7a and 3.7b, respectively.

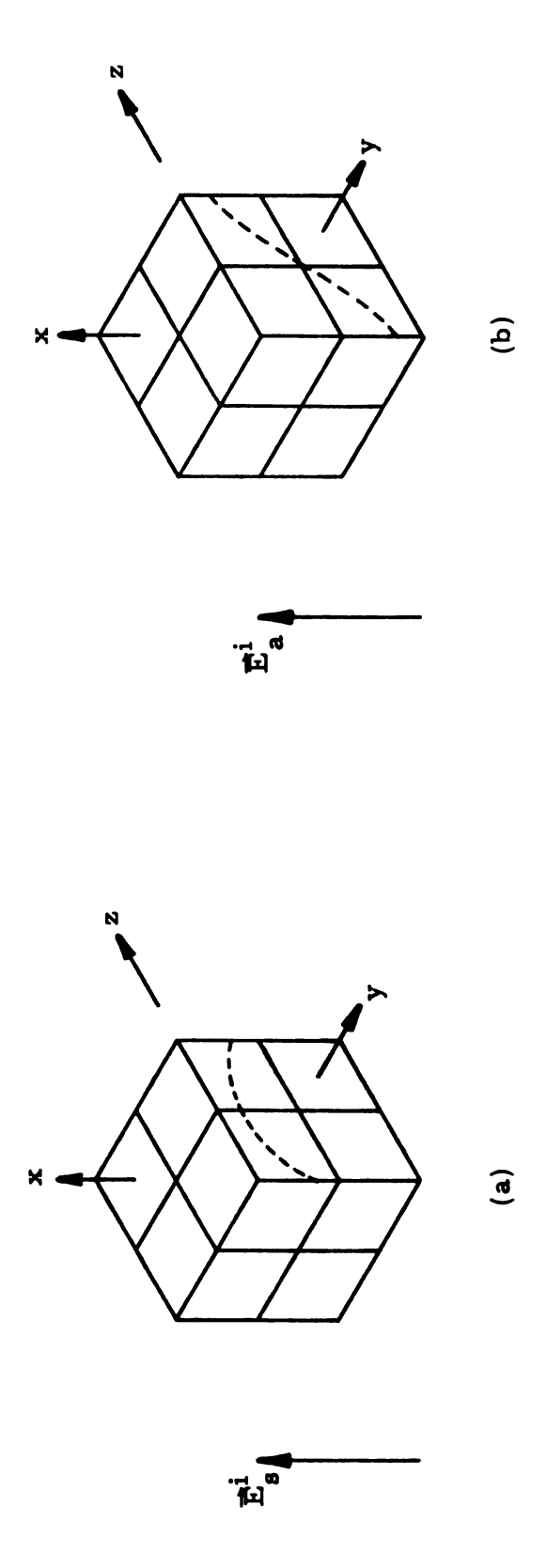
Let $\vec{E}_s(\vec{r})$ be the internal electric field induced by $\vec{E}_s^i(\vec{r})$. The components of $\vec{E}_s(\vec{r})$ obey the following relations:

$$E_{\mathbf{x}\mathbf{s}}(\vec{\mathbf{r}}_{\mathbf{m}_{1}}) = E_{\mathbf{x}\mathbf{s}}(\vec{\mathbf{r}}_{\mathbf{m}_{2}}) = E_{\mathbf{x}\mathbf{s}}(\vec{\mathbf{r}}_{\mathbf{m}_{3}}) = E_{\mathbf{x}\mathbf{s}}(\vec{\mathbf{r}}_{\mathbf{m}_{4}})$$

$$= E_{\mathbf{x}\mathbf{s}}(\vec{\mathbf{r}}_{\mathbf{m}_{5}}) = E_{\mathbf{x}\mathbf{s}}(\vec{\mathbf{r}}_{\mathbf{m}_{6}}) = E_{\mathbf{x}\mathbf{s}}(\vec{\mathbf{r}}_{\mathbf{m}_{7}}) = E_{\mathbf{x}\mathbf{s}}(\vec{\mathbf{r}}_{\mathbf{m}_{8}}) \qquad (3.5.12a)$$

$$E_{ys}(\vec{r}_{m_1}) = -E_{ys}(\vec{r}_{m_2}) = E_{ys}(\vec{r}_{m_3}) = -E_{ys}(\vec{r}_{m_4})$$

$$= E_{ys}(\vec{r}_{m_5}) = -E_{ys}(\vec{r}_{m_6}) = E_{ys}(\vec{r}_{m_7}) = -E_{ys}(\vec{r}_{m_8}) \quad (3.5.12b)$$



Cubical body excited by (a) the symmetric mode \vec{E}_{g} , and (b) the anti-symmetric mode \vec{E}_{g}^{i} . The octants of the cube are numbered as in Figure 3.6. Figure 3. 7.

$$E_{zs}(\vec{r}_{m_1}) = -E_{zs}(\vec{r}_{m_2}) = -E_{zs}(\vec{r}_{m_3}) = E_{zs}(\vec{r}_{m_4})$$

$$= -E_{zs}(\vec{r}_{m_5}) = E_{zs}(\vec{r}_{m_6}) = E_{zs}(\vec{r}_{m_7}) = -E_{zs}(\vec{r}_{m_8}) . (3.5.12c)$$

Similarly, let $\vec{E}_a(\vec{r})$ be the field induced by $\vec{E}_a^i(\vec{r})$. Then, the components of $\vec{E}_a(\vec{r})$ satisfy

$$E_{xa}(\vec{r}_{m_1}) = E_{xa}(\vec{r}_{m_2}) = E_{xa}(\vec{r}_{m_3}) = E_{xa}(\vec{r}_{m_4})$$

$$= -E_{xa}(\vec{r}_{m_5}) = -E_{xa}(\vec{r}_{m_6}) = -E_{xa}(\vec{r}_{m_7}) = -E_{xa}(\vec{r}_{m_8}) (3.5.13a)$$

$$E_{ya}(\vec{r}_{m_1}) = -E_{ya}(\vec{r}_{m_2}) = E_{ya}(\vec{r}_{m_3}) = -E_{ya}(\vec{r}_{m_4})$$

$$= -E_{ya}(\vec{r}_{m_5}) = E_{ya}(\vec{r}_{m_6}) = -E_{ya}(\vec{r}_{m_7}) = E_{ya}(\vec{r}_{m_8}) (3.5.13b)$$

$$E_{za}(\vec{r}_{m_1}) = -E_{za}(\vec{r}_{m_2}) = -E_{za}(\vec{r}_{m_3}) = E_{za}(\vec{r}_{m_4})$$

$$= E_{za}(\vec{r}_{m_5}) = -E_{za}(\vec{r}_{m_6}) = -E_{za}(\vec{r}_{m_7}) = E_{za}(\vec{r}_{m_8}) . (3.5.13c)$$

The total electric field inside the cube, with $\vec{E}^i(\vec{r})$ given by Equation (3.5.1), is found in three steps. First, using $\vec{E}^i_g(\vec{r})$ as the incident field, we require that Equation (3.2.16) be satisfied at each of the N points in the first octant. Proceeding as we did in the first part of this section, we use Equations (3.5.12a) through (3.5.12c) to reduce the number of unknowns by a factor of 8. After we solve the resulting matrix equation for $\vec{E}_g(\vec{r})$ in the first octant, we can find $\vec{E}_g(\vec{r})$ in the other octants via Equations (3.5.12a) through (3.5.12c).

Next, we use $\vec{E}_a^i(\vec{r})$ as the incident field, and compute $\vec{E}_a(\vec{r})$ in the first octant. We can again reduce the number of unknowns by using Equations (3.5.13a) through (3.5.13c). Once we have found $\vec{E}_a(\vec{r})$ in the first octant, we obtain $\vec{E}_a(\vec{r})$ in the other octants by employing Equations (3.5.13a) through (3.5.13c).

Finally, because of the linearity of Equation (3.2.16), the total induced electric field in the cube due to $\vec{E}^{i}(\vec{r})$ is simply

$$\vec{\mathbf{E}}(\vec{\mathbf{r}}) = \vec{\mathbf{E}}_{\mathbf{s}}(\vec{\mathbf{r}}) + \vec{\mathbf{E}}_{\mathbf{a}}(\vec{\mathbf{r}}) . \qquad (3.5.14)$$

Although we have reduced the number of unknowns by decomposing $\vec{E}^i(\vec{r})$ into symmetric and anti-symmetric modes, there are obvious disadvantages. First, we must solve two problems: a body excited by $\vec{E}^i_g(\vec{r})$, and a body excited by $\vec{E}^i_a(\vec{r})$. Second, each matrix element will contain eight terms. Finally, we must pay careful attention to the algebraic sign of the field components in the various octants when we add $\vec{E}_g(\vec{r})$ and $\vec{E}_a(\vec{r})$. Nevertheless, if computer storage space is limited, the decomposition of $\vec{E}^i(\vec{r})$ into symmetric and anti-symmetric modes may prove useful.

3.6. Calculation of External Scattered Field

We will frequently be interested in finding the scattered field outside the physiological system. Once $\vec{E}(\vec{r})$ has been determined inside the body, the external scattered field is given by Equations (3.2.6a) and (3.2.13):

$$\vec{\mathbf{E}}^{\mathbf{S}}(\vec{\mathbf{r}}) = \int_{\mathbf{V}} \boldsymbol{\tau}(\vec{\mathbf{r}}^{\scriptscriptstyle{\dagger}}) \, \vec{\mathbf{E}}(\vec{\mathbf{r}}^{\scriptscriptstyle{\dagger}}) \cdot \vec{\mathbf{G}}(\vec{\mathbf{r}}, \vec{\mathbf{r}}^{\scriptscriptstyle{\dagger}}) \, dV' \quad . \tag{3.6.1}$$

Using the notation developed in Section 3.3, we may write each scalar component of $\vec{E}^{s}(\vec{r})$ as

$$\mathbf{E}_{\mathbf{x}p}^{\mathbf{s}}(\vec{\mathbf{r}}) = \int_{\mathbf{V}} \tau(\vec{\mathbf{r}}) \begin{bmatrix} 3 \\ \Sigma \\ \mathbf{q} = 1 \end{bmatrix} \mathbf{G}_{\mathbf{x}p} \mathbf{x}_{\mathbf{q}} (\vec{\mathbf{r}}, \vec{\mathbf{r}}) \mathbf{E}_{\mathbf{x}q} (\vec{\mathbf{r}}) dV'$$

$$\mathbf{p} = 1, 2, 3.$$
(3.6.2)

Since the volume V has been partitioned into N cells, with $\tau(\vec{r})$ and $\vec{E}(\vec{r})$ assumed to be constant throughout each cell, Equation (3.6.2) becomes

$$E_{\mathbf{x}_{\mathbf{p}}}^{\mathbf{g}}(\vec{\mathbf{r}}) = \sum_{n=1}^{N} \int_{V_{\mathbf{p}}} \tau(\vec{\mathbf{r}}_{\mathbf{n}}) \left[\sum_{q=1}^{3} G_{\mathbf{x}_{\mathbf{p}}} \mathbf{x}_{\mathbf{q}}(\vec{\mathbf{r}}, \vec{\mathbf{r}}') E_{\mathbf{x}_{\mathbf{q}}}(\vec{\mathbf{r}}_{\mathbf{n}}) \right] dV' \qquad (3.6.3a)$$

or

$$E_{\mathbf{x}p}^{\mathbf{g}}(\vec{\mathbf{r}}) = \sum_{n=1}^{N} \sum_{q=1}^{3} \tau(\vec{\mathbf{r}}_{n}) E_{\mathbf{x}q}(\vec{\mathbf{r}}_{n}) \int_{V_{n}} G_{\mathbf{x}p}^{\mathbf{g}}(\vec{\mathbf{r}}, \vec{\mathbf{r}}') dV' \qquad (3.6.3b)$$

$$p = 1, 2, 3.$$

The integral in Equation (3.6.3b) has the same form as the integral in Equation (3.4.2), so it can be evaluated by the methods outlined in Section 3.4. Therefore, after we have found the N values of $\vec{E}(\vec{r})$ inside the physiological system, we can determine the scattered field at any exterior point by using Equation (3.6.3b).

3.7. Numerical and Experimental Results

A number of simple biological models have been studied using the moment solution of Equation (3.2.16). The results in this section illustrate the variety of problems which can be solved by this method. Since techniques for probing the induced field inside a conducting medium are still being perfected, the only experimental results to be presented are those describing the scattering from finite conducting cylinders. The data presented in this section is grouped into 4 general categories: testing and convergence, determination of the internal electric field, the external scattered field, and an investigation of the symmetric and anti-symmetric modes discussed in Section 3.5.

The incident electric field for all of the examples had a magnitude of 1 Volt per meter, and was polarized along the x-axis. Where possible, the symmetry methods of Section 3.5 were used; in most such cases, an illustration indicates the portion of the body in which the induced field was calculated. The subvolumes in all of the examples were cubes,

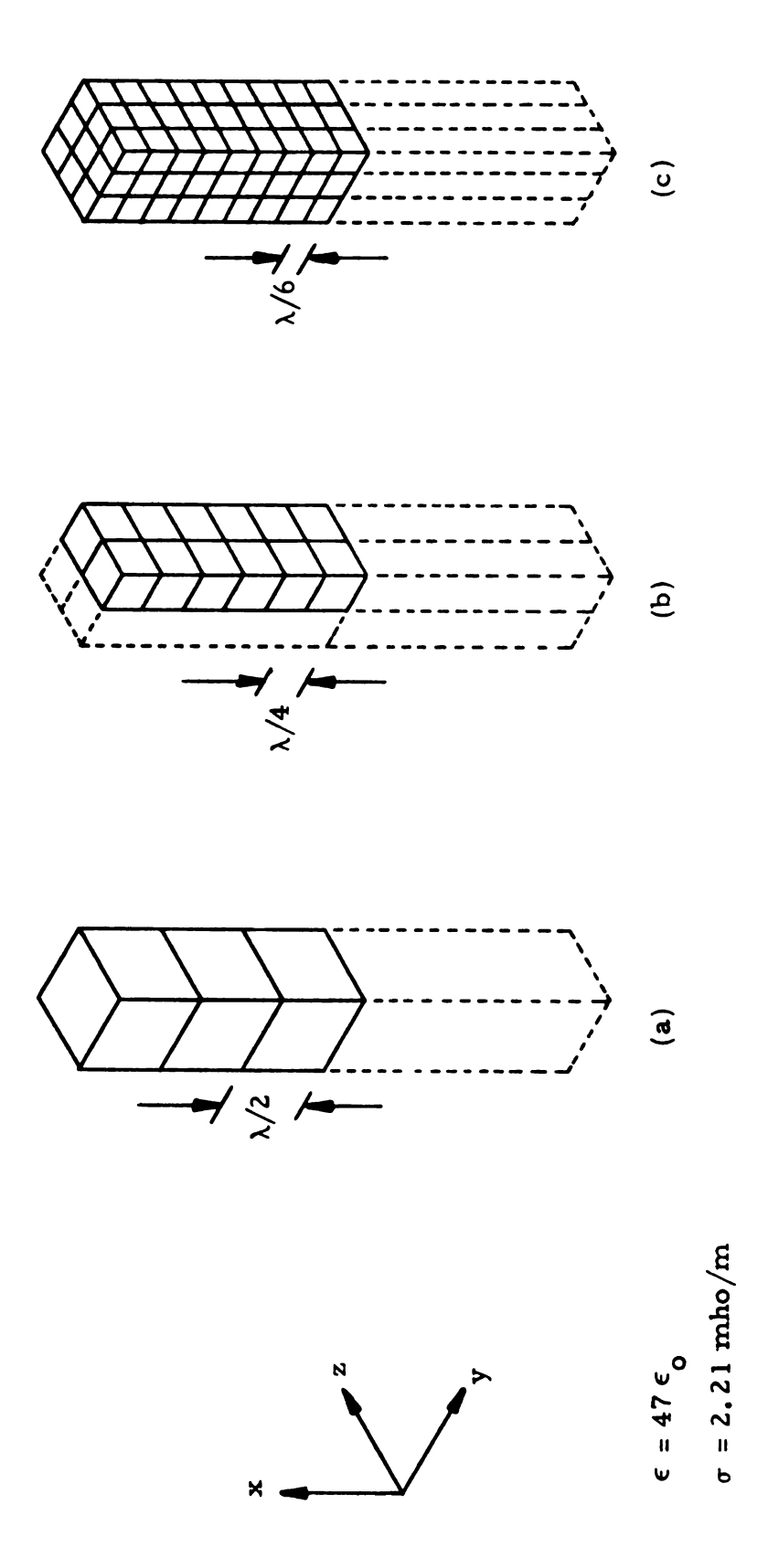
so that the expression for the diagonal matrix elements would be reasonably accurate, and the induced field was calculated at the center of each subvolume. Equation (3.4.5a) was used to evaluate the off-diagonal matrix elements for the examples shown in Figures 3.11 through 3.18. For the other examples, the off-diagonal elements were computed by numerically integrating Equation (3.4.2).

A. Testing and Convergence

This group of calculations was performed to test the convergence of the numerical solution, and to acquire confidence in its accuracy.

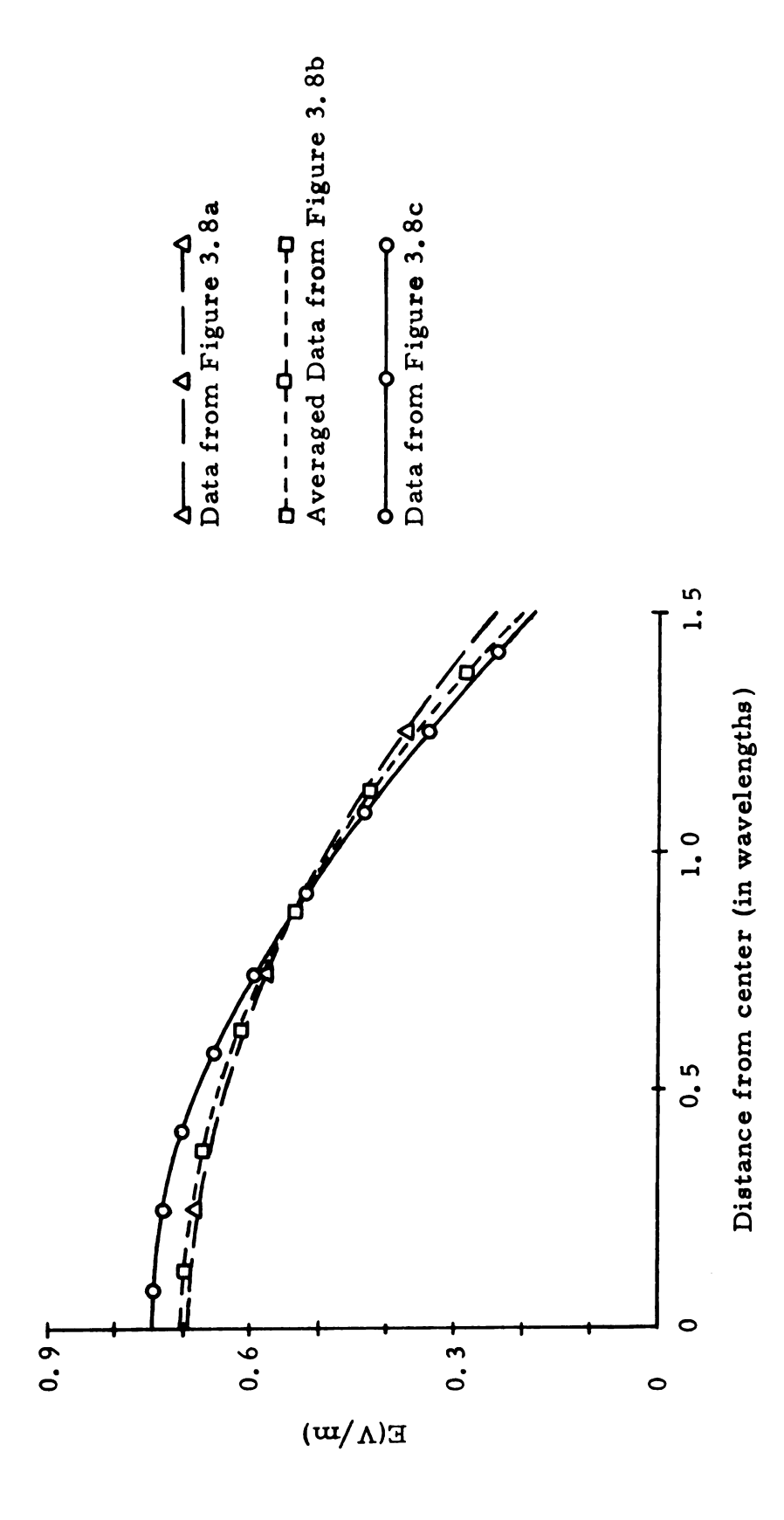
The following two examples examine the convergence of the solution as the size of each subvolume in the body is decreased. In the first test, a 2.45 GHz plane wave illuminated a muscle cylinder whose dimensions in wavelengths were $3 \times 1/2 \times 1/2$. The incident electric field was parallel to the axis of the cylinder, so that the induced field had essentially only an axial component. The cylinder was divided into a variable number of subvolumes, and the induced field was calculated for each configuration. The models for 6, 48, and 162 subvolumes are shown in Figures 3.8a, 3.8b, and 3.8c, respectively. The edges of each cell measured 1/2, 1/4, and 1/6 wavelength, respectively.

Figure 3. 9 shows the electric field intensity along the axis of the cylinder for each model depicted in Figure 3. 8. Since none of the subvolumes lie on the axis in Figure 3. 8b, the average of the fields in the front and back of the cylinder have been plotted to facilitate a comparison with the results from Figures 3. 8a and 3. 8c. All three models are in good agreement, indicating that using subvolumes as large as even 1/2 wavelength may yield useful data in some cases.



Frequency = 2.45 GHz

A cylinder of muscle partitioned into (a) 6, (b) 48, and (c) 162 subvolumes. The cylinder is illuminated by a 2.45 GHz plane wave, with the incident electric field \vec{E}^i parallel to the axis of the cylinder. $|\vec{E}^i|=1$ V/m. Figure 3.8.



Electric field intensity along the axis of the cylinder shown in Figure 3.8, for models (a), (b), and (c). $|\vec{E}^1| = 1 \text{ V/m}$. One wavelength in the cylinder is models (a), (b), and (c). 1.76 cm. Figure 3.9.

In the next test, the cube of muscle illustrated in Figure 3.10a was considered. The cube was exposed to a 2.45 GHz plane wave, and each of its edges measured 1 wavelength. The cube was treated as a single cell, and the electric field at its center was calculated. Next, the cube was partitioned into 27 subvolumes, as indicated in Figure 3.10b. The induced field was again determined, and the field intensity in the center cell was compared to the value obtained from the first calculation. The procedure was repeated for the quarter-wavelength cube shown in Figures 3.10c and 3.10d, and the results are presented in Table 3.1. Noting that the two values agree well for the quarter-wavelength cube, and recalling the results of the previous test, we will take 1/4 wavelength as an upper bound for the largest dimension of any subvolume.

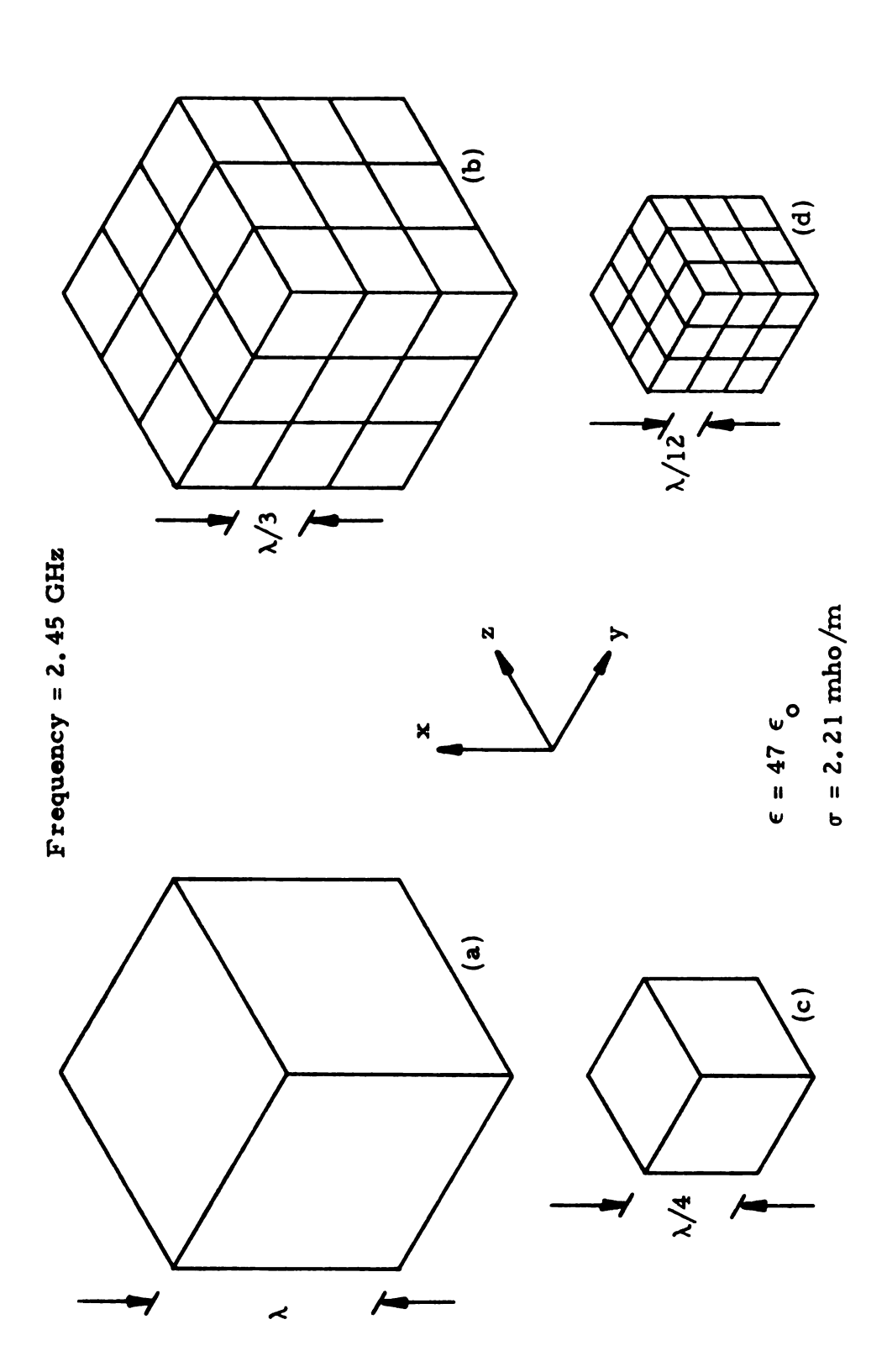
The last example was chosen to evidence the accuracy of the method. An electrically small dielectric cube (measuring 4 cm x 4 cm x 4 cm) was irradiated by a plane electromagnetic wave, for various values of frequency and dielectric constant, as illustrated in Figure 3.11. We expect the electric field near the center of the cube to be very nearly equal to the electric field near the center of a sphere with the same dielectric constant in a uniform electrostatic field. The field \vec{E} in the sphere is given by

$$\vec{E} = \frac{3}{\epsilon_r + 2} \vec{E}^i , \qquad (3.7.1)$$

where \vec{E}^i is the externally applied field, and $\epsilon_r = \epsilon/\epsilon_o$. The table in Figure 3.11 shows that the numerical solution is consistent with this expectation.

B. Internal Electric Field

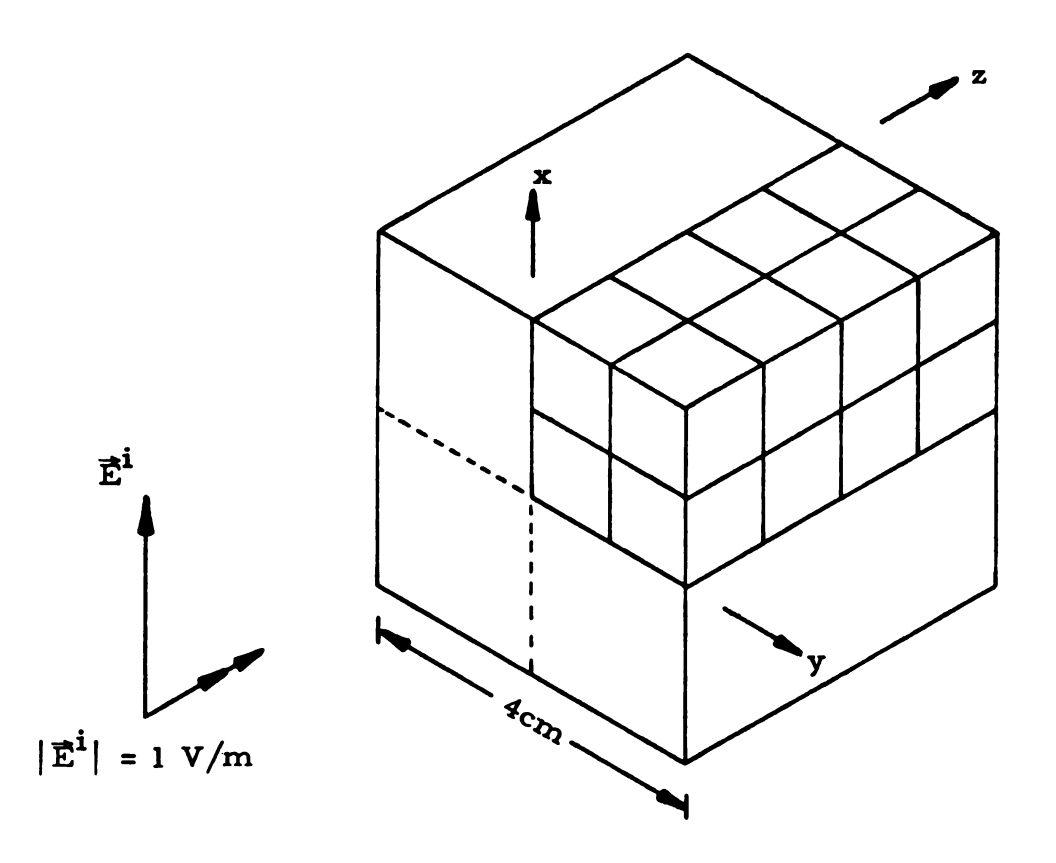
This group of examples is devoted to calculating the induced field in bodies of various shapes and sizes, with both uniform and nonuniform



Two cubes of muscle illuminated by a 2.45 GHz plane wave, treated as single cells in (a) and (c), and divided into 27 cubical subvolumes in (b) and (d). The edges of the cubes measure one wavelength and 1/4 wavelength, respectively. Figure 3. 10.

Number of cells	Size of each cell	Ē center (Volts/m)	Figure reference
1	λ	0.0789	3.10a
27	λ/3	0.0922	3.10b
1	$\lambda/4$	0.0592	3.10c
27	λ/12	0.0556	3.10d

Table 3.1. Induced electric field at the center of the muscle cubes shown in Figure 3.10 for various numbers of subvolumes. $|\vec{E}^i| = 1 \text{ V/m}.$



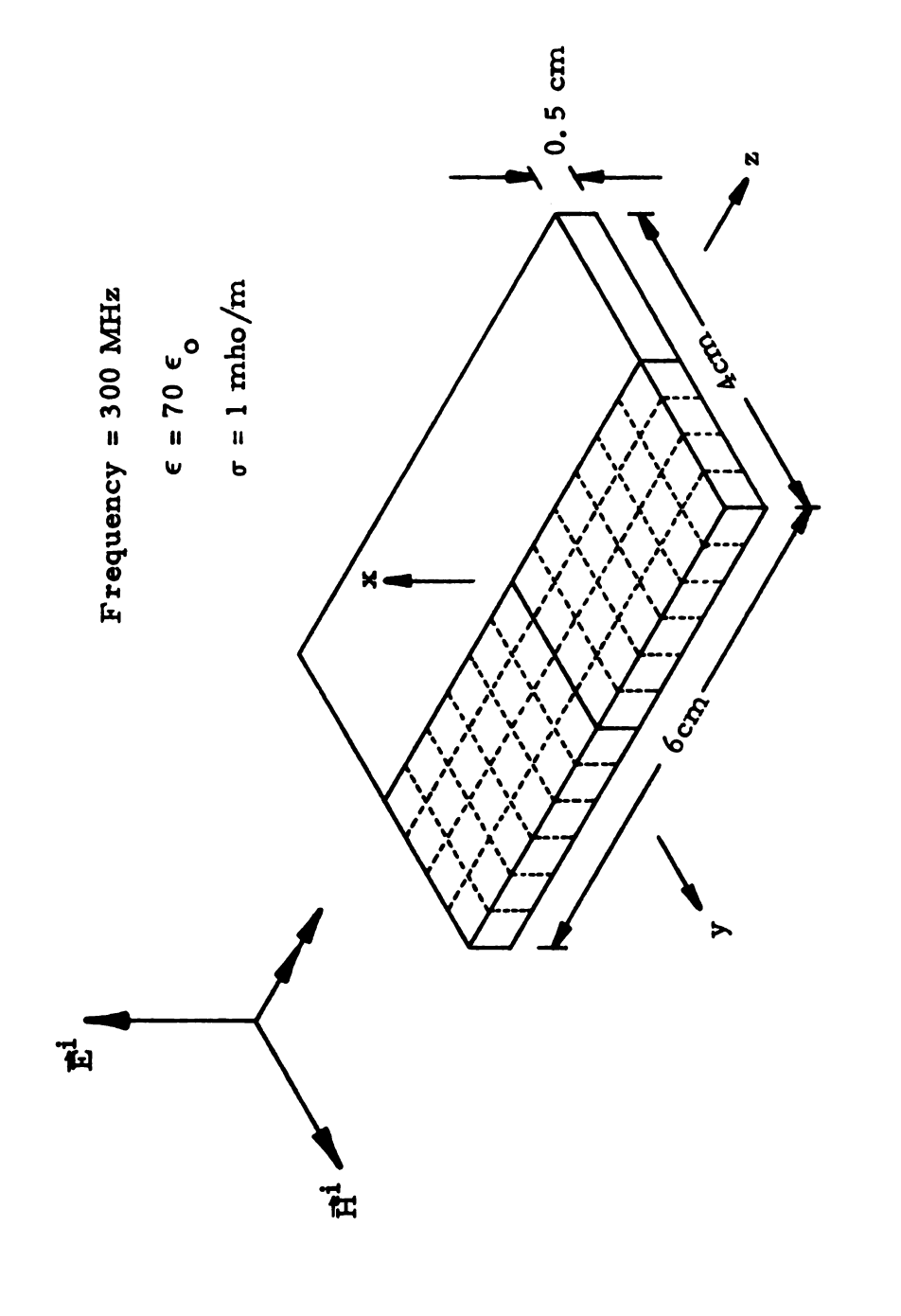
f (Hz)	λ _o (cm)	۴	λ _ε (cm)	$\frac{3}{\epsilon_{\mathbf{r}}+2}$	Ē center (Volts/m)
10 ⁷	3 x 10 ³	5.0	1.342 x 10 ³	0.4286	0. 4172
106	3 x 10 ⁴	5.0	1.342×10^4	0.4286	0.4172
10 ³	3 x 10 ⁷	5.0	1.342×10^7	0.4286	0. 4172
10 ³	3 x 10 ⁷	20.0	6.708 x 10 ⁶	0.1364	0. 1124
10 ³	3 x 10 ⁷	51.7	4. 172 x 10 ⁶	0.0559	0. 0503

Figure 3.11. Electric field induced at the center of a dielectric cube, for various values of frequency and dielectric constant. Incident electric field is a plane wave.

incident fields. The variety of examples presented here underscores the versatility of the moment method.

A 300 MHz plane wave impinges upon a plane conducting layer in Figure 3.12, with the incident electric field perpendicular to the plane of the layer. The dimensions of the layer are $6 \text{ cm} \times 4 \text{ cm} \times 0.5 \text{ cm}$, and its permittivity and conductivity are $70 \in 0$ and 1 mho/meter, respectively. The induced electric field, which has essentially only an x-component, is shown in Figure 3.13. The field is nearly uniform near the center of the layer, and is approximately $\epsilon_{\Omega}/|\epsilon + \sigma/j\omega|$ times the incident field. This result can be anticipated from the boundary conditions on E. In Figure 3.14, the plane of the layer is parallel to \vec{E}^{i} ; the x- and z-components of the induced field are presented in Figures 3.15 and 3.16, respectively. E_v is small compared to E_x and E_z . We note that E_x is about ten times larger than it was when the layer was perpendicular to \vec{E}^i . In some parts of the layer, E_z is about as large as E_x , even though the incident field has only an x-component. This example shows that the induced electric field in a conducting body depends very heavily upon the body's orientation with respect to the incident field.

Figure 3. 17 depicts a system of two tissue layers, fat and muscle, illuminated by a plane wave at 100 MHz. The body measures $16 \, \mathrm{cm} \, \mathrm{x}$ 12 cm x 4 cm, and each layer is 2 cm thick. In Figure 3. 18, the components of the induced field are shown. The magnitude of E_z is comparable to that of E_x in some portions of the fat layer; this result cannot be predicted by the plane slab model, since it assumes only an x-component in the body. In addition, the two models produce different values for E_x in the system. The plane slab model predicts that



Plane conducting layer exposed to a 300 MHz plane wave, with \vec{E}^i perpendicular to the plane of the layer. Figure 3. 12.

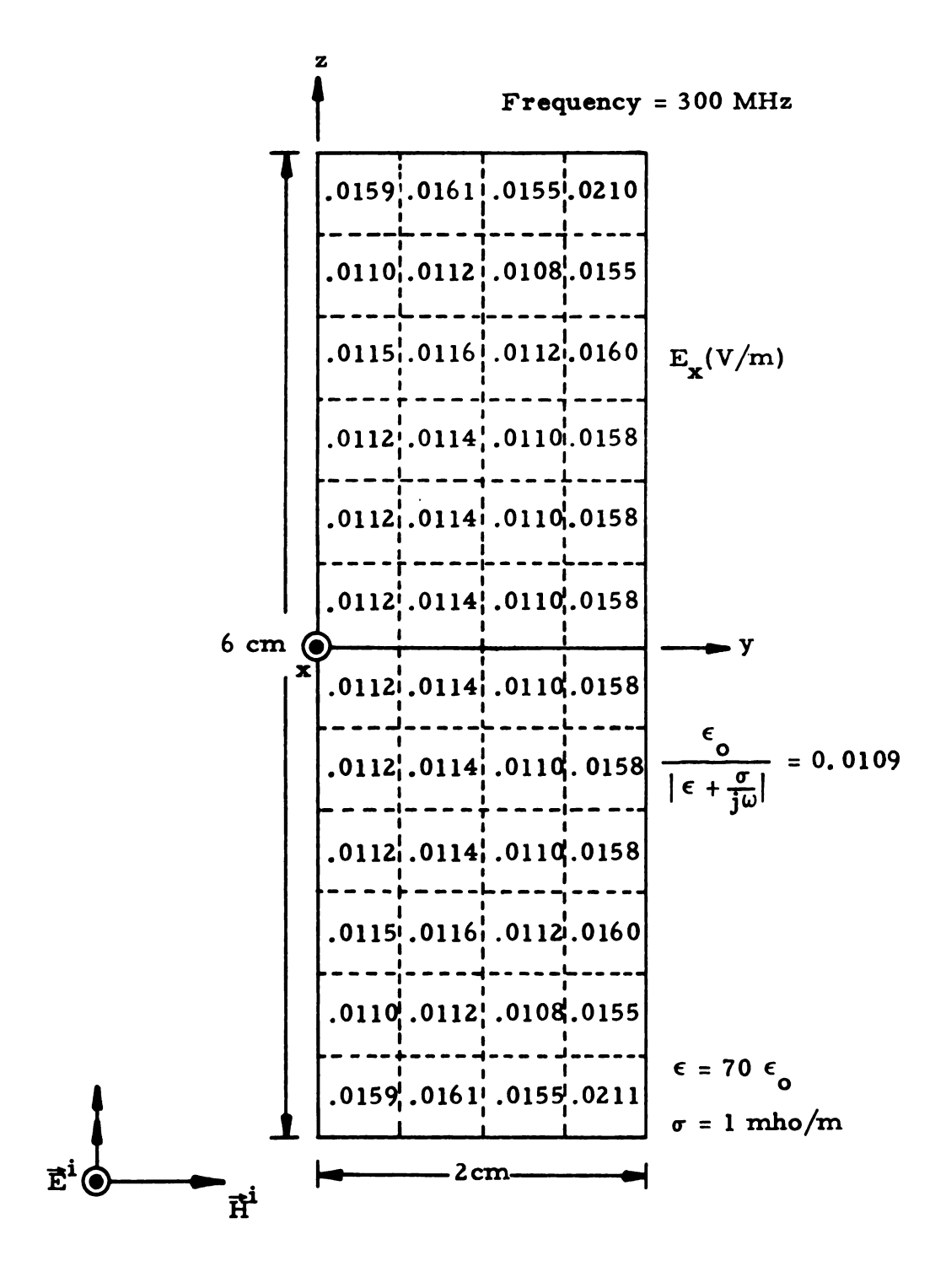
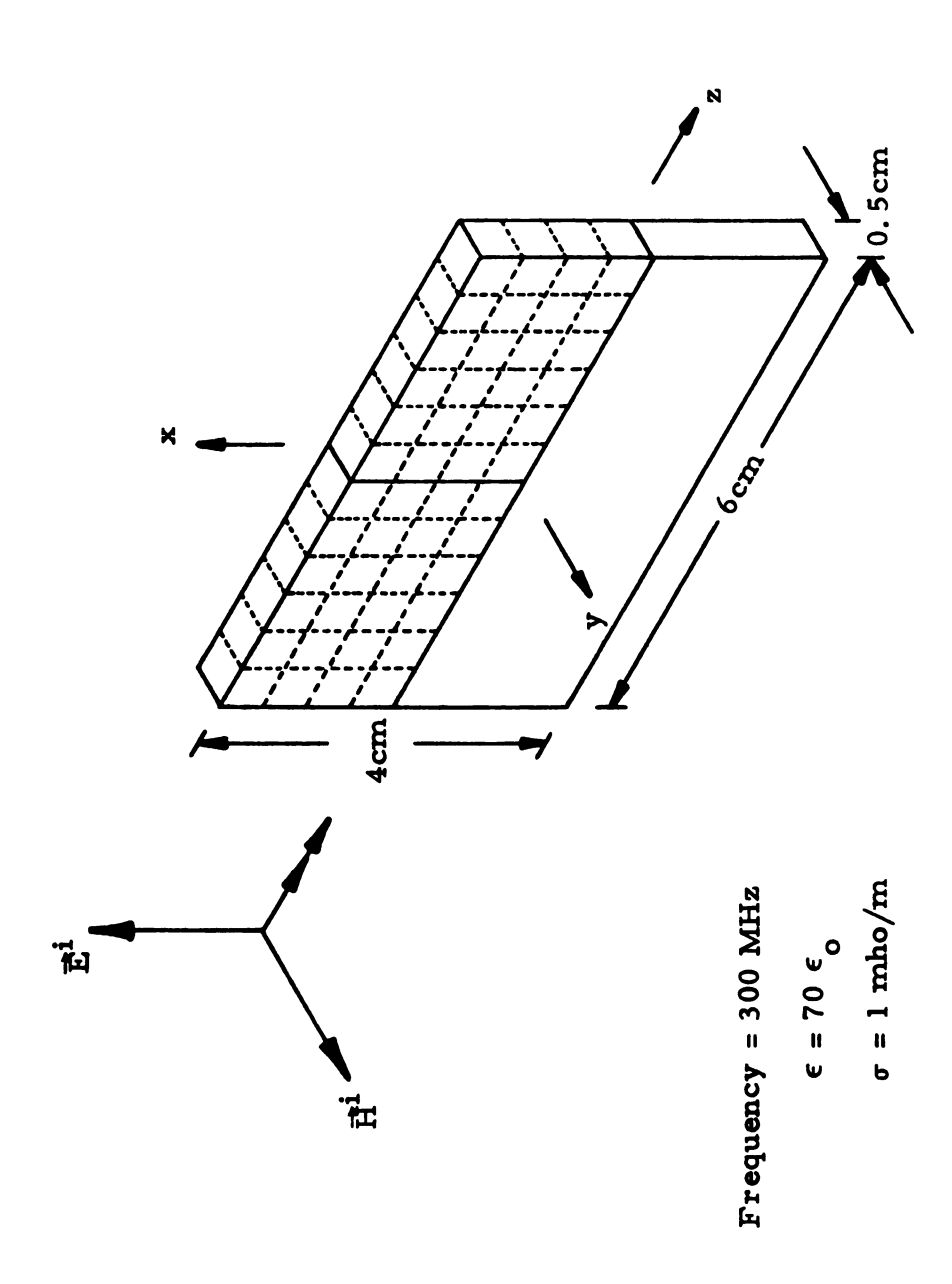
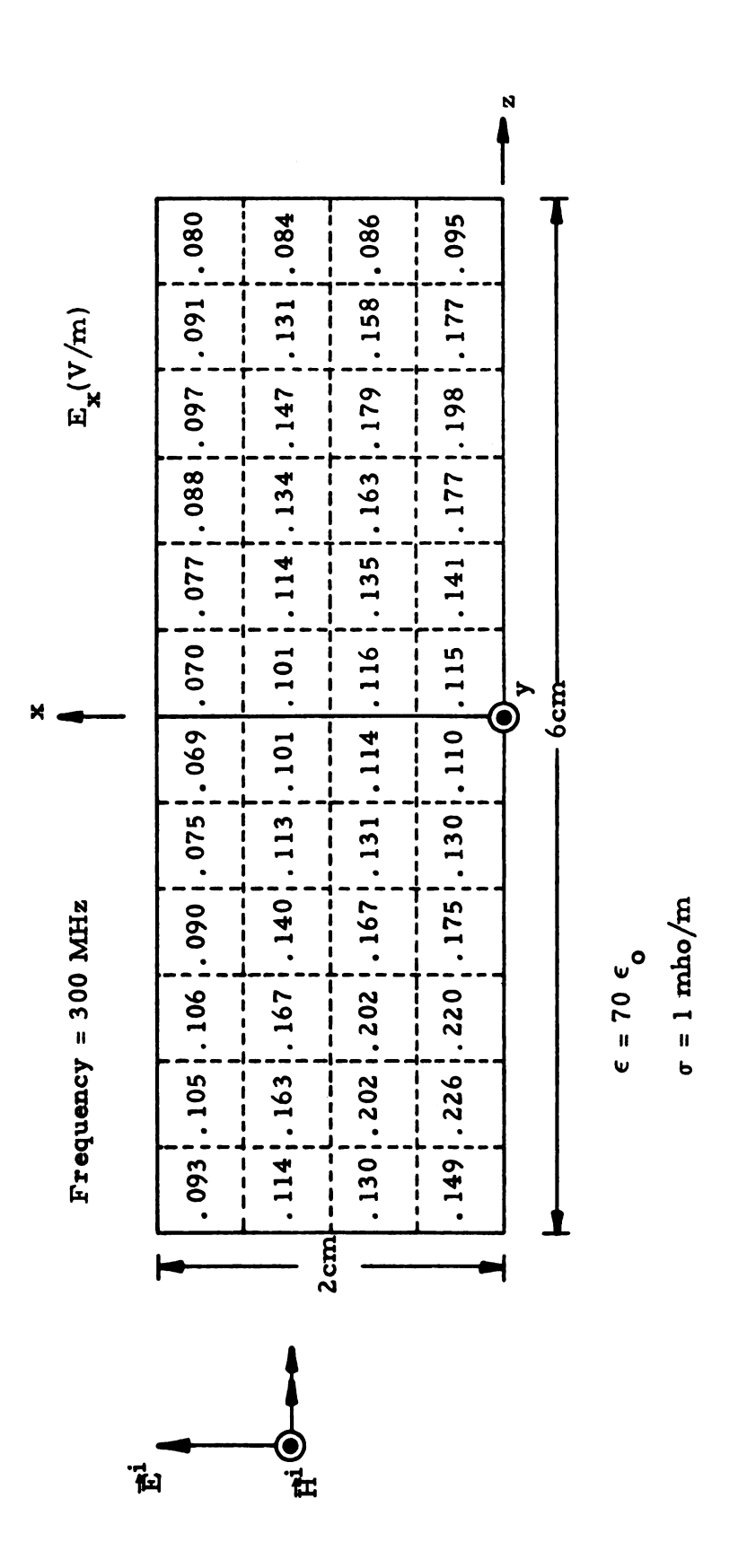


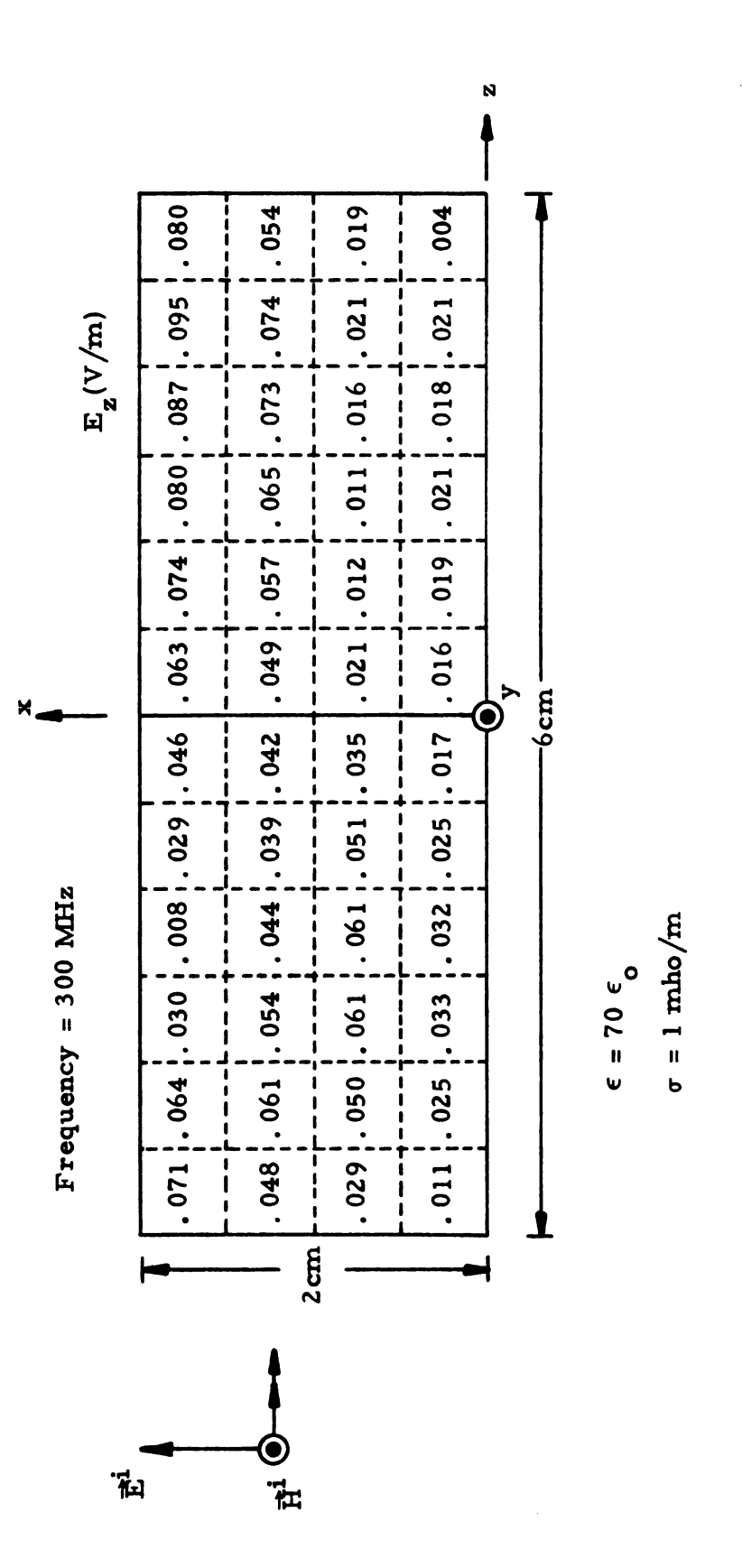
Figure 3.13. Electric field induced in the layer of Figure 3.12, with $\epsilon = 70 \epsilon_0$ and $\sigma = 1$ mho/m. Only half of the layer is shown above. E_y and E_z are negligible.



A 300 MHz plane wave impinges upon a plane conducting layer, with \vec{E}^i parallel to the plane of the layer. Figure 3, 14.



The x-component of the electric field induced in the layer of Figure 3. 14, with $\epsilon = 70\epsilon_0$ and $\sigma = 1 \text{ mho/m}$. Only half of the layer is shown above. Figure 3, 15.



The z-component of the electric field induced in the layer of Figure 3.14, with $\epsilon = 70 \epsilon_0$ Only half of the layer is shown above. and $\sigma = 1 \text{ mho/m}$. Figure 3. 16.

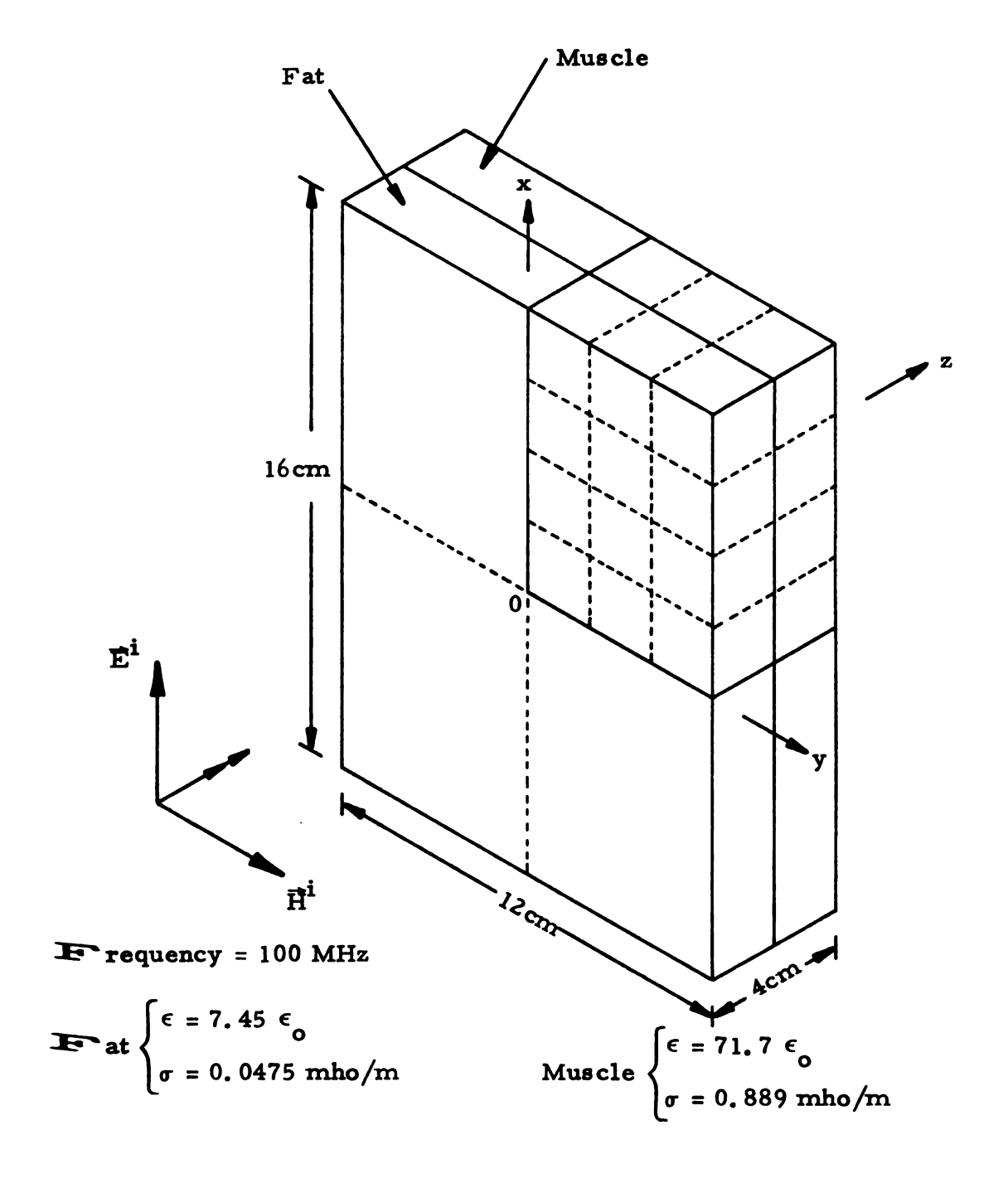


Figure 3.17. A block of tissue composed of a fat layer and a muscle layer, illuminated by a plane wave at 100 MHz.

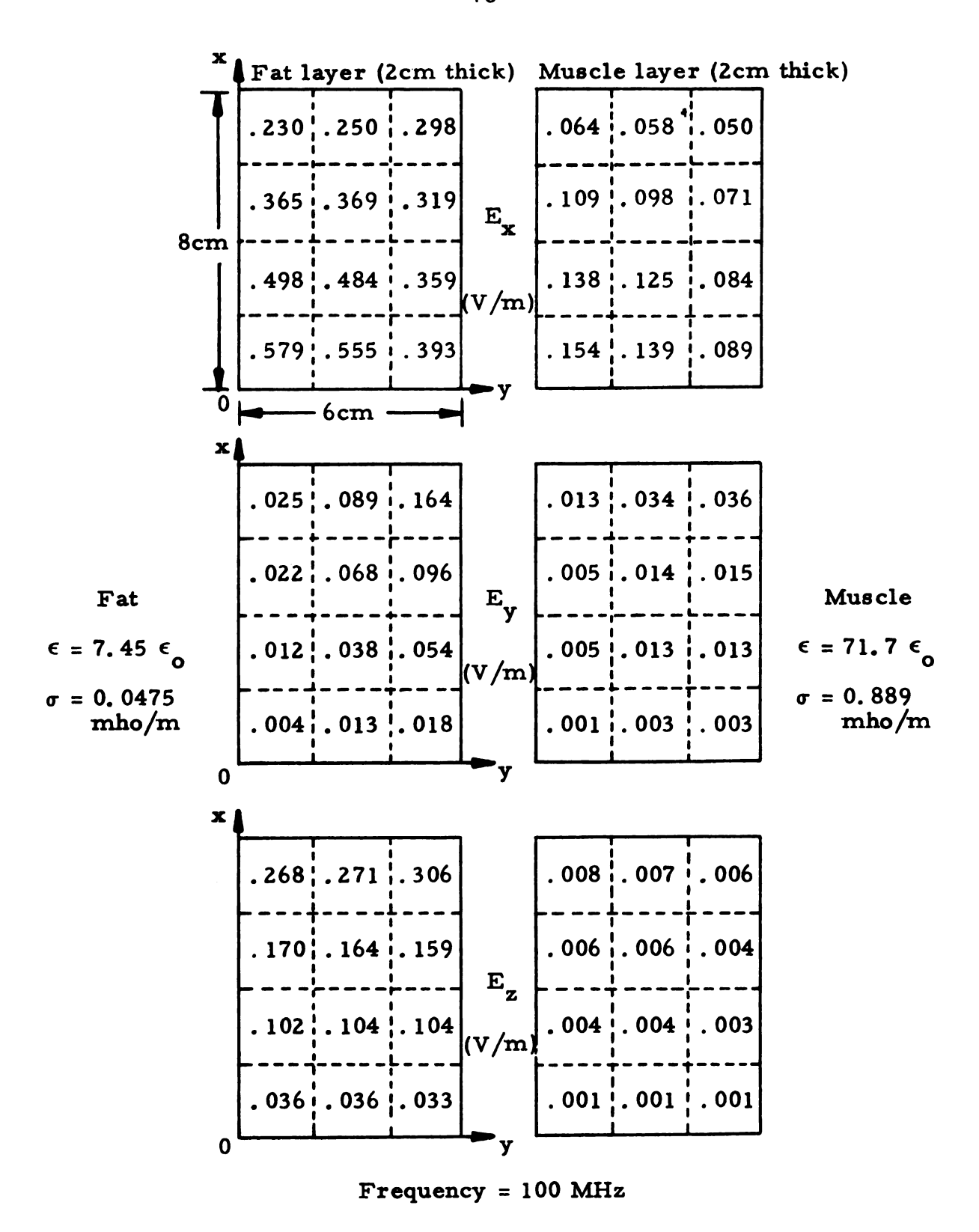


Figure 3.18. The electric field induced in the block of tissue pictured in Figure 3.17. Only 1/4 of each layer is shown above. For a corresponding plane slab model, $E_x = 0.197 \text{ V/m}$ at the center of the fat layer, and $E_x = 0.210 \text{ V/m}$ at the center of the muscle layer.

 $E_{x} = 0.197 \text{ V/m}$ at the center of the fat layer, and that $E_{x} = 0.210 \text{ V/m}$ at the center of the muscle layer.

In the next example we examine the induced axial electric field and the power density in cylinders of salt water, having 1 Normal, 2 Normal, and 5 Normal concentrations, and having various lengths. A typical cylinder, along with the coordinate system, is shown in Figure 3.19. At 9.45 GHz, the lengths of the cylinders are approximately $\lambda_0/4$, $\lambda_0/2$, λ_0 , and $3\lambda_0/2$, where λ_0 is the free-space wavelength. The electric field intensity, power density, and total absorbed power for each cylinder are given in Figures 3.20 through 3.25.

For a given cylinder length, the field distribution has the same general shape for all concentrations, although the total absorbed power is generally greater for the higher salt concentrations. We also note that the total absorbed power P_t reaches a relative maximum when the cylinder is about $\lambda_0/2$ in length.

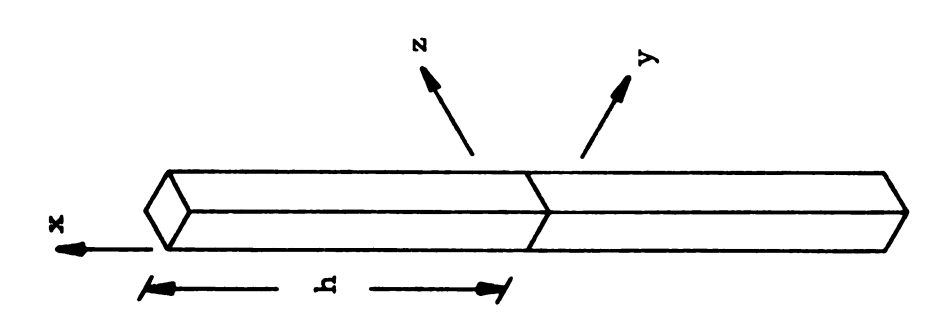
The next two examples investigate the effect of an inhomogeneity in a cylinder, as illustrated in Figure 3.26. Figure 3.26a shows a muscle cylinder, measuring 10 cm x 1 mm x 1 mm, illuminated by a 2.45 GHz plane wave polarized parallel to the axis of the cylinder. In Figure 3.26b, we have a similar muscle cylinder with a segment of fat 1 cm long at its center. The induced axial field and the power density for both cylinders are plotted in Figures 3.27a and 3.27b, respectively.

Since the electric field in the inhomogeneous cylinder is normal to the muscle-fat boundary, it obeys the boundary condition

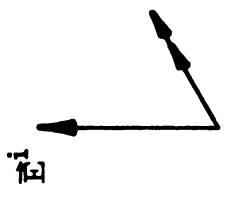
$$(\sigma_{\mathbf{M}} + j\omega \, \epsilon_{\mathbf{M}}) \, \mathbf{E}_{\mathbf{M}} = (\sigma_{\mathbf{F}} + j\omega \, \epsilon_{\mathbf{F}}) \, \mathbf{E}_{\mathbf{F}} , \qquad (3.7.2)$$

where the subscripts M and F refer to muscle and fat, respectively.

Thus, near the boundary, both the electric field and the power density



Frequency = 9.45 GHz



A saltwater cylinder of half-length h illuminated by a 9.45 GHz plane wave. The cross-section of the cylinder measures 1.8 mm x 1.8 mm. Figure 3. 19.

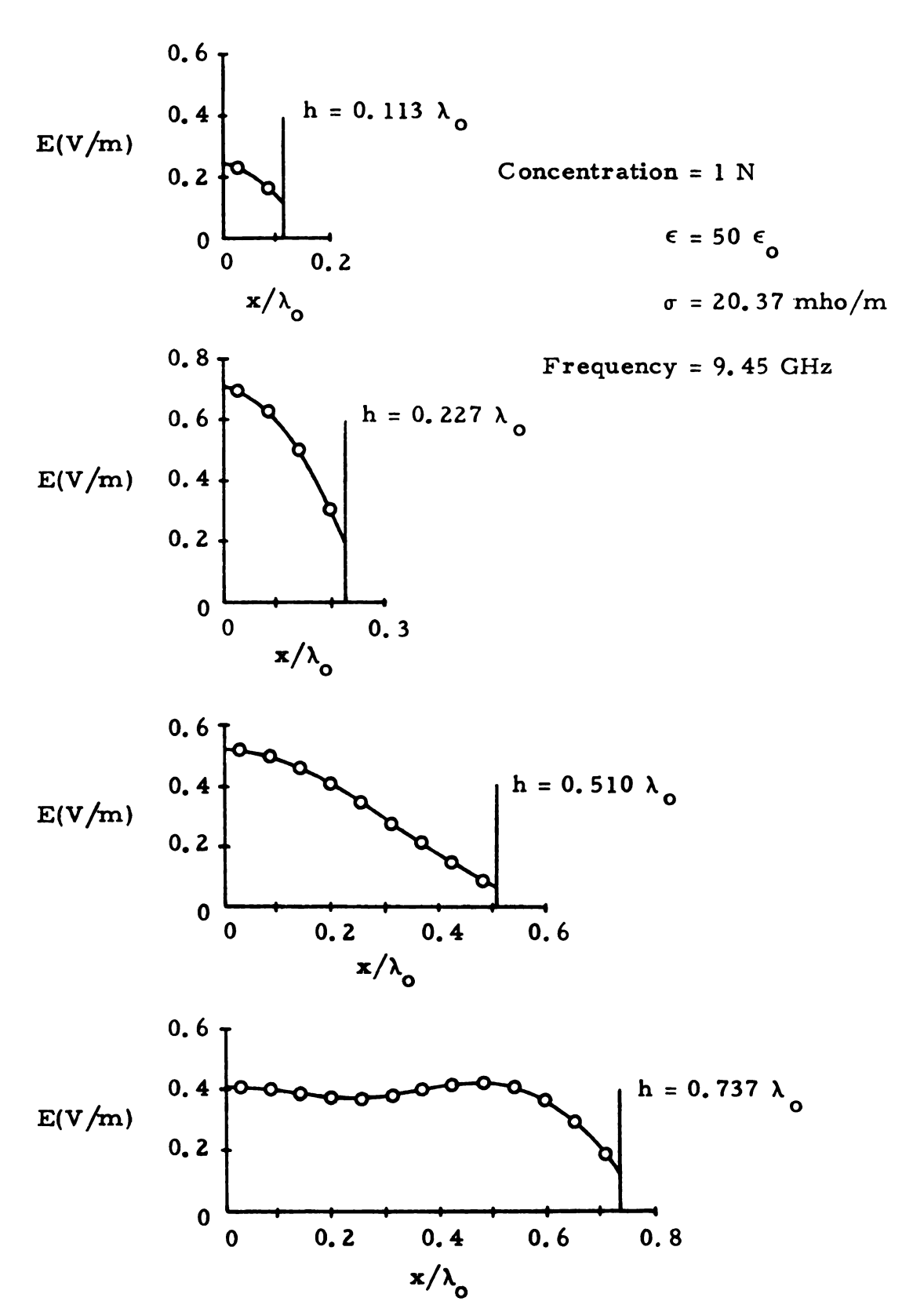


Figure 3.20. Electric field E along the axis of the saltwater cylinder shown in Figure 3.19, for $h/\lambda_0 = 0.113$, 0.227, 0.510, and 0.737. Concentration of the salt solution is 1 Normal, and the frequency is 9.45 GHz.

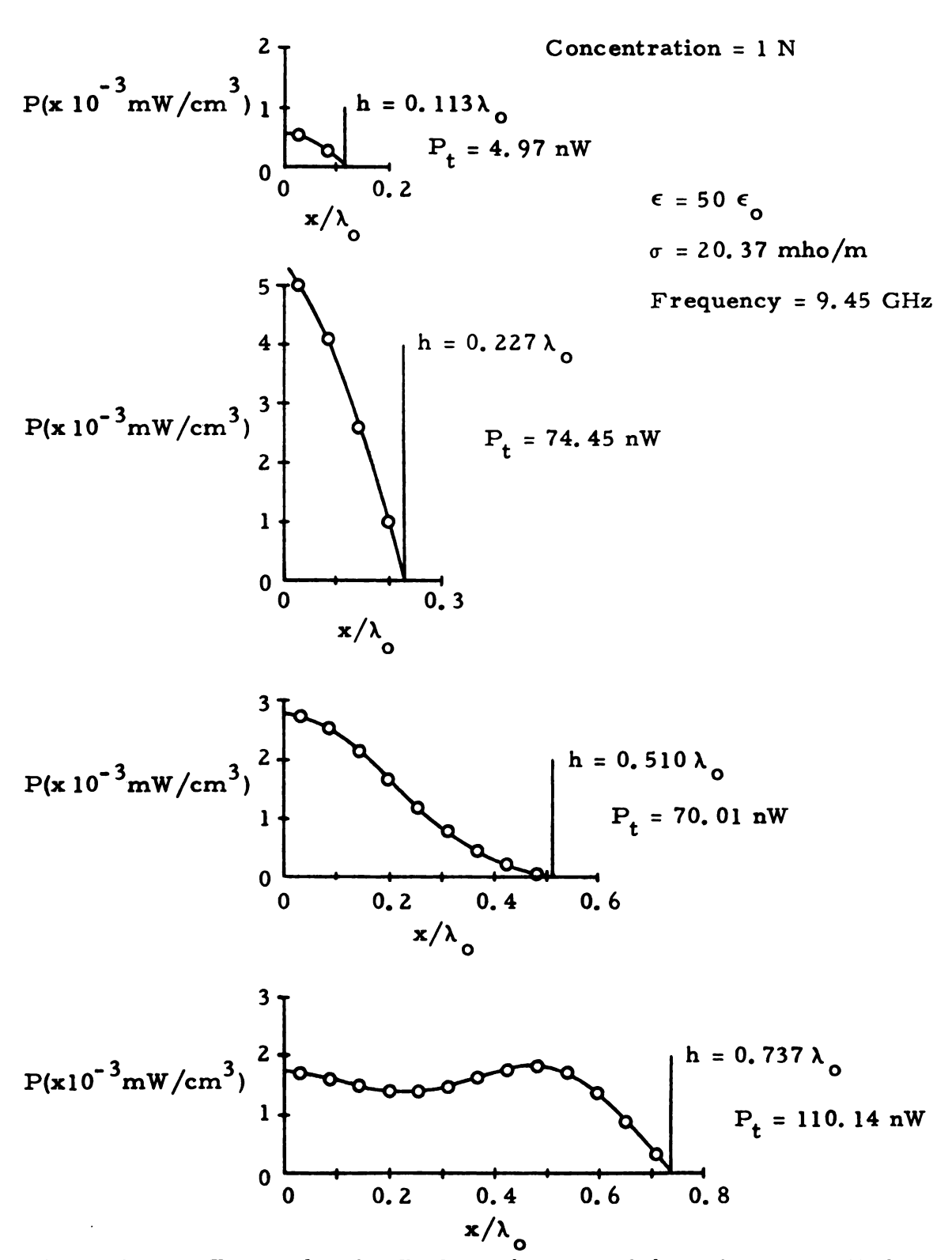


Figure 3.21. Power density P along the axis of the saltwater cylinder shown in Figure 3.19, and total absorbed power P_t , for $h/\lambda_0 = 0.113$, 0.227, 0.510, and 0.737. Concentration of the salt solution is 1 Normal, and the frequency is 9.45 GHz.

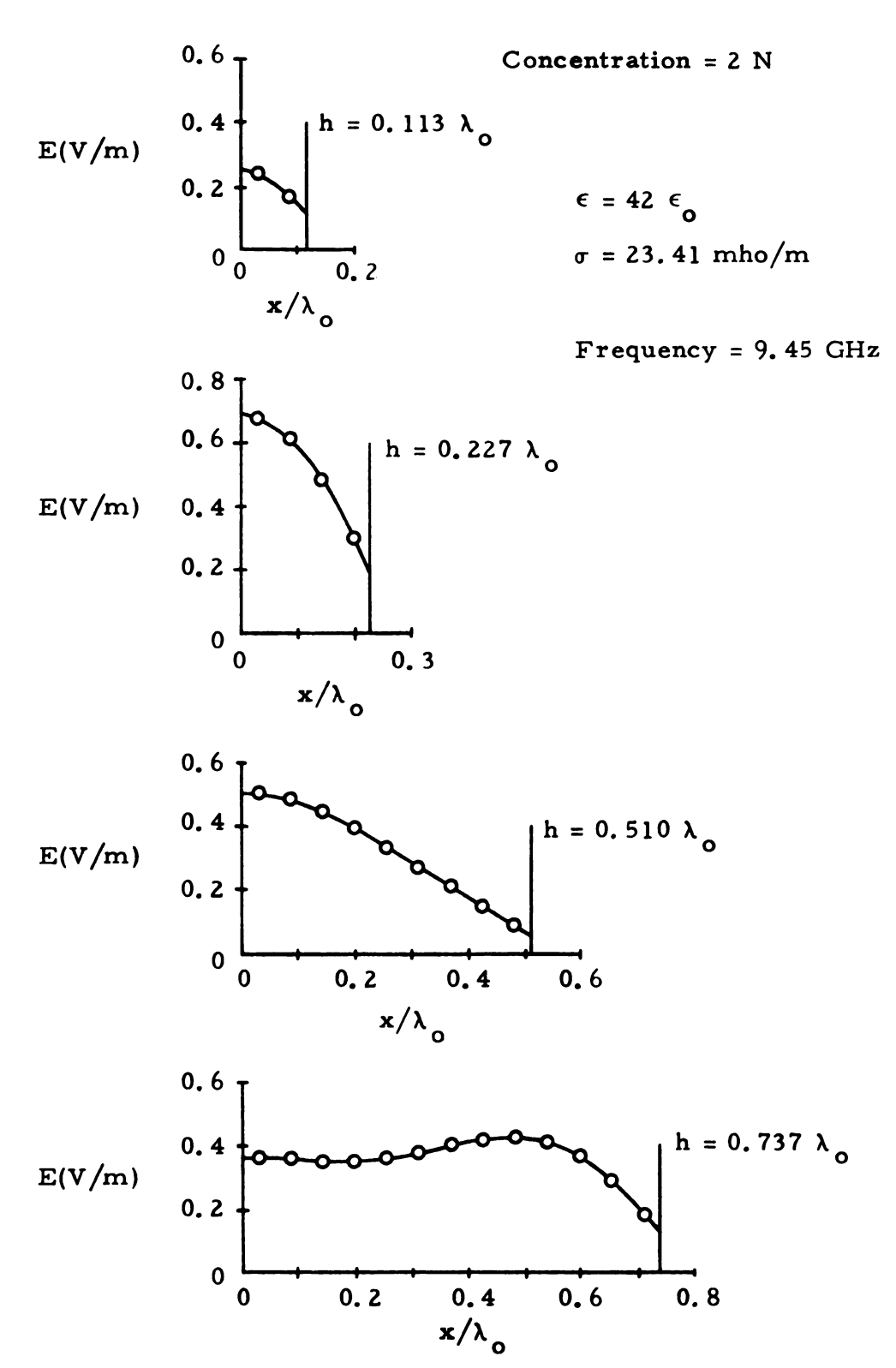


Figure 3.22. Electric field E along the axis of the saltwater cylinder shown in Figure 3.19, for $h/\lambda_0 = 0.113$, 0.227, 0.510, and 0.737. Concentration of the salt solution is 2 Normal, and the frequency is 9.45 GHz.

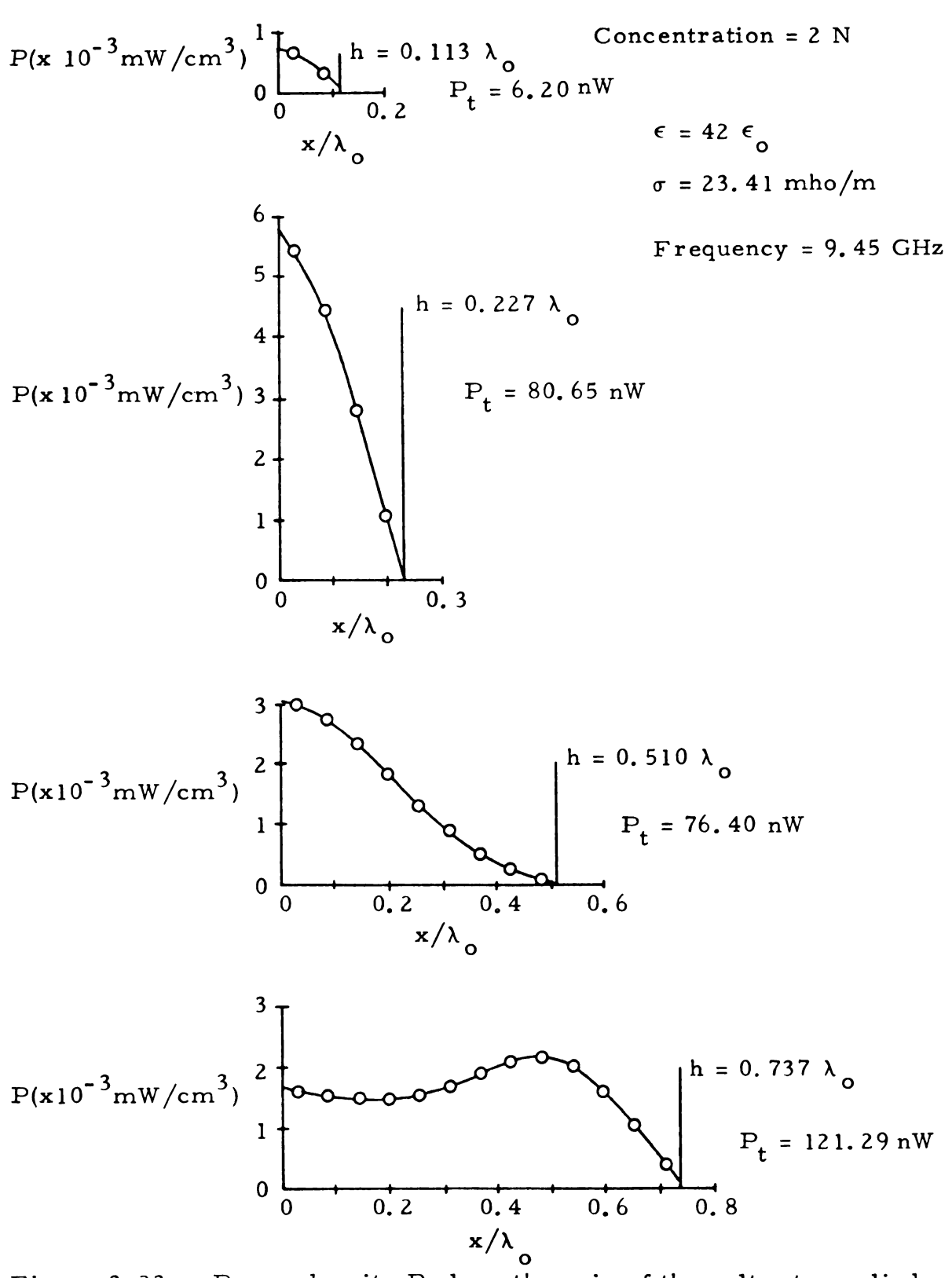


Figure 3.23. Power density P along the axis of the saltwater cylinder shown in Figure 3.19, and total absorbed power P_t , for $h/\lambda_0 = 0.113$, 0.227, 0.510, and 0.737. Concentration of the salt solution is 2 Normal, and the frequency is 9.45 GHz.

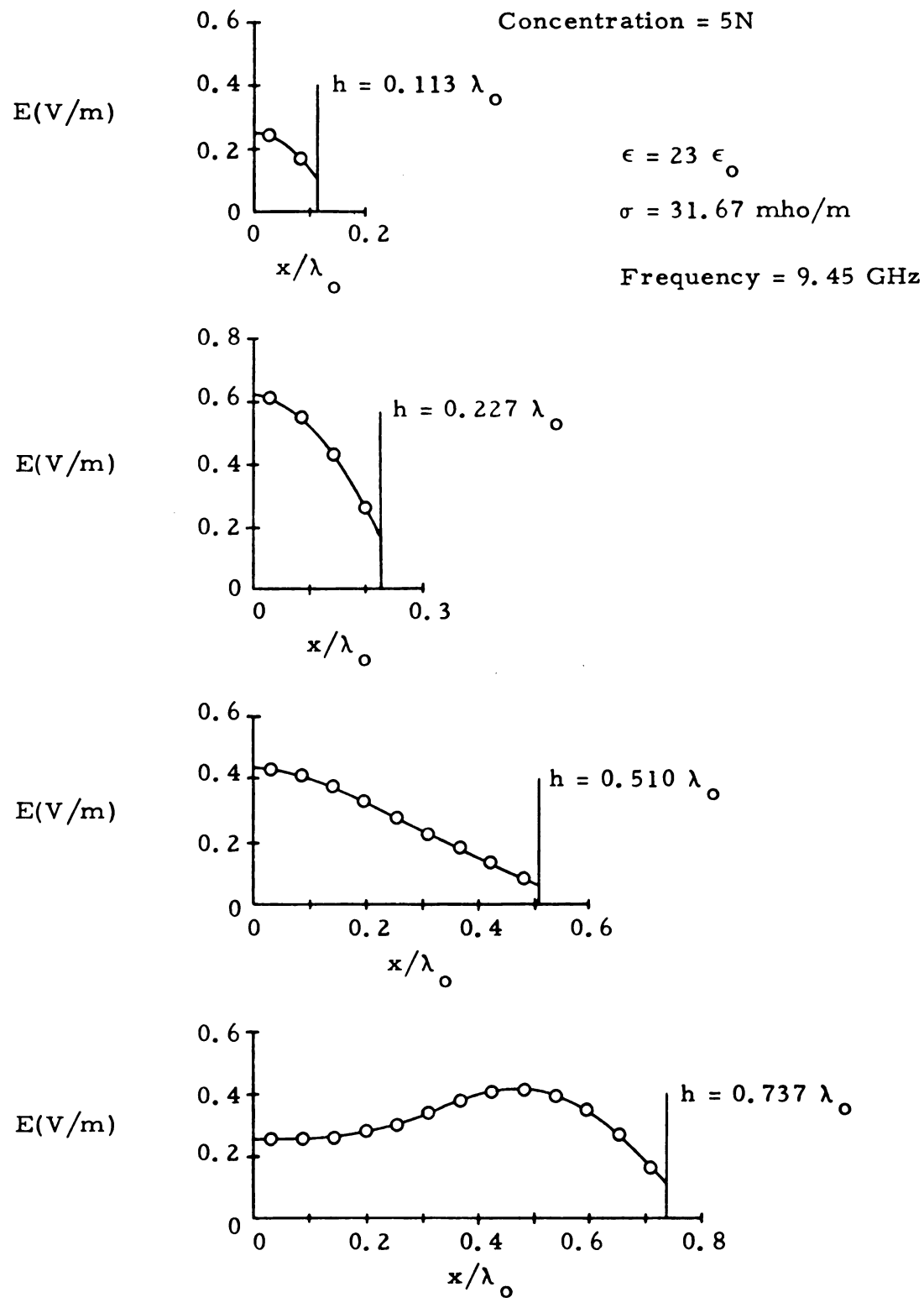


Figure 3.24. Electric field E along the axis of the saltwater cylinder shown in Figure 3.19, for $h/\lambda_0 = 0.113$, 0.227, 0.510, and 0.737. Concentration of the salt solution is 5 Normal, and the frequency is 9.45 GHz.

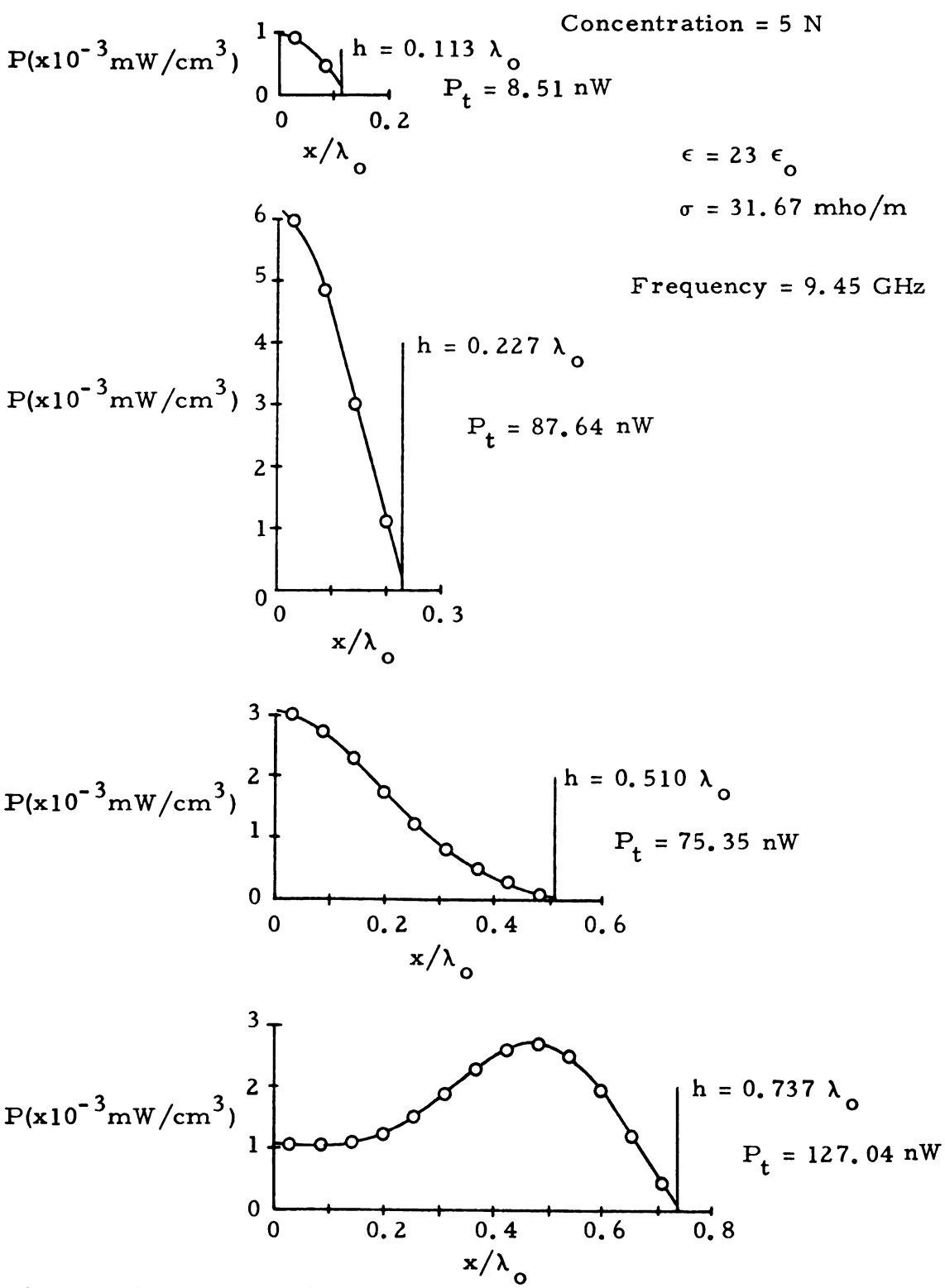
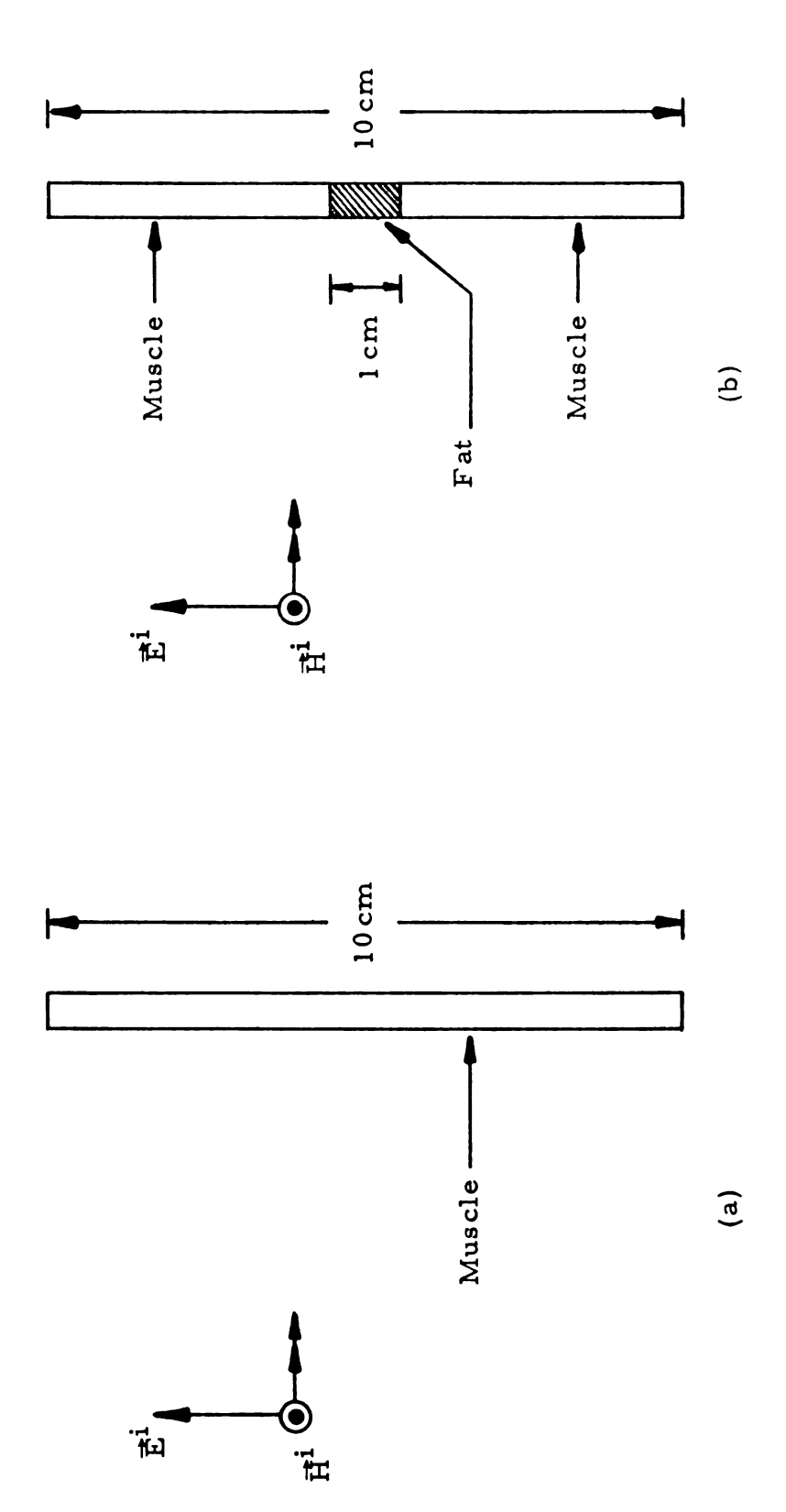
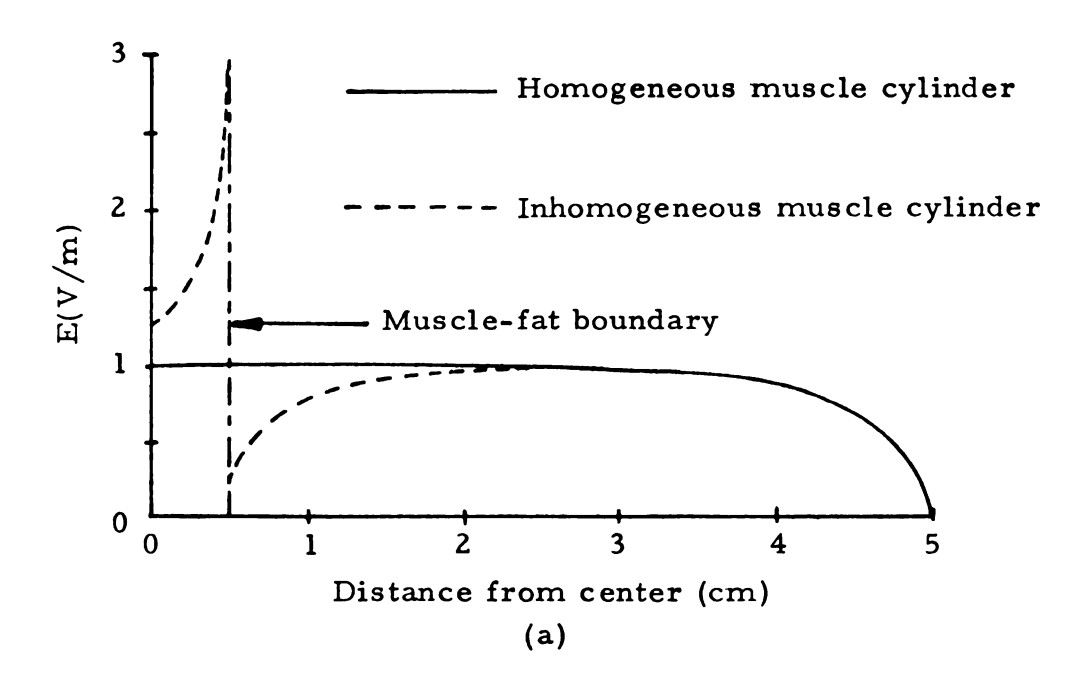


Figure 3.25. Power density P along the axis of the saltwater cylinder shown in Figure 3.19, and total absorbed power P_t , for $h/\lambda_0 = 0.113$, 0.227, 0.510, and 0.737. Concentration of the salt solution is 5 Normal, and the frequency is 9.45 GHz.



Frequency = 2.45 GHz

(a) A homogeneous muscle cylinder, and (b) an inhomogeneous muscle cylinder irradiated by a 2.45 GHz plane wave. Figure 3, 26.



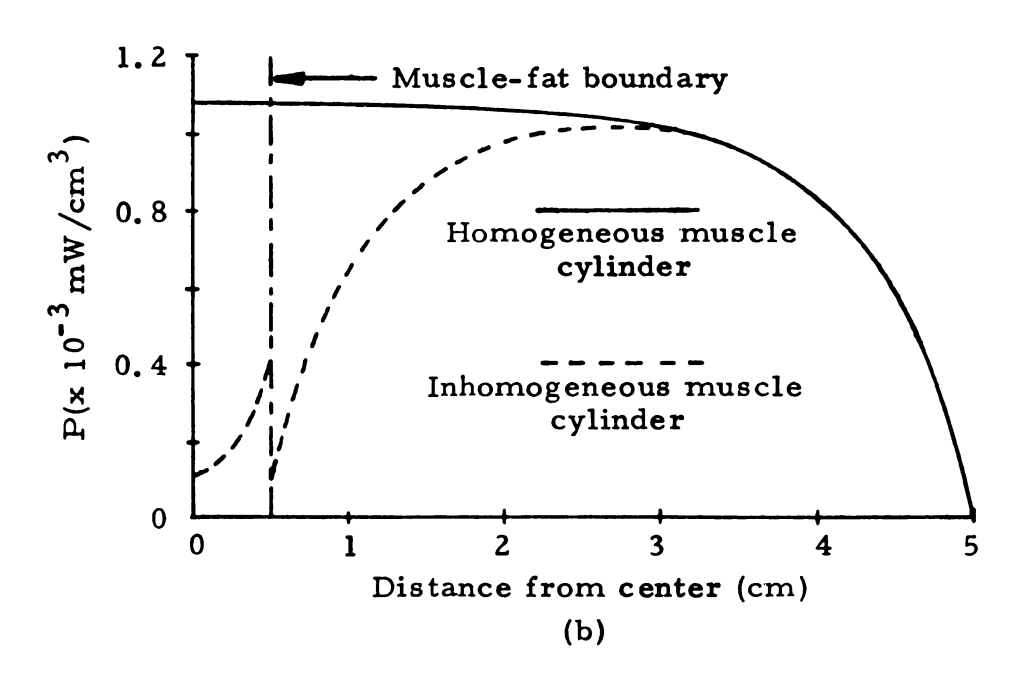


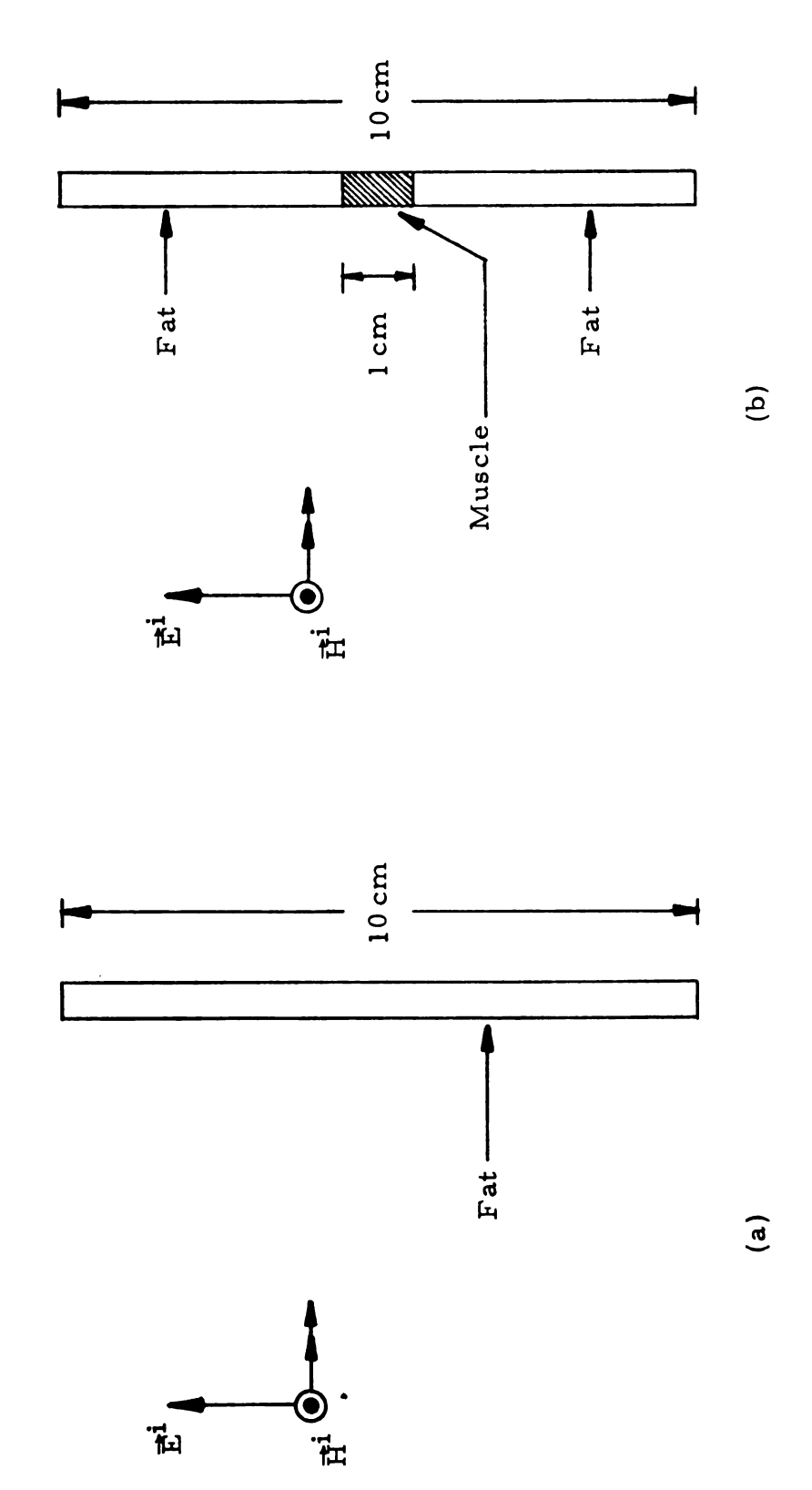
Figure 3.27. (a) Induced electric field E, and (b) power density P along the axes of the muscle cylinders shown in Figure 3.26. The frequency is 2.45 GHz, and $|\vec{E}^i| = 1 \text{ V/m}$. Each cylinder was partitioned lengthwise into 100 subvolumes of equal size.

in the fat are larger than in the muscle, thereby creating a local "hot spot". However, the overall heating near the center of the inhomogeneous cylinder is considerably less than that for the homogeneous muscle cylinder.

In Figures 3.28 and 3.29, the roles of the fat and muscle have been reversed. We again see a "hot spot" on the fat side of the muscle-fat interface in the inhomogeneous cylinder. However, the heating near the center of the cylinder is markedly greater when the muscle segment is present. Thus, the temperature of a cylindrical fat structure exposed to electromagnetic radiation could be significantly increased by the presence of one or more small muscle segments.

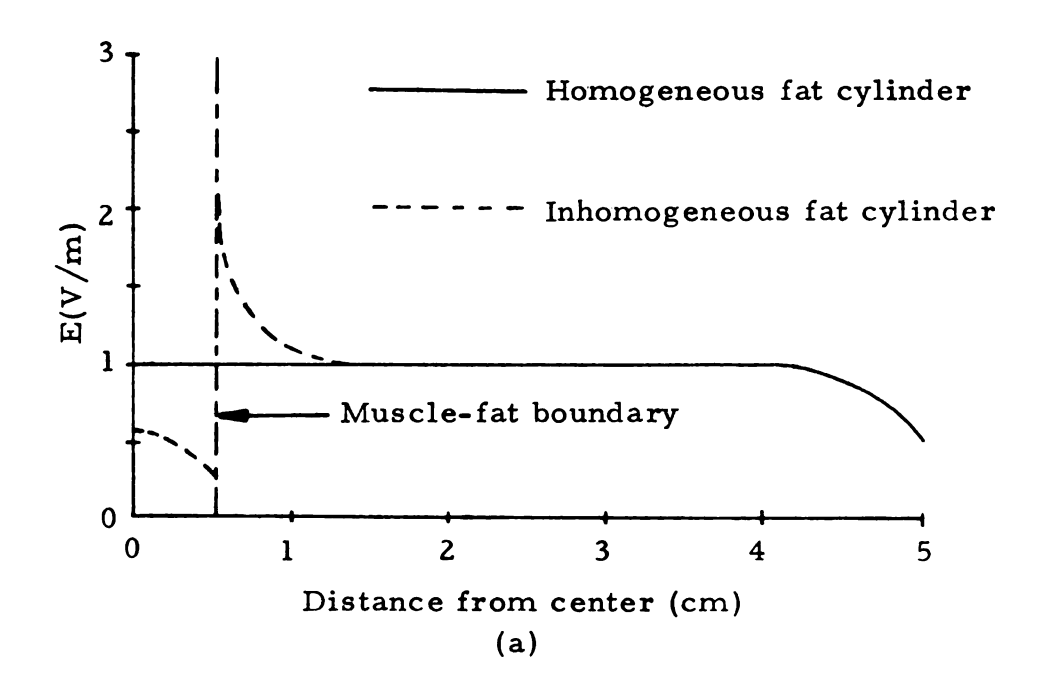
An inhomogeneous layer of fat is exposed to a 600 MHz plane wave in Figure 3.30. The layer measures 5 cm x 5 cm x 1 cm, and has a 1 cm x 1 cm x 1 cm cube of muscle imbedded near its center. Figures 3.31 and 3.32 show the x- and y-components, respectively, of the induced field; E_z is negligible. We note that E_x becomes quite large in the subvolumes immediately above and below the muscle cube, while the field in the muscle is small. Again, this is due to the boundary condition expressed in Equation (3.7.2).

As the last example in this group, we examine the induced field produced by nonuniform illumination of a homogeneous muscle layer. The layer measures $2.5 \, \text{cm} \times 2.5 \, \text{cm} \times 0.5 \, \text{cm}$, as shown in Figure 3.33, and is illuminated in a small area near one corner by a 600 MHz plane wave. E_x and E_y are presented in Figures 3.34 and 3.35, respectively; the z-component is negligible. E_x is largest in the subvolume which was directly irradiated, and decays rapidly as we move away from the site of incidence. E_y varies considerably throughout



Frequency = 2.45 GHz

(a) A homogeneous fat cylinder, and (b) an inhomogeneous fat cylinder irradiated by a 2.45 GHz plane wave. Figure 3.28.



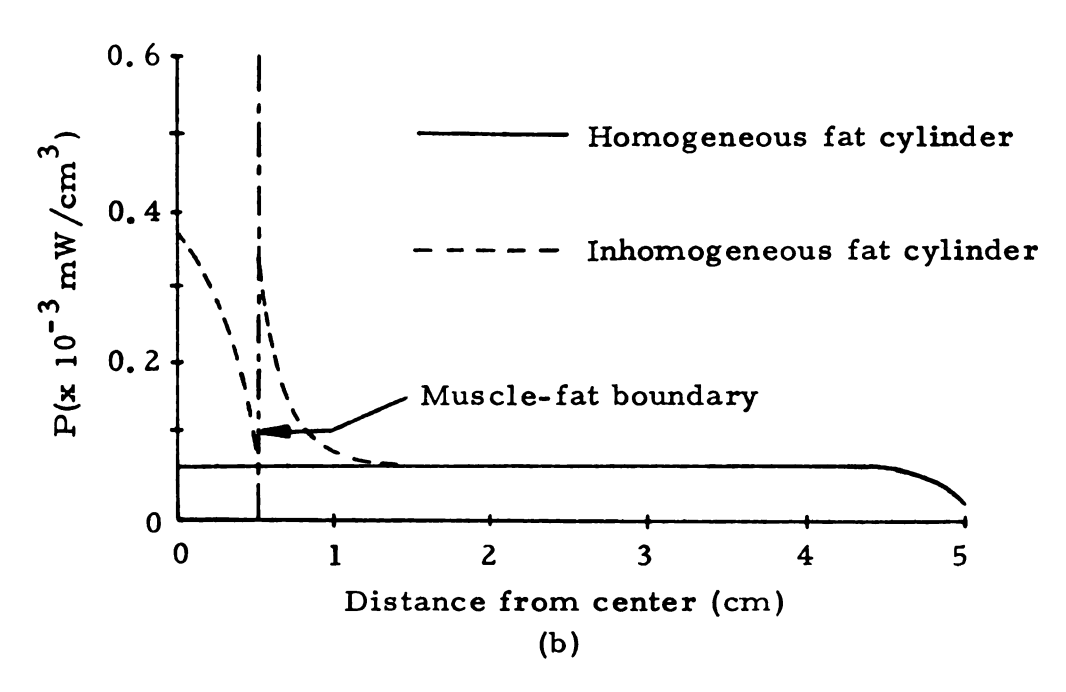


Figure 3.29. (a) Induced electric field E, and (b) power density P along the axes of the fat cylinders shown in Figure 3.28. The frequency is 2.45 GHz, and $|\vec{E}^i| = 1 \text{ V/m}$. Each cylinder was partitioned lengthwise into 100 subvolumes of equal size.

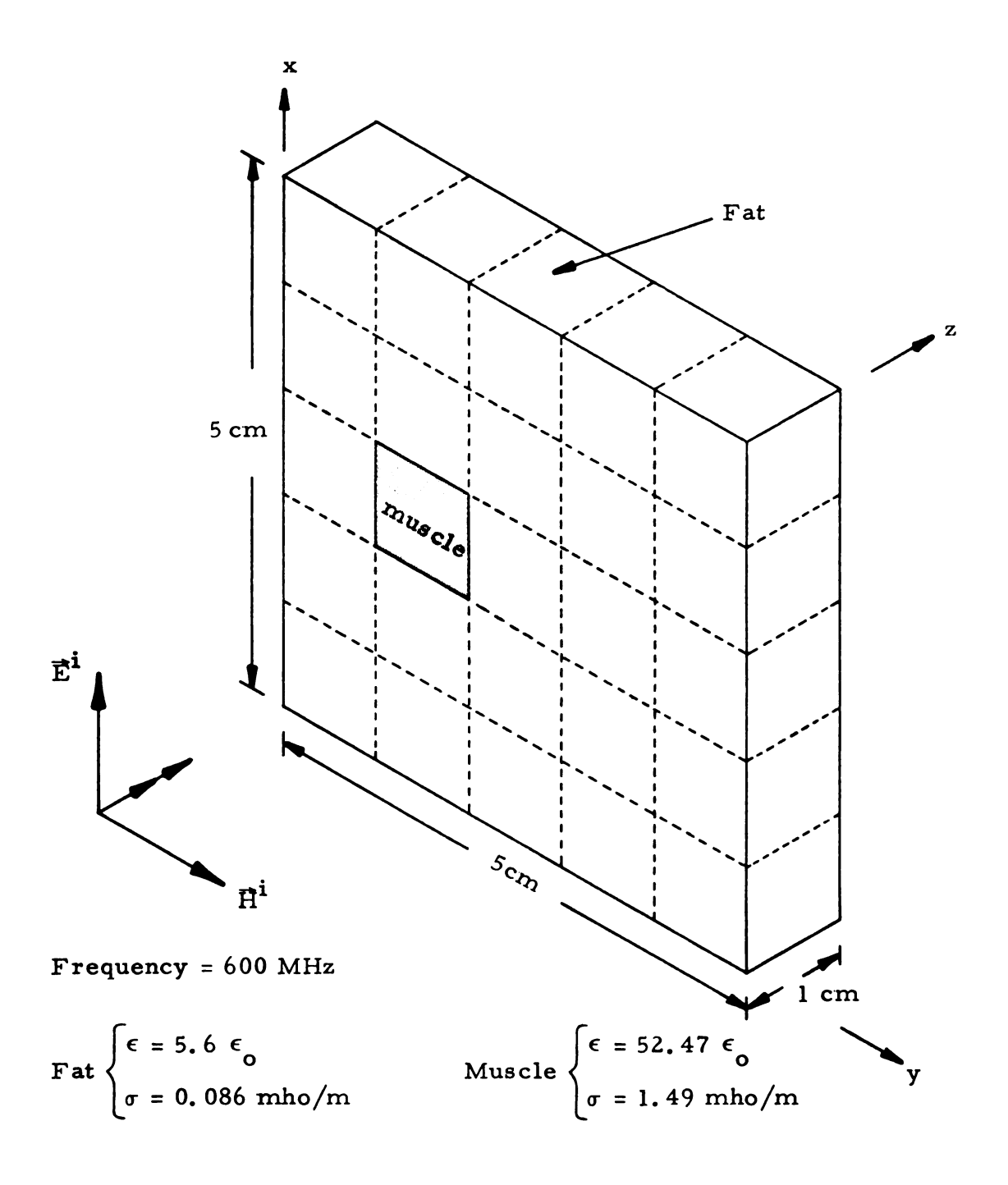
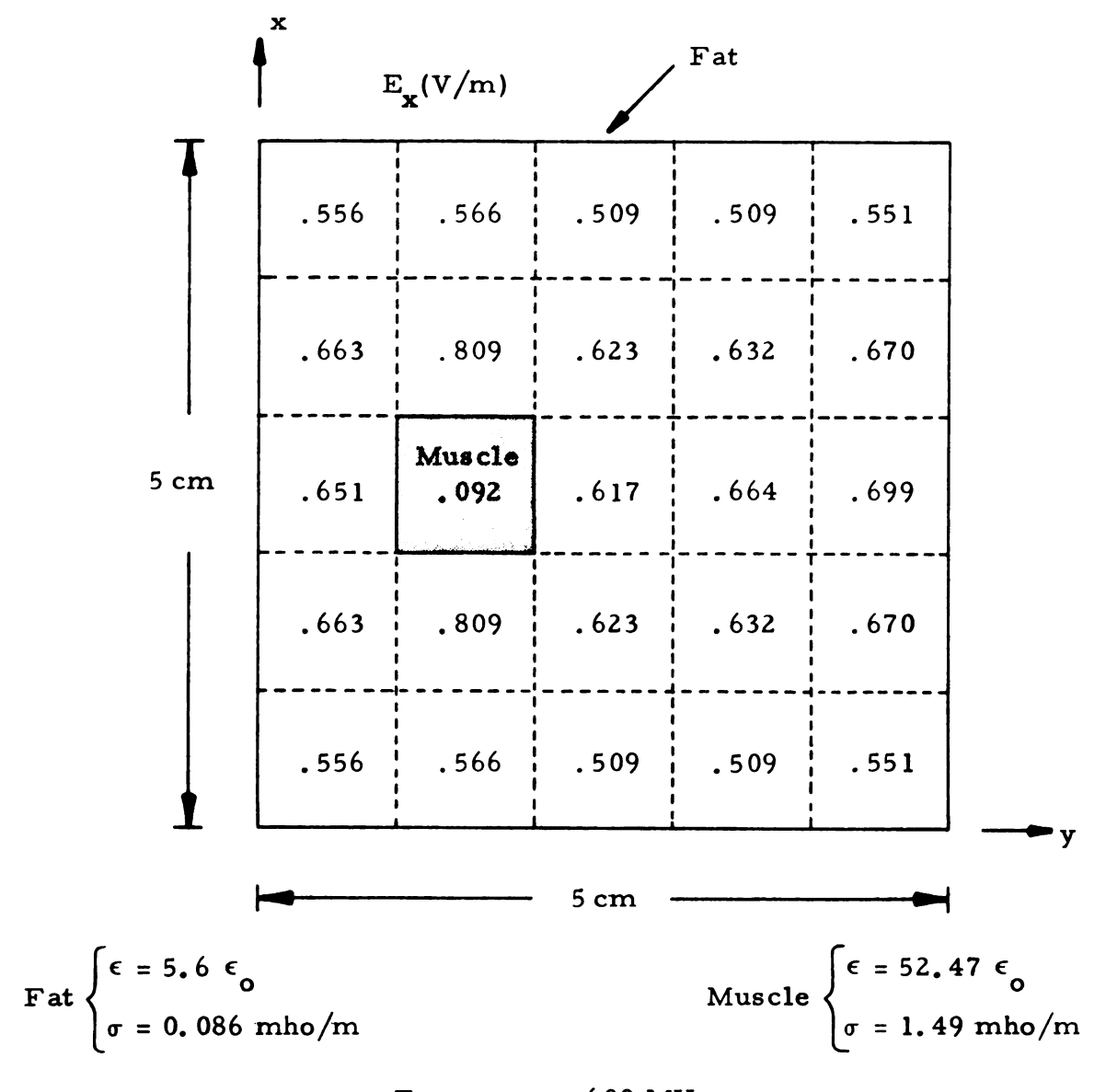
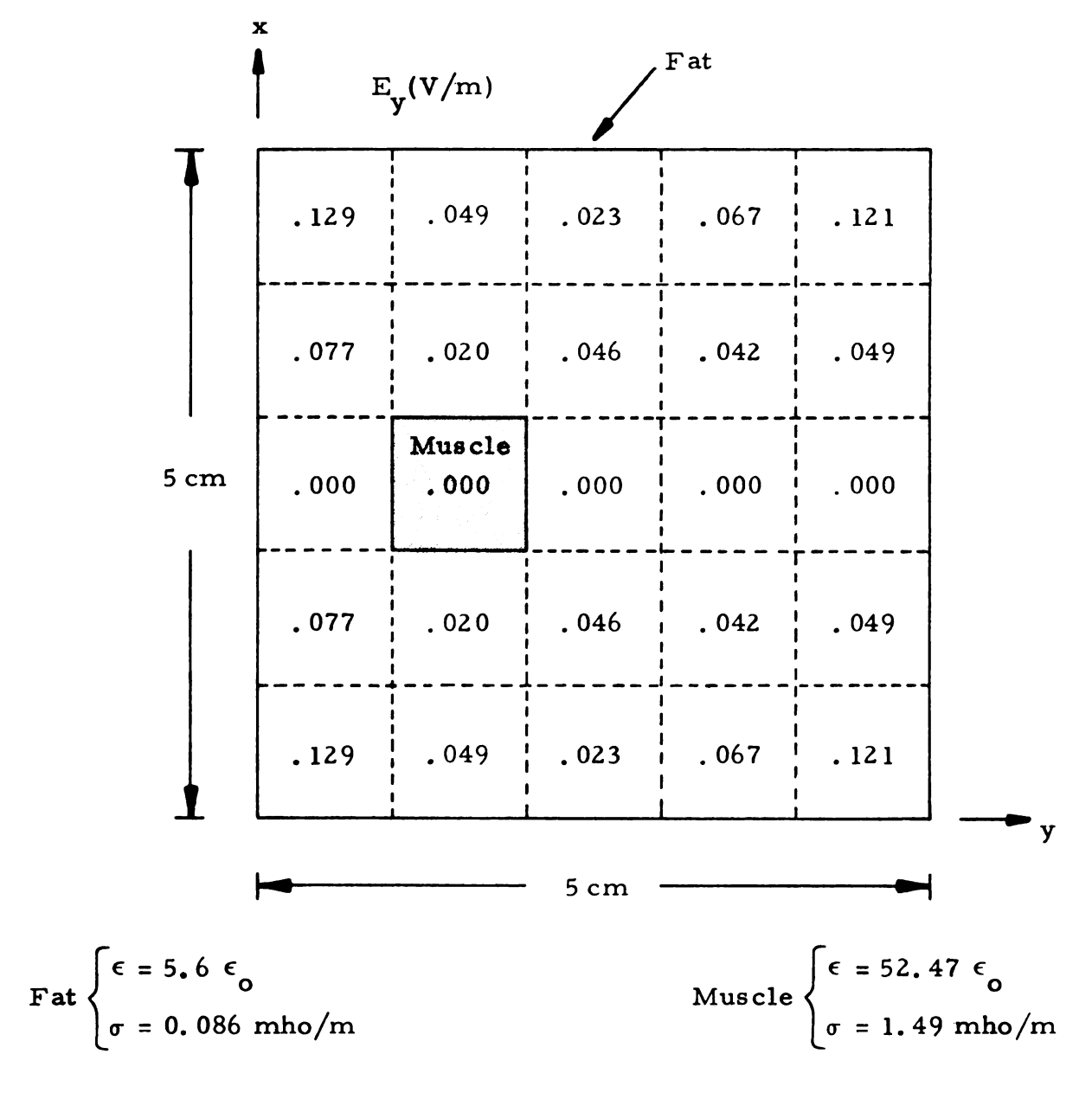


Figure 3.30. An inhomogeneous fat layer illuminated by a uniform plane wave at 600 MHz.



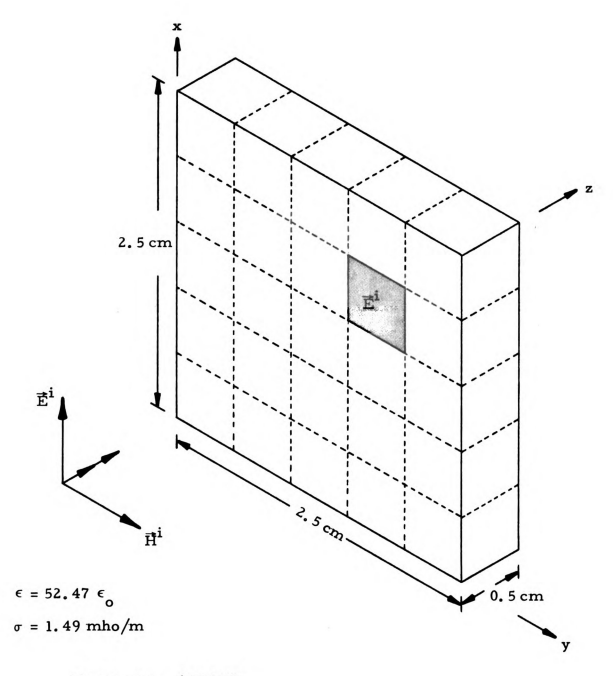
Frequency = 600 MHz

Figure 3.31. The x-component of the electric field induced in the layer illustrated in Figure 3.30. The incident field is polarized along the x-axis.



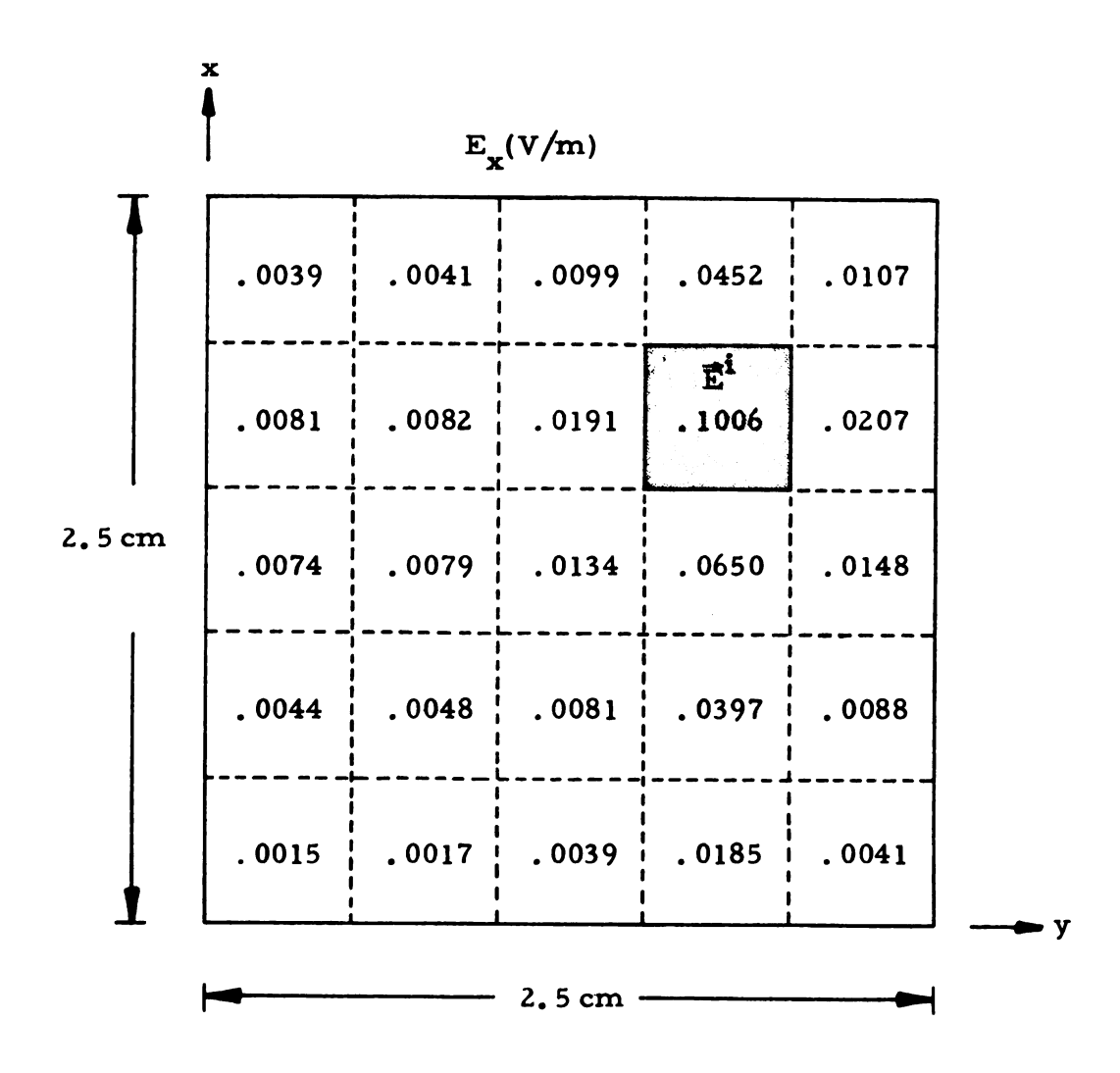
Frequency = 600 MHz

Figure 3.32. The y-component of the electric field induced in the layer illustrated in Figure 3.30. The incident field is polarized along the x-axis.



Frequency = 600 MHz

Figure 3.33. A homogeneous layer of muscle, illuminated only in the shaded area by a 600 MHz plane wave.

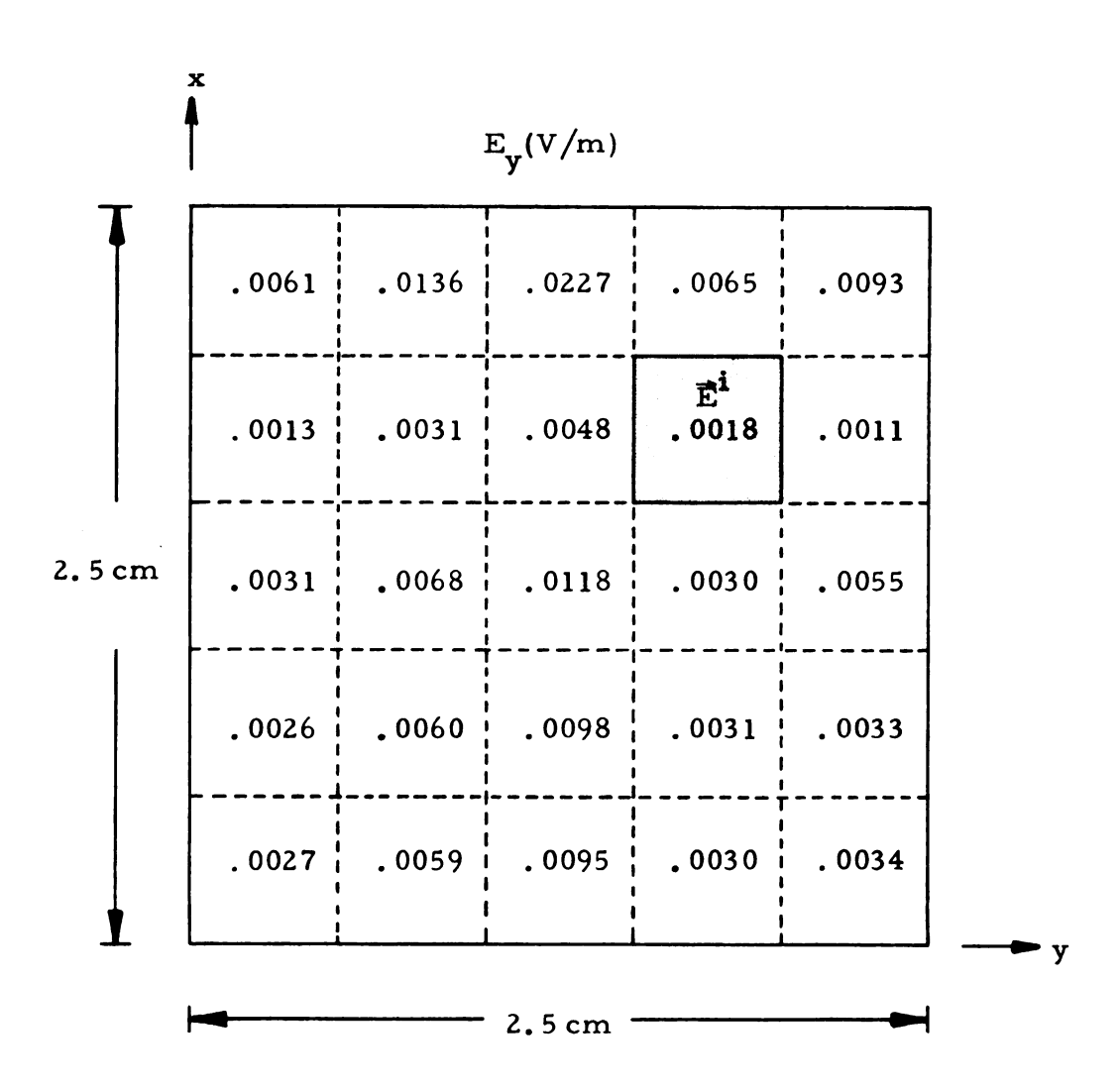


 ϵ = 52.47 ϵ_{0}

 $\sigma = 1.49 \text{ mho/m}$

Frequency = 600 MHz

Figure 3.34. The x-component of the electric field induced in the layer pictured in Figure 3.33. The incident field is polarized along the x-axis, and irradiates only the shaded portion of the layer.



$$\epsilon = 52.47 \epsilon_{o}$$

 $\sigma = 1.49 \text{ mho/m}$

Frequency = 600 MHz

Figure 3.35. The y-component of the electric field induced in the layer pictured in Figure 3.33. The incident field is polarized along the x-axis, and irradiates only the shaded portion of the layer.

the layer, but we note that its maximum value is attained in a subvolume other than the one illuminated.

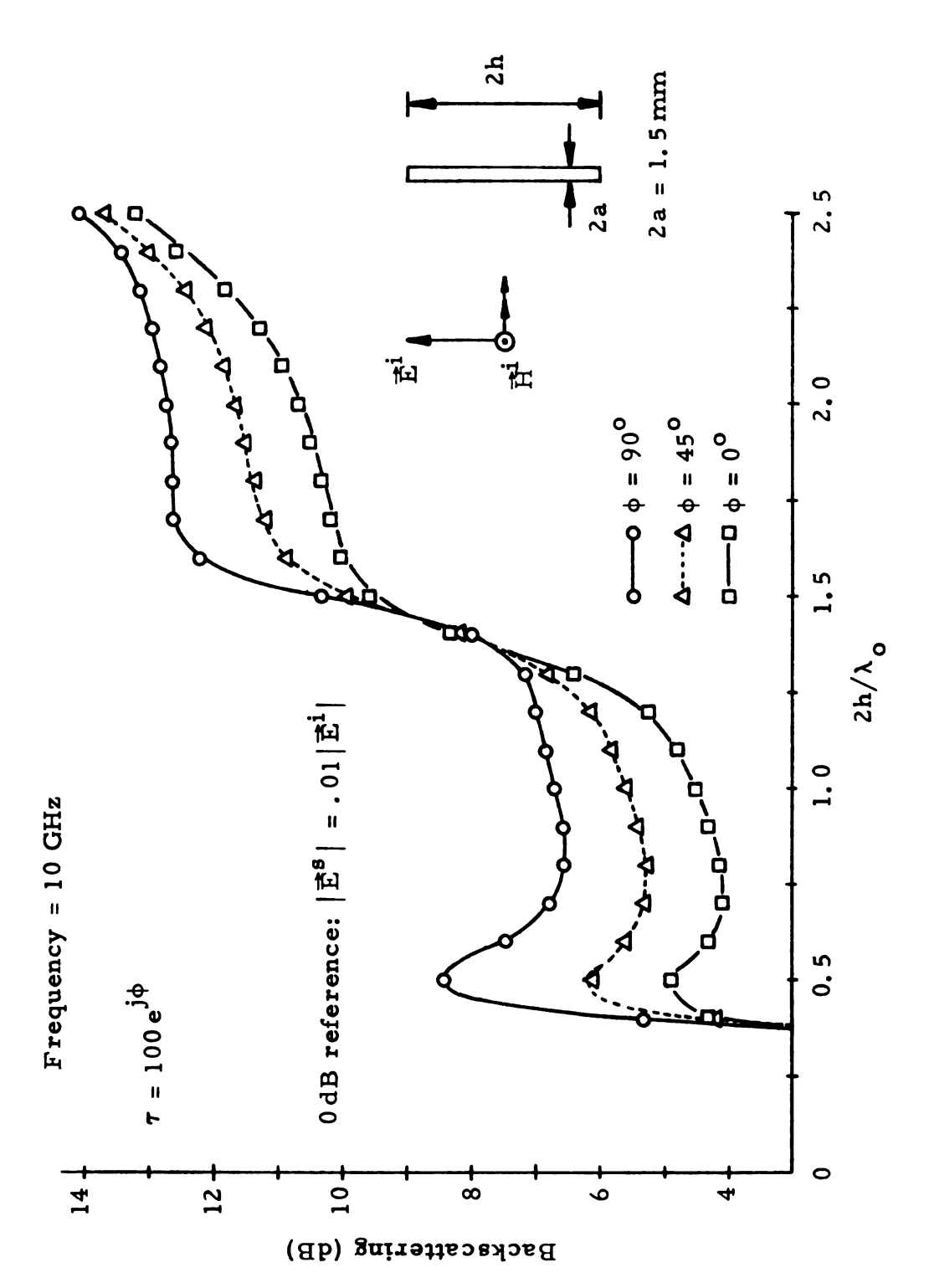
C. External Scattered Field

In the following group of examples, we examine the backscattering characteristics of various thin cylinders exposed to uniform plane waves. The incident field is parallel to the cylinder axis, so that only an axial field is induced. Equation (3.6.3b) is used to compute the backscattered field. The 0 dB reference for all figures in this group is $|\vec{E}^s| = 0.01|\vec{E}^i|$.

The first example investigates how the phase angle of τ affects the scattering behavior of a cylinder. We note that τ , given by Equation (3.2.6b), can be thought of as a complex conductivity, having a magnitude $|\tau|$ and a phase angle ϕ . \vec{J}_{eq} is purely a conduction current when $\phi = 0^{\circ}$, while $\phi = 90^{\circ}$ implies that \vec{J}_{eq} is solely a polarization current; if $\phi = 45^{\circ}$, the conduction and polarization components of \vec{J}_{eq} are equal.

In Figure 3.36 we have plotted the backscattering, calculated at a distance of 30 cm, as a function of length for three different cylinders. The magnitude of τ was 100 in all three cylinders, but ϕ was different for each one; the respective values were 0° , 45° , and 90° . We note that the backscattering increases with ϕ . Although all three cylinders exhibit a resonance at $\lambda_{\circ}/2$, the peak grows sharper as ϕ increases. This occurs because the losses in the cylinder decrease as ϕ grows larger. Hence, for a fixed value of $|\tau|$, the scattering will increase with the ratio of polarization current to conduction current.

We compare theory and recent experimental results [10] in the next four examples. In each case, the scattered field was determined



Backscattering from three different homogeneous cylinders exposed to a 10 GHz plane wave. The magnitude of r was 100 in each case, but the respective values of the phase angle of r were 0°, 45°, and 90°. The observation point was 30 cm from each cylinder. Figure 3.36.

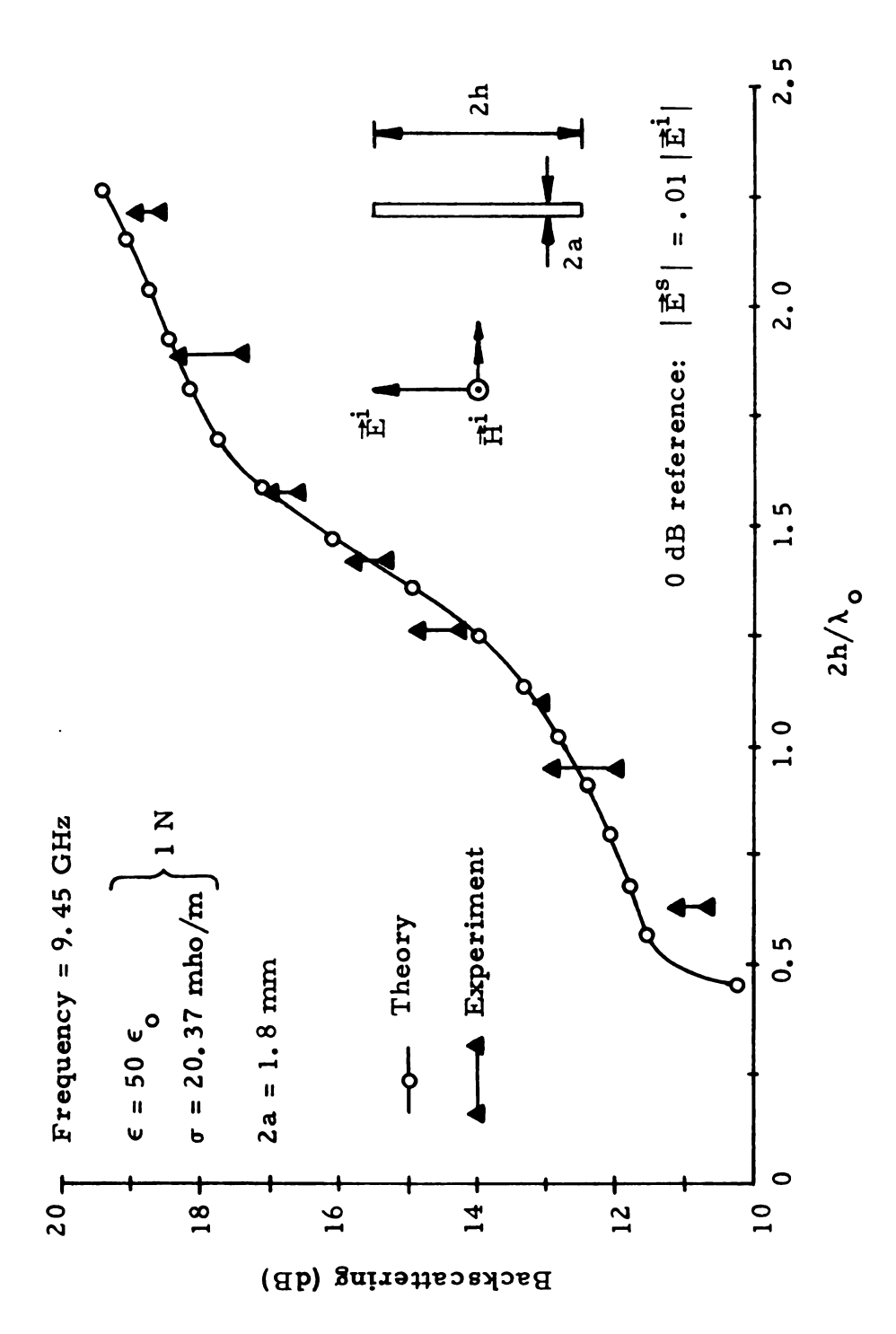
15 cm from the corresponding cylinder. Figures 3.37 and 3.38 illustrate the backscattering from salt water cylinders at 9.45 GHz. The concentrations of the salt solutions are 1 Normal and 5 Normal, respectively. In both figures the agreement between theory and experiment is very good. We note the absence of resonances at $\lambda_0/2$, even though, as we recall, the total absorbed power reaches a relative maximum at this length (see Figures 3.21, 3.23, and 3.25).

Although the assumptions we made in developing the moment solution are not valid for a good conductor at microwave frequencies unless the number of subvolumes is extremely large, an attempt has been made to calculate the backscattering from a brass cylinder at 9.45 GHz. We have compared the theoretical results with experiment in Figure 3.39, and find the agreement to be surprisingly good. Although the current in the brass cylinder is essentially a surface current, the model used here can provide useful data on scattering from metallic cylinders.

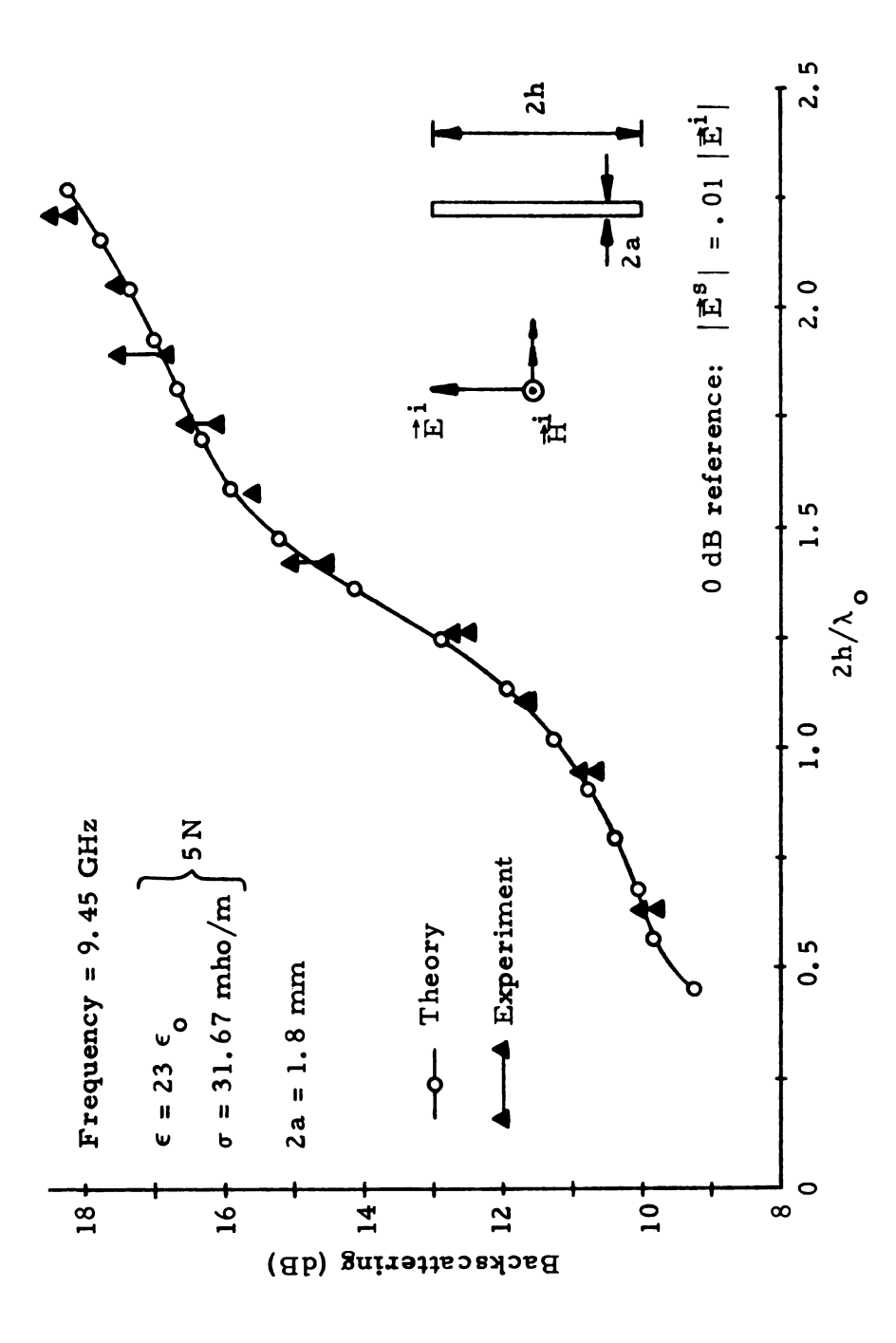
In Figure 3.40 we have compared the relative backscattering from a 1 Normal saltwater cylinder and a brass cylinder at 9.45 GHz. The experimental results agree well with theory. When the cylinder lengths are odd multiples of $\lambda_0/2$, the brass cylinder exhibits resonances, and scatters more than the saltwater cylinder. At lengths which are even multiples of $\lambda_0/2$, the saline solution scatters more. Thus, it is possible that a cylindrical biological structure, such as man, could scatter more microwave energy than a similar metallic cylinder.

D. Symmetric and Antisymmetric Modes

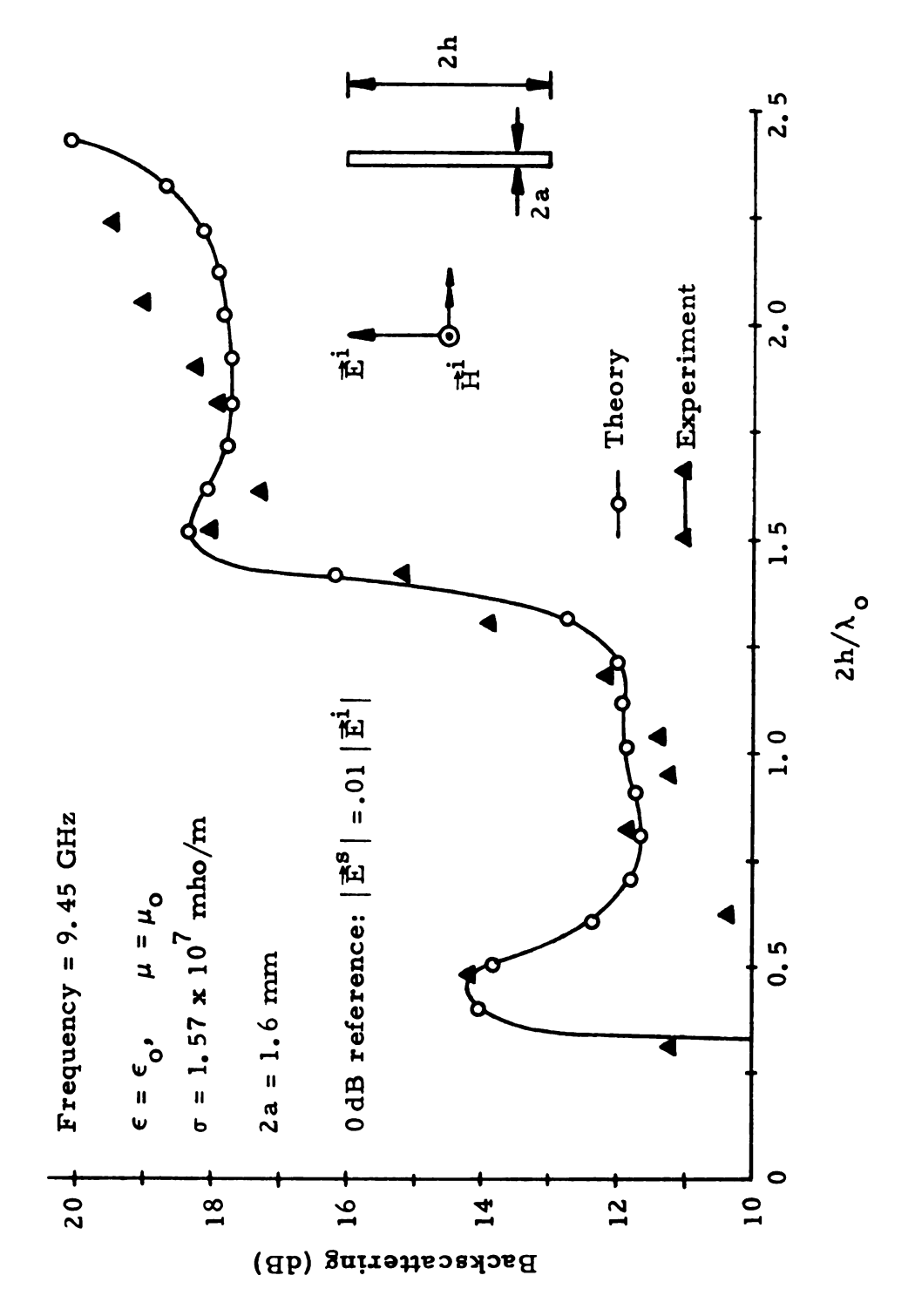
In Section 3.5, we discussed the decomposition of an incident plane wave \vec{E}^i into a symmetric component \vec{E}^i_s and an antisymmetric component \vec{E}^i_a , given respectively by Equations (3.5.11b) and (3.5.11c). When the



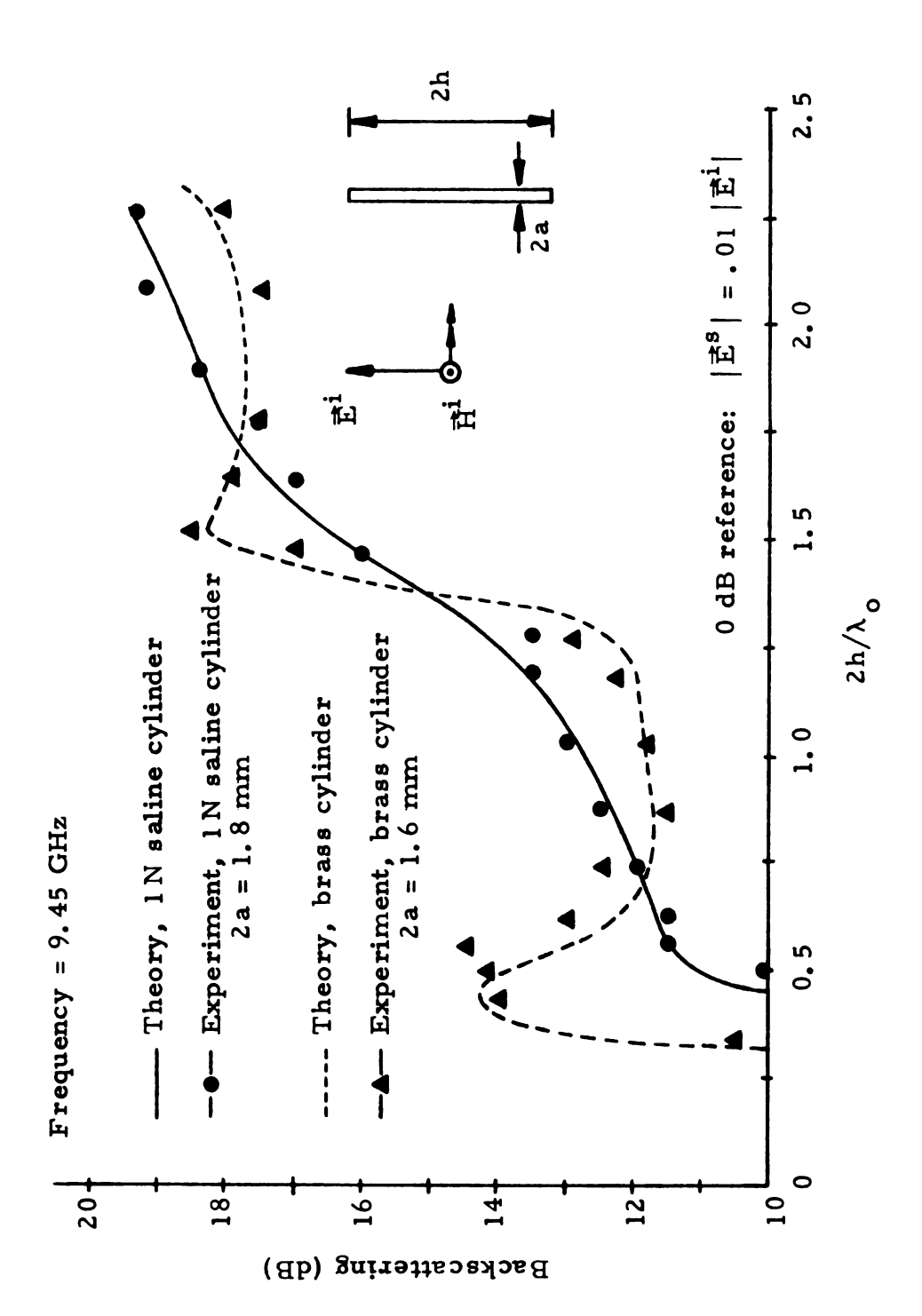
Comparison of theory and experiment for backscattering from a saltwater cylinder of l Normal concentration at 9.45 GHz. The observation point was 15 cm from the cylinder. Figure 3.37.



Comparison of theory and experiment for backscattering from a saltwater cylinder of 5 Normal concentration at 9.45 GHz. The observation point was 15 cm from the cylinder. Figure 3, 38.



Comparison of theory and experiment for backscattering from a brass cylinder at 9.45 GHz. The observation point was 15 cm from the cylinder. Figure 3.39.



Comparison of theory and experiment for relative backscattering from a brass cylinder The frequency was 9.45 GHz, and and a saltwater cylinder of I Normal concentration. the observation point was 15 cm from each cylinder. Figure 3.40.

plane wave impinges upon a biological body, each of these components induces a partial field inside the body; \vec{E}_s^i excites a symmetric mode \vec{E}_s , while \vec{E}_a^i induces an antisymmetric mode \vec{E}_a . The total electric field \vec{E} inside the body is simply the sum of \vec{E}_s and \vec{E}_a . The examples in this group illustrate some of the characteristics of the symmetric and antisymmetric modes. In each example, both \vec{E}_s and \vec{E}_a exhibit nearly linear polarization; they differ markedly, however, in their spatial distributions. \vec{E}_s is generated mainly by the incident electric field, while \vec{E}_a is due primarily to the incident magnetic field.

Figure 3.41 shows the symmetric mode \vec{E}_s in a muscle layer measuring 5 cm x 5 cm x 0.5 cm, irradiated by a 1 GHz plane wave. \vec{E}^i is parallel to the plane of the layer, while \vec{H}^i is perpendicular to it. The magnitude of the symmetric mode is greatest at the center of the layer, and decreases toward the edges. We note that \vec{E}_s is roughly parallel to \vec{E}^i throughout the layer.

The antisymmetric mode \vec{E}_a in the same layer is illustrated in Figure 3.42. \vec{E}_a is small near the center of the layer, and generally increases toward the edges. In contrast to the symmetric mode, the field lines of the antisymmetric mode circulate about \vec{H}^i . $|\vec{E}_s|$ and $|\vec{E}_a|$ are roughly equal in this example.

Since \vec{E}_s and \vec{E}_a are not in phase, the total electric field in the layer is elliptically polarized. The ellipse traced out by the electric field vector in each subvolume is plotted in Figure 3.43. The polarization varies throughout the layer from almost linear to nearly circular.

Figure 3.44 depicts a 100 MHz plane wave irradiating a loop of muscle measuring 10 cm x 10 cm x 1 cm. \vec{E}^i and \vec{H}^i are parallel and perpendicular, respectively, to the plane of the loop. The symmetric

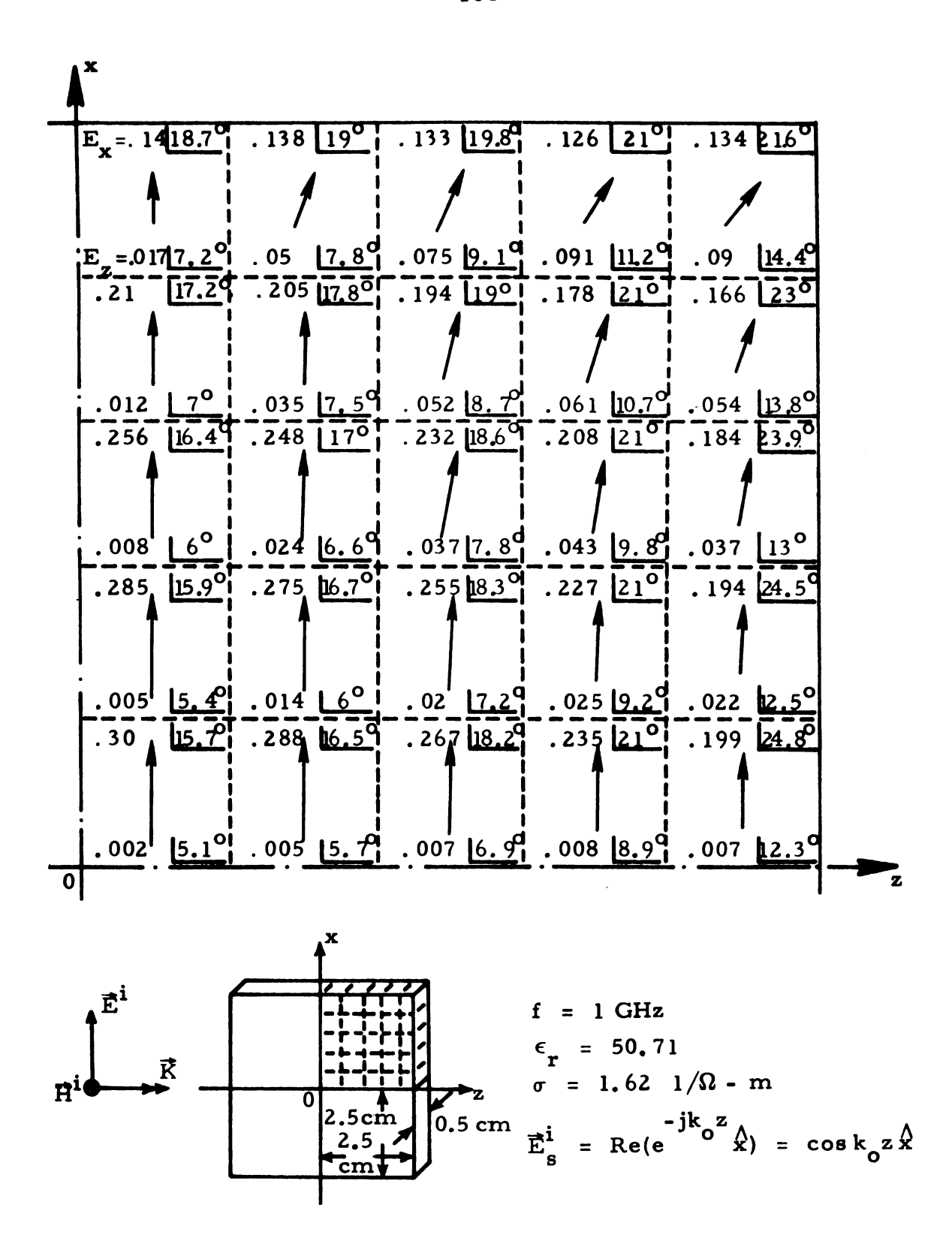


Figure 3.41. The symmetric mode of the electric field in a muscle layer exposed to a 1 GHz plane wave. The symmetric mode is induced by the symmetric component ($\cos k$ z $\stackrel{?}{E}$) of $\stackrel{?}{E}$. Only 1/4 of the layer is shown above.

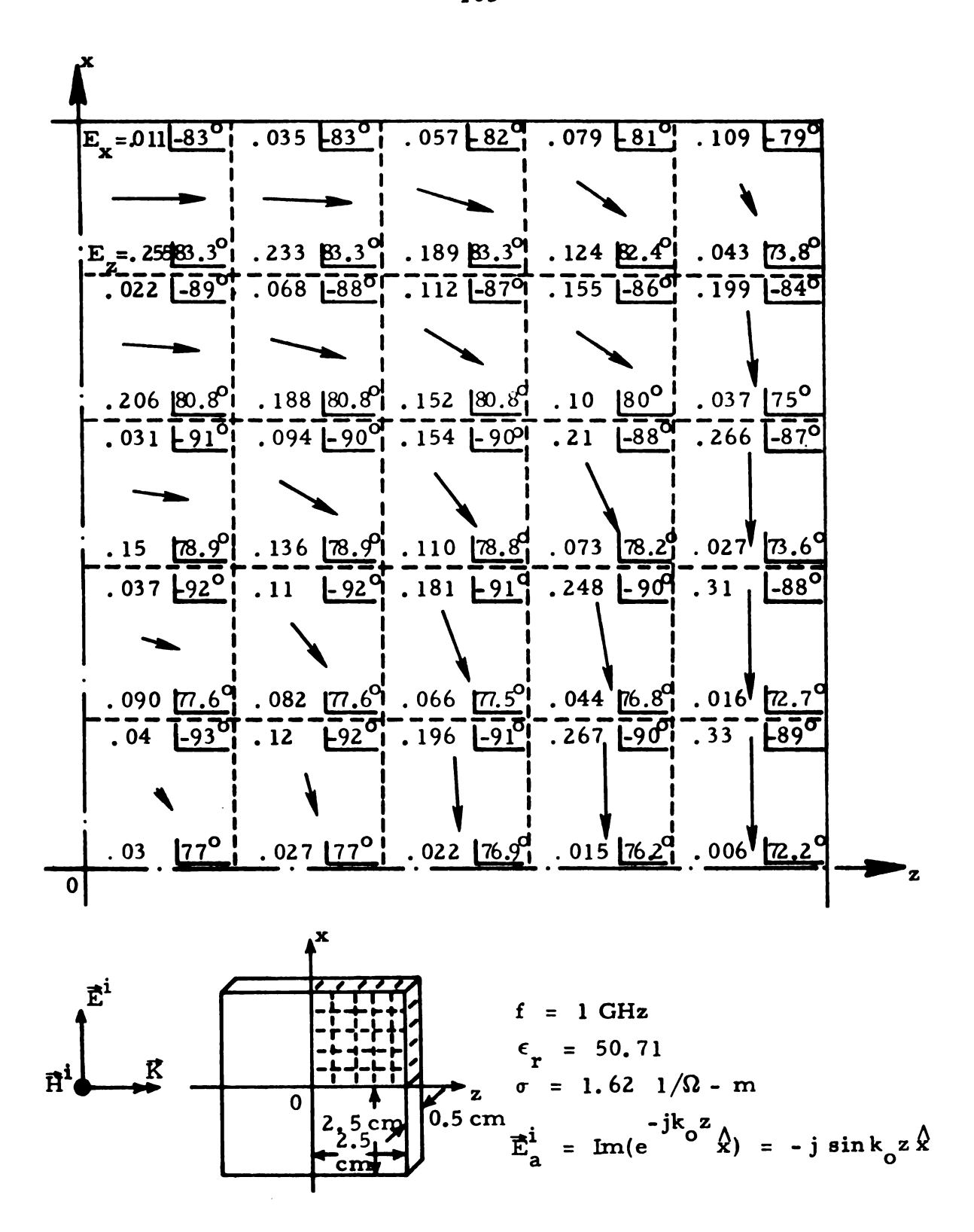


Figure 3.42. The antisymmetric mode of the electric field in a muscle layer exposed to a 1 GHz plane wave. The antisymmetric mode is induced by the antisymmetric component (-j sink₀z x) of Eⁱ. Only 1/4 of the layer is shown above.

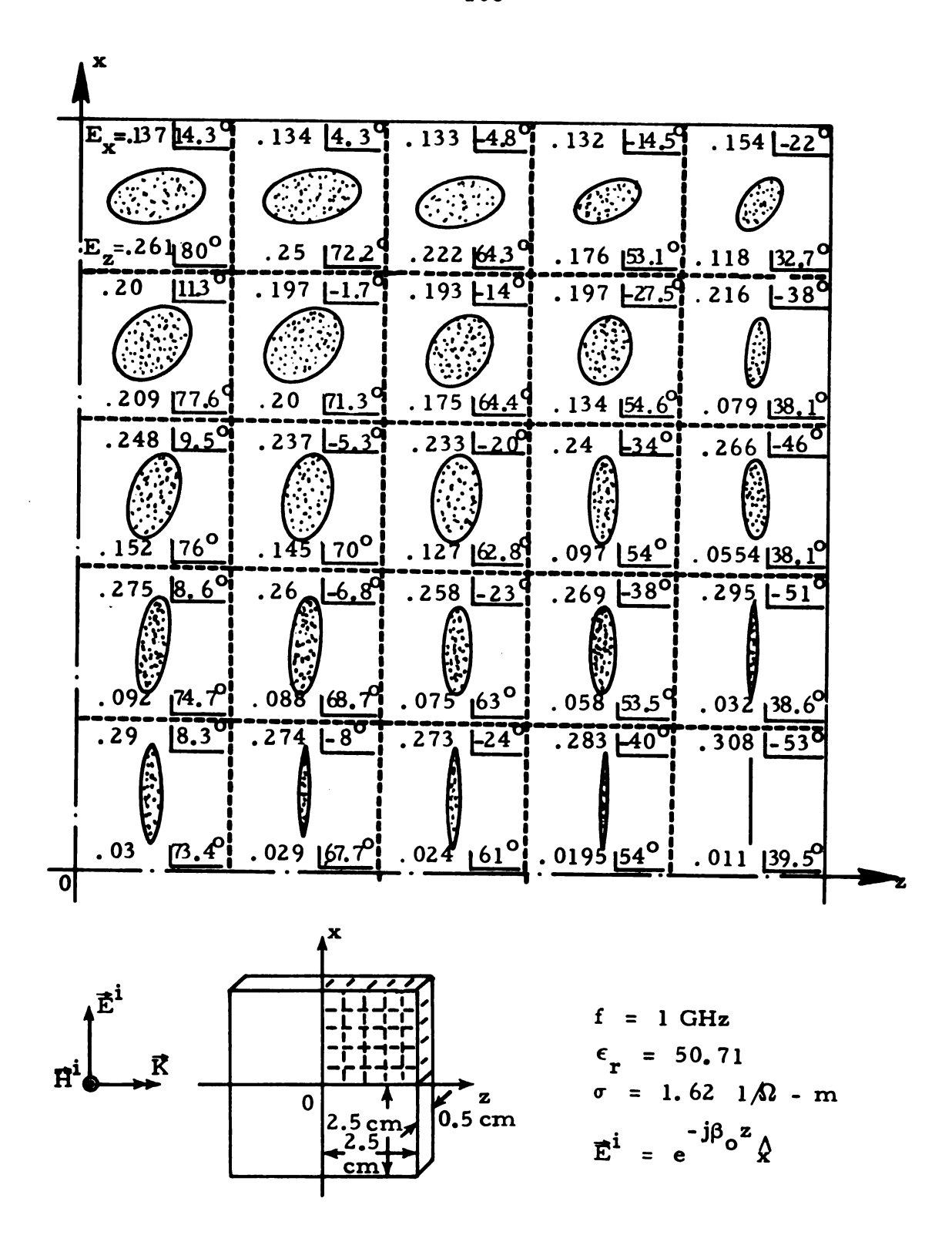
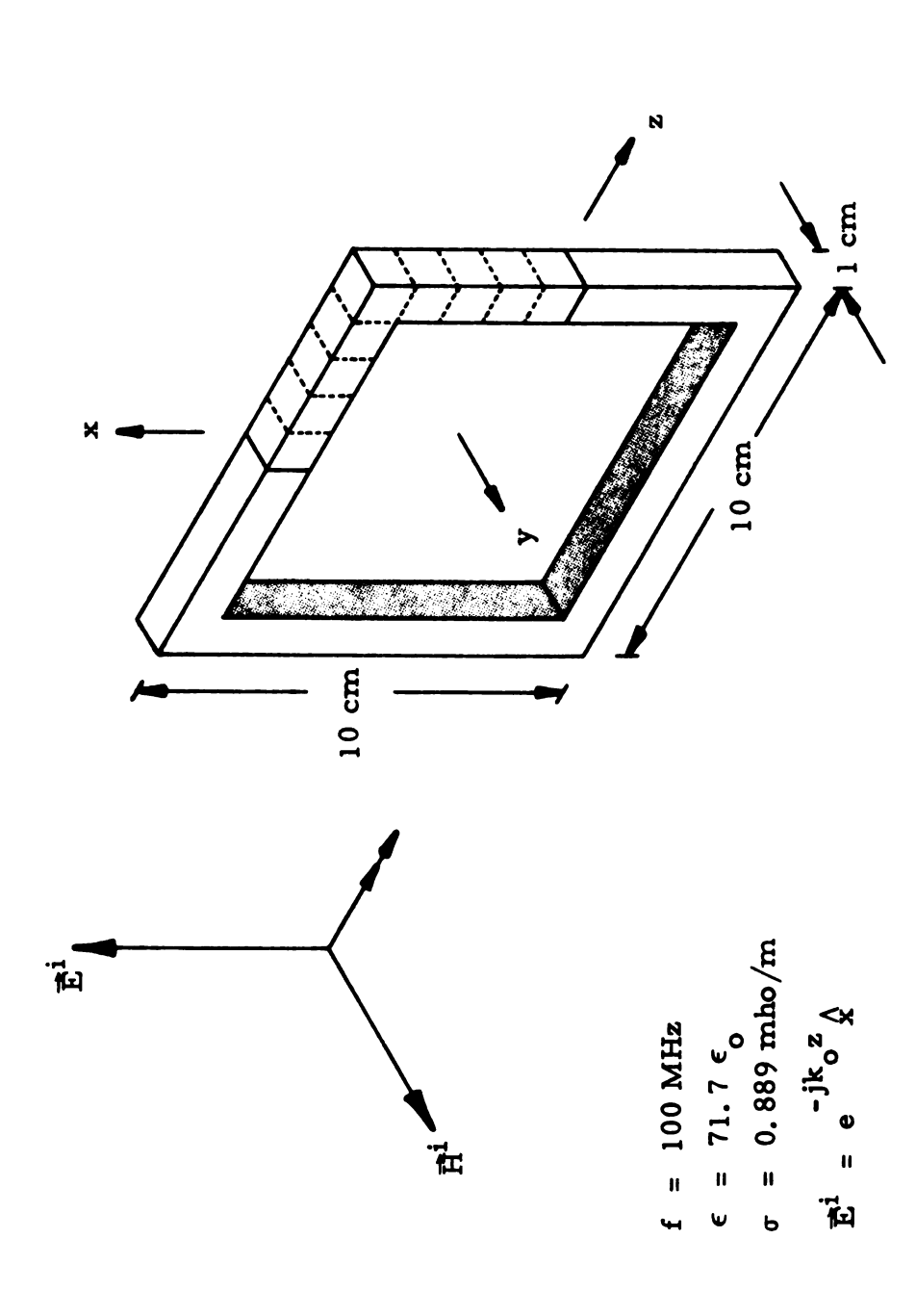


Figure 3.43. The total electric field induced in a muscle layer by a 1 GHz plane wave. Only 1/4 of the layer is shown above.



A square loop of muscle irradiated by a 100 MHz plane wave. E lies in the plane of the loop, while H^i is normal to the plane of the loop. Figure 3. 44.

and antisymmetric modes are illustrated in Figures 3.45 and 3.46, respectively. We note that \vec{E}_s is largest in the segments of the loop which are parallel to \vec{E}^i . As in the previous example, \vec{E}_a circulates about the incident magnetic field. Because the loop in this example is electrically small, $|\vec{E}_a|$ is generally much less than $|\vec{E}_s|$. Therefore, the total electric field in the loop has not been plotted.

Two features characterize the symmetric mode: it is excited by the incident electric field, and it resembles an oscillating dipole. The antisymmetric mode, on the other hand, is a circulatory field generated by the incident magnetic field.

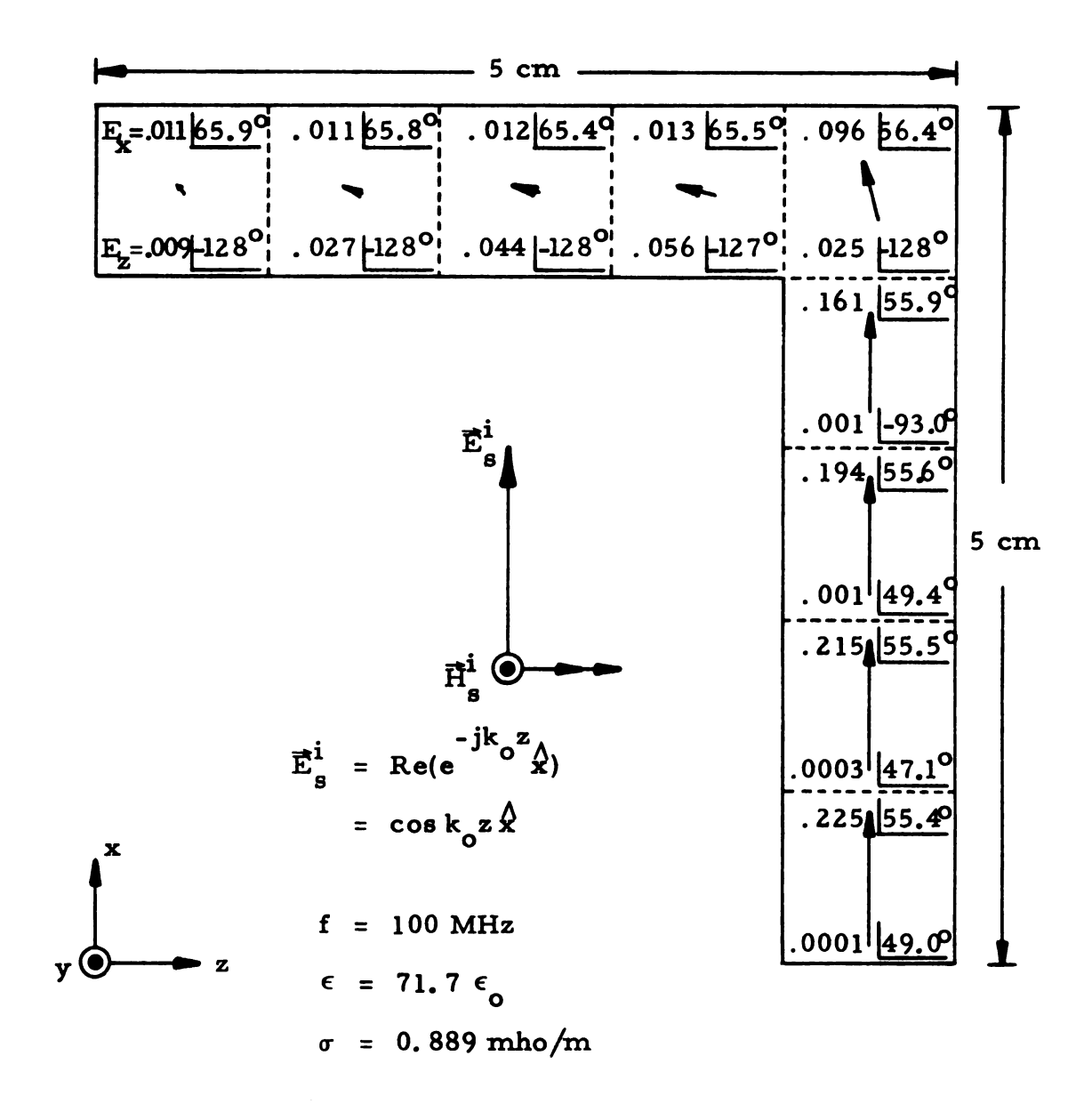


Figure 3.45. The symmetric mode of the electric field in the loop of muscle shown in Figure 3.44. The symmetric mode is induced by the symmetric component (cos k oz k) of the incident field. Only 1/4 of the loop is shown above.

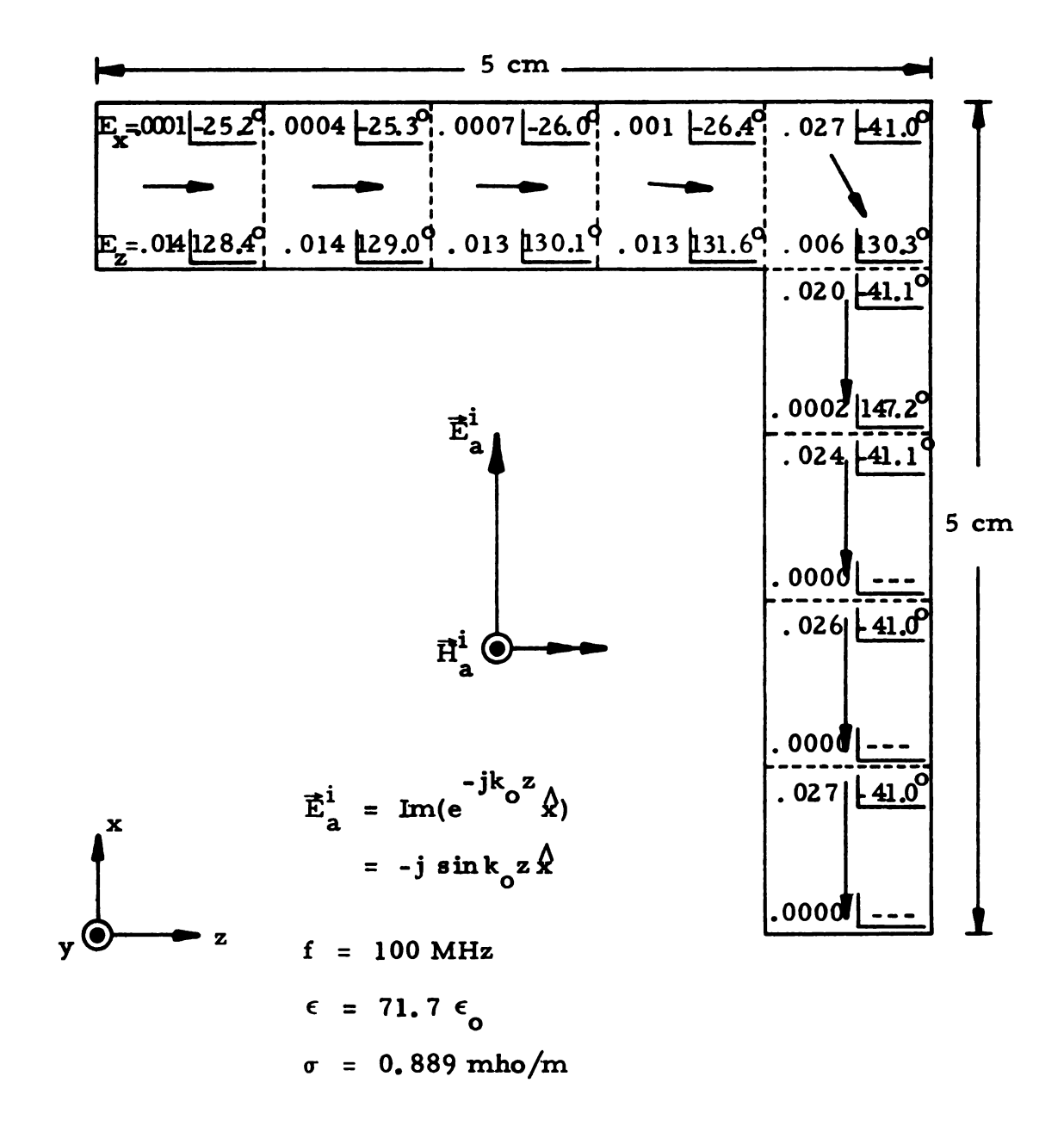


Figure 3.46. The antisymmetric mode of the electric field in the loop of muscle shown in Figure 3.44. The antisymmetric mode is induced by the antisymmetric component (-j sink_oz x) of the incident field. Only 1/4 of the loop is shown above.

CHAPTER IV

A DESCRIPTION OF THE COMPUTER PROGRAM USED TO DETERMINE THE INDUCED ELECTRIC FIELD IN AN ARBITRARY, FINITE PHYSIOLOGICAL SYSTEM

This chapter includes a description of the computer program used to obtain the numerical results presented in Chapter III. A listing of the program deck and instructions for its use are also provided.

4.1. Description of the Program

Figure 4.1 shows a rectangular block of tissue, illuminated by an electromagnetic plane wave. Only normal incidence will be considered here. The incident field is given by

$$\vec{E}^{i}(\vec{r}) = \lambda e^{-jk} o^{z} . \qquad (4.1.1)$$

PRØGRAM BLØCK will calculate the induced electric field and the power density at a prescribed number of uniformly spaced points inside the tissue block by solving the matrix equation

$$[G][E] = -[E^{i}]$$
 (4.1.2)

Given the necessary data, the program constructs a mathematical model of the body, calculates the elements of [G], then solves Equation (4.1.2) for [E]. If the user wishes, BLØCK will also calculate the external scattered field.

The block of tissue is partitioned into N identical rectangular subvolumes, and the induced electric field is calculated at the center of each subvolume. Since the program can accommodate a matrix [G] of any size up to 100×100 , N can be no larger than 33 in the most general

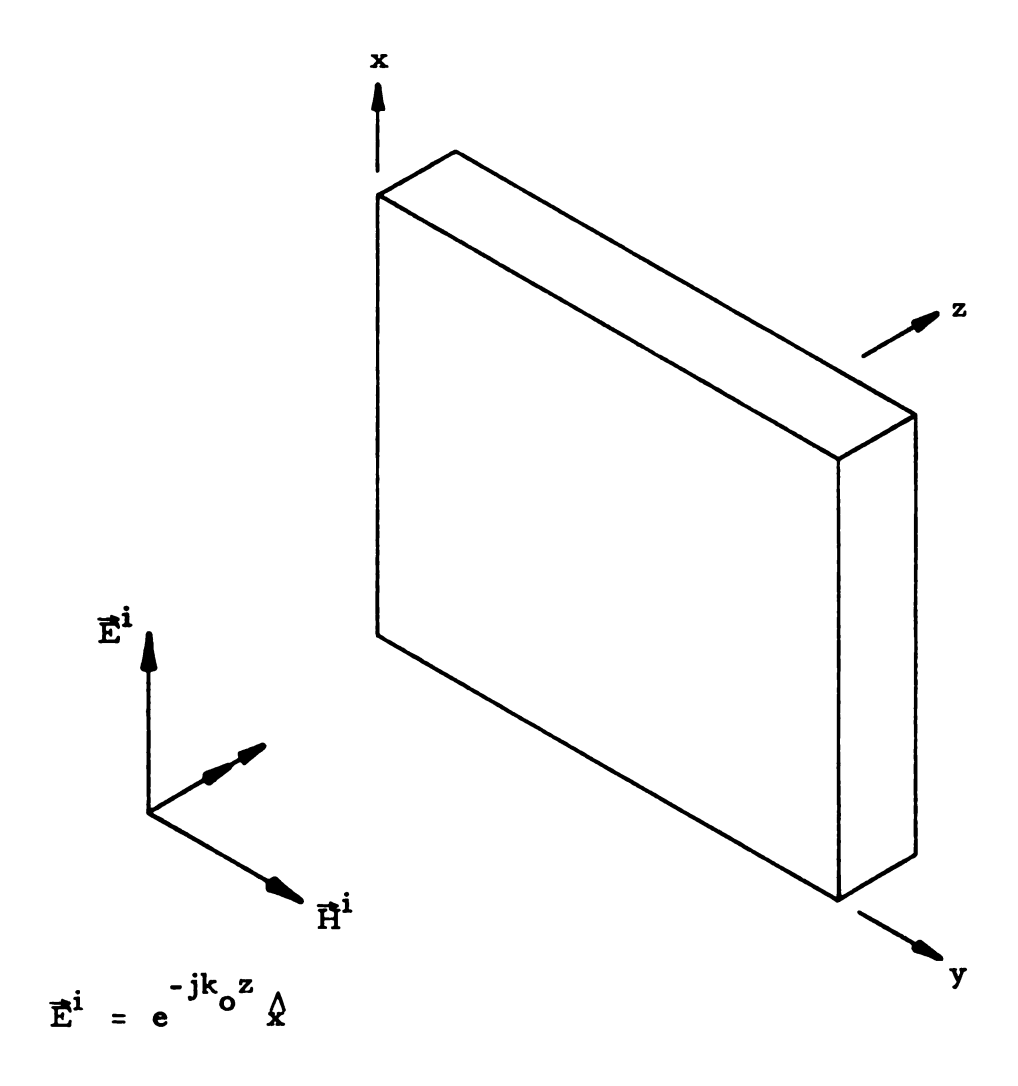


Figure 4.1. An electromagnetic plane wave, incident normally upon a rectangular block of tissue.

case. Often, however, by exploiting the body's symmetry (if any) and by neglecting certain components of the induced field, we can, in effect, increase this number several times. In fact, we can use as many as 400 subvolumes in certain cases. The details will be given in Section 4.3.

The following options are available to the user:

- 1. The block of tissue can be homogeneous or inhomogeneous.
- 2. The block may be illuminated uniformly over its crosssection, or only in selected areas.
- 3. The user can neglect certain components of the induced field, thereby reducing the size of [G] and increasing the limit on the number of subvolumes allowed. If the partitioning scheme has even symmetry, the user can further reduce the size of [G].
- 4. The scattered field may be calculated at any point outside the block, using either rectangular or spherical polar coordinates.

4.2. Structure of the Data File

The data file for PRØGRAM BLØCK, showing the input variables, their FØRMAT specifications, and their locations within the file, is outlined in Table 4.1. A detailed description of the variables is given in Section 4.3.

A sample partitioning scheme for an arbitrary block is shown in Figure 4.2. The block is divided into layers along the z-axis; each layer is partitioned into rows and columns of subvolumes along the x-and y-axes, respectively. The simplest model for the program to work with is a block in which each layer is homogeneous, and whose cross-

CARD NØ.	CØLUMN(S)	VARIABLE NAME	<u>FØRMAT</u>
1	48	NDIV	I 1
2	1-5 11-20 21-28	CØMP * FMEG IQARR(J), J=1, 8	A5 F10.0 811
3	1-2 6-7 11-12	NX NY NZ	12 12 12
4	1-10 11-20 21-30	DXCM DYCM DZCM	F10.0 F10.0 F10.0
5.1,,5.NZ	1-10 11-20	RLEP1 SIG1	F10.0 F10.0
6	41-47	FILE1 *	A 7
6a,6b, (Subfile #1)	1-2 6-7 11-13	IX IY INDEX1	12 12 A3
7	38-44	FILE2 *	A 7
7a, 7b, (Subfile #2)	1-2 6-7 11-12 21-30 31-40 41-43	MX MY MZ RLEP2 SIG2 INDEX2	12 12 12 F10.0 F10.0
8	33-39	FILE3 *	A7
8a, 8b, (Subfile #3)	1-5 11-20 21-30 31-40 41-43 51-56	CØØRD * C1 C2 C3 INDEX3 ACTIØN AXIS *	A5 F10.0 F10.0 F10.0 A3 A6 A1

Table 4.1. The structure of the data file for PRØGRAM BLØCK. If any of the variables marked with an asterisk does not match its prescribed codes, the program will be aborted.

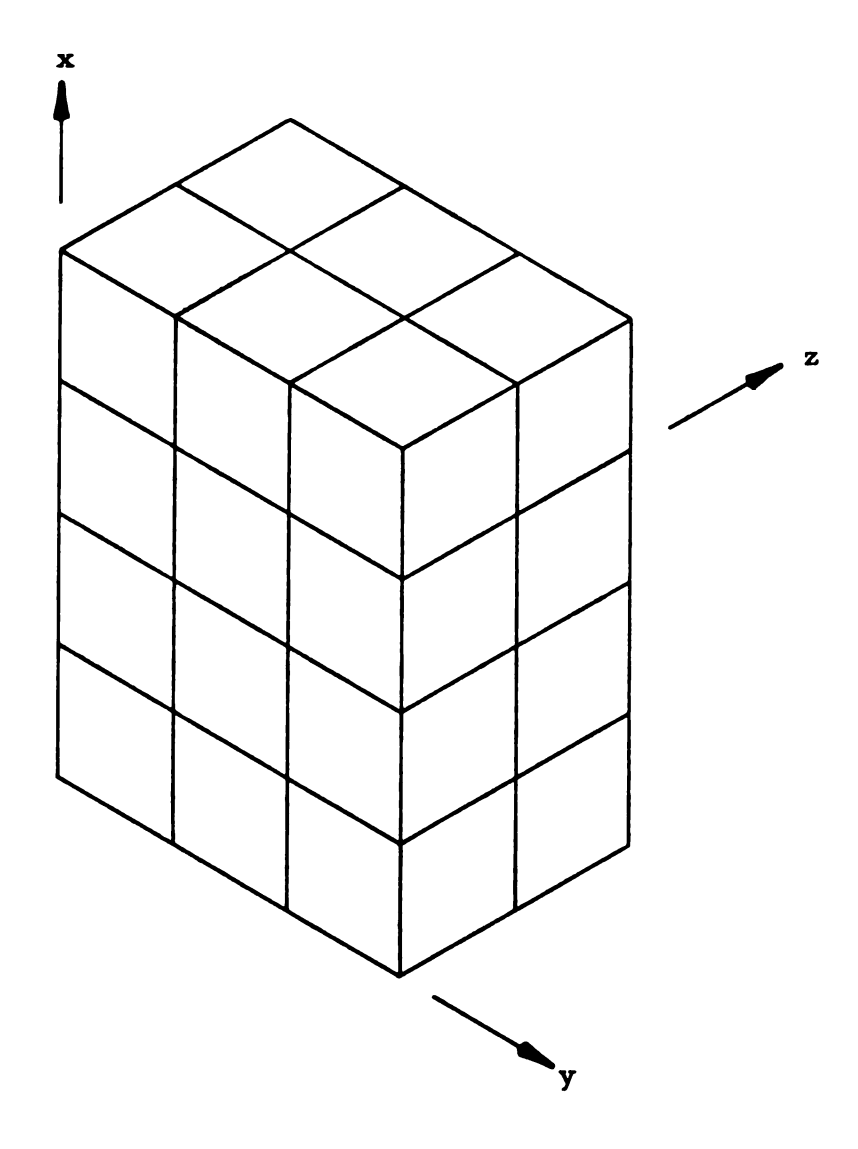


Figure 4.2. A block of tissue partitioned into rows, columns, and layers of subvolumes along the x-, y-, and z-axes, respectively.

section is uniformly illuminated by the incident wave. Hence, BLØCK uses the first few data cards to construct such a model; the user makes any necessary changes with the remaining data cards. The next few paragraphs describe this procedure.

The first four cards contain variables which describe the geometry of the tissue block. The "fifth card" is actually a "subfile" containing one card for each layer of subvolumes. Each card in this group specifies the relative permittivity and conductivity of its respective layer. If a particular layer is inhomogeneous, its data card gives the prevalent values of $\epsilon_{\mathbf{r}}$ and σ in that layer.

The program uses the above data to construct the simple model described above. The remainder of the data file consists of three subfiles which enable the user to make any desired changes. On Card 6, for example, he indicates whether or not the incident field is collimated, illuminating only selected portions of the block. If it is collimated, each card in the first subfile (Cards 6a, 6b, etc.) locates one incident beam. If the block is uniformly illuminated, Subfile #1 is omitted.

Similarly, Card 7 indicates whether any of the layers in the body are inhomogeneous. If so, each card in Subfile #2 (Cards 7a, 7b, etc.) specifies the location and electrical parameters of one inhomogeneity. The subfile is excluded if each layer is homogeneous.

On Card 8, the user states whether or not he wishes to calculate the scattered field. If he does, each card in the third subfile provides the data needed to calculate the scattered field at one exterior point.

Otherwise, the subfile is omitted.

4.3. Description of the Input Variables

In this section we describe the function of each input variable and explain how it is used in PRØGRAM BLØCK. The variables are presented in their order of appearance in the data file.

NDIV -- This variable allows the user to control the accuracy with which the elements of [G] are evaluated. Each subvolume is divided into NDIV³ identical cells in order to perform the numerical integration. Thus, as NDIV is increased, the matrix elements will be evaluated more accurately, although at greater cost. Using NDIV = 1 leads to the approximation given by Equation (3.4.5a). Setting NDIV = 2 usually gives satisfactory results at a reasonable cost. Beginning in Column 1, the first card reads:

NUMBER ØF DIVISIØNS PER EDGE FØR INTEGRATIØN = 2.

CØMP -- In some cases, various components of the induced field are so small in comparison with the others that they may be assumed to be zero. Consequently, considerable time, cost, and computer storage can be saved. The program can accommodate a matrix [G] of any size up to 100 x 100. If all three components of Ē are non-zero, [G] is 3N x 3N, thereby allowing up to 33 subvolumes. If the internal field has only x- and y-components, [G] is 2N x 2N, enabling us to use up to 50 subvolumes.

The limit is 100 subvolumes if E_x is the only nonzero component of the induced field, since [G] is N x N in that case. CØMP is a 5-character code indicating which components of the internal electric field are assumed to be nonzero. Only the three cases discussed above are permitted; their respective codes are "X, Y, Z", "XANDY", and "XØNLY". Any other code will abort the program.

- FMEG -- FMEG is the frequency of the incident field, in MHz.
- IQARR -- As shown in Figure 4.3, the body under consideration may exhibit up to four quadrants of symmetry. We can take advantage of this to save time, money, and storage. Because the induced field will also be symmetrical, [E] is calculated only in the first quadrant of the block. The number of unknowns in Equation (4.1.2) is therefore reduced up to 4 times. IQARR is an array indicating which quadrants of symmetry are present. The block's geometry and partitioning scheme are specified in the first quadrant only; this configuration is then reflected into the appropriate quadrants to obtain a model for the entire block. The quadrants may be listed in any order; blanks and duplicates will be ignored. Quadrant 1 is automatically supplied by the program. Since no combination of 3 quadrants can be symmetrical, any such combination on the data card will abort the program.
- NX, NY, NZ -- NX, NY, and NZ represent the number of partitions along the coordinate axes in the first quadrant. Thus, in Figure 4.3, the block's first quadrant will be divided into NX rows of subvolumes along the x-axis, into NY columns along the y-axis, and into NZ layers along the z-axis.
- DXCM, DYCM, DZCM -- These are the x-, y-, and z-dimensions, respectively, of each subvolume, in centimeters. For best results, each subvolume should be a cube.
- RLEP1, SIG1 -- If a particular layer is homogeneous, these variables are the relative permittivity and conductivity, respectively, of that layer. They represent the predominant values of $\epsilon_{\mathbf{r}}$ and σ if the layer is inhomogeneous.

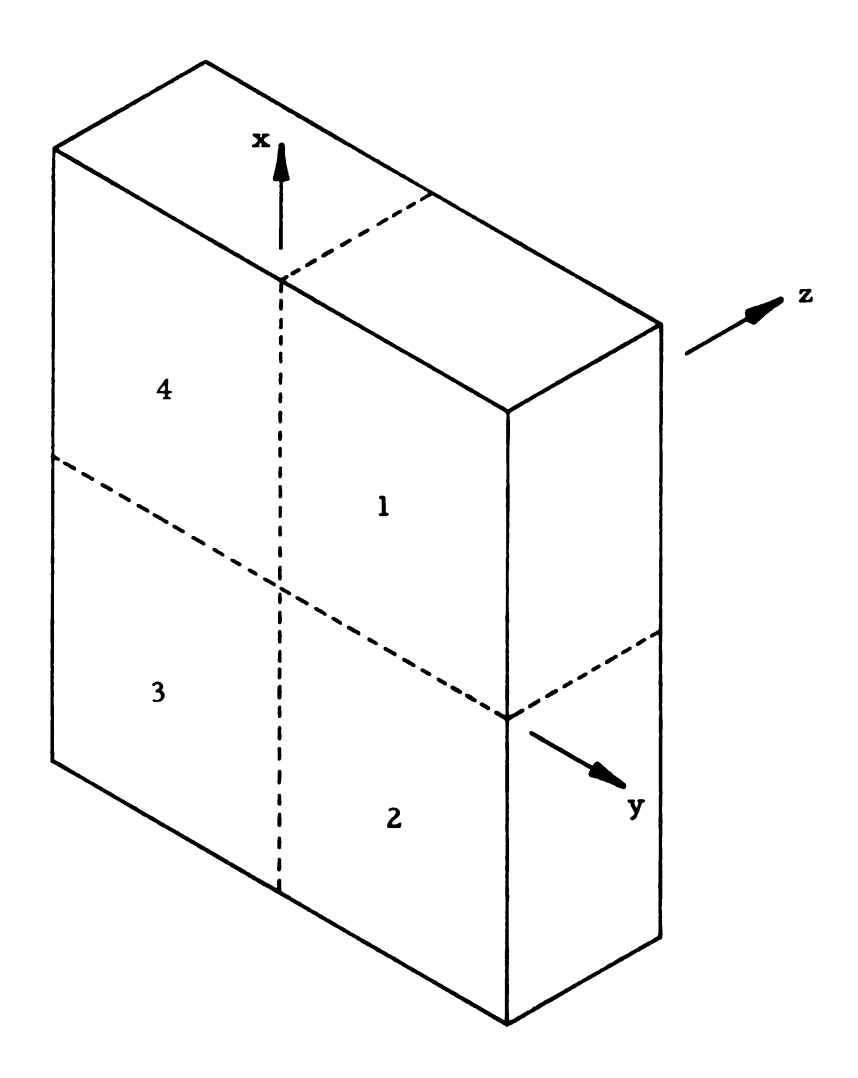


Figure 4.3. A block of tissue divided into 4 symmetrical quadrants. If the incident field is likewise symmetrical, calculating the induced field in only one quadrant will determine the induced field in the entire block.

FILE1 -- FILE1, FILE2, and FILE3 are 7-letter codes which indicate whether or not their respective subfiles are to be included in the data file. The code is "NULLSET" if the subfile in question is to be omitted, and "FØLLØWS" if the subfile is to be included. Any other code will abort the program. FILE1 signifies whether the incident field is uniform or collimated. Beginning in Column 1, the data card reads:

DATA FILE FØR NØNUNIFØRM ILLUMINATIØN = NULLSET FØLLØWS.

- IX, IY -- The collimated incident field impinges upon the intersection of the IXth row and the IYth column of subvolumes in the first quadrant. If symmetry is used in calculating the induced field, the incident field and the tissue block must have the same quadrants of symmetry.
- INDEX1 -- INDEX1, INDEX2, and INDEX3 identify the last card of their respective subfiles by the code "END" or "END FILE". They are blank elsewhere.
- FILE2 -- FILE2 denotes whether or not there are any inhomogeneities in the block. Beginning in Column 1, the data card reads:

 DATA FILE FØR INHØMØGENEØUS LAYERS = NULLSET FØLLØWS.

 See FILE1 for details.
- MX, MY, MZ -- These variables locate an inhomogeneity in the body.

 It is found at the intersection of the MXth row and the MYth column of subvolumes in the MZth layer.
- RLEP2, SIG2 -- These are the relative permittivity and conductivity, respectively, of the subvolume identified by MX, MY, and MZ as the inhomogeneity.
- INDEX2 -- See INDEX1 for details.

FILE3 -- FILE3 indicates whether or not the scattered field is to be computed. Beginning in Column 1, the card reads:

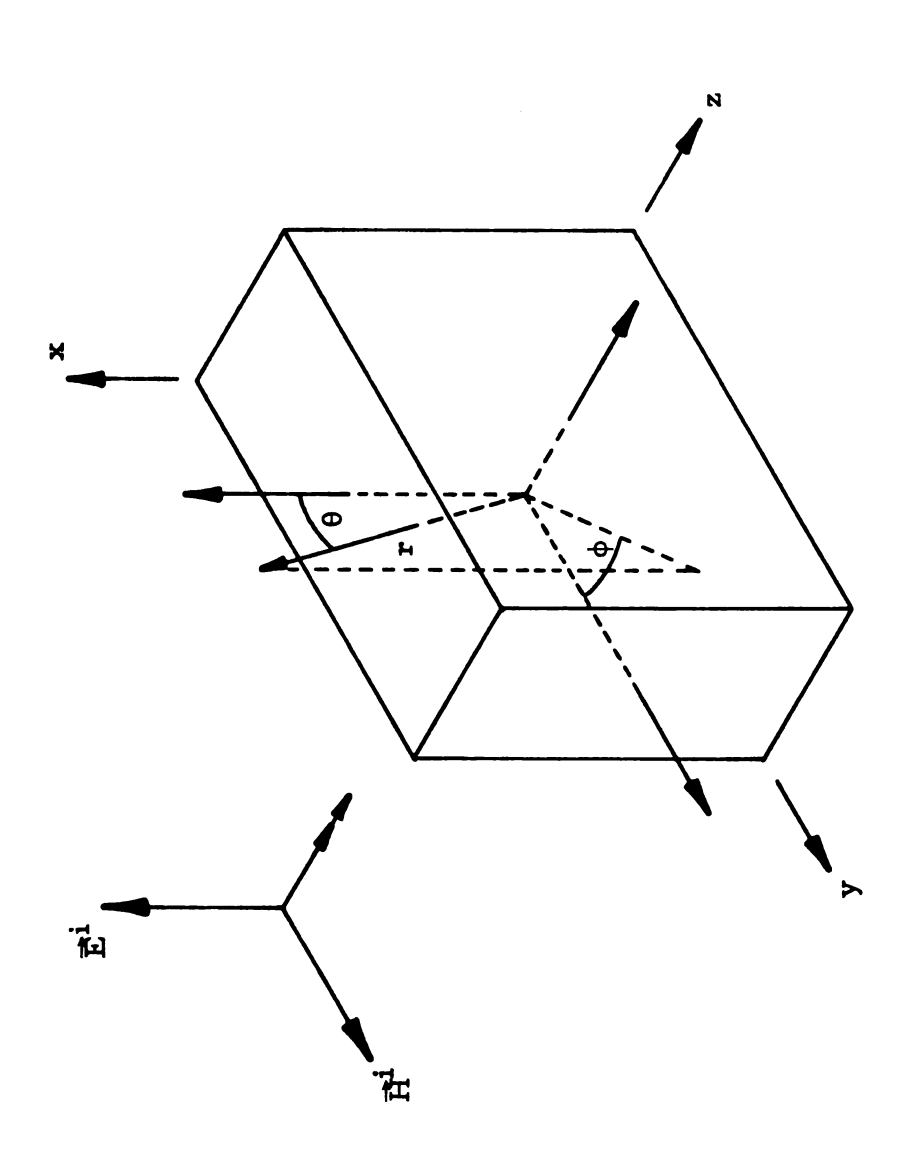
DATA FILE FØR SCATTERED FIELD = $\begin{subarray}{l} NULLSET \\ FØLLØWS \end{subarray}$ See FILE1 for details.

- CØØRD -- This 5-character code identifies the coordinate system in which the field point will be expressed--either rectangular or spherical polar coordinates. The respective codes are "RECT." and "PØLAR". Any other code will abort the program.
- C1, C2, C3 -- These are the coordinates of the field point. In rectangular coordinates they represent x, y, and z, respectively, in meters. The coordinate system is shown in Figure 4.1 or 4.3. If polar coordinates are used, C1 is the r-coordinate, in meters, while C2 and C3 give θ and φ, respectively, in degrees. The origin of the polar coordinate system is the center of the block, as shown in Figure 4.4. The polar axis of the spherical system may be changed by the user, as explained below.

INDEX3 -- See INDEX1 for details.

ACTION, AXIS -- These alphabetic codes are blank unless the user wishes to substitute a new polar coordinate system for the one shown in Figure 4.4. ACTION and AXIS are ignored if the coordinate system being used is rectangular. The new coordinate system will be right-handed. ACTION expresses the user's intent to change the system, and AXIS names the new polar axis. To alter the polar coordinate system, the card reads, beginning in Column 51:

CHANGE PØLAR AXIS TØ Y.



A spherical polar coordinate system used in calculations of the external scattered field. This system is used unless the program user changes it. Figure 4.4.

Any character other than "X", "Y", or "Z" will abort the program. If "CHANGE" is incorrectly punched, it will be ignored. The message "CHANGE PØLAR AXIS TØ Y", for example, will construct the coordinate system shown in Figure 4.5. We note that \vec{E}^i is perpendicular to the new polar axis. By suitably orienting the block of tissue in the original system, this technique enables the user to study scattering from bodies illuminated by a wave polarized along the y-axis, without changing the program.

To get a better understanding of how these variables are used, we will discuss some examples in the next section.

4.4. Using the Program

We will construct the data files for two sample problems in this section, in order to see how the input variables are used. After we examine the data files, we will discuss some of the important features of the printed output.

First, we consider the block of tissue shown in Figure 4.6, which comprises a homogeneous layer of fat and a homogeneous layer of muscle. The face of the block measures 4 cm x 4 cm, and each layer is 1 cm thick. The incident field is a 915 MHz plane wave, and it illuminates the body uniformly. In addition, we wish to calculate the scattered field at the point x = y = 0, z = -1 meter.

Letting NDIV = 2, the first data card looks like this:

NUMBER ØF DIVISIØNS PER EDGE FØR INTEGRATIØN = 2.

The block is symmetrical in all four of the quadrants shown in Figure 4.3, and we cannot assume that any components of the induced field are zero. Thus, the second card is:

X,Y,Z 915. 1234

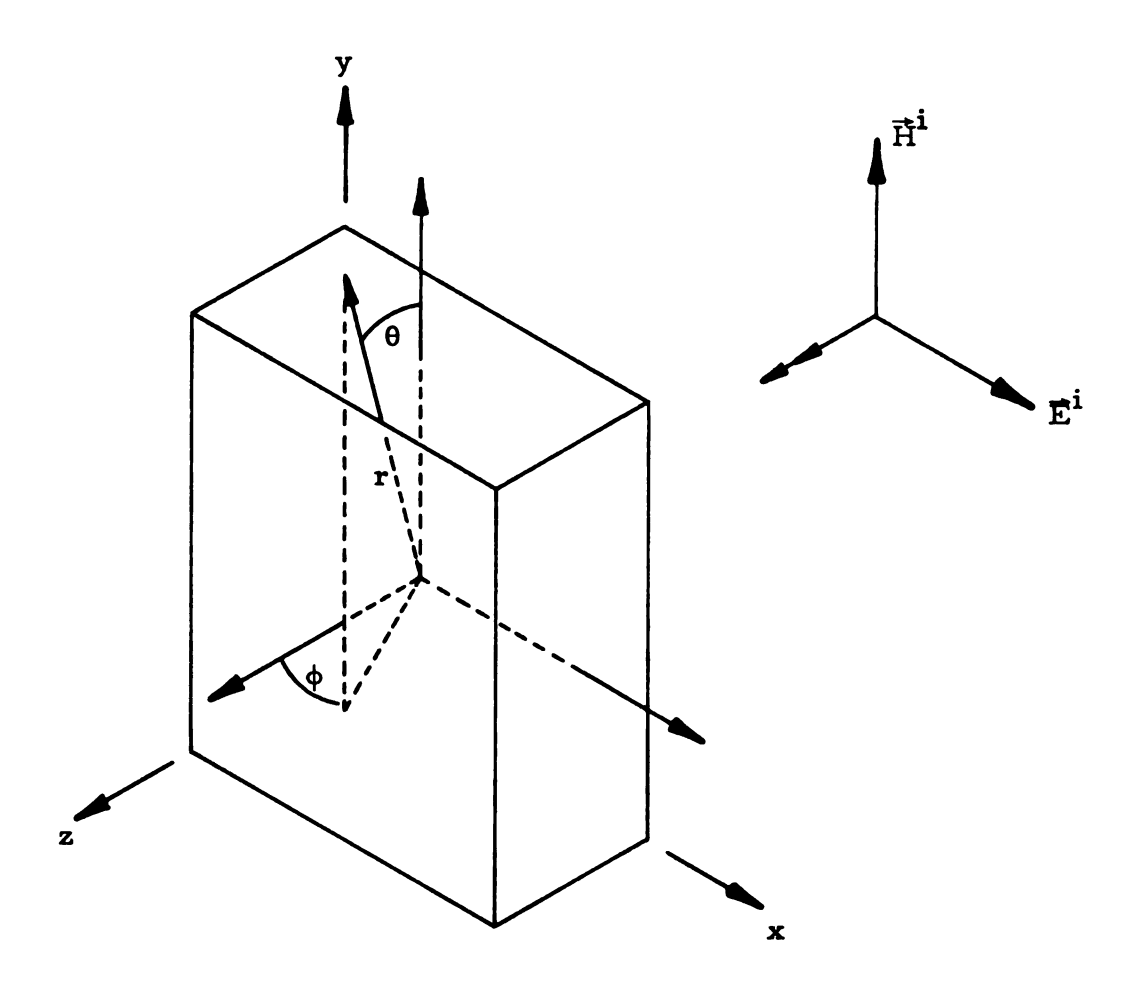


Figure 4.5. An alternate spherical polar coordinate system for scattering calculations. This system uses the y-axis as the polar axis.

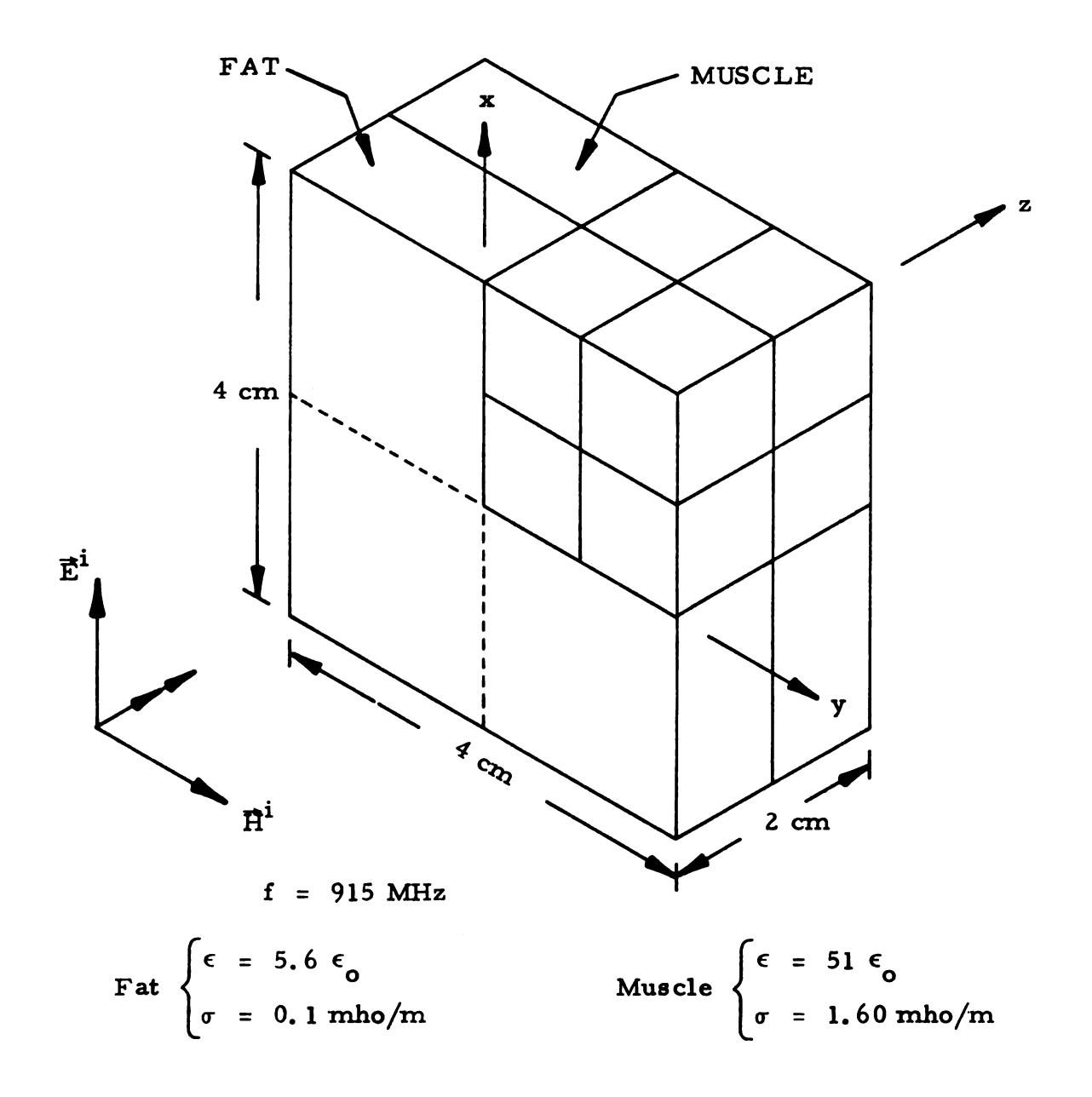


Figure 4.6. A block of tissue composed of a homogeneous fat layer and a homogeneous layer of muscle, illuminated by a 915 MHz plane wave.

The first quadrant has been partitioned into 8 subvolumes--two rows and two columns in each layer. Each subvolume is a cube measuring 1 cm x 1 cm x 1 cm. The next two cards, therefore, appear as follows:

At 915 MHz, the permittivity of fat is 5.6 ϵ_0 , and its conductivity is about 0.1 mho/meter. The values for muscle are 51 ϵ_0 and 1.60 mho/meter, respectively. This data appears on the next two cards as shown below:

Since the illumination is uniform, and since each layer is homogeneous, the next two cards are:

DATA FILE FØR NØNUNIFØRM ILLUMINATIØN = NULLSET

DATA FILE FØR INHØMØGENEØUS LAYERS = NULLSET

We will compute the scattered field in rectangular coordinates.

The scattering file contains only one card, so the last two data cards are:

In the second example, we will calculate only the induced field in the inhomogeneous layer of fat shown in Figure 4.7. The layer measures 3 cm x 3 cm x 1 cm, and each subvolume is 1 cm x 1 cm x 1 cm. The subvolume in the 2nd row, 3rd column, is composed of muscle, as shown in the figure. The incident field is again a 915 MHz plane wave, but it illuminates only the subvolume in the lower left-hand corner of the layer (IX = IY = 1).

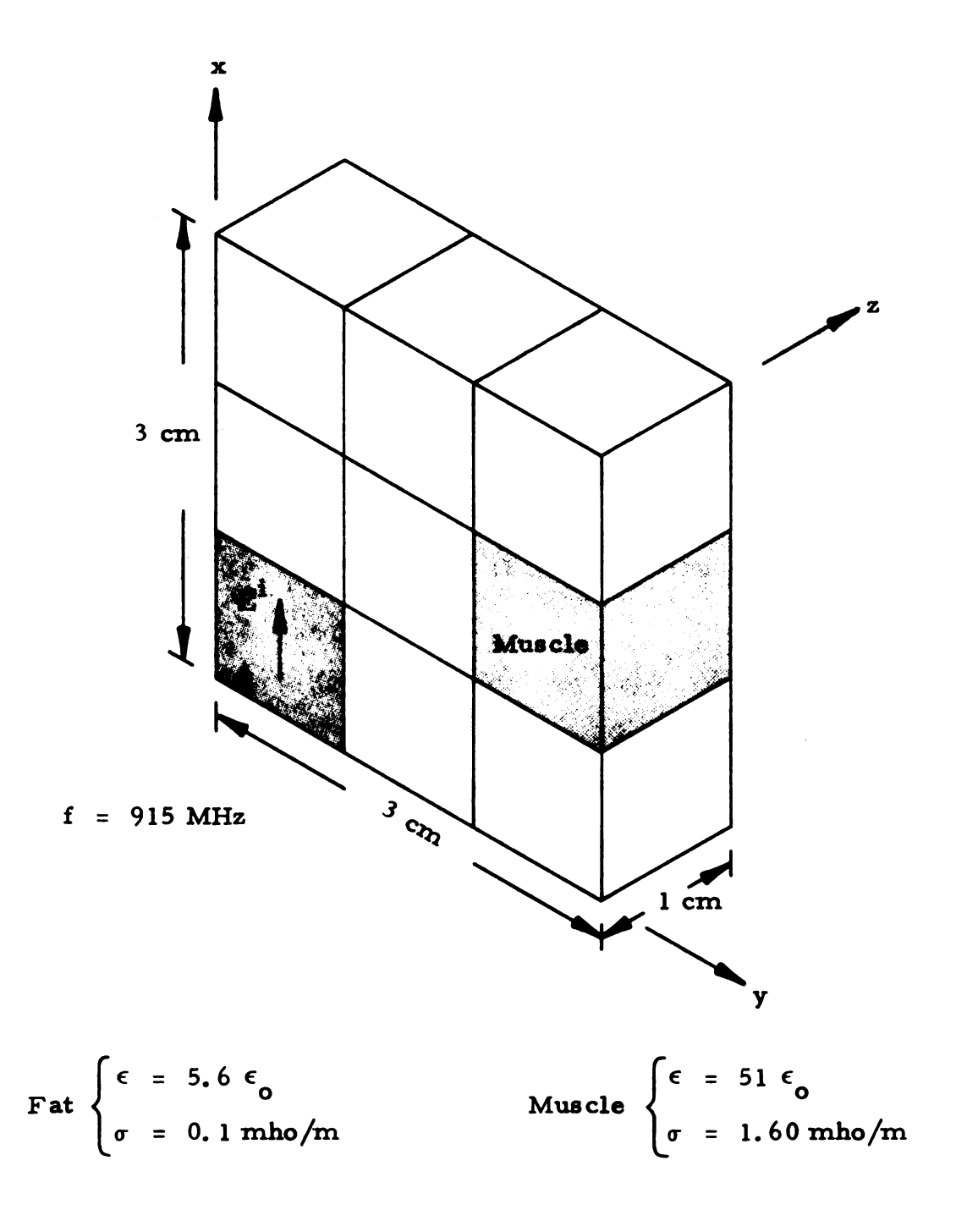


Figure 4.7. An inhomogeneous layer of fat, illuminated only in one corner by a 915 MHz plane wave.

The configuration of subvolumes shown cannot be obtained by reflecting a smaller group of subvolumes about one or more axes of symmetry. Hence, only the first quadrant of Figure 4.3 can be used. Since the z-component of the induced field in a single layer of subvolumes is often negligible, we will assume that only E_x and E_y are nonzero. We will again use NDIV = 2.

The data file for this example is as follows:

NUMBER ØF DIVISIØNS PER EDGE FØR INTEGRATIØN = 2

XANDY 915.0 1 03 03 01 1.0 1.0 1.0

0.1

DATA FILE FØR NØNUNIFØRM ILLUMINATIØN = FØLLØWS

01 01 END FILE

5.6

DATA FILE FØR INHØMØGENEØUS LAYERS = FØLLØWS

02 03 01 51.0 1.60 END FILE

DATA FILE FØR SCATTERED FIELD = NULLSET

The printed output from the second example is shown on Page 129. Although most of the items in the output are self-explanatory, a few of them need to be explained. The indices of each subvolume in the first quadrant (the row, column, and layer) are given under the columns marked "IX", "IY", and "IZ". The column labeled "N" gives a simple numbering scheme which assigns a single index to each subvolume in the first quadrant.

The column marked "IRR" is blank when the incident field illuminates the block uniformly. When \vec{E}^i is collimated, an "X" appears under the "IRR" column next to each subvolume which is directly irradiated by the incident wave.

INTERNAL FIELD

FREQUENCY = 915.000000 MHZ.	C NX N	NY B 3 NZ B	INVESTIGATION OF THE TRANSPORTED TO THE TRANSPORTED		ILLUMINATION = COLL.	
	QUADRANTS USED = 1.	H 1.				
	EX	Ę	£2	a a	EPS	916
38	.42885230E+00	.81650960E-02	0.	.91990483E-02	5.60	•10000E •00
37	.51371019E-01	.21894284E-01	0.	.15591706E-03	2.60	.10000E+00
Ţ	.10419839E-01	.877317796-02	••	.92770847E-05	2.60	.10000E .00
955	•12855070E•00	.16514802E-01	••	.83990100E-03	2.60	.10000E .00
907	.13907050E-01	.42486125E-01	••	.99923843E-04	2.60	.10000E+00
3	.14165134E-02	.17524916E-02	••	.40621897E-05	51.00	.16000E+01
2	.46021170E-01	.78307229E-02	••	.10896342E-03	5.60	.10000E+00
92	•29023635E-02	.20038935E-01	0.	.20499131E-04	5.60	.10000E+00
2	.23920035E-02	.94409008E-02	••	.47426144E-05	5.60	.10000E .00

TOTAL POWER ABSURBED IN BODY # .10442335E-07 WATTS.

NUMBER OF PARTITIONS PER EDGE IN INTEGRATION = 2

"DELTA X", "DELTA Y", and "DELTA Z" at the bottom of the page denote the dimensions of each subvolume.

The output describing the scattered field from the first example is shown on Page 131. Most of the columns on the page have two headings separated by a "/". The first heading in each pair is employed when rectangular coordinates are used; the second heading is used when polar coordinates have been given. Thus, in our example, the first three numbers are the x-, y-, and z-coordinates, respectively, in meters, of the field point. The next three numbers are E_x^S , E_y^S , and E_z^S at that point. The "PØLAR AXIS" column is blank when rectangular coordinates are used.

The magnitude of each field component, as well as the magnitude of the total field, is also given in dB. The 0 dB reference is $|\vec{E}^s| = 0.01 |\vec{E}^i|$.

When polar coordinates are used, the first three columns of numbers give, respectively, the r-coordinate of the field point in meters, and the θ - and φ -coordinates in degrees. The next three columns show E_r^s , E_{θ}^s , and E_{φ}^s at that point.

4.5. Listing of Program and Subroutines

The listing of PRØGRAM BLØCK and its subroutines begins on Page 132. A "\$" is used to separate consecutive FØRTRAN statements, allowing more than one statement per card. The program requires approximately 70000 octal words of storage.

SCATTERED FIELD

COORU	X/R	Y/THETA	1H4/2	EXZER	EY/ETH	Е2/ЕРН	POLAR AXIS
HECT.	0000	0000•	-1.0000	.36745505E-02	.66186866E-19	.53220256E-19	
				-8.70 DB	-343.58 08	-345.48 DB	
				TOTAL SC	TOTAL SCATTERED FIFTD = -0.70 DB	-0-70 DB	

0 DB REFERENCE IS ES = 0.01 EI .

```
IZ**4X**N**4X**IRR**10X**EX**19X*
**10X**51G*)
3X*4(E16*8*4X)*F10*2*6X*E12*5)
** CM***7X**DELTA Y = **F7*4** CM*
                                                                RID.PART.START1.START2.START3.ADD1.ADD2.ADD3.
FCTR2.TAUN2.GMAT.DET
IE(10.10).TAUDATA(20.2).DUMMY(20200).IQ(8).
                                                                                                                                                                                                                                                                                                                                                   SORBED IN BODY = * E16.8 * WATT
                                                                                                                                                                                                                                                                                                                                                                              SPECIFYING FILE3.4
                            1.121,74.NERR
1.KZ.PI.EPS.MU.HVN.OMEG
LTAY.DELTAZ.NX.NY.NZ
                                                                                                                                               .
289
.
                                                                                                                                                                                                                                                                                                                                                                               160
                                                                                                             SOOO
                                                                                                                                                                                                                                  ပ
```

		るファファファ	~~~@@@@@	00000000000000000000000000000000000000
<u> </u>	بالبالبالباليا	بالالالباليال	اللالبال الماليال	00000000000000000000000000000000000000
EAC 100.NDIV S READ 101.COMP.FMEG.(IGARR(J).J=1.8) EAC 102.NX.NY.NZ S READ 101.COMP.FMEG.(IGARR(J).J=1.8) EAC 102.NX.NY.NZ S READ 103.DXCM.DYCM.DZCM O 300 KZ=1.NZ S READ 104.RLEP1.SIG1 S TAUDATA(KZ.1)=RLEP1 B AUCATA(KZ.2)=SIG1 F(COMP .EQ. SHXONLY) GO TO 500 F(COMP .EQ. SHXNDY) GO TO 502 F(COMP .EQ. SHXNDY) GO TO 502 F(COMP .EQ. SHX.Y.Z) GO TO 502 RON=1 S GO TO 503 BON=2 S GO TO 503	MEG=2.*PI*FMEG*1.0E6 S WVN=OMEG*SQRT(MU*EPS) S NERR=0 B	T GUADRANTS, ELIMINATING BLANKS AND DUPLICATES 0.301 I=188	DO 303 JJ=2.8	REAC 106.1X.1Y.1NDEX]
0 000	MM 00	× 24 %		0 0 0 0 0 0 0 0 0 0 0 0 0 0 0 0 0 0 0

! :	

```
M2=1
                                                                                                                                                                                                                                                                                                                                                                                                                                                                                                                                                                                                                                                                   519
                                                                                                                                                                                                                                                                                                                                                                                                                                                                                                                                 307
                                                                                                                                                                                                                                                                                                                         ၁၀
                                                                                                                                                                                                                                                                                                                                                                                                                                                                                                                                                                                                                                                                                                                     Z,M.RAD,EFI,EFZ,EF3,POWER,VOL(M,S),VOL(M,6)
57,DXGM,DYCM,DZCM S PRINT 158,PTOT
                                                                                                                                                                                                                                                                                                                                                                                                                                                                                                                                                                                                                                                                                                                                                                             R NOT SCATTERED FIELD IS TO BE CALCULATED IF IF (FILE3 * EG* 7 HNULLSET) 60 TO 999 (COUNS) 60 TO 521 (COUNS) 60 999 (COUNS) FIELD: IF DESIRED (COUNS) KRON)
                                                                                                                                                                                                                                                                                                                                                                                                                                                                                                                                                                                                                                               FILE . EQ. 7HNULLSET 60
S RAD=1HX S 60 T0 520
                                                                                                                                                                                                                                                                                                                          99
                                                                                                                                                                                                                                                                                                                                                                                                                                                             4.FMEG.NX.NY.NZ.ZILL, COMP. (INTARR (J), J=1.ICOUNT)
                                                                                                                                                                                                                                                                                                                          333
                                                        S
                                                                                                                                                                                                                                                                                                                                                                                                                                                                                                                                    8999
                                                                                                                                                                                                                                            -10+N+H1
                                                                                                                                                                                                                                                                                                                                                                                                                                                                                                                                 516
516
517
                                                                                                                                                                                                                                                                                                                                                                                                  RIX EQUATION FOR INTERNAL ELECTRIC FIELD STATES AND STA
                                                                                                                                                                                                                                                                                                                                                                                                                                                                                                                                    $22
                                                                                                                                                                                                                                                                                                                                                                                                                                                                                                                                 $ 00 308 1X=1,NX
IF(KRON .EQ. 1) GO
IF(KRON .EQ. 2) GO
GO TO S18
                                                                                                                                                                                                                                                                                                                                                                                                                                                                                                                                                                                                                                               M.6) # (EF1 ** 2 + EF2 * + R*VOL (M.4) S IF (M.4) NE. I) 60 10 519
                                                                                                                                                                                                                                                                                                                                                                                                                                                                                                                                  S
S
S
S
S
S
                                                                                                                                                                                                                                                                                                                                           3015
0015
0015
0015
0015
 3000
3000
0600
0600
0600
0600
                                                                                                                                                                                                                                                                                                                                                                                                                                                                                                                                                                                                                                                                                                                                                                                                                                                          521
999
                                                                                                                                                                                                                                                                                                                                                                                                                                                                                                                                                                                                                                                                                                         322
308
308
                                                                                                                                                       511
                                                                                                                                                                                                                     51,
                                                                                                                                                                                                               ပ
                                                                                                                                                                                                                                                                                                                                                                                                                                                                                                                     C
                                                                                                                                                                                                                                                                                                                                                                                                                                                                                                                                                                                                                                                                                                                                                                                     S
                                                                              ပ
```

		;

		!

E 222 22 22 22 23 25 25 25 25 25 25 25 25 25 25 25 25 25	
52 FUNC=FCTR1*(FCTR2*CMPLX(-1.*ALPHA**21.*ALPHA)) 53 TOTAL=TOTAL+FUNC 30 U(2)=U(2)+ADD2 31 U(1)=U(1)*ADD1 32 U(3)=U(3)*ADD3 32 U(3)=U(3)*ADD3 33 U(1)=U(1)*ADD3 34 U(1)=U(1)*ADD3 35 U(3)=U(3)*ADD3 36 MAT=(0.*-1.)*REX1*TAUMZ*DVMZ*TOTAL/DENOM S GO TO 99 54 IF(1 *EQ. 1) & GO TO SG 55 GMAT=(0.*-1.)*Z**OMEG*MU**TAUMZ/(10.*3.)*OMEG*EPS)) 56 A=((3.*DVMZ)/(4.*PI))**(1.*,3.)*OMEG*EPS)) 57 CTR1=(0.*-1.)*Z**OMEG*MU**TAUMZ/(10.*3.)*OMEG*EPS)) 58 CONTINUE S RETURN S END	SUBROUTINE RFN(19) COMMON VOL(100.6)*XO*YO*ZO*IN*NERR COMMON VOL(110.6)*ENO.YO*ZO*IN*NERR COMMON VOL(110.6)*ENO.YO*ZO*IN*NERR COMMON VOL(110.6)*ENO.YO*ZO*IN*NERR LONG TO COMMON VOL(110.6)*ENO.YO*ZO*IN*NERR LONG TO COMMON VOL(110.6)*ENO.YO*ZO*IN*NERR LONG TO COMMON VOL(110.6)*ENO.YO*ZO*IN*NERR LONG ECC. COLO. ENO. EMPROPER QUADRANT NUMBER.*/ LONG ECC. COLO. ENO. ENO. ENC. ENC. ENC. ENC. ENC. ENC. ENC. ENC
order en	

2444444 1111111			44444444	00000000000000000000000000000000000000
CARTON TO THE TOTAL TOTA	3 A(J.NPI)=0. 2 D0 4 J=1.NM1 S C=CABS(A(J.J)) S JP D=CABS(A(I.J)) S IF(C=D) 6.5.5 S B=A(I.K) A(J.K) S C=D T K=J.NPM S B=A(I.K) S CONTINUE S IF(CABS(A(J.J))=FP) 14.1 S D0 4 A(I.K)=CONST=A(J.K) S IF(CABS A(J.K) S IF(CABS A) S IF(CABS A(J.K) S IF(CABS A) S	AND THE CANAL TH	SUBROUTINE SCATTER(G.10.MA.N.KRON) COMFLEX G.GMAI.TOTAL.SUM.EF REAL HU.INDEX3 DIMENSION G(100.101).EF(3).X(3).EPOL(3).EREC(3).IQ(8) COMMON FIELD/SIZE(3).KI.KZ.PI.EPS.MU.WVN.OMEG COMMON/FIELD/SIZE(3).KI.KZ.PI.EPS.MU.WVN.OMEG COMMON/GADSCA/XC.YC.ZC COMMON/GADSCA/XC.YC.ZC	3(5X.F10.4).3(4X.E16.3(5X.F10.4).3(4X.E16.6).3(5X.F10.4).3(4X.E16.6).3(5X.F10.4).3(4X.E16.6).3(10X.F7.2).4 DB+)/6

```
PULAX=1HX
                              900
                              00
     150, COORD $ 60 TO
E2DB=20.*AL0610(EREC(2))
                                          FIELD TO BOEAR
```

CHAPTER V

SUMMARY

This thesis has presented a technique for calculating the electric field induced in a finite biological body having arbitrary shape and composition, when the body is irradiated by an electromagnetic wave. A knowledge of the induced field is important to researchers investigating the biological effects of nonionizing radiation.

As an introduction to the study of induced electromagnetic fields in biological media, a plane slab model of a human trunk was analyzed. It was noted that the electromagnetic field induced in the model by a uniform plane wave can be obtained by two methods: (1) by a direct application of boundary conditions, and (2) by transmission line techniques. A group of numerical examples was presented to illustrate the behavior of the human trunk model at various frequencies from 100 Hz to 10 GHz.

The problem of calculating the electric field induced in a finite body was considered next. An integral equation for the induced electric field was derived using the free-space dyadic Green's function. The method of moments was then used to transform the integral equation to a matrix equation for numerical solution. Techniques for calculating the external scattered field, and for using symmetry to reduce the matrix size, were included. A variety of numerical examples, along with some experimental data, were presented to illustrate the versatility and the accuracy of the moment solution. In addition, the computer

program used to calculate the numerical examples was described, and instructions for its use were given.

The numerical technique presented in this thesis has a serious drawback: if a researcher wishes to study a model which must be sectioned into a large number of subvolumes, his computer system must be able to invert enormous matrices. Such a case might occur if one or more of the following applies: (1) very high frequencies are used; (2) the model is quite large; (3) the model's shape or composition is complicated; (4) a "fine-grained" solution is required. Thus, a useful topic for further research would be that of developing an efficient way to invert very large matrices.

Also, a great deal of work has yet to be done on probing the induced field in a body of biological material. There is at present a conspicuous lack of experimental data on this subject.



APPENDIX A

EVALUATION OF THE SCALAR COMPONENTS OF THE FREE-SPACE DYADIC GREEN'S FUNCTION

The free-space dyadic Green's function may be written as

$$\vec{G}(\vec{r}, \vec{r}') = -j\omega\mu_{o} \left[\vec{T} + \frac{\nabla\nabla}{k_{o}^{2}}\right] \frac{e^{-jk_{o}|\vec{r} - \vec{r}'|}}{4\pi|\vec{r} - \vec{r}'|}, \quad (A1)$$

where $\overrightarrow{1} = \overrightarrow{x} \overrightarrow{x} + \overrightarrow{y} \overrightarrow{y} + \overrightarrow{z} \overrightarrow{z}$,

and
$$k_0 = \omega \sqrt{\mu_0 \epsilon_0}$$
.

The scalar components of $\overrightarrow{G}(\overrightarrow{r},\overrightarrow{r}')$ are given by

$$G_{\mathbf{x}_{\mathbf{p}}\mathbf{x}_{\mathbf{q}}}(\mathbf{r},\mathbf{r}') = -j\omega\mu_{\mathbf{o}}\left[\psi \delta_{\mathbf{p}\mathbf{q}} + \frac{1}{k_{\mathbf{o}}^{2}} \frac{\partial^{2}\psi}{\partial \mathbf{x}_{\mathbf{q}}\partial \mathbf{x}_{\mathbf{p}}}\right], \qquad (A2)$$

$$\mathbf{p}_{\mathbf{q}} = 1, 2, 3 ,$$

where

$$\psi = \psi(R) = \frac{e^{-jk_0R}}{4\pi R} ,$$

$$R = |\vec{r} - \vec{r}'| = (u_1^2 + u_2^2 + u_3^2)^{1/2} ,$$
(A3)

$$u_{i} = x_{i} - x_{i}!$$
 $i = 1, 2, 3$,

and
$$x_1 = x$$
, $x_2 = y$, $x_3 = z$.

Since $\frac{\partial R}{\partial x_p} = \frac{u_p}{R}$, we have

$$\frac{\partial \psi}{\partial \mathbf{x}_{\mathbf{p}}} = \frac{d\psi}{d\mathbf{R}} \frac{\partial \mathbf{R}}{\partial \mathbf{x}_{\mathbf{p}}} = \frac{d\psi}{d\mathbf{R}} \frac{\mathbf{u}_{\mathbf{p}}}{\mathbf{R}} . \tag{A4}$$

Then.

$$\frac{\partial^{2} \psi}{\partial \mathbf{x}_{\mathbf{q}} \partial \mathbf{x}_{\mathbf{p}}} = \frac{\partial}{\partial \mathbf{x}_{\mathbf{q}}} \left(\frac{d\psi}{dR} \frac{\mathbf{u}_{\mathbf{p}}}{R} \right) = \frac{\mathbf{u}_{\mathbf{p}}}{R} \frac{\partial}{\partial \mathbf{x}_{\mathbf{q}}} \left(\frac{d\psi}{dR} \right) + \frac{d\psi}{dR} \frac{\partial}{\partial \mathbf{x}_{\mathbf{q}}} \left(\frac{\mathbf{u}_{\mathbf{p}}}{R} \right)$$

$$= \frac{\mathbf{u}_{\mathbf{p}}}{R} \frac{d^{2} \psi}{dR^{2}} \frac{\partial R}{\partial \mathbf{x}_{\mathbf{q}}} + \frac{1}{R^{2}} \frac{d\psi}{dR} \left[R \frac{\partial \mathbf{u}_{\mathbf{p}}}{\partial \mathbf{x}_{\mathbf{q}}} - \mathbf{u}_{\mathbf{p}} \frac{\partial R}{\partial \mathbf{x}_{\mathbf{q}}} \right] . \tag{A5}$$

Or,

$$\frac{\partial^2 \psi}{\partial \mathbf{x}_q \partial \mathbf{x}_p} = \frac{\mathbf{u}_p \mathbf{u}_q}{R^2} \frac{d^2 \psi}{dR^2} + \frac{1}{R} \frac{d \psi}{dR} \left[\delta_{pq} - \frac{\mathbf{u}_p \mathbf{u}_q}{R^2} \right] , \qquad (A6)$$

since
$$\frac{\partial \mathbf{u}_{\mathbf{p}}}{\partial \mathbf{x}_{\mathbf{q}}} = \delta_{\mathbf{pq}}$$
.

Substituting Equation (A6) into Equation (A2) and rearranging terms gives

$$G_{\mathbf{x}_{\mathbf{p}}\mathbf{x}_{\mathbf{q}}}(\vec{\mathbf{r}},\vec{\mathbf{r}}') = -j\omega\mu_{\mathbf{o}}\left[\left(\psi + \frac{1}{k_{\mathbf{o}R}^{2}}\frac{d\psi}{dR}\right)\delta_{\mathbf{p}\mathbf{q}} + \frac{u_{\mathbf{p}}u_{\mathbf{q}}}{k_{\mathbf{o}R}^{2}}\left(\frac{d^{2}\psi}{dR^{2}} - \frac{1}{R}\frac{d\psi}{dR}\right)\right]. \quad (A7)$$

With ψ given by Equation (A3), it can be readily demonstrated that

$$\frac{d\psi}{dR} = -\psi \left[j k_0 + \frac{1}{R} \right] . \tag{A8}$$

Thus,

$$\frac{d^2\psi}{dR^2} = -\psi \frac{d}{dR} \left[j k_o + \frac{1}{R} \right] - \left[j k_o + \frac{1}{R} \right] \frac{d\psi}{dR}$$

$$= \frac{\psi}{R^2} + \psi \left[j k_o + \frac{1}{R} \right]^2 . \tag{A9}$$

Or,

$$\frac{d^2\psi}{dR^2} = \psi \left[\frac{2}{R^2} + \frac{2jk_0}{R} - k_0^2 \right] . \tag{A10}$$

Substituting Equations (A8) and (A10) into Equation (A7) gives

$$G_{\mathbf{x}_{\mathbf{p}}\mathbf{x}_{\mathbf{q}}}(\vec{\mathbf{r}}, \vec{\mathbf{r}}') = -j\omega\mu_{\mathbf{o}} \left\{ \left[\psi - \frac{\psi}{k_{\mathbf{o}}^{2}R} \left(\frac{1}{R} + j k_{\mathbf{o}} \right) \right] \delta_{\mathbf{p}\mathbf{q}} + \frac{u_{\mathbf{p}}u_{\mathbf{q}}}{k_{\mathbf{o}}^{2}R^{2}} \left[\psi \left(\frac{2}{R^{2}} + \frac{2jk_{\mathbf{o}}}{R} - k_{\mathbf{o}}^{2} \right) + \frac{\psi}{R} \left(\frac{1}{R} + j k_{\mathbf{o}} \right) \right] \right\} . \quad (A11)$$

Equation (All) may be rewritten as

$$G_{\mathbf{x}_{p}}\mathbf{x}_{q}^{(\overrightarrow{\mathbf{r}},\overrightarrow{\mathbf{r}}')} = \frac{-j\omega_{\mu_{o}}\psi}{k_{o}^{2}R^{2}} \left[(k_{o}^{2}R^{2} - 1 - jk_{o}R)\delta_{pq} + \frac{u_{p}}{R} \frac{u_{q}}{R} (3 - k_{o}^{2}R^{2} + 3jk_{o}R) \right] . \tag{A12}$$

$$\text{Letting} \quad \alpha = k_{o}R, \quad \cos\theta_{\mathbf{x}_{p}} = \frac{u_{p}}{R},$$

$$\cos\theta_{\mathbf{x}_{q}} = \frac{u_{q}}{R}, \quad \text{and using Equation (A3),}$$

we have

$$G_{\mathbf{x}_{p}}\mathbf{x}_{q}^{(\vec{r},\vec{r}')} = \frac{-j\omega_{\mu_{o}}k_{o}e^{-j\alpha}}{4\pi\alpha^{3}}[(\alpha^{2}-1-j\alpha)\delta_{pq} + \cos\theta_{\mathbf{x}_{p}}\cos\theta_{\mathbf{x}_{q}}^{(3-\alpha^{2}+3j\alpha)]},$$
(A13)

which is Equation (3.3.4).



BIBLIOGRAPHY

- 1. Collin, R. E., and F. J. Zucker, Antenna Theory Part 1, pp. 41-43, McGraw-Hill, 1969.
- 2. Harrington, R. F., Field Computation by Moment Methods, ch. 1, Macmillan, 1968.
- 3. Harrington, R. F., <u>Time-Harmonic Electromagnetic Fields</u>, pp. 123-125, McGraw-Hill, 1961.
- 4. Ho, H. S., A. W. Guy, R. A. Sigelmann, and J. F. Lehmann, "Electromagnetic heating patterns in circular cylindrical models of human tissue," in <u>Proc. 8th Ann. Conf. Medical and Biological Engineering</u> (Chicago, Ill.), July 1969, p. 27.
- 5. Johnson, C. C., and A. W. Guy, "Nonionizing electromagnetic wave effects in biological materials and systems," Proc. IEEE, Vol. 60, No. 6, pp. 692-718, June 1972.
- 6. Kritikos, H. N., and H. P. Schwan, "Hot spots generated in conducting spheres by electromagnetic waves and biological implications," IEEE Trans. Biomedical Engineering, Vol. BME-19, No. 1, pp. 53-58, January 1972.
- 7. Lehmann, J. F., A. W. Guy, V. C. Johnston, G. D. Brunner, and J. W. Bell, "Comparison of relative heating patterns produced in tissues by exposure to microwave energy at frequencies of 2450 and 900 megacycles," Arch. Phys. Med. Rehabil., Vol. 43, pp. 69-76, February 1962.
- 8. Lepley, L. K., and W. M. Adams, "Electromagnetic dispersion curves for natural waters," <u>Water Resources Research</u>, Vol. 7, No. 6, pp. 1538-1547, December 1971.
- 9. Lin, J. C., A. W. Guy, and C. C. Johnson, "Power deposition in a spherical model of man exposed to 1-20 MHz electromagnetic fields," IEEE Trans. Microwave Theory Tech., Vol. MTT-21, No. 12, pp. 791-797, December 1973.
- 10. Livesay, D. E., B. S. Guru, and K. M. Chen, "Scattering from finite biological and metallic cylinders," presented at 1975 International IEEE/AP-S Symposium, Univ. Ill. at Urbana-Champaign, June 2-4, 1975.
- 11. Plonsey, R., Bioelectric Phenomena, pp. 204-206, McGraw-Hill, 1969.

- 12. Ramo, S., J. R. Whinnery, and T. Van Duzer, Fields and Waves in Communication Electronics, ch. 6, Wiley & Sons, 1965.
- 13. Richmond, J. H., "Scattering by a dielectric cylinder of arbitrary cross-section shape," <u>IEEE Trans. Antennas Propagat.</u>, Vol. AP-13, No. 3, pp. 334-341, May 1965.
- 14. Richmond, J. H., "TE-wave scattering by a dielectric cylinder of arbitrary cross-section shape," IEEE Trans. Antennas Propagat., Vol. AP-14, No. 4, pp. 460-464, July 1966.
- 15. Saxton, J. A., and J. A. Lane, "Electrical properties of sea water," Wireless Engineer, pp. 269-275, October 1952.
- 16. Schwan, H. P., "Radiation biology, medical applications, and radiation hazards," in Microwave Power Engineering, Vol. 2, E. C. Okress, Ed., pp. 215-232, Academic Press, 1968.
- 17. Shapiro, A. R., R. F. Lutomirski, and H. T. Yura, "Induced fields and heating within a cranial structure irradiated by an electromagnetic plane wave," IEEE Trans. Microwave Theory Tech., Vol. MTT-19, No. 2, pp. 187-196, February 1971.
- 18. Van Bladel, J., "Some remarks on Green's dyadic for infinite space," IRE Trans. Antennas Propagat., Vol. AP-9, pp. 563-566, November 1961.
- 19. Van Doeren, R. E., "An integral equation approach to scattering by dielectric rings," <u>IEEE Trans. Antennas Propagat.</u> (Communications), Vol. AP-17, No. 3, pp. 373-374, May 1969.

MICHIGAN STATE UNIV. LIBRARIES 31293000939250